Calhoun
Institutional Archive of the Naval Postgraduate School

Calhoun: The NPS Institutional Archive

DSpace Repository

Theses and Dissertations | 1. Thesis and Dissertation Collection, all items

1965-06-01

A comprehensive analysis of cryogenic magnets suitable for magnetohydrodynamic applications.

McMorris, John Allen

Massachusetts Institute of Technology

http://hdl.handle.net/10945/11816

Downloaded from NPS Archive: Calhoun

DUDLEY KNOX LIBRARY

http://www.nps.edu/library

Calhoun is the Naval Postgraduate School's public access digital repository for research materials and institutional publications created by the NPS community. Calhoun is named for Professor of Mathematics Guy K. Calhoun, NPS's first appointed -- and published -- scholarly author.

Dudley Knox Library / Naval Postgraduate School
411 Dyer Road / 1 University Circle
Monterey, California USA 93943

NPS ARCHIVE
1965.06
MCMORRIS, J.

A COMPREHENSIVE ANALYSIS OF CRYOGENIC MAGNETS SUITABLE FOR MAGNETOHYDRODYNAMIC APPLICATIONS

by

JOHN ALLEN McMORRIS II, LIEUTENANT, U.S. NAVY

B.S., U.S. Naval Academy
(1957)

S.M., Nav. Eng., Massachusetts Institute of Technology
(1963)

SUBMITTED IN PARTIAL FULFILLMENT OF THE
REQUIREMENTS FOR THE DEGREE OF
DOCTOR OF SCIENCE
at the
MASSACHUSETTS INSTITUTE OF TECHNOLOGY
June, 1965

THESIS SUPERVISOR: HERBERT H. WOODSON, SC.D.
Professor of Electrical Engineering

Library
U. S. Naval Postgraduate School
Monterey, California

A COMPREHENSIVE ANALYSIS OF CRYOGENIC MAGNETS SUITABLE FOR MAGNETOHYDRODYNAMIC APPLICATIONS

by

JOHN ALLEN McMORRIS II, LIEUTENANT, U. S. NAVY

B. S., U. S. Naval Academy
(1957)

S. M., Nav. Eng., Massachusetts Institute of Technology
(1963)

SUBMITTED IN PARTIAL FULFILLMENT OF THE
REQUIREMENTS FOR THE DEGREE OF
DOCTOR OF SCIENCE
at the
MASSACHUSETTS INSTITUTE OF TECHNOLOGY
June, 1965

THESIS SUPERVISOR: HERBERT H. WOODSON, SC. D.
Professor of Electrical Engineering

NPS ARCHIVE
1969
MCMORRIS, J.

Thesis
M2554

Library
U. S. Naval Postgraduate School
Monterey, California

A COMPREHENSIVE ANALYSIS OF CRYOGENIC MAGNETS SUITABLE FOR MAGNETOHYDRODYNAMIC APPLICATIONS

by

JOHN ALLEN McMORRIS II, LIEUTENANT, U. S. NAVY

B. S., U. S. Naval Academy
(1957)

S. M., Nav. Eng., Massachusetts Institute of Technology
(1963)

SUBMITTED IN PARTIAL FULFILLMENT OF THE
REQUIREMENTS FOR THE DEGREE OF
DOCTOR OF SCIENCE
at the
MASSACHUSETTS INSTITUTE OF TECHNOLOGY
June, 1965

Signature of Author: _____

Department of Electrical Engineering, May 14, 1965

Certified by: _____

Thesis Supervisor

Accepted by: _____

Chairman, Departmental Committee on Graduate Students

A COMPREHENSIVE ANALYSIS OF CRYOGENIC MAGNETS SUITABLE FOR MAGNETOHYDRODYNAMIC APPLICATIONS

by

JOHN ALLEN McMORRIS II, LIEUTENANT, U.S. NAVY

Submitted to the Department of Electrical Engineering
on May 14, 1965 in partial fulfillment of the
requirements for the degree of Doctor of Science

ABSTRACT

This work constitutes a comprehensive investigation of the application of cryogenic technology to coils suitable for MHD applications. Detailed background studies are conducted in the specific areas of resistive behavior of metals, coil structural requirements, cryogenic refrigerator characteristics, properties of coolants, and cooling system design. These studies were utilized to develope a series of characteristic curves, suitable for use in the preliminary design phase of this type of cryogenic magnet. The range of the investigation covers coils suitable for generating fields of up to 100 KG, for use with MHD channels of cross section between .01 and 10 square meters.

Consideration is given to the optimization of operating temperature and coil geometry. A simplified procedure for preliminary coil analysis, utilizing the characteristic curves, is presented in the form of a flow diagram. Example problems indicate that "minimum loss" coils appear highly attractive for use with seeded-gas MHD generators of 50 Mw output, or larger. In general, "optimized" cryogenic coils should provide at least an order of magnitude reduction in total power requirements, compared to "conventional" copper coils. A reasonable evaluation of present data indicates that eventually, this may be improved by yet another factor of four.

Thesis Supervisor: Herbert H. Woodson
Title: Professor of Electrical Engineering

ACKNOWLEDGEMENTS

The author is deeply indebted to Professor H. H. Woodson, for his encouragement and guidance, as supervisor of this thesis, and to Professors J.L. Smith, Jr., P. E. Gray, and A. E. Bergles, for their valuable assistance as members of the thesis committee. Their constructive criticism has contributed greatly to the final form of this work.

This work was accomplished, in part, through use of the facilities of the M. I. T. Computation Center, at Cambridge, Massachusetts.

CONTENTS

		Page
I.	Introduction	9
	A. Background	9
	B. State-of-the-art	12
	C. Application to MHD	13
II.	Resistivity of metals	18
	A. Background	18
	B. Limitations of the theory	21
	C. "Residual" or "Impurity" resistance	24
	D. "Intrinsic" or "Ideal" resistance	27
	E. Zero-field resistance standards	36
	F. Magnetoresistance	43
III.	Structural design considerations	55
	A. Basic concepts	55
	B. Internal structure	56
	C. Superposition model for internal structure	64
	D. Support of "self field"	65
	E. Support of "adjacent field"	71
	F. External structure	73
IV.	Refrigeration	77
	A. Efficiency	77
	B. Other factors	80
V.	Heat transfer	82
	A. Basic concepts	82
	B. Pool boiling characteristics	84
	C. Pool boiling data	87
	D. Qualitative influence of forced convection	91
VI.	Coolant flow	96
	A. Geometric considerations	96
	B. Properties of coolants	98
	Saturation property coefficients	99
	Helium	101
	Parahydrogen	102
	Neon	103
	Nitrogen	103
	C. Single-phase flow	104

CONTENTS (cont'd)

Page

D. Two-phase flow 105
No-slip model 109
No-mixing model 112
Utilization of above models 115
Correction for subcooling at inlet 117
E. Other coolant considerations 120
VII. Generation and use of characteristic curves 123
A. Curves of coil geometry 123
Generation 123
Use 124
B. Mean coil resistivity curves 125
Generation 125
Use 128
C. Structural curves 129
Generation 129
Use 131
D. Coolant curves 131
Generation 132
Use 134
VIII. Design of cryogenic saddle coils 136
A. General design characteristics 136
B. Simplified design procedure 141
C. Example problem: minimum power consumption 144
D. Example problem: "lightweight" coil 149
IX. Conclusions 151
X. Recommendations 156

APPENDICES

A. Coil geometry curves 158
B. Mean coil resistivity curves 162
25 KG coils 163
50 KG coils 167
75 KG coils 171

CONTENTS (cont'd)

		Page
	100 KG coils	175
C.	Structural curves	179
D.	Coolant curves	184
	Nitrogen	185
	Neon	194
	Parahydrogen	203
	Helium	212
E.	Computer programs	221
	Coil geometry / resistivity	222
	Structural analysis	228
	Data fitting	232
	Coolant flow analysis	235
F.	Bibliography	249

LIST OF FIGURES

		Page
1.	Saddle coil	15
2.	Resistivity of indium	28
3.	Resistivity of sodium	29
4.	Resistivity of copper	30
5.	Resistivity of aluminum	31
6.	Field-free resistance standards	42
7.	Magnetoresistance of indium	46
8.	Magnetoresistance of sodium	47
9.	Magnetoresistance of copper	48
10.	Magnetoresistance of aluminum	49
11.	Magnetoresistance standards	52
12.	Normalized magnetic stress distribution for F = 2.7	58
13.	Normalized magnetic stress distribution for F = 1.9	59
14.	Normalized magnetic stress distribution for F = 1.7	60
15.	Normalized magnetic stress distribution for F = 1.5	61
16.	Normalized magnetic stress distribution for F = 1.3	62
17.	Simaltaneous solution of linear and cubic equations	69
18.	Refrigeration power vs. temperature	79
19.	"Typical" saturated boiling curves for cryogenic liquids	85
20.	a. Qualitative variation of heat transfer coefficient with quality.	93
	b. Qualitative variation of critical flux with quality	93
21.	"Typical" flow development	107
22.	a. "Typical" flow characteristics	121
	b. Possible flow instability	121
23.	Electrical plus refrigeration power for 50 kg saddle coils with $A_{ch} = 0.1$, $F = 2$, $\lambda = 1$	137
24.	Relative power consumption vs. F for $\lambda = 1$	140
25.	Simplified flow diagram for saddle coil design	142

LIST OF TABULATED DATA

		Page
1.	Field free resistivity of indium	38
2.	Field free resistivity of sodium	39
3.	Field free resistivity of copper	40
4.	Field free resistivity of aluminum	41
5.	Magnetoresistance design standards	52
6.	Saturation property coefficients	99

I. INTRODUCTION

A. Background:

Recent developments in the field of magnetohydrodynamics point toward an increasing need for high-field electromagnets combining large physical size with low power requirements: In particular, the application of seeded-gas MHD generators to commercial power generation (1, 2) indicates a probable need for fields of the order of 20-50 kilogauss, with channel lengths ranging between 1 and 30 meters and widths between 0.1 and 5 meters (the larger sizes corresponding to the lower fields). Further, recent interest in the application of MHD to marine propulsion (3, 4) suggests a possible need for fields of up to 200 KG, with channel dimensions scaling upwards from the larger figures cited above. It has been shown (2, 5) that the unprecedented size and high field requirements, coupled with the demand for operating economy, preclude the use of conventional electromagnets for these applications.

The startling advance of superconductor technology within the last decade has led to the consideration of superconducting magnets, to the exclusion of all others, for applications such as the above. Indeed, investigation of the Vanadium-Gallium system indicates the possibility that "hard" superconductors may be capable of operation in fields up to 500 KG (6). Despite this promise, however, superconducting magnets exhibit several less-than-desirable characteristics which have hampered their development, to date:

1. The elements utilized in superconducting alloys and compounds are relatively rare, and correspondingly expensive.

2. The mechanical properties of these alloys and compounds--- most notably, brittleness--- lead to severe problems in the manufacture and

operation of high-field coils.

3. The present "standard of the industry"--- ten mil wire--- poses serious problems regarding the assembly of physically large coils.

4. Due to the fact that hard superconductors become relatively poor conductors when quenched, the magnetic field of a suddenly quenched superconducting magnet is prone to rapid collapse. This leads, at best, to the problem of rapid disposal of a great deal of stored energy, and can lead, at worst, to local arcing and/or destruction of the coil. Subsequently, local impairment of the cooling system associated with such a coil--- if sufficient to permit a local temperature fluctuation to the vicinity of the quench point--- could necessitate immediate and total shutdown. This, in itself, could be disastrous, particularly in marine propulsion applications.

5. To date, the current density attainable in large superconducting coils has fallen far below that predicted on the basis of short-sample testing, thus adding an additional complication to the design of high-field magnets.

Although significant advances have been made in the search for solutions to these problems--- particularly, as regards coil protection (7), and determination of the factors underlying degraded performance in large coils (8-14)--- the successful synthesis of a large, high-field superconducting coil has proven to be an elusive, and as yet unrealized, goal. This fact has become a critical roadblock to the advance of MHD technology: so much so, that background studies leading to the development of a commercial MHD generator have perforce been conducted with a large, pulse-operated conventional copper-coil electromagnet (15, 16).

An alternative to the utilization of superconducting magnets for the

above applications would be the use of so-called "cryogenic" magnets: that is, magnets utilizing coils wound of any of several highly-purified and carefully annealed metals, designed to take advantage of the marked resistance decrease of "ordinary" conductors at cryogenic temperatures, as contrasted with superconductivity. Such magnets share the promise of relatively economical generation of intense magnetic fields over large volumes, but not the problems cited above. Specifically:

1. Initial material cost is less.
2. Mechanical properties tend toward ductility.
3. No significant restrictions need be placed on conductor size.
4. The metals contemplated are those considered "good" conductors, even at room temperature. Thus, resistivity is not critically sensitive to minor temperature fluctuations.
5. No serious scaling problems are known to exist. In fact, many of the problems associated with cryogenic magnet design become less severe as size is increased.

Of course, these advantages are offset by relative disadvantages: For example, since cryogenic coils do have non-zero resistivity, ohmic heating occures within the coil dewar, and an appreciably larger refrigeration system may be required for a given cryogenic coil than for a comparable superconducting coil. This implies both higher operating costs and higher equipment costs, with the relative increase depending primarily on coil size. Again, larger coils would appear more competitive on a relative basis. However, two facts seem pertinent, here: First, even relatively small cryogenic coils can be designed to operate considerably more economically than comparable room-temperature magnets. Second, cryogenic magnets have been built and successfully tested in sizes larger than those yet attainable by superconducting technology.

B. State-of-the-art:

Interestingly enough, although at least one study indicates that large cryogenic coils might closely approach the anticipated efficiency of the yet elusive superconducting coils for large-scale MHD applications (2), none have been built for this purpose, and in fact, no detailed study of such an application has been published to date. Perhaps this can be attributed to the glamour of superconducting magnets. However, considerable interest has been exhibited in the development of cryogenic magnets in geometries suitable for controlled fusion experiments, as can be seen from a brief description of coils already constructed in this country:

Los Alamos Scientific Laboratory (A. E. C.)(17, 18):

Size: 2-1/2" I. D. x 7-1/2" O. D. x 5" long. Construction: "Jelly roll": 120 turns of 5" x .010" copper foil, separated by inert spacers for coolant channels. Coolant: Liquid hydrogen (immersion). Field: 60 KG steady, 62 KG for 5 second pulse. Status: Operational.

Project Sherwood (N. B. S.) (19, 20):

Size: 3" I. D. x 12" O. D. x 7" long. Construction: "Tape wound": 14 stacked pancakes, each 0. 4" thick, wound of 14, 000 turns of 4 mil aluminum foil (insulated by 0. 17 mil paper strip) and encapsulated in epoxy. Radial slots machined in inert spacers between pancakes for coolant flow. Coolant: Liquid hydrogen (forced flow). Field: Tested to 95 KG. Status: Structural failure at 95 KG: magnet burst when Lorentz forces exceeded inherent strength of epoxy-bonded Al foil.

Lewis Research Center (N. A. S. A.) (21, 22):

Size: 30 cm. I. D. x 90 cm. O. D. x 60 cm. long. Construction: "Jelly roll": 12 stacked pancakes, each with 75 turns of 5 cm. x 0. 2 cm. aluminum strip, separated for coolant flow. Coolant: Liquid neon (immersion).

Field: Designed for 200 KG. Status: Undergoing preliminary testing.

Lawrence Radiation Laboratory (U. C.) (23, 24):

Size: 7-1/8" I. D. x 16" O. D. x 12" long. Construction: 77 turns of 0.625" square conductor (sodium cast into .010" stainless tubing), wound in four layers with coolant grooves and stainless support cylinders between adjacent layers. Coolant: Gaseous helium (forced flow). Field: Designed for 100 KG. Status: Failed during testing at 21 KG when Lorentz force extruded sodium through small crack in stainless jacket. Being rebuilt.

The above coils share many common features: All are cylindrical solenoids, such as might be suitable for construction of a magnetic mirror. All have what has hitherto been considered a large bore, for high-field magnets. All but the last (designed by Taylor and Post) are of extremely simple design, and even the last design appears simple contrasted with what might be required to perform the same task with "conventional" electromagnets.

Taylor and Post are evolving what might be considered the second generation of cryogenic magnets: Their design represents the first attempt to obtain the best possible performance (25-27) from a cryogenic magnet, as contrasted with previous attempts to obtain performance, period. They have attempted to optimize their design in two respects: first, they have attempted to identify that operating temperature which minimizes total power expended in removing I^2R losses from the coil, and second, they have identified the particular geometry which maximizes magnetic energy density per unit dissipation for a cylindrical solenoid.

C. Application to MHD:

The coil model which will be used throughout this analysis is the overlapping cylinder or "saddle coil" model discussed by Stekly, et al.

(2) (Fig. 1). Conceptually, this model consists of two identical, parallel, circular cylinders, carrying a uniform, equal axial current in opposite directions, which have been brought together until they actually overlap. Since, by superposition, no current flows in the region of overlap, the material in this region can be removed to provide the "working area" of the coil. Such a configuration confers many advantages for transverse-field MHD applications: First, referring to the axes depicted in Fig. 1, it can be shown that in the working area, the magnetic field produced by the overlapping cylinders is uniform everywhere and is given by:

$$B_x = B_y = 0, \qquad B_z = \mu_o J_e a \tag{1}$$

where J_e is the effective current density in either cylinder and a is the offset between the center of either cylinder and the center of the working area. Next, insofar as MHD channels tend to be relatively long and narrow, the saddle coil configuration offers a relatively efficient utilization of conductor material, in that the coil windings are so arranged that the individual conductors are kept close to the MHD channel which they serve. Finally, the configuration is practical from an engineering viewpoint: The indicated cylinders would, in practice, be comprised of a large number of individual conductors, so that the "crescent moon" shape of the coil lobes could be readily approximated by the assembly of modular units. In short, it seems reasonable to assume that actual MHD coils would closely resemble such a model, with the degree of similarity probably controlled by a compromise between desired field homogeneity and ease of assembly.

It is apparent that many of the characteristics of a particular coil will be determined by the application for which it is intended. For example, it has been shown (28, 29) that the length of a transverse-field MHD channel

FIGURE 1

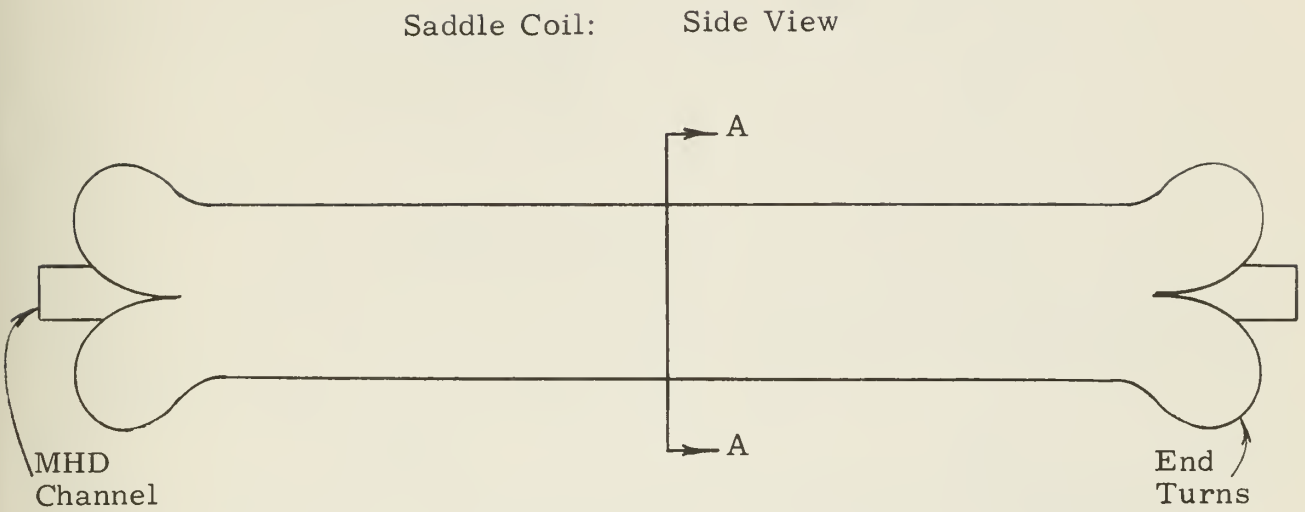
Saddle Coil: Side View
A
A
MHD
Channel
End
Turns

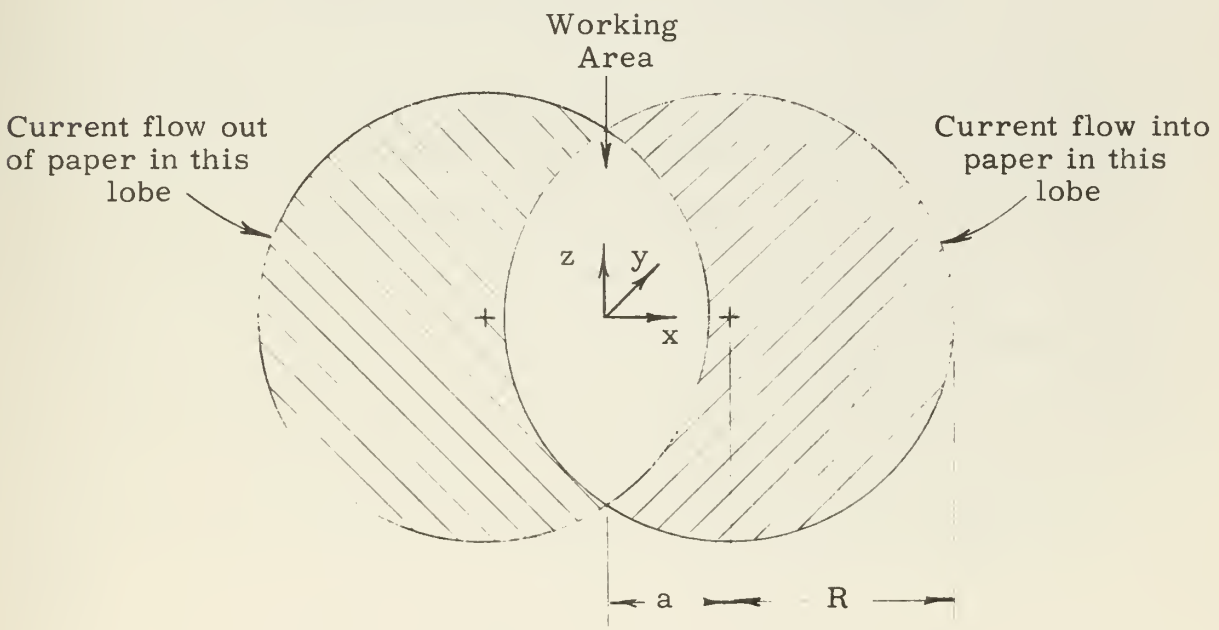
Working
Area
Current flow out
of paper in this
lobe
Current flow into
paper in this
lobe
z
y
x
+
+
a
R
Section A-A

should be 5-10 times the mean channel width, to minimize degrading end effects. It will be assumed here that the contemplated MHD channel is of rectangular cross section, with width 2w and height 2h. The largest such rectangle which can be inserted into a given working area has:

$$w = \frac{-3a + \sqrt{a^2 + 8R^2}}{4} \qquad (2)$$

and

$$A_{ch} = 4w\sqrt{R^2 - (a + w)^2} \qquad (3)$$

where R is the radius of either cylinder. The length of the coil associated with such a channel will be taken to be:

$$L = 10\sqrt{A_{ch}} \qquad (4)$$

The total cross section (both lobes) of the coil is related to the above parameters by:

$$A_{cl} = 2R^2\left[\pi - (2\gamma - \sin 2\gamma)\right], \quad \gamma = \cos^{-1}(a/R) \qquad (5)$$

One additional concept must be included in the discussion of such coils: At either end of the coil, the individual conductors must pass up and over (or down and under) the MHD channel. It will be assumed here that these "end turns" do not contribute to the useful magnetic field, but do contribute to total loss. Obviously, one would desire to minimize the mean length of the end turns, within the constraints imposed by the above parameters. Considering this, the mean length of an end turn will be estimated as one half the circumference of the circumscribing circle: that is,

$$L_e \cong \pi(R + a).$$

It is then useful to define a form factor, F, as follows:

$$F = 1 + L_e/L \qquad (6)$$

Thus, geometrically similar coils can be described by the common value of their form factor. Further, total coil volume, etc., can be estimated

as:

$$V_{tot} = F A_{cl} L \qquad (7)$$

The purpose of this work, then, is to examine the application of cryogenic technology to coils such as those described above. The basic philosophy of this investigation is to seek that information required to support a realistic appraisal of the desirability of cryogenic magnets for a particular MHD application, to identify those parameters which can be used most conveniently to define a coil during the preliminary design process, and to illuminate, in detail, the relationships between those parameters and the resultant coil. The range of the investigation covers coils suitable for generating fields of up to 100 KG, for use with MHD channels of cross section between .01 and 10 square meters. It might be noted that, aside from the apparent geometric differences, such coils differ from the solenoidal coils discussed earlier in that the constraints imposed imply approximate coincidence in size between the smallest coils considered here, and the largest cryogenic solenoids built to date.

II. RESISTIVITY OF METALS

A. Background:

It is appropriate to begin this analysis of cryogenic magnets with a brief resume of the physical reasons which favor the application of cryogenic technology to magnet design: Essentially, the resistivity of pure metals is a sufficiently strong function of temperature that refrigeration to the cryogenic range can reduce magnet power consumption by more than the additional power required to run the refrigerator. For this reason, cryogenic magnets can be made to operate with significantly less power consumption than comparable "conventional" magnets.

MacDonald (30) provides an excellent summary of the development of the underlying theory: Briefly, Mathiessen (31) first recognized that the resistance of metals could be separated into two components, one dependent upon the degree of purity, and the other upon the temperature. He postulated that these components were independent, and therefore directly additive. They have come to be generally known as "residual" or "impurity" resistance and "intrinsic" or "ideal" resistance, respectively. The former is attributed to scattering of conduction electrons by local deformation of the crystal lattice (e. g., by the presence of impurity atoms, or dislocations), and the latter, to scattering by thermal vibration of the lattice. Thus, the "ideal" resistance goes to zero as the absolute temperature goes to zero.

No significant advance was made in quantitative analysis of the thermal behavior of ideal resistance until quantum theory became fairly well developed: In 1929, Bloch (32), utilizing a lattice model first postulated by Debye (33) in 1911, evolved the first strictly theoretical treatment to predict accurately the low-temperature resistive behavior of "ideal"

metals. Bloch's Law states:

$$\rho = \left(\frac{T}{\Theta}\right)^5 \int_0^{\Theta/T} \frac{x^5\,dx}{(e^x - 1)(1 - e^x)} \qquad \Theta = \frac{h\nu_m}{k} \qquad (8)$$

where Θ, the "Debye temperature", is a constant, characteristic of a particular lattice. (Actually, Bloch's original solution considered only the low- and high-temperature limiting cases, but subsequent investigators have found that the above integral expression, derived by him, is essentially valid for all temperatures. For $T \ll \Theta$, the above expression reduces to $\rho \sim (T/\Theta)^5$, while for $T \geq \Theta$, $\rho \sim T/\Theta$.)

Within a few years, Gruneisen (34) noted that Bloch's theory could be modified to provide a more accurate prediction of the resistive behavior of real metals by use of an empirical correction factor: He suggested that the resistivity derived from eqn. (8) be multiplied by a factor of the form $(1 + \alpha_1 T + \alpha_2 T^2)$, where α_1 and α_2 were to be determined experimentally for the various metals. While admitting that this technique could not be defended on strictly theoretical grounds, he advanced heuristic arguments defending the form of the indicated correction, and observed that in most cases, the resultant "fit" to experimental data was accurate to within about 10% of the value of the residual resistance. (Later investigators (35) have introduced an equivalent, though somewhat less convenient, concept of describing "real" resistive behavior by use of a variable Debye temperature.)

Concurrently with the above developments, several investigators became interested in the fact that the resistance of metallic conductors increases in the presence of a magnetic field. In 1938, Kohler (36) was able to show that:

$$\frac{\Delta r}{r_o} = \Psi\left(\frac{H}{r_o}\right) \qquad (9)$$

where $r_o = r(0, T)$ is the total resistance at temperature T, in the absence

of any magnetic field, and $\Delta r = r(H, T) - r(0, T)$ is the resistance increase in the presence of the field. Kohler was unable to obtain a general solution for the functional form of Ψ, though he predicted that in the limit of small arguments,

$$\Psi(H/r_o) \rightarrow a(H/r_o)^2,$$

while in the limit of large arguments,

$$\Psi(H/r_o) \rightarrow b(H/r_o)^0,$$

i. e., the magnetoresistance (Δr) saturates. Obviously, magnetoresistance is more important at cryogenic temperatures than at "ordinary" temperatures, since the reduced value of r_o leads to a more rapid increase of magnetoresistance with field for any given metal. Further, though Kohler did not obtain a general solution for Ψ, mere recognition that the functional relationship exists suggests a plotting technique by which the results of limited testing may be generalized to predict the magnetoresistance of samples of different purity, or at different temperatures. Plots of magnetoresistance vs. H/r_o have come to be known as "Kohler diagrams". (Equivalently, one can plot magnetoresistance vs. the ratio of mean free path in the lattice to the radius of the orbit of a free electron in the magnetic field: However, though this latter concept may be more elegant in a physical sense, the former technique is generally more convenient for the experimenter.)

In 1940, Justi(37) recommended the use of a so-called reduced Kohler diagram, in which magnetoresistance is plotted vs. $H(r_\Theta/r_o)$, rather than H/r_o. It was his hope that normalizing the field-free resistivity to its value at the Debye temperature for the particular lattice would eliminate differences due to the variation in "intrinsic" scattering between different lattice structures. Unfortunately, such normalization does not cause the data for all metals to fall on a single curve, though the curves for the

various metals, when so plotted, do tend to fall in a rather broad band. Nevertheless, many experimenters have adopted the practice of plotting magnetoresistance data with field-free resistivity normalized in this manner. Actually, little is gained, and much is lost, through this technique: In general, authorities cannot agree on the exact value of the Debye temperature for a particular metal. Further, since Debye temperatures for most metals fall well out of the range in which detailed experimental resistivity figures are available, the normalizing standard for a particular metal must often be generated from the theory. Aside from the approzimations inherent in the theory, there is the problem of which version to use: Bloch's original version, the Gruneisen modification thereto, or some more recent derivation. Thus, one is faced with data normalized to a rather fuzzily defined standard, and all too often, published data lack any indication of the normalizing standard used. Even when the standard can be determined, this practice obscures any direct comparison between different metals. About all that can be said to recommend the practice is that it reduces the size of the numbers involved.

Despite continued interest in the theory of the magnetoresistive behavior of metals, little significant advance has been made in the last several years. To quote from a second article by MacDonald (38):

> "---it appears that the theory is quite unable to give any detailed explanation of such bizarre behavior: Wilson says 'It does not seem likely that any model simple enough to be tractable theoretically would give a magnetoresistance curve of the complexity of those actually observed.'"

B. Limitations of the theory:

The above relations, taken together, comprise the theoretical motivation for the use of cryogenic magnets: In theory, careful purification and annealing will result in a residual resistance several orders smaller than the room temperature resistance of a given metal. Cooling to cryo-

genic temperatures can make the ideal resistance arbitrarily small compared to the residual resistance. Then, if the magnetoresistance saturates at a sufficiently low value--- or, at least, does not rise too rapidly with increasing field--- cryogenic magnets can be made to operate much more economically than conventional electromagnets.

Unfortunately, as might be inferred from the above discussion, the approximations inherent in the foregoing concepts preclude their direct application to magnet design:

1. The theory does not quantize the relationship between degree of impurity, or extent of cold work, and the magnitude of the resultant residual resistance. Nor is anything said regarding the feasibility of attaining a specified degree of purity in a particular metal.

2. Experimental data indicate that Mathiessen's rule is an best an approximation. Assuming its validity, one can compute the "ideal" resistance-temperature curve for a given metal by extrapolating an experimental curve to 0^{o} K to determine the residual resistance, then subtracting that constant from the original curve. In general, curves so computed from observation of samples of lesser purity (34, 39) lie well above those computed from measurements on highly pure samples (40-43), at least for the liquid hydrogen-liquid helium range. Maimoni's date (48) indicate a similar discrepancy for aluminum samples of the same purity, in which the resistance ratio was varied by controlling the degree of anneal. One can only conclude that either the scattering due to lattice deformation is energy dependent, or some energy dependent coupling exists between intrinsic and residual resistivity.

In essence, the original assumption of independence between these components of resistance implies the assumption that the density of "impurity"-type scattering centers is so low as to have negligible influ-

ence on the overall lattice. Recent investigations may indicate the severity of this restriction: Several metals (e. g., Ag, Au, Cu, Mg) exhibit an anomalous resistance minimum, below which resistance increases as temperature is decreased (30, 44-46). MacDonald and Pearson (47), working with extremely dilute copper alloys, traced this behavior to the presence of specific impurities: They reported that as few as 5-10 p. p. m. of such elements as Fe, Bi, Pb, Sn, Ga, In, Ge, and Si sufficed to produce the phenomenon. In the absence of these elements, no minimum was observed. (A later paper (48) describes iron as the primary culprit, suggesting that the latter five elements listed serve primarily to replace traces of Fe originally tied up in oxides, thus releasing them into solid solution.)

3. Attempts to "improve the fit" between Bloch's law and experimental data--- such as that proposed by Gruneisen--- do not alter the asymptotic behavior predicted by that law at low temperatures. However, it has been found that several metals deviate from the predicted T^5 dependency: for example, the resistivity of platinum apparently goes to zero as T^2 (49, 50), and that of iron and nickel, as T^3 (51). Perhaps the most startling deviation is that reported by Mendoza and Thomas (52): Working with copper and gold specimens which did not exhibit the minima discussed above (which occurs at about 10° K for copper), they found "normal" behavior down to about 0.25° K, below which the resistance of both metals rose asymptotically toward the ordinate as temperature was further decreased.

4. Although Kohler predicted that magnetoresistance should saturate at sufficiently high fields, only two metals--- aluminum and indium (37, 53)--- have experimentally displayed such saturation, to date. Further, though data from various sources correlate rather well for some metals,

when plotted on Kohler diagrams, other metals display considerable "scatter".

Lest the trees obscure the forest, it should be noted that the behavior of most metals conforms reasonably well to that predicted by the theory, especially above the liquid hydrogen range. Even in the "exceptional cases", the absolute magnitude of the deviations is small, if only because total resistance is small at the temperatures in question. However, from a practical viewpoint, a relative error of a factor of two--- or even, 10% --- might be the difference between success or failure for a particular cryogenic magnet. Thus, it is unwise to predict quantitative results, a priori, from the theory alone.

Because of these considerations, the decision was made to conduct a careful, detailed survey of the literature regarding the experimental resistive behavior of various cryogenic conductors, as a starting point for this study. The specific metals investigated were aluminum, copper, sodium, and indium: The first three have already been used in the construction of various cryogenic solenoids, and the last has been proposed for use in cryogenic coils, in view of its magnetoresistive behavior. The results of this investigation are summarized in the remaining sections of this chapter. TO FACILITATE DIRECT COMPARISON BETWEEN CRYOGENIC CONDUCTORS, ALL RESISTIVITY FIGURES IN THIS AND SUBSEQUENT CHAPTERS HAVE BEEN NORMALIZED TO THE RESISTIVITY OF "STANDARD" COPPER AT 300^{o} K (WHICH IS TAKEN TO BE 1.7715 MICRO-OHM CENTIMETERS), except that data displayed in Figs. 2-5.

C. "Residual" or "Impurity" resistivity:

As a rough rule of thumb, most metals can be purified sufficiently to achieve a residual resistivity approximately four orders of magnitude

below their room temperature resistivity. Whether or not such purification is feasible, in a particular case, depends on the cost and complexity of the necessary metallurigical processing, as balanced against the contemplated application:

For example, at liquid nitrogen temperatures, residual resistance is generally negligible compared to intrinsic resistance, for metals of "commercial" purity. Thus, the conductors of coils intended for use with this coolant need not be of highest purity: Far more importance should be assigned to the selection of a conductor with a high Debye temperature, to obtain (hopefully) lower intrinsic resistance. (Approximate figures for the Debye temperatures of the metals covered by tlis study are: indium, 100^{o} K; sodium, 202^{o} K; copper, 333^{o} K; aluminum, 395^{o} K.)

By contrast, in the liquid neon range (i. e., about 30^{o} K) and below, residual resistance becomes increasingly important: Ultimately, the lowest residual resistance attainable for a given metal generally determines the minimum operating power attainable for a coil wound of that metal. Obviously, then, the minimum residual resistance attainable, and the ease with which it can be attained, become important factors in the evaluation of prospective cryogenic conductors.

In general, metals such as indium and sodium, with low Debye temperatures, can be readily purified by vacuum distilation: indium, to a residual resistance ratio as low as $r_0/r_{300} = 4.4 \times 10^{-5}$ (54), and sodium, to about $r_0/r_{300} = 3 \times 10^{-4}$ (41, 55, 56). Or, normalizing these figures to the resistance standard cited above, the ratio for indium becomes $r_0/r_s = 2 \times 10^{-4}$, and for sodium, $r_0/r_s = 8 \times 10^{-4}$. It is worth noting that metals with such low Debye temperatures are fully annealed at room temperature: Thus, once residual resistivity has been decreased to a

particular level, it will not increase due to "cold work" in the manufacture of a coil.

Aluminum, despite its high Debye temperature, can be readily purified by the zone refining process (57-59). This technique has proven a relatively economical source of aluminum with residual resistance ratios as low as $r_0/r_{300} = 1.4 \times 10^{-4}$ ($r_0/r_s = 2.2 \times 10^{-4}$). However, both Maimoni's data (40) and the Project Sherwood report (20) indicate that the resistivity of aluminum is quite sensitive to cold work. If aluminum cryogenic coils are to derive maximum benefit from the use of highly pure metal, conductors must be carefully annealed--- after assembly, if possible--- and structural support provided to ensure that working stress in the windings does not exceed the proportional limit. (It might be noted, also, that elimination of impurities tends to reduce the yield strength, as well as the resistivity, of most metals.)

Copper poses a unique problem: although methods have recently been perfected to zone refine this metal (60), its high conductivity complicates the use of induction heaters in the refining process, thus rendering the technique relatively difficult. To date, most of the ultra-pure copper used in recent experiments has been prepared by a complex electrolytic process developed in 1941 (61). Minimum residual resistance ratios have been in the vicinity of $r_0/r_{300} = 5 \times 10^{-4}$, or $r_0/r_s = 4.8 \times 10^{-4}$ (17, 48, 62). However, though the resistivity of pure copper is apparently not so sensitive to cold work as that of aluminum, it is acutely sensitive to the presence of Fe in solid solution (as has been discussed above): so much so, that actual attainment of the minimum cited is a rare phenomenon. (As contrasted with the usual correspondence between decreased impurity content and lower residual resistivity, MacDonald and Pearson (47) indicate that the resistivity of Fe-contaminated copper can be decreased by reacting

the iron contaminant with oxygen, thus raising the total impurity content, but converting the iron to less critical iron oxide.) It would appear advisable to avoid even the use of steel dies in drawing pure copper into wire, and even then, a copper-wound coil might be a questionable choice for low temperature applications.

The above resistance figures do not, by any means, constitute an absolute minimum: Gold, et al. (48) report a specimen of purest natural copper with a resistance ratio of 3.1×10^{-4}. Even more significantly, Post and Taylor have recently developed a process (63) which, while altering neither the purity nor the degree of anneal, lowers the residual resistance ratio for sodium from the level cited above to $r_0/r_{300} = 1.5 \times 10^{-4}$ ($r_0/r_s = 4.3 \times 10^{-4}$). It is at least possible that their process may be effective for other metals. It might also be noted that the advancing state-of-the-art has roughly reduced minimum residual resistance ratios by two orders of magnitude since the 1930's. It would seem reasonable to assume that at least some further improvement is probable. Again, any further reduction in residual resistance will generally permit further reduction of the minimum attainable operating cost for cryogenic coils.

D. "Intrinsic" or "Ideal" resistance:

Figures 2-5 present a summary of the available experimental data on the intrinsic resistance of indium, sodium, copper, and aluminum.

In processing this data, occasional interpretation has been necessary: Some of the data were originally presented in the form of curves of "total" resistance, with no specification as to the residual resistance of the specimen tested. Such curves have been graphically extrapolated to 0° K, and the intrinsic resistance computed as discussed earlier. A few experimenters have presented curves normalized to their estimate of the

FIGURE 2

Resistivity of Indium

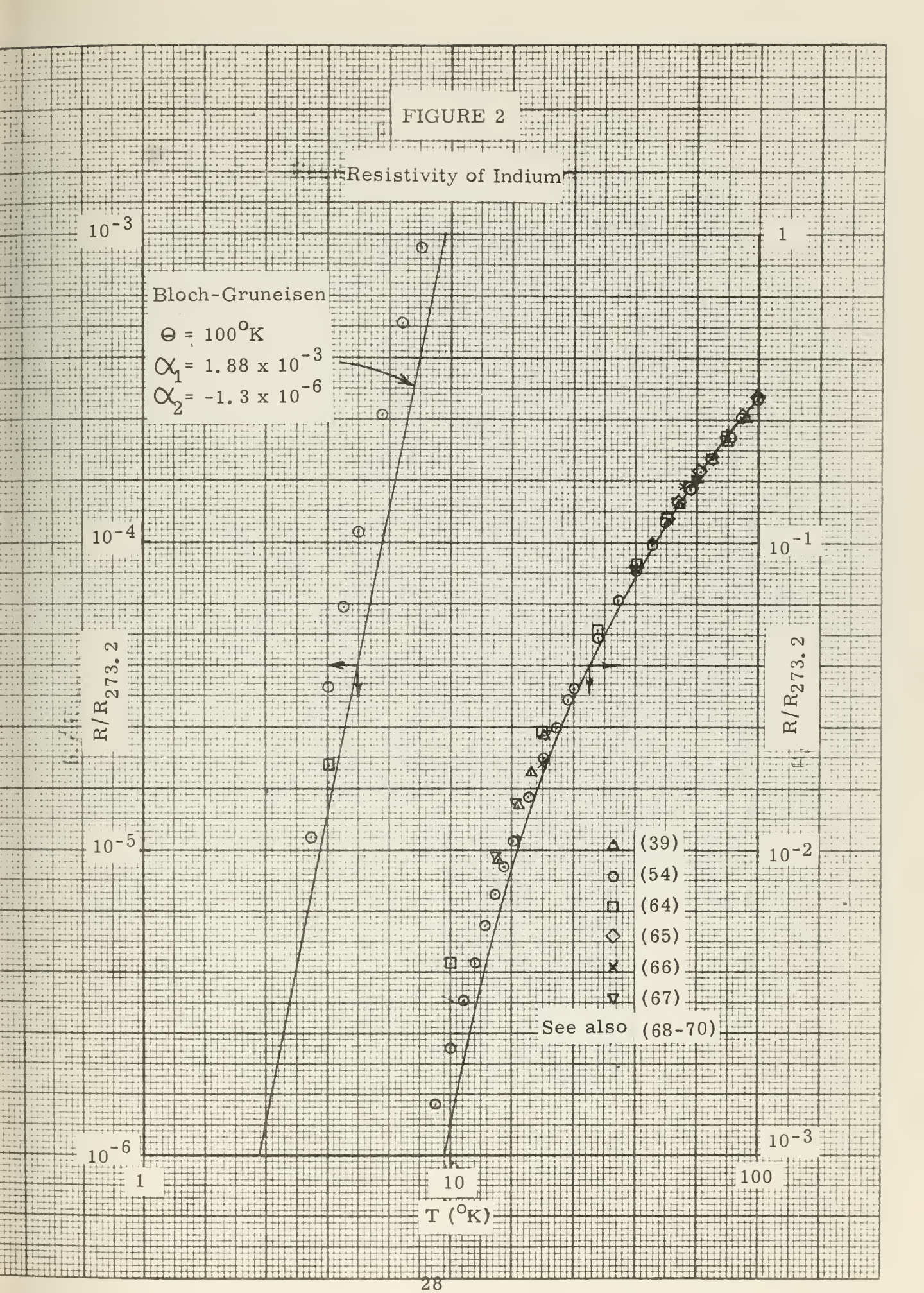

FIGURE 3

Resistivity of Sodium

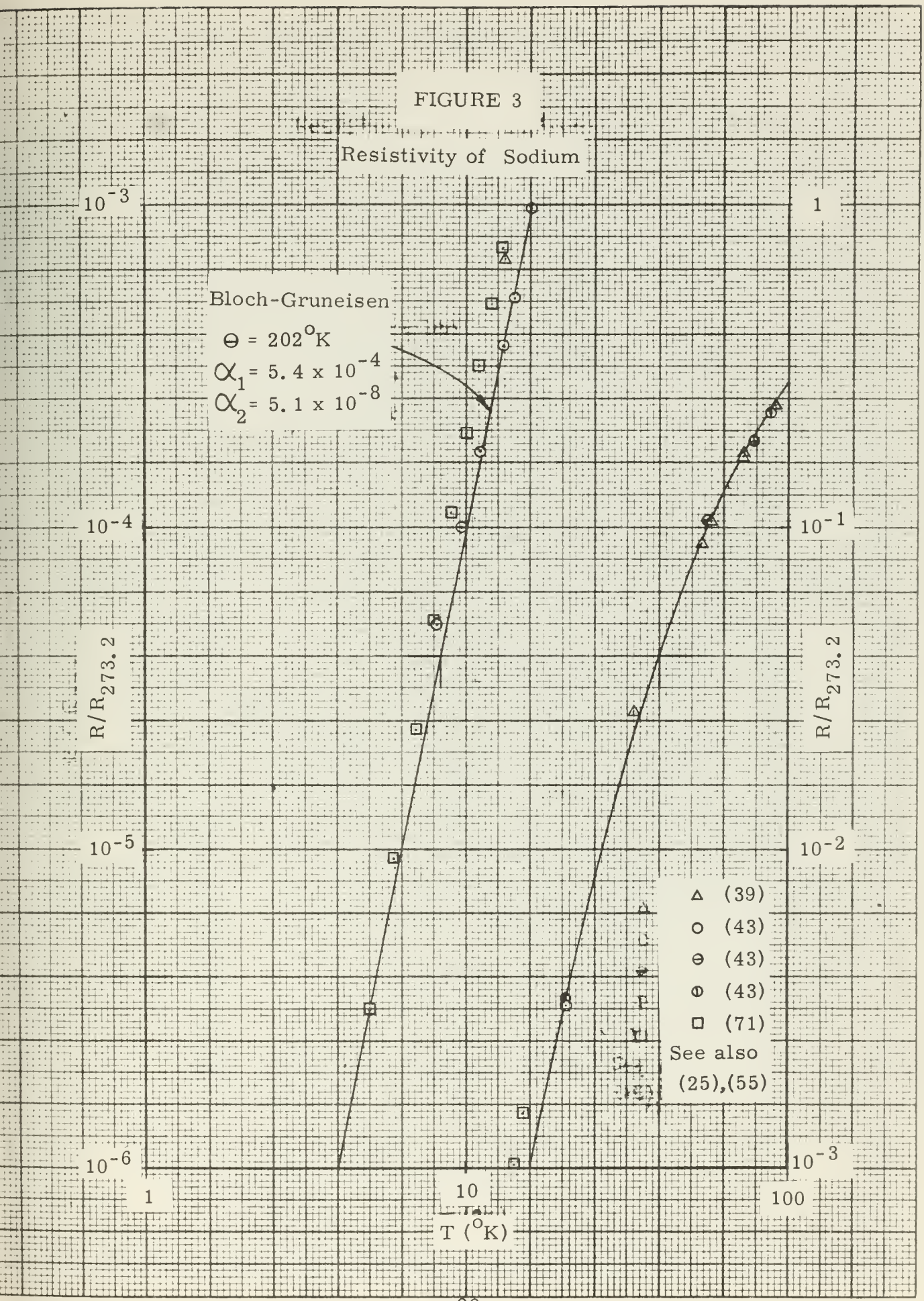

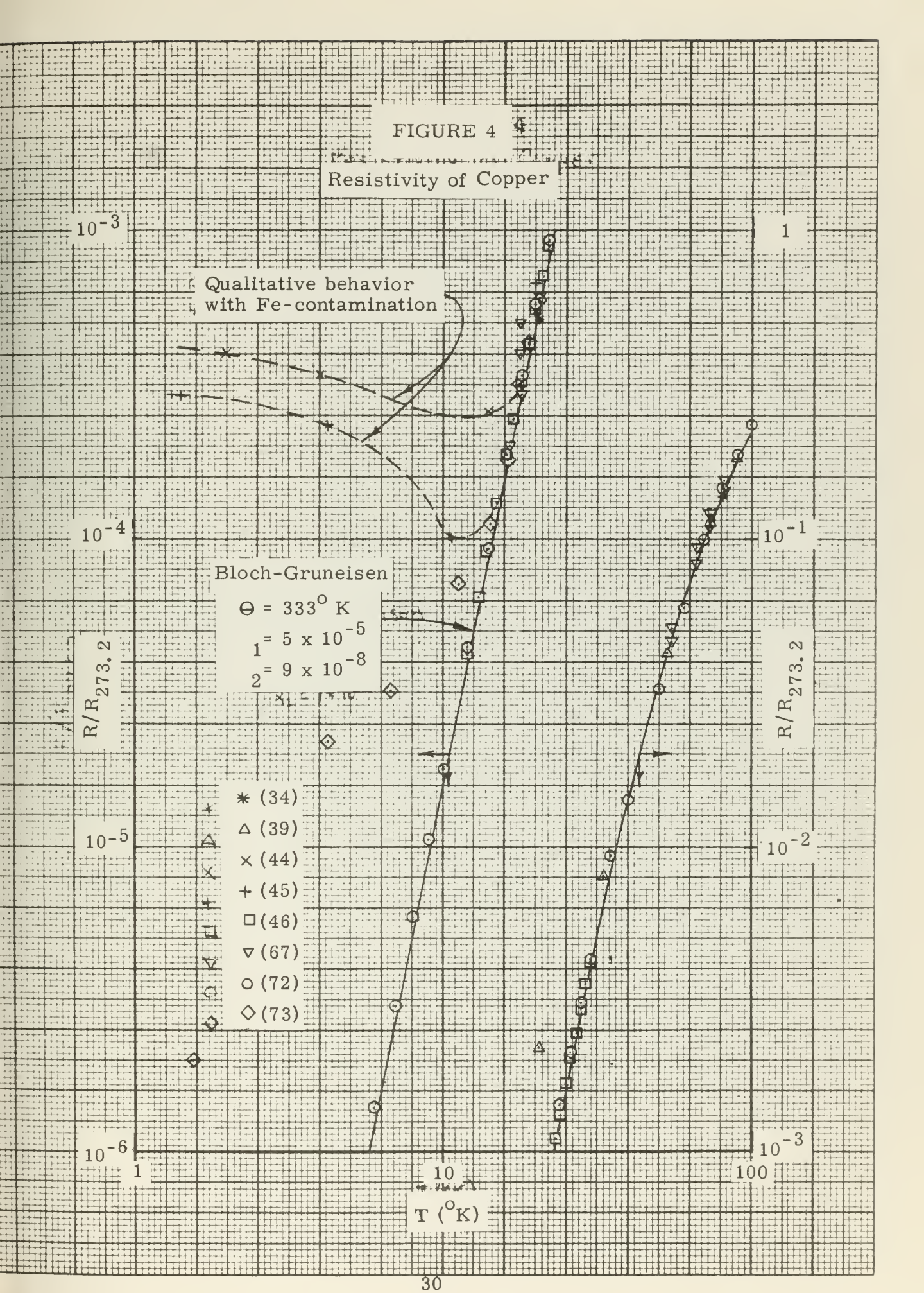
FIGURE 4
Resistivity of Copper
Qualitative behavior with Fe-contamination
Bloch-Gruneisen
Θ = 333° K
1 = 5 x 10^-5
2 = 9 x 10^-8
* (34)
△ (39)
× (44)
+ (45)
□ (46)
▽ (67)
○ (72)
◇ (73)
R/R273.2
T (°K)
10^-3
10^-4
10^-5
10^-6
1
10
100
10^-1
10^-2
10^-3

FIGURE 5

Resistivity of Aluminum

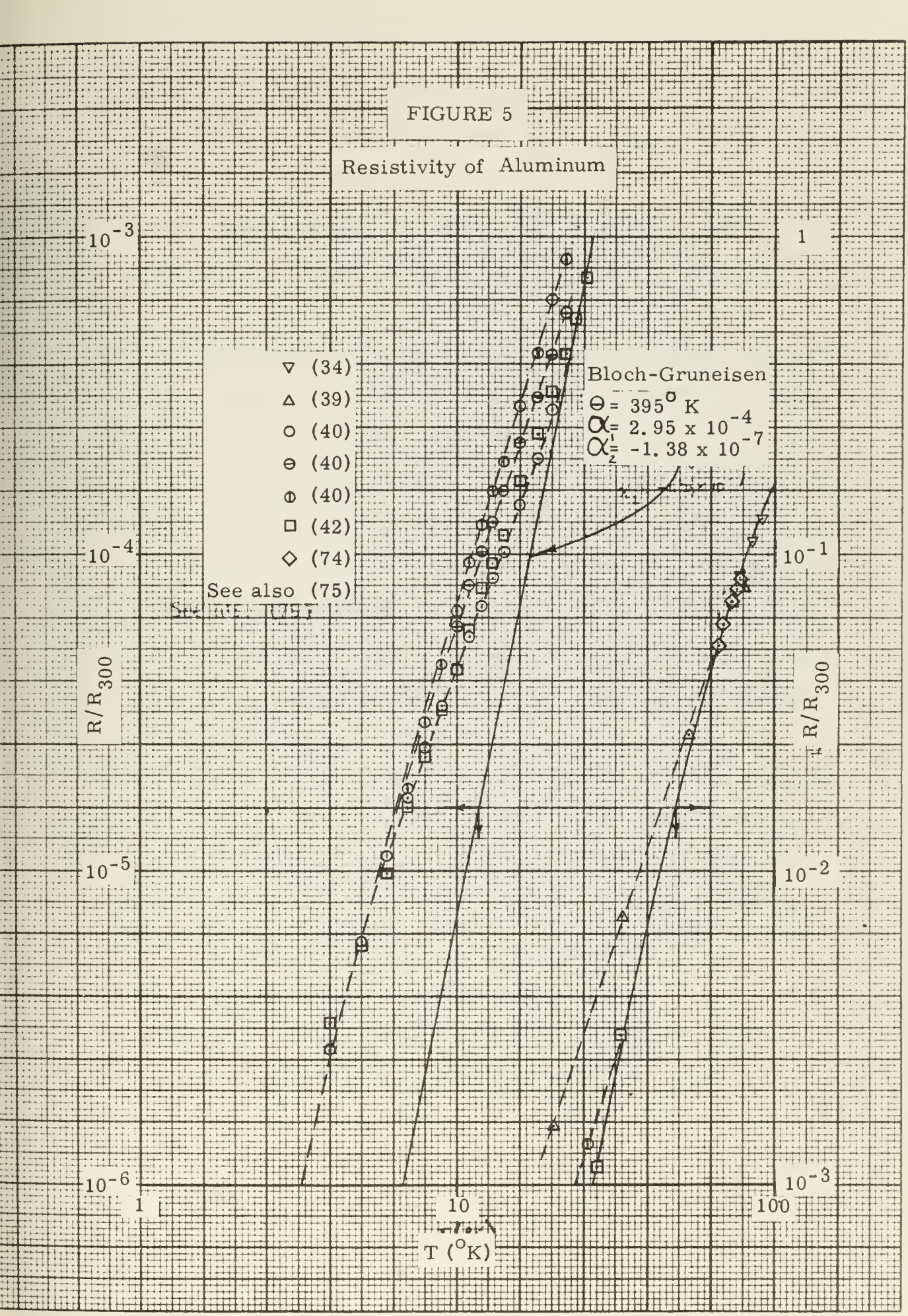

Debye temperature resistivity of the specimen tested. In such cases, the data have been converted in accord with the Bloch-Gruneisen theory to the form presented here: Where the original author specified a value for the Debye temperature, that value was used in the conversion. Where no value was indicated, the temperatures cited in the preceding section were used.

Since the great bulk of resistivity data for indium, sodium, and copper were originally normalized to the 0°C resistivity of the specimen tested, the experimental data presented in Figures 2-4 are all normalized to that standard. Conversely, published data for aluminum has most frequently been normalized to the 300° K resistivity, and is so normalized in Fig. 5.

For comparison, the Bloch-Gruneisen curve for each metal is plotted along with the experimental data. For sodium, copper, and aluminum, the coefficients α_1 and α_2 used in computing the theoretical curve were those determined by Gruneisen (34). For indium, the values were determined by the author.

Not all available data have been included in Figs. 2-5: However, all recent works known to the author are included, and the data presented are considered fairly representative of the total information available. (In fact, it would seem that the trends which appear in the data presented are established with sufficient clarity to warrant, perhaps, greater confidence in the "overall picture" than in any single work.)

As is apparent in Fig. 2, experimental data for indium conform quite well to the Bloch-Gruneisen theory down to about 50° K. Below this temperature, the data lie above the theory: The greatest divergence occurs in the range 4° K to 12° K, where some experimental points lie more than a factor of 3 above the theoretical prediction. Despite this divergence, the experimental curves exhibit approximate parallelism to the theoretical

curve: In fact, it would appear--- though available data are scanty--- that the experimental curves again converge toward the theoretical curve below 4° K. Note that, due to its low Debye temperature, the intrinsic resistance of indium exceeds the residual resistance figures cited earlier down to about 3° -4° K. Considering this, there would be little gained by seeking further decrease in residual resistance for this particular metal. Indium undergoes a field-free transition to superconductivity at 3.41° K. However, since it is a "soft" superconductor, this transition would presumably be quenched, in the unlikely event that indium high-field coils were designed for operation below that temperature.

In many respects, the resistive behavior of sodium resembles that of indium, as can be seen by comparing Figs. 2 and 3. However, there is generally better correspondence between experimental data and the Bloch-Gruneisen theory for sodium. Although some divergence is again apparent below 50° K, the data of MacDonald and Mendelssohn coincide with the theory to 11° K. The greatest divergence is that reported by Woods, at about 10° K, and amounts to no more than a factor of 2. Again, the experimental data appear to reconverge to the Bloch-Gruneisen curve at low temperatures. The residual and intrinsic resistivities of pure sodium are of roughly equal magnitude around 10°-11° K, in keeping with its higher Debye temperature. One would expect that at least some advantage could be gained from further reduction of the residual resistivity of sodium, since Taylor and Post (26) indicate that "minimum power" sodium coils should be operated at about 10° K.

Fig. 4 indicates remarkably close correlation between experimental data and theory for copper, provided that no iron contamination is present: in such cases, divergence is generally less than 10%. (The scarcity of data

points below 15° K again represents the severity of this restriction!) The data of Los and Gerritsen, and of Gerritsen and Linde, represent typical behavior in the more normal situation, when iron contamination is present. (These curves are labelled "qualitative" behavior, due to the difficulty of determining any "constant" value for residual resistance, when total resistance rises with decreasing temperature.) Were it not for the difficulty of obtaining iron-free copper, these data would indicate that copper might be an ideal choice for low-temperature coils, since its intrinsic resistance decreases so rapidly. Actually, the magnetoresistive behavior of copper is the least desirable of the four metals considered here, as will be shown in a later section of this chapter. These facts, taken together, limit the desirability of copper cryogenic coils to the upper end of the 0°-100° K temperature range under investigation.

The resistive behavior of aluminum, as depicted in Fig. 5, is unique in many respects: First, strong coupling between residual and intrinsic resistivity is apparent. The three curves plotted from Maimoni's data represent specimens with $r_0/r_{300} = 1.476 \times 10^{-4}$, 4.94×10^{-4}, and 3.62×10^{-3}, respectively, with direct correspondence between increased intrinsic resistivity and increased residual resistivity. This, of course, is in direct disagreement with Mathiessen's rule, and is the apparent source of the noted strain sensitivity of aluminum conductors. Aside from the fact that this behavior results in marked deviation from the Bloch-Gruneisen curve (as did Fe-contamination in copper), the nature of that deviation is also unique: At the upper end of the temperature span investigated, aluminum conforms even more closely than did copper to the behavior predicted by the theory. There is virtually no deviation between experimental data and the theoretical curve. However, at some tem-

perature between 65° K and 25° K--- depending upon the residual resistance of the specimen--- the experimental curves shear sharply away from the theory, after which they exhibit a T^3 dependence, while the theoretical curve rapidly approaches the usual T^5 dependence. This behavior does not appear to persist for long: Around 10° K, the experimental curves converge rapidly, and thereafter appear to parallel the theoretical curve, though they do not converge to it. (Fenton, et al., reported that their data conformed to the relationship

$$\rho = 5.68 \times 10^{-10} + 1.5 \times 10^{-13} T^{2.9} \Omega\text{-cm}$$

throughout the range 0°-30° K. Actually, their data points appear to fall increasingly under this line at temperatures below 4° K, and over it at temperatures above 25° K.) Because of this "sidestep", one faces the paradoxical situation that predictions from the theory appear to be precisely correct, for purest aluminum, down to about 25° K, but more than an order of magnitude too low at temperatures much below 25° K.

It is interesting to speculate that aluminum, above all metals, would profit from the further advance in metallurgical technique required to further reduce minimum residual resistance levels: Even with the above behavior, aluminum has such a high Debye temperature that its intrinsic resistance decreases more rapidly with temperature than was the case with the other metals covered here. Since the magnetoresistance of aluminum apparently saturates at a low value, residual resistance tends to dominate the performance of low-temperature aluminum cryogenic coils. Further reduction of residual resistance would apparently decrease both components of "field-free" resistance, and (if $\Delta r/r_o$ does indeed saturate at a constant value) decrease the maximum Δr due to magnetic effects, as well. Such a three-fold gain could only result in a direct reduction of coil operating cost, again provided that care is taken to ensure

that "cold work" does not occur during assembly and operation of the coil.

One additional conclusion can be drawn from the data plotted in Figs. 2-5: The Bloch-Gruneisen theory is a useful asymptotic limit for the experimentally derived curves. At liquid nitrogen temperatures, data points tend to fall on the theoretical curve, or so near it, that the theory itself is a perfectly adequate design criterion. But to repeat the observation made earlier, the theory should not be used as a design standard for cryogenic coils intended for service in the liquid neon range, or below. Recourse must be made to experimental data for such applications.

E. Zero-field resistance standards:

If the Bloch-Gruneisen theory is not to be used as a design standard for cryogenic coils, the time has come to develope a standard. Given the above data, this is a relatively simple task, but first, it may be profitable to digress to a point of philosophy:

The primary motivation for use of cryogenic coils for any application is the desire to reduce operating costs. Even if a particular cryogenic coil is not designed to seek minimum operating cost (for example, geometry may be altered from the "minimum cost" optimum to reduce coil size, or operating temperature altered, because of preference for a particular coolant, etc.), the primary justification for accepting the greater complexity and initial cost of cryogenic coils, as compared to "conventional" coils, is still the same.

Bearing this in mind, the "total field-free resistivity" standards evolved here will assume that every effort has been made to achieve minimum residual resistivity, in each case. As was pointed out above, this probably would not be done for liquid-nitrogen-cooled coils: However,

intrinsic resistance tends to dominate the performance of such coils to such an extent that the error incurred by assuming too low a value for residual resistivity is negligible. If, on the other hand, a coil is designed for operation at temperatures where residual resistance is a significant part of total field-free resistance, the above assumption is strongly justified: At such temperatures, total operating cost is dominated by refrigeration costs. For every unit of heat generated in the coil, many units of work must be expended in refrigeration. It is highly probable that the additional cost and effort required to obtain and maintain minimum residual resistance would be repaid many times over the operating life of the coil. The importance of this fact cannot be overemphasized!

For this reason, the residual components of the resistance standards presented in Tables 1-4 are the minimum figures previously cited for each metal. The intrinsic component corresponds to the Bloch-Gruneisen theory, down to the temperature at which the purest specimens tested diverge from that theory, and then follows the experimental trend. All figures have been normalized to the 1.7715 micro-ohm centimeter standard. The design standards for all four metals are also plotted in Fig. 6, for ease of direct comparison.

The detailed application of these resistance standards to the analysis of cryogenic saddle coils is discussed in Chapter VII, and the mean resistivity design curves resulting from that analysis are presented in Appendix B.

TABLE 1

FIELD FREE RESISTIVITY OF INDIUM

	0	1	2	3	4	5	6	7	8	9
0	1.987	1.987	2.00	2.15	3.52	6.86	13.44	25.2	44.4	69.4
1	103.3	146.2	197.8	258	326	404	485	576	675	779
2	892	1002	1129	1255	1381	1507	1642	1773	1913	2060
3	2200	2350	2500	2650	2790	2940	3090	3240	3390	3540
4	3690	3840	3990	4140	4300	4450	4600	4760	4910	5060
5	5220	5380	5540	5700	5850	6010	6170	6330	6490	6650
6	6800	6960	7110	7280	7440	7600	7750	7810	8060	8220
7	8380	8540	8700	8860	9010	9160	9320	9480	9640	9800
8	9950	10110	10260	10420	10570	10730	10880	11040	11190	11350
9	11510	11660	11820	11980	12140	12300	12460	12620	12780	12960

Values of $10^4 r/r_s$ are tabulated vs. temperature in degrees Kelvin.

Top temperature scale: units. Left temperature scale: tens.

TABLE 2

FIELD FREE RESISTIVITY OF SODIUM

	0	1	2	3	4	5	6	7	8	9
0	4.33	4.33	4.33	4.33	4.35	4.40	4.51	4.73	5.11	5.75
1	6.74	8.15	10.30	13.23	17.10	22.3	29.1	37.2	47.9	59.8
2	75.9	94.8	115.1	140.0	165.7	195.9	230	268	308	352
3	399	450	504	559	619	680	743	810	880	953
4	1027	1103	1182	1262	1343	1424	1507	1590	1673	1758
5	1843	1930	2020	2110	2200	2300	2390	2490	2580	2670
6	2760	2850	2940	3040	3130	3230	3330	3430	3530	3630
7	3730	3830	3930	4030	4130	4230	4330	4430	4530	4630
8	4730	4830	4930	5030	5130	5230	5330	5420	5510	5610
9	5710	5810	5910	6010	6110	6210	6310	6410	6510	6600

Values of $10^4 r/r_s$ are tabulated vs. temperature in degrees Kelvin.

Top temperature scale: units. Left temperature scale: tens.

TABLE 4

FIELD FREE RESISTIVITY OF ALUMINUM

	0	1	2	3	4	5	6	7	8	9
0	2.16	2.16	2.17	2.18	2.20	2.25	2.31	2.40	2.51	2.65
1	2.83	3.02	3.22	3.46	3.72	4.02	4.37	4.79	5.27	5.84
2	6.52	7.30	8.23	9.39	10.80	12.67	14.91	17.61	20.6	24.1
3	28.1	32.7	37.8	43.7	50.1	57.3	65.3	74.1	84.0	94.9
4	106.7	119.3	133.2	147.8	163.0	179.9	197.0	215	234	255
5	277	300	324	350	378	407	436	467	498	529
6	561	595	630	666	703	741	781	822	865	908
7	952	998	1044	1091	1138	1185	1232	1279	1326	1374
8	1422	1470	1519	1569	1620	1673	1727	1781	1835	1890
9	1946	2003	2060	2117	2174	2231	2288	2345	2402	2459

Values of $10^4 r/r_s$ are tabulated vs. temperature in degrees Kelvin.

Top temperature scale: units. Left temperature scale: tens.

FIGURE 6

Field-Free Resistance Standards

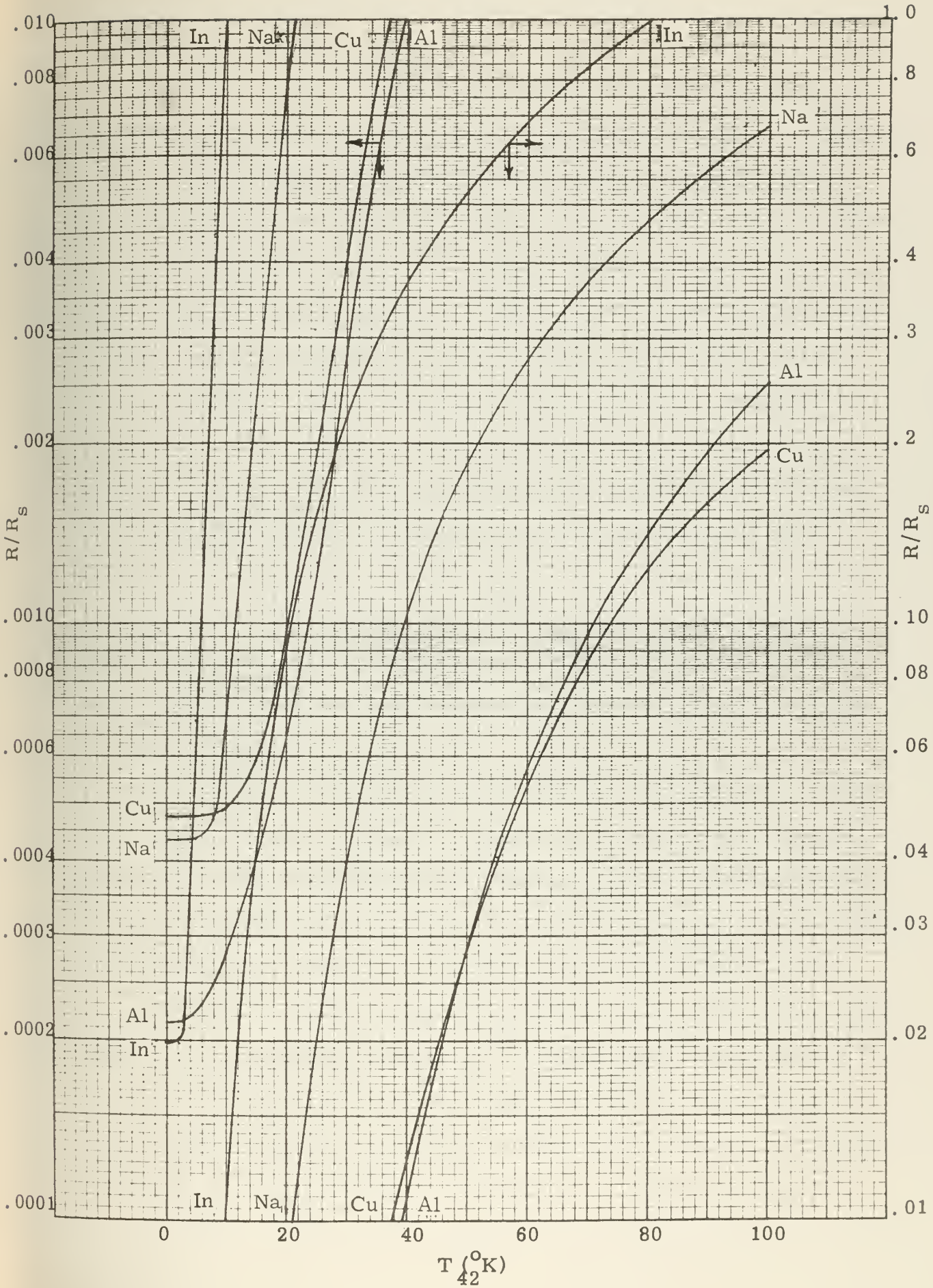

F. Magnetoresistance:

Basically, the comments in Section D of this chapter regarding the processing of experimental data apply as well to this section. In addition, a few of the problems associated with the collection of experimental magnetoresistance data bear discussion, prior to presentation of that data.

Assuming that Kohler's rule is valid, the most convenient manner to collect magnetoresistance data is to obtain the purest specimen available, immerse it in liquid helium, and subject it to various magnetic fields while conducting resistance readings: The purity and low temperature will assure a low value for r_o, and thus a high value of H/r_o for relatively low values of H. These data can then be projected to much higher field intensities, for coils operating above the temperature of liquid helium.

Unfortunately, aside from the obvious problems of instrumentation and measurement, and the difficulties inherent to any work in liquid helium, such collection of magnetoresistance data is beset by a number of unique problems:

As zero-field resistivity is quite low, it would be convenient to work with a relatively long, thin wire to maintain conveniently large resistance values. However, size effects are known to influence magnetoresistance readings: The resistance of a fine wire actually decreases in the presence of a magnetic field, until the field intensity reaches the point that the Larmour radius of a free electron in the field is of the order of the radius of the wire. Beyond this point, magnetoresistive behavior is more in keeping with the theory. Still, the extent to which size effects may continue to influence behavior, even beyond this crossover point, is difficult to determine. Unfortunately, the working area available to the experi-

menter is obviously limited by the size of both the dewar and the magnet providing the test field. Due to these problems, very little data have been taken from "large" specimens: that is, specimens approaching the size of conductors which might be used in cryogenic coils. In fact, the very small size of some specimens tested leads to problems in correlating the available data, and questions as to whether such data can be accurately projected to coil performance.

Orientation is a second problem: it is known that the magnetoresistance of a polycrystalline specimen rises more rapidly if the field is applied transverse to the specimen, than if the field is applied longitudinally. The data presented here are all transverse-field data, in keeping with the anticipated application. Yet this factor also introduces an obvious element of uncertainty.

Finally, the range of the data becomes a problem: Specimens are not always so pure and strain-free as might be desired, and attainment of sufficiently high values of H/r_o can be a problem. The usual solution is to use a pulsed magnetic field, since few magnets exist which are capable of producing the necessary field intensities on a steady-state basis. Such dynamic readings introduce yet another element of uncertainty: The specific heat of most metals is quite low at the temperature in question. Pulsed fields induce eddy currents in the specimen; eddy currents result in ohmic heating; and the temperature of the specimen--- and therefore its resistivity--- may rise from this effect. Some experimenters have corrected their data for such factors, or have estimated the effect to be negligible. Others do not even discuss the problem. One would anticipate that such an effect might lead to artificially high values of Δr, particularly at high field intensities, but the degree of correction required to compensate for this may be a moot point.

In any event, it is apparent that the collection of magnetoresistance

data is a somewhat more arduous undertaking than the collection of zero-field resistance data, so it is perhaps not surprising that the data displayed in Figs. 7-10 exhibit somewhat more scatter than was apparent in Figs. 2-5!

Figures 7 and 10 reveal marked similarity in the magnetoresistive behavior of indium and aluminum: For both metals, $\Delta r_n/r_n$ apparently saturates at $H/r_n = 10^4$ KG (where $r_n = r/r_s$), and thus never rises much above the value of 1.5. Further, though sources of data for indium are relatively limited, it is generally true for both metals that experimental data from different sources correlate reasonably well. (Purcell's data, as published in NBS Report 8481 (20), are an exception to this: His data, on aluminum foils, exhibit significantly higher values of $\Delta r/r_o$ than have been reported elsewhere. Further, the magnetoresistance of Purcell's specimens apparently increased with increasing temperature, for a given field strength. Due to this latter phenomenon, his data cannot be reduced to a single curve by application of Kohler's law, and are not reproduced here. The extent to which size effects may be responsible for such behavior is not known.)

Of the data reproduced in Fig. 10, the only significant deviation from the trend cited above is that reported by Cotti, et al.: Their data points indicate a possible departure from saturated behavior at high field intensities. Other experimenters have generally failed to observe such a phenomenon, and Cotti describes any such departure as "spurious". In particular, Callaghan--- whose 3/8" diameter specimen may be the largest aluminum specimen for which magnetoresistance figures are available--- tested to virtually the same range, with no apparent deviation from saturation.

Figure 8 presents the experimental data for sodium, and is, in itself,

FIGURE 7

Magnetoresistance of Indium

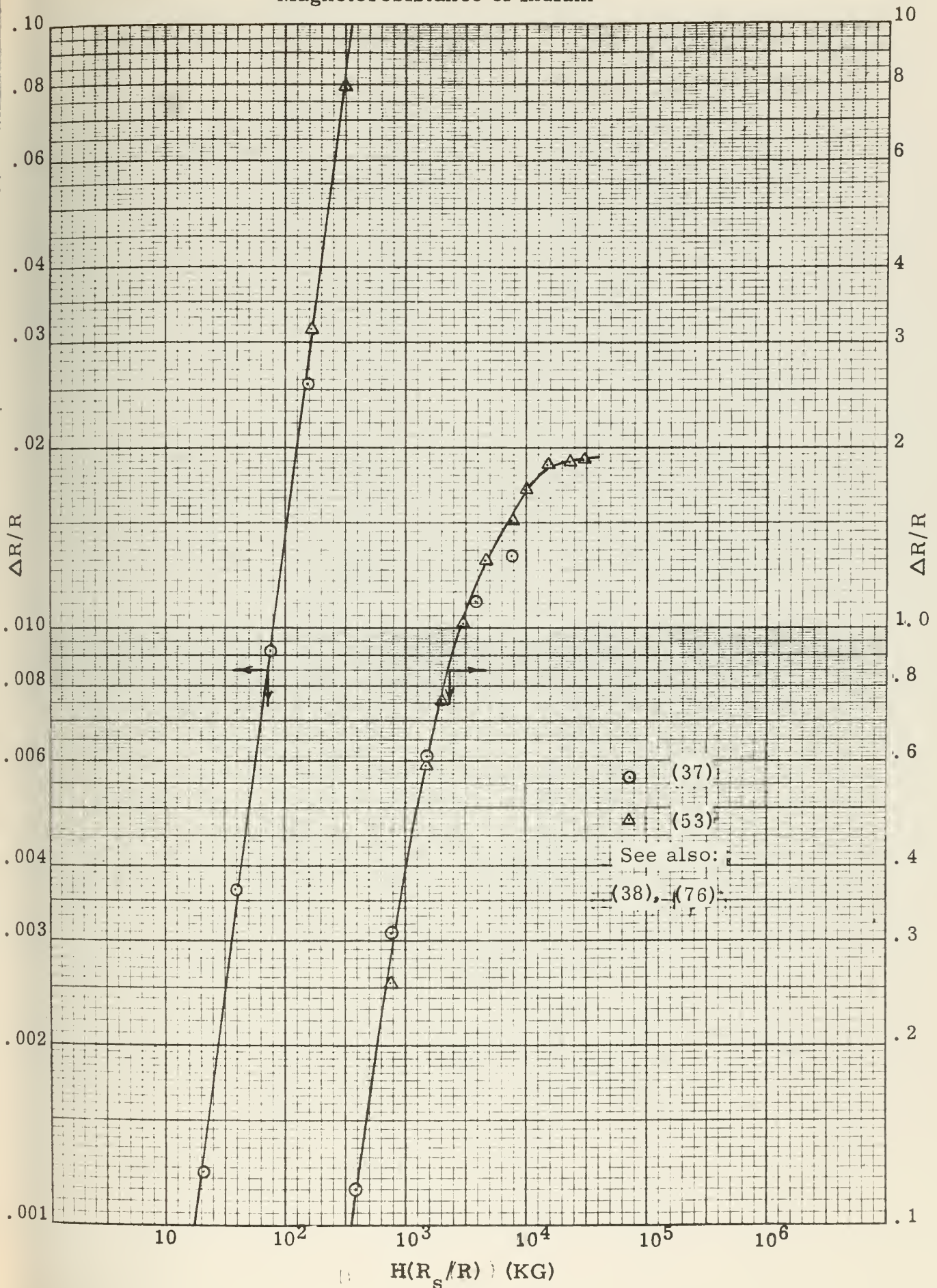

FIGURE 8

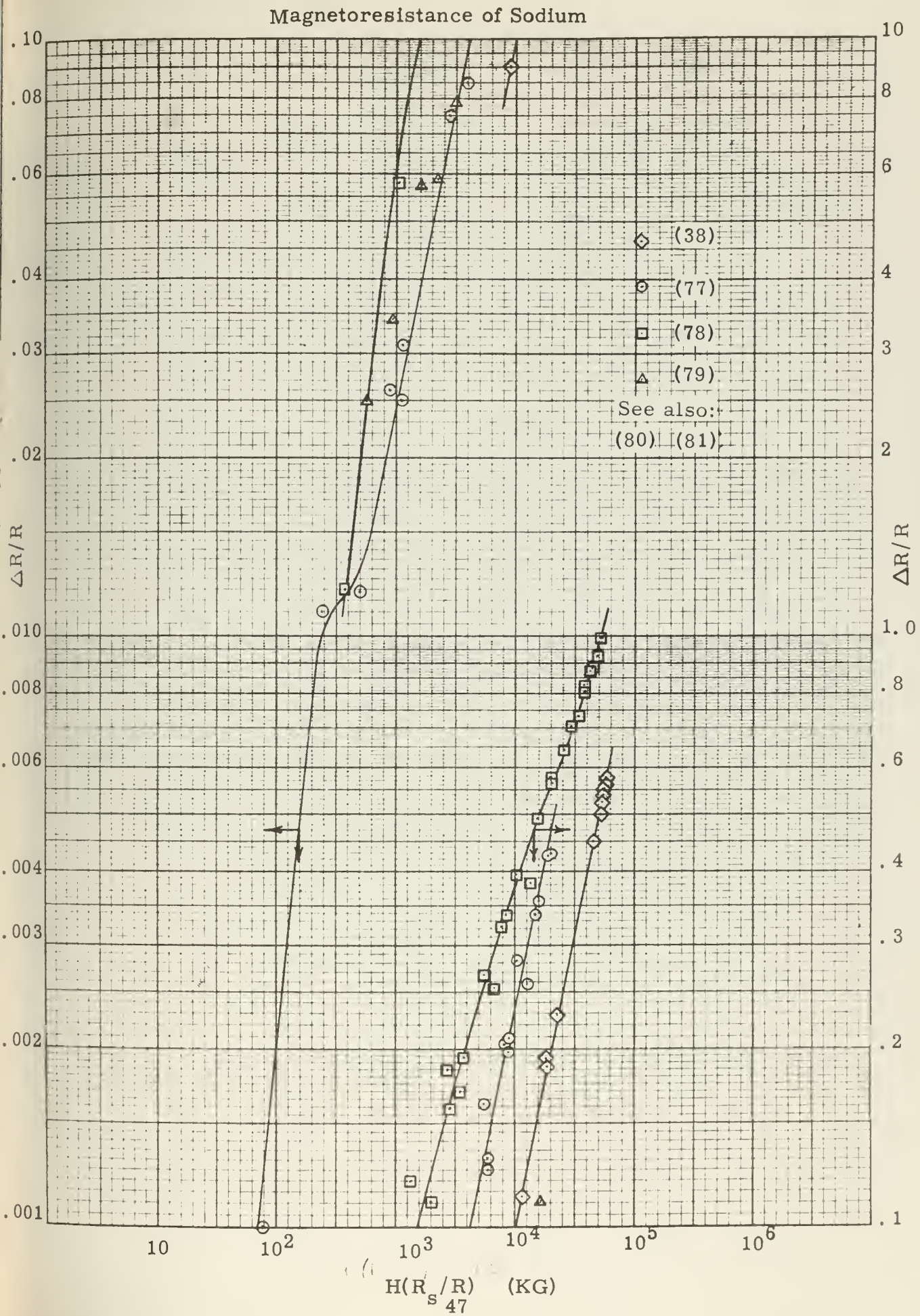
Magnetoresistance of Sodium
(38)
(77)
(78)
(79)
See also:
(80) (81)
ΔR/R
ΔR/R
H(R_s/R) (KG)
10
10^2
10^3
10^4
10^5
10^6
.10
.08
.06
.04
.03
.02
.010
.008
.006
.004
.003
.002
.001
10
8
6
4
3
2
1.0
.8
.6
.4
.3
.2
.1

FIGURE 9

Magnetoresistance of Copper

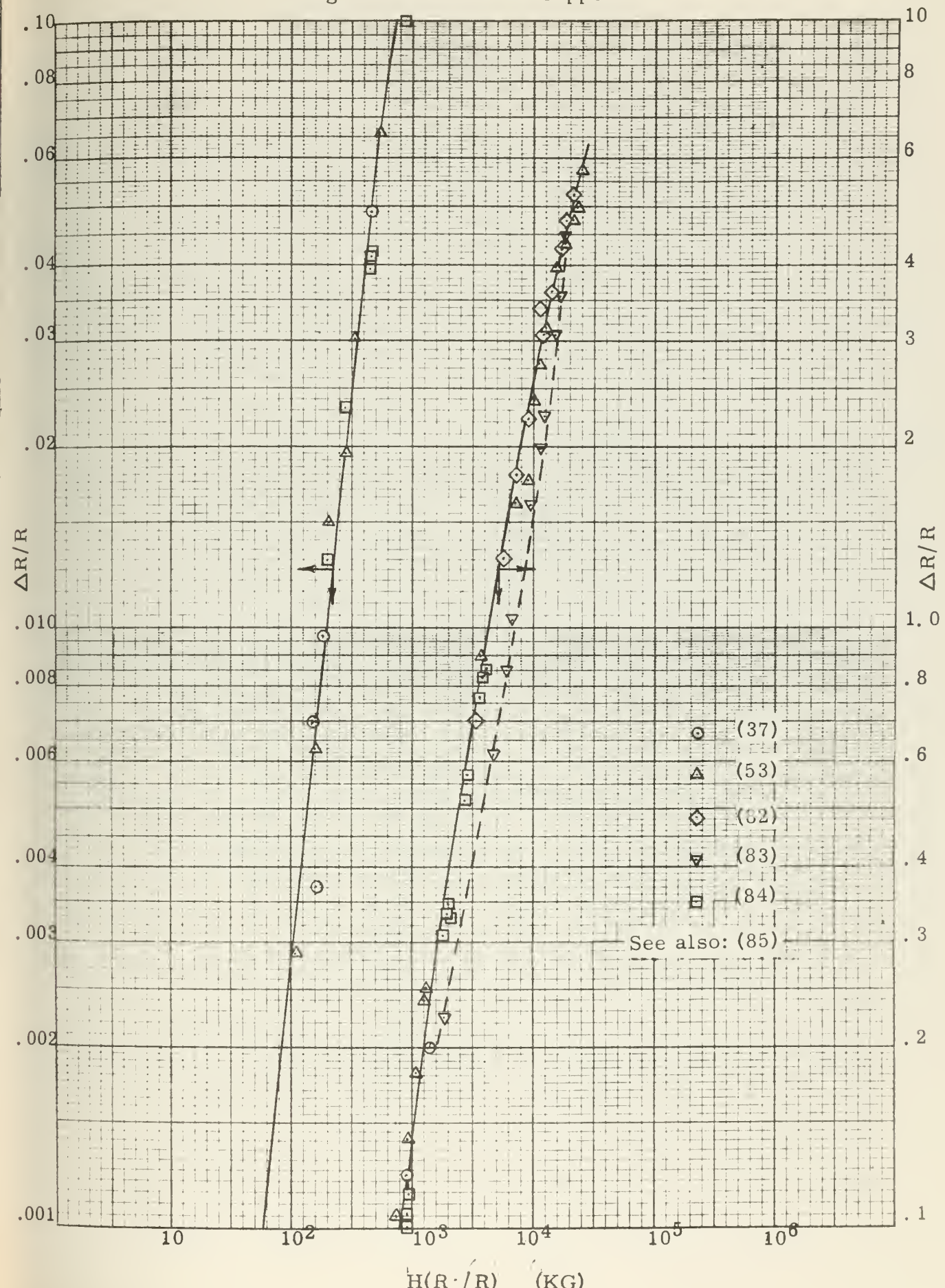

FIGURE 10

Magnetoresistance of Aluminum

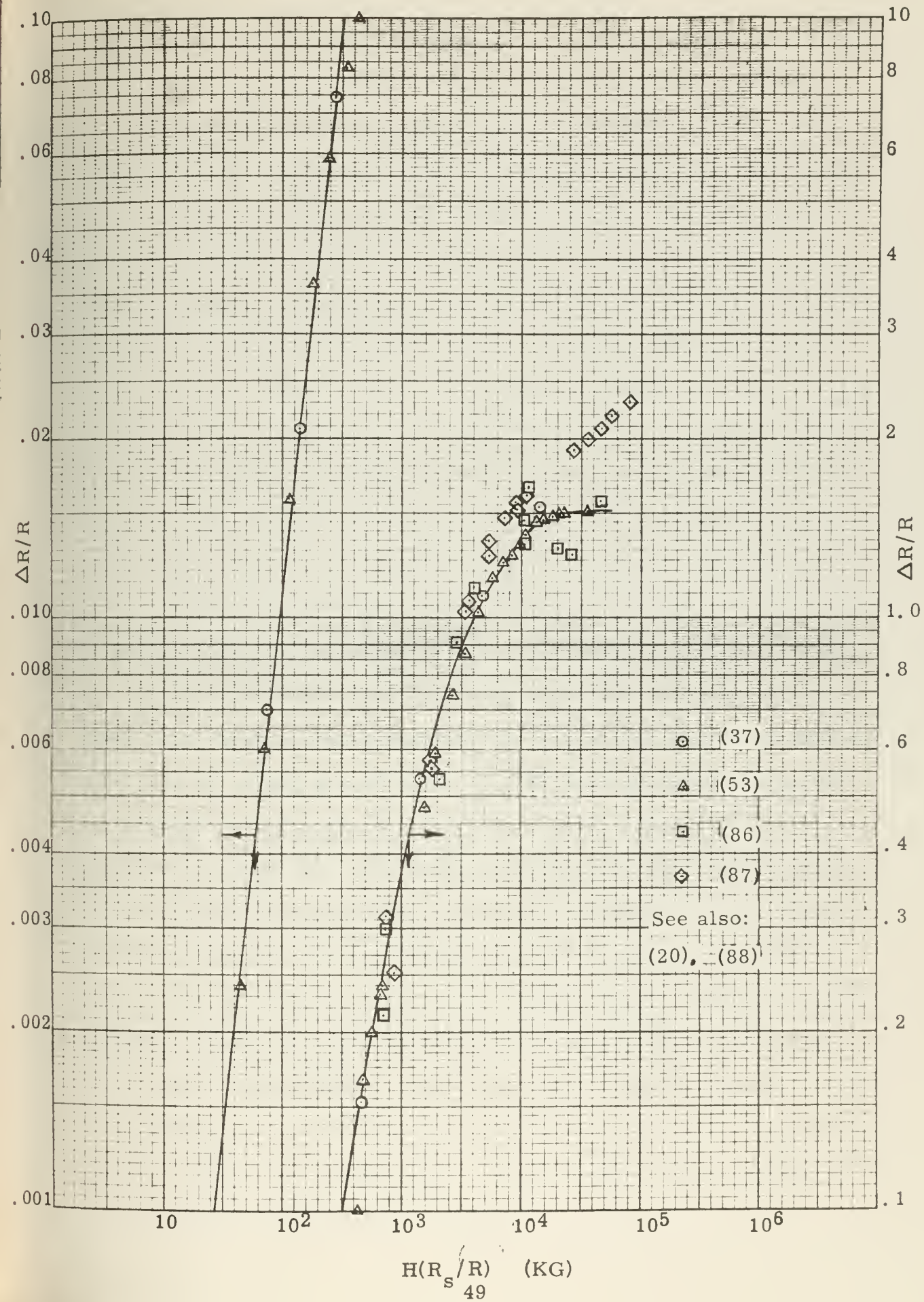

ample evidence of the "bizarre behavior" alluded to earlier. Hopefully, the situation may not be quite so chaotic as it would seem, at first.

White and Woods worked with very fine (less than .35 mm) rods of sodium, and as a result, the magnetoresistance of their specimens was found, initially, to decrease with increasing field. The data points reproduced here are limited to those which fell above the "crossover point" discussed earlier, but again, the extent to which size effects might still exert an influence is not known. In any event, the experimental curve exhibits a "knee" at about H/r_n = 300 KG, as though magnetoresistance had begun to saturate, but then passes through a point of inflection and asymptotically approaches a linear dependency at high fields. MacDonald's data overlap the upper end of this range, and confirm the linear dependency at high fields: however, MacDonald's curve is displaced laterally from that of White and Woods. This may, in part, be attributable to the fact that MacDonald indicates his calibration to be "approximate".

The most recent data reproduced here are from Taylor and Post: Their curve results from measurements on a particularly large (sodium cast into a 20' length of 0.5" O.D. x 0.035" wall stainless tubing) and partucularly pure ($r_{273}/r_{4.2} \sim 6500$) specimen, wound into a 4-1/2" diameter coil. Qualitatively, the behavior of this larger specimen is similar to that described above. The curve exhibits a "knee", though a much more gradual one, and apparently passes through a point of inflection near the upper end of the range investigated. Whether or not the quantitative differences are attributable to size effects is a matter for speculation. Regrettably, current data do not extend to sufficiently high values of H/r_n to confirm whether or not this last curve would eventually approach a linear field dependency. Taylor indicates that additional testing will extend the data to higher fields.

Finally, Fig. 9 summarizes the experimental data for copper. Contrasted with the other metals described here, the magnetoresistance curve for copper seems almost simple: It initially exhibits an H^2 dependence, then falls gradually to a linear dependence. This fact has been confirmed by numerous investigators, and all reports correlate remarkably well, except for that of Olsen and Rinderer. Although the magnetoresistance of copper is relatively low at low fields, it rises so rapidly that by $H/r_n = 10^4$ KG, copper exhibits greater magnetoresistance than all other metals considered. As ultra-low-temperature, ultra-high-purity high-field copper coils would exceed this value of H/r_n by an appreciable margin, one faces the problem discussed above: High-purity copper coils are unattractive in the liquid hydrogen range because of magnetoresistance. Coils of lesser purity are unattractive in that range due to the overwhelming probability of iron contamination. Thus, it is advisable to restrict the use of copper coils to the liquid nitrogen range and above.

The design standards derived from Figs. 7-10 are presented in Table 5, and plotted in Fig. 11. In order to permit analysis of high-field coil performance in the liquid helium range, it has been necessary to extrapolate the data to $H/r_n = 10^6$ KG. Indium and aluminum have been extrapolated at constant Δr; copper has been extrapolated under the assumption that Δr varies linearly with field intensity; and sodium has been extrapolated under the assumption that magnetoresistance asymptotically approaches a linear field dependency. Extrapolated values are indicated by parentheses in the table, and broken lines in the curves.

TABLE 5

MAGNETORESISTANCE DESIGN STANDARDS

H/r_n (KG)	In: $\Delta r/r$	Na: $\Delta r/r$	Cu: $\Delta r/r$	Al: $\Delta r/r$
1×10^1	--	--	--	--
2	.00150	--	--	--
3	.00270	--	--	.00110
4	.00409	--	--	.00197
5	.00565	--	--	.00309
6	.00730	--	--	.00448
7	.00855	--	.00140	.00606
8	.00949	--	.00182	.00794
9	.01067	--	.00229	.01008
1×10^2	.01228	.00100	.00284	.01234
2	.0418	.00390	.01093	.0448
3	.0811	.00830	.0230	.0840
4	.1232	.01352	.0378	.1268
5	.1660	.01915	.0545	.1701
6	.212	.0270	.0716	.214
7	.258	.0316	.0894	.256
8	.304	.0382	.1080	.298
9	.349	.0447	.1273	.339
1×10^3	.393	.0513	.1470	.563
2	.762	.1101	.364	.676
3	1.020	.1613	.599	.872
4	1.205	.206	.838	1.008
5	1.340	.243	1.111	1.112
6	1.441	.276	1.342	1.187
7	1.523	.306	1.591	1.249
8	1.589	.334	1.844	1.295
9	1.640	.358	2.11	1.338

Continued on next page

TABLE 5

(CONTINUED)

H/r_n (KG)	In: $\Delta r/r$	Na: $\Delta r/r$	Cu: $\Delta r/r$	Al: $\Delta r/r$
1×10^4	1.668	.381	2.36	1.369
2	1.870	.552	4.94	1.489
3	1.906	.704	(7.41)	1.508
4	(1.906)	.842	(9.86)	1.513
5	(1.906)	.969	(12.30)	(1.513)
6	(1.906)	(1.097)	(14.77)	(1.513)
7	(1.906)	(1.217)	(17.30)	(1.513)
8	(1.906)	(1.330)	(19.78)	(1.513)
9	(1.906)	(1.440)	(22.2)	(1.513)
1×10^5	(1.906)	(1.552)	(24.7)	(1.513)
2	(1.906)	(2.54)	(49.5)	(1.513)
3	(1.906)	(3.42)	(74.4)	(1.513)
4	(1.906)	(4.26)	(99.6)	(1.513)
5	(1.906)	(5.06)	(124.9)	(1.513)
6	(1.906)	(5.86)	(150.0)	(1.513)
7	(1.906)	(6.67)	(174.7)	(1.513)
8	(1.906)	(7.47)	(199.6)	(1.513)
9	(1.906)	(8.32)	(225)	(1.513)

$r_n = r/r_s$

$r_s = 1.7715 \times 10^{-6}$ ohm-centimeters

FIGURE 11

Magnetoresistance Standards

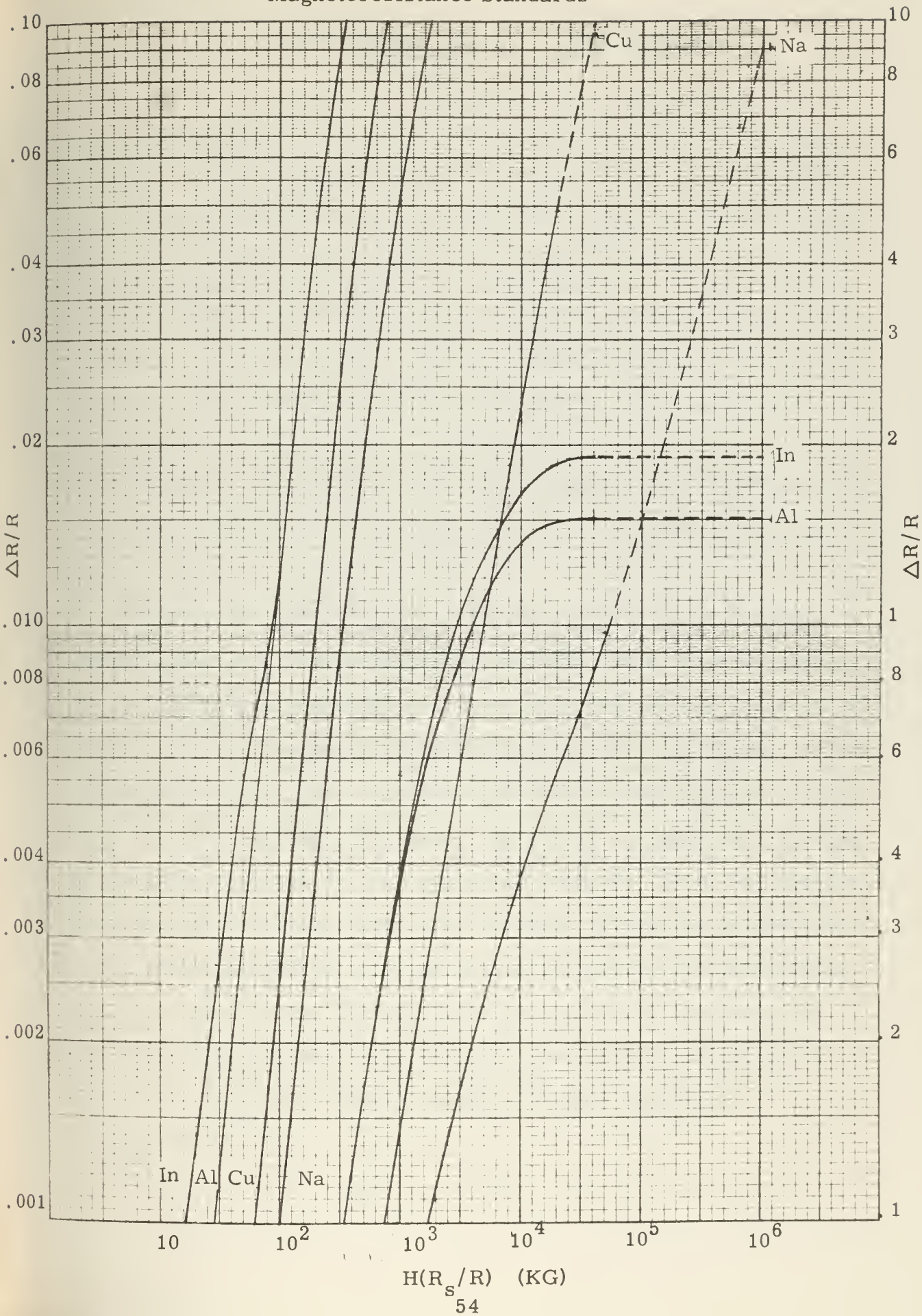

III. STRUCTURAL DESIGN CONSIDERATIONS

A. Basic concepts:

The non-conducting structural components of any air-core electromagnet must be regarded as a necessary evil: While necessary to support the coil against the various stresses developed, such components contribute nothing to the desired objective of generating a specified field throughout a specified region. Suffice it to say that if coils could be made to operate without such elements, they would be. Since this is generally impossible, this chapter will be devoted to the development of a model with which the minimum structural requirements of a cryogenic saddle coil may be estimated, as a function of the basic variables defining the coil.

Note that the above does not imply that the model used provides answers which can be directly applied to "real" coils. For one thing, the minimum structural fraction achievable in real coils is a function of such things as the ingenuity of the designer, the need to provide for ease of construction, etc. For another, a model which determines the minimum structure "needed" for support may quite reasonably predict that no structure is necessary, in a particular instance. This, for example, would be true for small, "jelly-roll" cryogenic solenoids, in which the configuration permits the conductors to be essentially self-supporting. However, even in small "jelly-roll" coils, it is convenient to use non-conducting elements to ensure centering, provide for coolant flow, etc. Thus, the structural volume fraction of a "real" coil may not be large, but will not be zero.

Nevertheless, the model proposed here provides answers which are useful in the preliminary design phase, which is consistent with the spirit

of this work. No attempt will be made to evaluate those variables which are primarily a function of the discretion of the designer. Corrections for such items can best be injected during the detailed design phase, after preliminary analysis has broadly defined the form of the desired coil.

In proceeding with this analysis, it will be convenient to discriminate between two classes of structural elements:

Internal structure is here defined as those structural components contained entirely within the coil dewar (and therefore, within the coil windings). The primary influence of such structure on the design is to reduce the packing factor attainable, and thus increase the conductor current required to obtain a given effective current density. (Note that equations (1), (3), and (5) essentially define the form of a coil in terms of effective current density.)

External structure is defined as those structural components which are external to the coil windings, including the dewar and those structural elements which penetrate the dewar. External structure has no influence on the effective current density, but does decrease the available working area, add to coil weight, and contribute to heat leak.

B. Internal structure:

There are two significant differences between the internal structure of a saddle coil and that of a solenoid, such as those described earlier:

First, the conductors of a tape-wound or "jelly roll" solenoid have structural continuity in the plane of main stress, while those of a saddle coil do not. The structural strength of the conductors of a tape-wound coil can directly support part or all of the stress load. By contrast, the conductors of a saddle coil run axially, while the major stresses occur

in the transverse plane. The latter situation is clearly less favorable.

Second, the magnetic stresses developed in a high field solenoid tend to pull the coil apart. Thus, it is relatively easy to design internal structural elements so that all structural components are in tension. The normalized magnetic stress distribution for various saddle coils is shown in Figs. 12-16. (These figures also indicate coil profile, as a function of the form factor defined in eqn. (6).) As can readily be seen, it is impossible to support such a stress distribution by components entirely in tension. The point, here, is that structural components bearing compressive loads may be subject to elastic instabilities--- i. e., buckling--- at stress levels well under the yield stress of the material used. Allowance must be made for this in coil design.

Two other considerations apply to the internal structure of cryogenic coils, in general. Mention has been made of the necessity to minimize residual resistance for ultra-low-temperature coils. This might necessitate designing to allow for a final anneal after the coil has been assembled. (Or, if the coil is to be built up from modular units--- that is, pre-formed "bundles" of conductors--- designing for anneal of such units, after shaping.) Such goals probably preclude the use of any structural materials which depend on elaborate heat treatment to develope structural strength. However, the designer has one consolation if "as annealed" metals must be used for internal structure. Engineering metals which do not become brittle at cryogenic temperatures exhibit an appreciable increase in strength, over room-temperature characteristics. (See McClintock and Hauser (89) for a discussion of factors influencing mechanical properties.) Since internal structure will be maintained entirely at cryogenic temperatures while the coil is operating--- and magnetic stresses do not exist while the coil is not operating--- advantage can be taken of the increased

FIGURE 12 F = 2.7

FIGURE 12.

Normalized magnetic stress distribution for F = 2.7

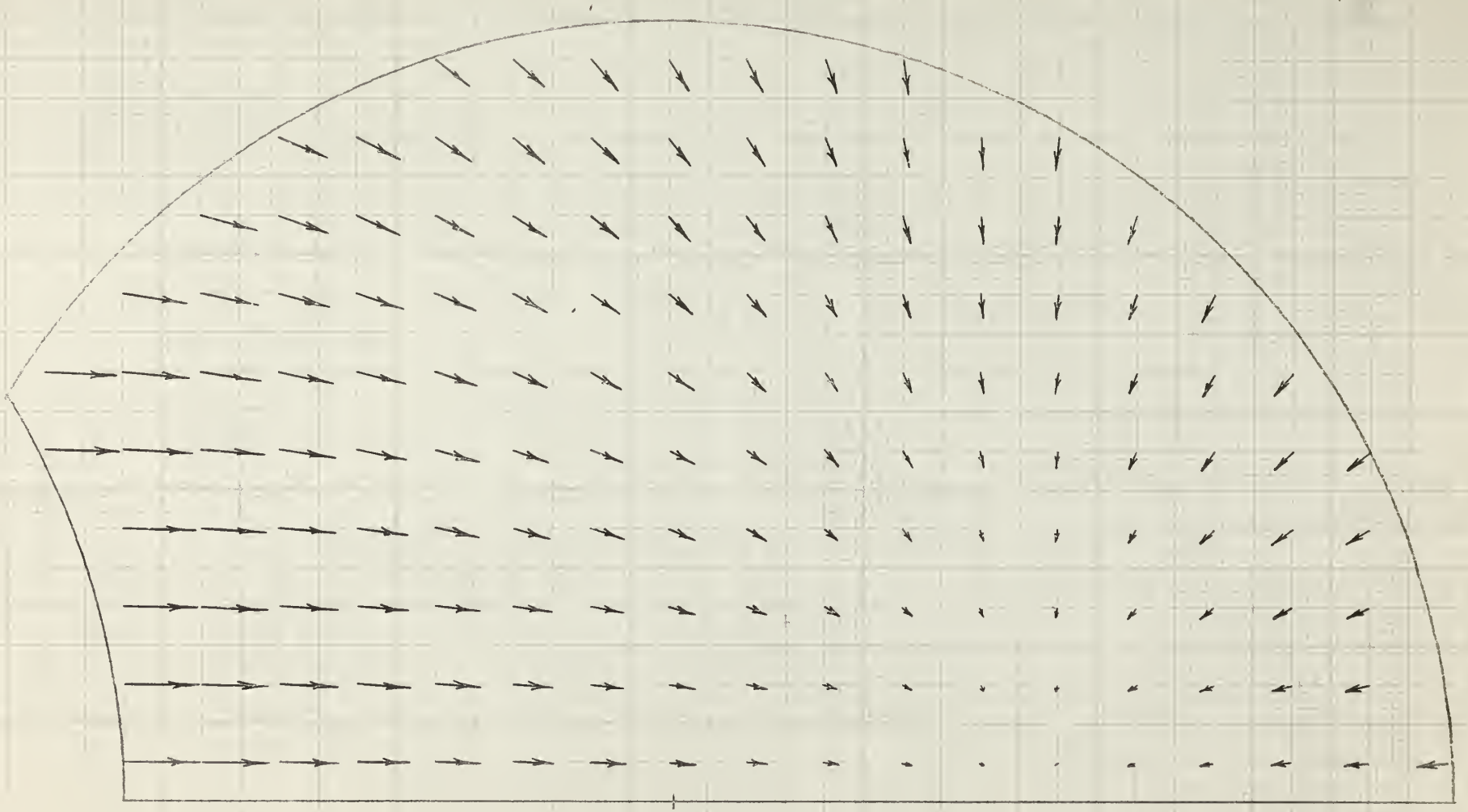

FIGURE 13 F = 1.9

FIGURE 13

Normalized magnetic stress distribution for F = 1.9

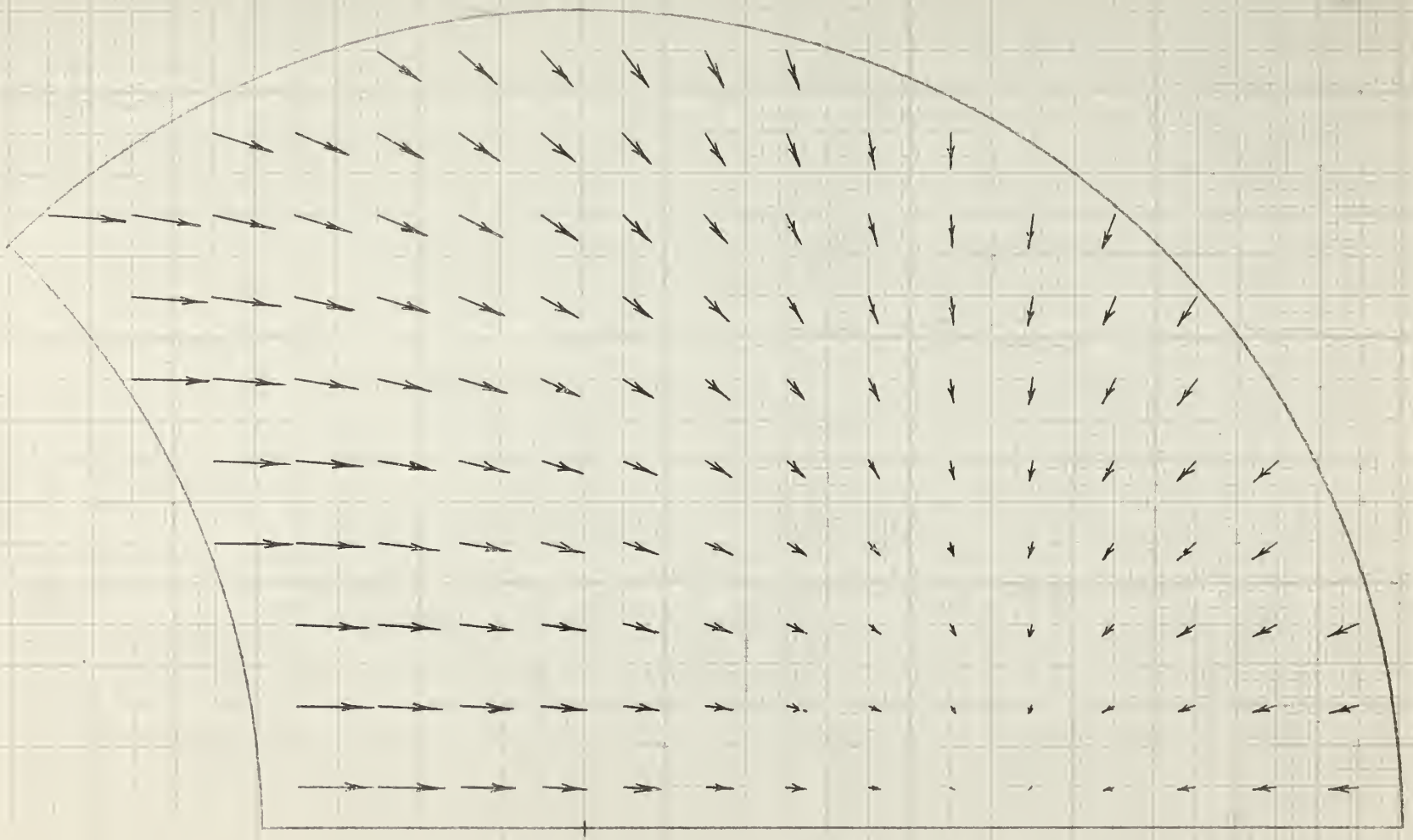

FIGURE 14 F=1.7

FIGURE 14.

Normalized magnetic stress distribution for F = 1.7

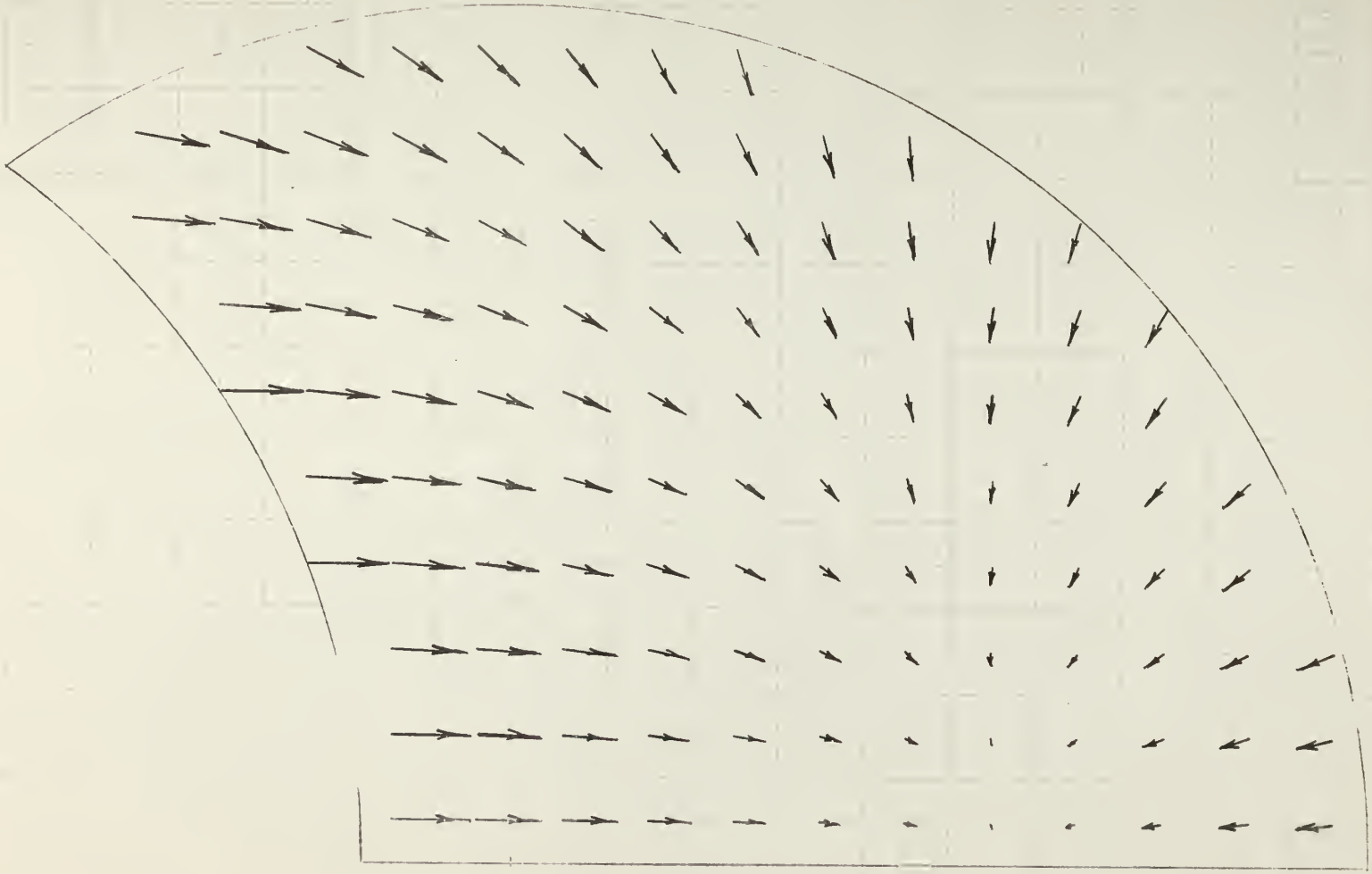

FIGURE 15 F = 1.5

FIGURE 15

Normalized magnetic stress distribution for F = 1.5

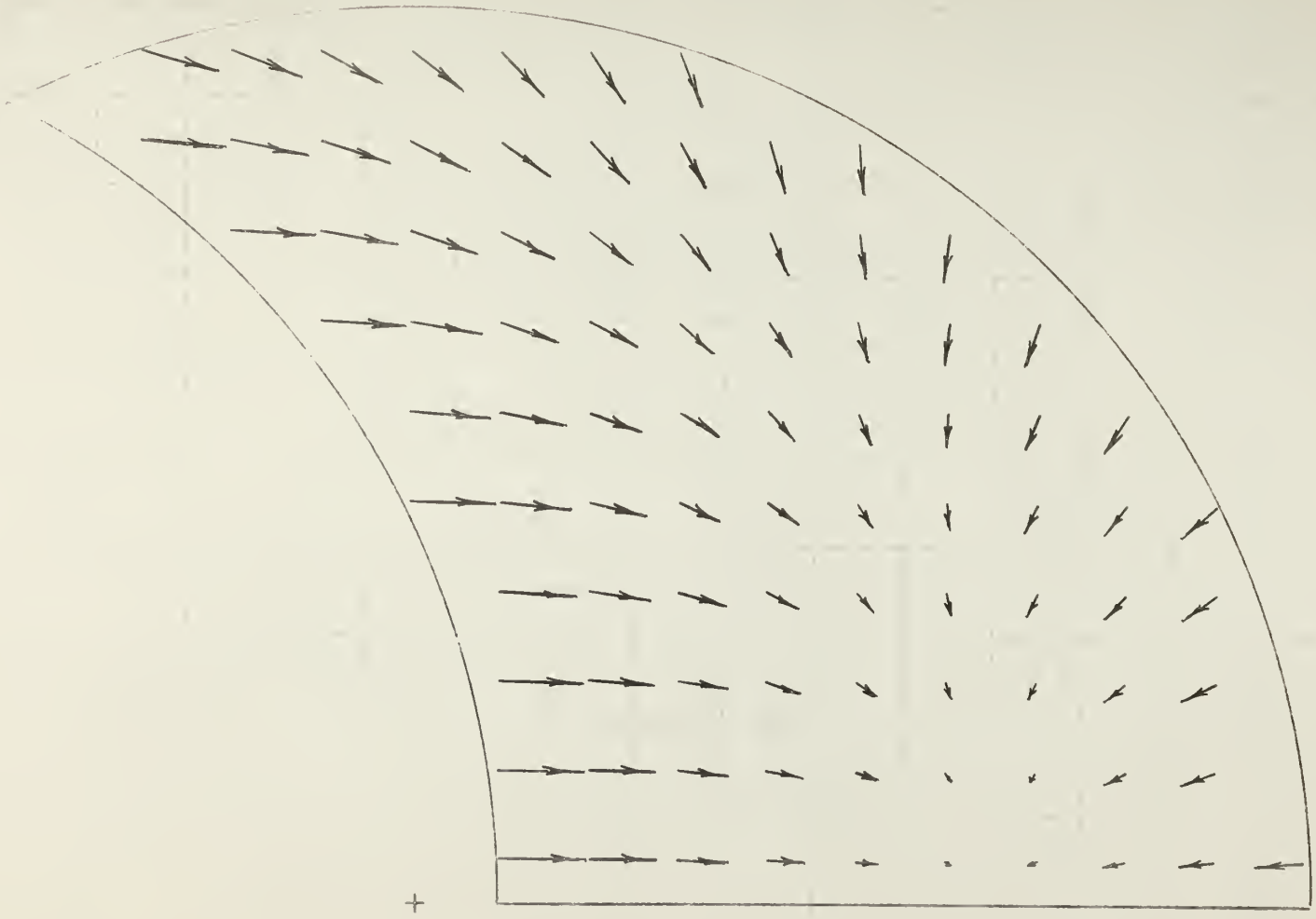

FIGURE 16 F = 1.3

FIGURE 16

Normalized magnetic stress distribution for F = 1.3

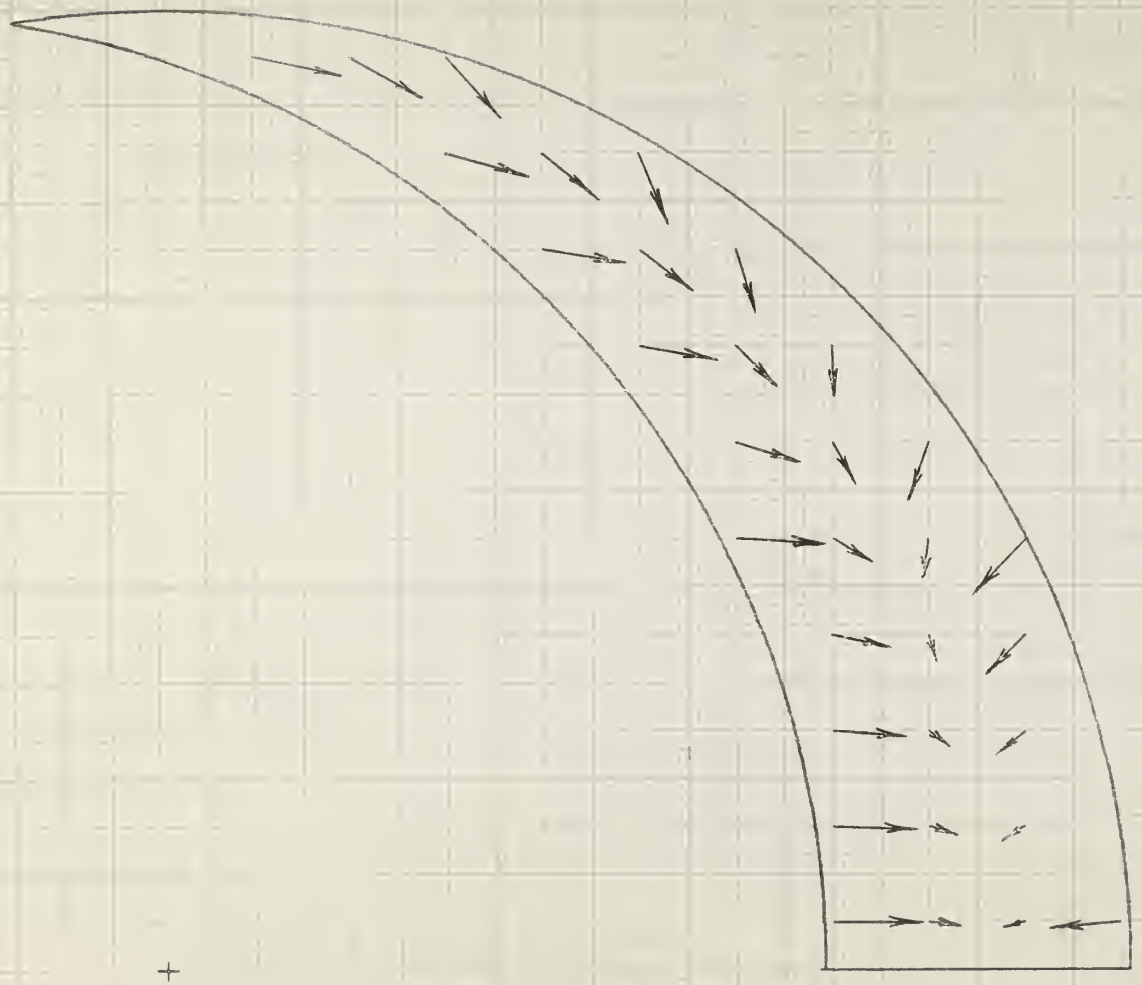

low-temperature strength of structural metals. (For example, Swenson (90) found that the compressive yield strength of Type 304 stainless steel increased from about 75,000 p. s. i. at room temperature to over 110,000 p. s. i. at 20° K. For additional information, see also (91).)

C. Superposition model for internal structure:

As is apparent in Figs. 12-16, the stress distribution in a high-field saddle coil is rather complex. It is probable that detailed structural design will be a difficult, iterative analysis, with the final outcome strongly dependent upon the arrangement scheme initially assumed. In order to reduce this situation to one which is sufficiently tractable for preliminary analysis, a superposition model will be used. Basically, the illustrated stress pattern results from two separate force fields: that due to the interaction between the current and magnetic field of a single coil lobe, and that due to the interaction of the current of one lobe with the field of the other. Each of these force fields will be treated separately, and the optimum structural arrangement to support each field will be determined. The structural volume fraction required for the combined fields will be estimated as the sum of the structural volume fractions so determined.

As will be seen, this is equivalent to assuming that the support structure of the coil is fabricated from a series of interlocking segments of circular shells. This probably would not be feasible, for a "real" coil, due to the obvious problems of assembly. However, the circular shell model does indicate those regions of the coil which most need structural support, and provides a tentative arrangement which could be successively modified in an orderly fashion.

Specifically, application of the superposition technique to this problem involves the following approximations:

1. Interactions between the two force fields are ignored. (If one were to draw an "X" through the center of either cylinder, the two force fields would be found, generally, to oppose each other on that side of the "X" away from the channel. Thus, less structure would actually be required in that

region than the model would predict.)

2. Interactions between support shells are ignored. (The shells required to support "self field" are subjected to compressive loading, and must be designed in accord with the appropriate elastic stability criteria. Actually, the interlocking shells resulting from the "adjacent field" analysis would provide some additional stiffening, not considered in the "self field" analysis. On the other hand, if either set of shells were to shift position slightly under load, part of that load would be transferred to the other set. Such load transferral is also neglected.)

Basically, predictions from such a model should be reasonable, but conservative. At least, the model provides a systematic means to estimate the additional structure required due to the inability to avoid compressive loading. Further, it is well to be conservative at this point. Deviations from the idealized circular shell model--- in the interest of ease of assembly--- will probably necessitate a somewhat higher structural volume fraction than would result from an "optimum support" arrangement.

D. Support of "self field":

The force distribution in a circular cylinder, due to interaction of uniform, axial current flow with the magnetic field generated by that current flow, is directed radially inward and has a magnitude given by:

$$f_m = \text{magnetic force density} = \frac{\mu_o r J^2}{2} \qquad (10)$$

To return to our original hypothesis, where the use of structure can be avoided, it will be. If the cylinder is comprised of many individual conductors, those near the center of the cylinder are in such a region. Force densities are low, and directed so as to hold the coil together. It

is reasonable to assume that the wires in any circular shell would tend to "jam together", as do the keyed stones of a circular arch. Certainly, the conductors could be shaped to accentuate this tendency. Stability would not be a problem, since this region is essentially solidly filled with conductors. To what radius does this region extend?

Consider a thin shell of conductors at radius r. If we assume this shell to be "keyed together", it is essentially self-supporting. The magnetic force distributed within this shell is equivalent to an external pressure, directed inward, of magnitude

$$p_e = \frac{\mu_o J^2 r\, dr}{2}$$

Neglecting stability, this is simply the classic "hoop stress" problem. If we desire to limit the internal stress in the conductors to a maximum level σ_c, we have:

$$\sigma_c = \frac{r p_e}{t} = \frac{\mu_o J^2 r^2 dr}{2\, dr}$$

and therefore

$$r_{max} = \frac{1}{J}\sqrt{\frac{2\sigma_c}{\mu_o}} \qquad (11)$$

That is, the individual conductors must not be "keyed together" at $r > r_{max}$, or the resultant hoop stress will exceed the specified stress limit of the conductor. If the coil must be designed to prevent self support in shells at greater radii, the conductors in such shells will be forced inward by the magnetic pressure, due to lack of structural continuity. The resultant stress must not be transferred to the shell at $r = r_{max}$, since the conductors of that shell have already been "stressed to the limit". Therefore, the first structural support shell must be located at $r_1 = r_{max}$.

Assuming the conductors located outside the first support shell all transfer their load inward, those located immediately adjacent to the sup-

port shell will be subjected to the greatest load, in the form of simple radial compression. Again, this must not exceed the specified limit, σ_c. The position of the second support shell can then be determined by integrating eqn. (10) radially, subject to this condition.

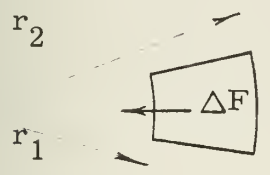

In a slab of width $\Delta\Theta$,

$$\Delta F = \iint \frac{(\mu_o r J^2)(r\, dr\, d\Theta)}{2} = \frac{\mu_o J^2}{6}(r_2^3 - r_1^3)\,\Delta\Theta$$

The "equivalent pressure" on the structural shell is thus:

$$p_e = \Delta F / \Delta A = \frac{\mu_o J^2}{6}(r_2^3 - r_1^3)\Delta\Theta / r_1 \Delta\Theta = \frac{\mu_o J^2}{6}\left[\frac{r_2^3 - r_1^3}{r_1}\right] \qquad (12)$$

And the radius of the second structural shell must be:

$$r_2 = r_1 \left[1 + \frac{6\sigma_c}{\mu_o J^2 r_1^2}\right]^{1/3} \qquad (13)$$

Obviously, this can be repeated until the outer radius of the cylinder is reached. Eqn. (13) is used to determine the radius of each successive shell, since it is known that $p_e = \sigma_c$ in eqn. (12). For the last shell, eqn. (12) is solved for the effective pressure on the shell, by setting $r_2 = r_o$, the outer radius of the cylinder.

The above analysis of "effective pressure" has ignored the thickness of the support shells. The reason is this: Consider a slab of height h,

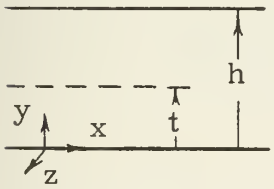

mounted on a zero-thickness shell at y = 0, and carrying a uniform current J_e in the -z direction. In the presence of a uniform, x-directed magnetic field, B_x, the slab will exert a pressure $p_e = B_x J_e h$ on the support. Now let the support have non-zero thickness, so that it extends from y = 0 to y = t. If we require the same total current in the slab, the current density must become $J = J_e/\lambda$, where $\lambda = (h-t)h$. The pressure exerted on the support is now given by $p_e = B_x(J_e/\lambda)(h\lambda) = B_x J_e h$, as before. An analogous situation exists in the "self field" problem above, since the magnetic field

at a given radius in such a composite cylindrical conductor is primarily determined by the "effective" current flow within that radius. Thus, to a first approximation, the location of the "next" shell is not influenced by the non-zero thickness of the "present" shell, and the appropriate current density to use in eqns. 10-13 is J_e, the effective current density of the coil. Obviously, field perturbations due to the presence of non-conducting structure become more severe, and therefore the accuracy of this model decreases, as $\lambda \rightarrow 0$. (In fact, when the stability criteria are applied to determine shell thickness, it is quite possible to compute a "structural volume fraction" greater than unity.) However, if the analysis indicates that support structure alone would result in a packing factor less than, say, 0.25, the coil is obviously not of interest.

Once the position of each shell has been determined, its required thickness must be found. Windenburg (92) summarized, in 1947, the equations required for this process. They are:

$L < L_{crit}$

$$p = \frac{2}{1.05} \sigma_y \frac{t}{D} \qquad (14)$$

$$p = \frac{2.42E}{(1-\mu^2)^{3/4}} \left[\frac{(t/D)^{5/2}}{L/D - .045(t/D^{1/2}} \right] \qquad (15)$$

$L > L_{crit}$

$$p = \frac{1}{1.27} \left(\frac{2E}{1-\mu^2} \right) (t/D)^3 \qquad (16)$$

$$p = 2.34 \sigma_y \frac{t}{D} - 1.06(\sigma_y/E)^{1/2} \qquad (17)$$

Equations (14) and (15) apply to "short" cylinders, while (16) and (17) apply to "long" cylinders. Essentially, if a cylinder is very short, elastic instability is no problem, and (14)--- which is a slightly more conservative version of the hoop stress equation--- applies. As the cylinder is lengthened, a simple, two-lobe instability collapse is possible at stress levels below yield. The "critical pressure" in this region is a function of the

elastic modulus, t/D, and L/D, as shown in (15). At still greater lengths, the ends are so remote that further removal has no significant influence on stability. At this point, (16) applies. However, as (16) was derived from elastic stability considerations, it does not recognize that a proportional limit exists. Thus, collapse can occur from yielding, vice instability, at pressures lower than predicted from (16). The appropriate equation to predict this mode of failure is (17).

In using these equations to determine shell thickness, one must obviously know p, t/D, L/D, the design stress limit specified for the structural material (which would presumably be an order of magnitude higher than that established for the conductor), and the elastic modulus and Poisson's ratio for the structural material. For "short" cylinders, one would solve both (14) and (15). The larger (t/D) so obtained would be correct. For "long" cylinders, (16) and (17) would be applied in similar fashion. To aid in distinguishing "short" from "long", Windenburg defines the parameter:

$$X = \left(\frac{29 \times 10^6}{E}\right)\left(\frac{\sigma_y}{27,500}\right)\left(\frac{L}{D}\right).$$

If $X \leq 5$, (14) and (15) apply. If $X \geq 20$, (16) and (17) apply. If $5 < X < 20$, try both (14) and (15), and (16) and (17), as above, then keep the smaller of the two resultant values for (t/D).

One problem arises, regarding the crossover from (16) to (17) for high-yield-strength metals. For a given metal (and a particular L and D), the simaltaneous solution of these two equations involves a cubic in(t/D). Such a solution can assume one of three forms, illustrated in Fig. 17. In case (A), there are three real, unequal roots. In (B), there are still three

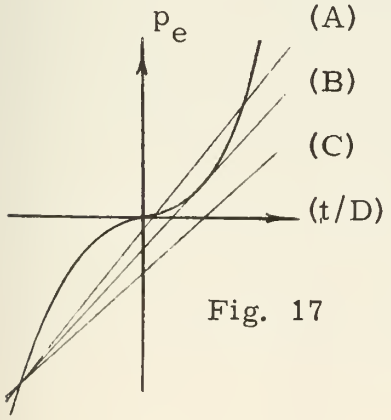

Fig. 17

real roots, but two are identical. In (C), there is only one real root, and two imaginary roots (i. e., no physical solution). Equations (16) and (17) were originally derived for mild steel. Equation (17) is an attempt to express case (B) in terms of the physical parameters of any metal, and is successful for mild steels. The physical solution in this case follows (16) to the point of tangency, then (17) at higher pressures. Unfortunately, for yield strengths in excess of about 50,000 p. s. i., substitution of the appropriate parameters into (16) and (17) results in case (C): That is, (17) no longer provides the equation of a straight line, tangent to (16) at the desired crossover point.

To circumvent this situation, it is necessary to re-examine the physical reasons underlying the necessity for "crossover". Eqn. (16) becomes invalid at high pressures, for a particular goemetry, because "real" metals reach their proportional limit and thereafter deviate from Hooke's Law. Thus, (16) predicts too low a value for (t/D), since it assumes a constant elastic modulus. Eqn. (17) attempts to correct for this by assuming that shell thickness must be increased in direct proportion to pressure, beyond a specified point. This specified crossover point would presumably lie somewhere between the proportional limit and the yield point (2% offset), depending on the characteristics of the metal used.

A conservative approach will be used here. Following the solution of (16), the value of (t/D) so obtained, along with the known value of P_e, will be inserted in the hoop stress equation to determine whether or not the resultant stress in the shell exceeds the proportional limit of the metal in question. If so, the effective pressure corresponding to the proportional limit for the given shell will be determined, and the slope of eqn. (16) will then be found at that pressure. Assuming this to be the

desired crossover point, these data will be used to generate the equation of a straight line, tangent to (16) at the pressure corresponding to the proportional limit. The projection of this straight line will then be used to determine a corrected value for (t/D) at the effective pressure.

Finally, after the radius and thickness of each shell have been determined, the total volume of these "compressive" shells can be determined, and divided by the volume of the composite cylindrical conductor. It will be assumed here that the compressive volume fraction of the "crescent moon" of a saddle coil lobe is approximately equal to the compressive volume fraction of a cylinder of the same radius, carrying the same effective current.

E. Support of "adjacent field":

The force distribution in either coil lobe, due to interaction of uniform, axial current flow with the magnetic field generated by a similar, but oppositely directed, current flow in the adjacent lobe, is directed radially outward from the center of the adjacent lobe and has a magnitude given by:

$$f_m = \frac{\mu_o r_o^2 J^2}{2r} ,$$

where r_o is the outer radius of the adjacent lobe. A natural structural arrangement to support such a force distribution consists of a series of circular arcs, concentric with the adjacent lobe. The problem here is similar to that preceding. The position, thickness, and in this case, length of each such arc must be determined. Since this set of structural shells is in tension, no stability problems exist.

To determine the location of the first tensile shell, let us refer to a coordinate system centered on the "adjacent" lobe, henceforth called the

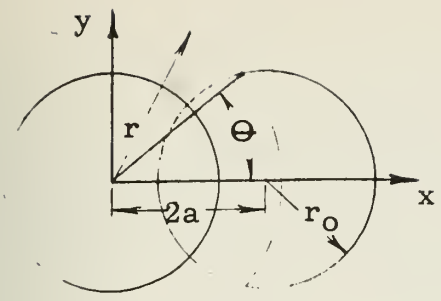

left lobe. Again considering the lack of structural continuity in the transverse plane, since the magnetic force considered here tends to "pull apart" the individual conductors, it will be assumed that the load will be transferred radially outward from the center of the coordinate system. In the most severely stressed conductors, immediately adjacent to the structural shell, we have:

$$p_e = dF/dA = \int_{r_o}^{r} 2r\Theta f_m dr / 2r_1\Theta = \frac{\mu_o r_o^2 J_e^2 \int \Theta \, dr}{2r_1\Theta} \qquad (18)$$

where 2Θ is the angle subtended by the circle bounding the right lobe at a given radius. Referred to the indicated coordinate system, this circle is:

$$(x - 2a)^2 + y^2 = r_o^2,$$

where 2a is the distance between lobe centers. Further, the equation of a circular arc, centered on the origin, of radius r, is:

$$x^2 + y^2 = r^2$$

Thus, the x-coordinate of the intercept of the circle bounding the right lobe, and above circular arc, is:

$$x = \frac{r^2 + 4a^2 - r_o^2}{4a} \qquad (19)$$

and therefore

$$\Theta = \cos^{-1}(x/r) = \cos^{-1}\left(\frac{r^2 + 4a^2 - r_o^2}{4ar}\right) \qquad (20)$$

The above is a bit messy for explicit solution, but can be programmed readily for numerical solution. Conceptually, the procedure is the same as before. Shells are positioned in accord with the requirement that $p_e = \sigma_c$ at each shell. Shell thickness is determined from the requirement that:

$$t_i = \frac{\sigma_c}{\sigma_d} r_i \qquad (21)$$

where σ_d is the design stress limit for the structural material. The "tensile" volume fraction then becomes:

$$T.V.F. = \frac{\sum 2(\sigma_c/\sigma_d) r_i^2 \Theta_i}{A_c}, \qquad (22)$$

where A_c is the cross sectional area of either lobe.

Essentially, the above shells transfer the magnetic stresses distributed within the windings to the outer edge of the coil: i. e., the ends of such shells must be "anchored" by structure bounding the outer surface of the lobe. Further, as there is a net repulsive force tending to separate the two lobes, provision must be made to tie the bounding structure of the two lobes together. However, such structure does not penetrate the windings, and therefore has no effect on the packing factor of the coil. It is therefore treated as "external structure", as defined above.

It is interesting to note the role of σ_c and σ_d, in determining the structural volume fraction predicted by this model. Basically, the number of structural shells--- both tensile and compressive--- is determined by σ_c, and the thickness of each shell by σ_d.

The details of the actual computational procedure followed in applying this model to the coils investigated are provided in Chapter VII, and the results of those calculations, in Appendix C.

F. External structure:

The external structure associated with a "real" MHD coil is a sufficiently strong function of the intended application as to preclude quantitative discussion in a study of this nature. Nevertheless, a few points

bear mentioning, qualitatively:

The phrase "external structure" has been defined to include the structural elements bounding each coil lobe, as well as those members connecting the two lobes, the dewar required to maintain the cryogenic environment, and the structural members which support the assembled coil, both against gravity, and against any drag or thrust generated by the MHD channel.

Most probably, the structure bounding and connecting the coil lobes would form the inner vacuum wall of the dewar. Again, advantage could be taken of the increased low-temperature strength of materials.

For coils designed for operation below liquid nitrogen temperatures, it is likely that the dewar itself would be of "two-stage" construction. That is, everything within the "cold" side of the dewar would be maintained at the coil operating temperature, but a "middle layer" of the dewar would interpose a "sandwich" of liquid nitrogen between the cold side and ambient temperature. This would reduce heat leak by conduction and radiation through the dewar, but far more importantly, allow greatly reduced heat leak by conduction along structural elements and electrical leads piercing the dewar, into the "cold box". Most of the heat leak along such elements could be removed, with reduced refrigeration cost, from the liquid nitrogen layer.

Most probably, the vacuum layers of the dewar would contain either a multi-layer "superinsulation" (93-97), or one of the somewhat less effective but more readily applied opacified powders (96-98), to minimize heat leak. Such construction would ensure that heat leak through the dewar would be negligible compared to other losses. (A reasonable estimate, given such construction, would be .05 watts per square meter.)

From a strictly structural viewpoint, arrangements would presumably be made to ensure that heat leak along electrical leads was also negligible. McFee (99) indicates a "passive" method of minimizing such heat leak by control of lead geometry. "Active" methods light involve using boil-off vapor from the cold box to refrigerate the leads. However, for steady-state, closed-loop operation, it would be necessary to provide for recondensation of such vapor, and its return to the cold box.

Probably, the most efficient geometry for support structure which pierces the dewar would be the so-called "bicycle-spoke" arrangement, in which the coil is supported by a network of long, thin spokes. Careful design of such supports will ensure maximum path length from ambient to cryogenic temperatures, and therefore minimum heat leak, along each support member. Obviously, this is not the most convenient arrangement from the viewpoint of ease of construction. In small cryogenic coils, I^2R losses dominate so strongly that one might prefer to utilize fewer, and more easily installed supports, even at the cost of added heat leak. In larger coils, structural leak may be more important. Stekly and Woodson (100) provide a means by which the magnitude of such heat leak may be readily estimated: Let F be the total force to be supported in a given direction (weight, thrust, etc.). Then,

$$A_s = F/\sigma_s$$

where σ_s is the design stress in the support material (note that since supports penetrate the dewar, room temperature figures must be used), and A_s is the required effective cross section of support structure. Since the rate of heat leak along such structure is given by:

$$q = k\frac{A_s}{L_s}\Delta T,$$

where k is the mean thermal conductivity (see (101) or (102) for typical values), L_s the mean length, and ΔT the temperature drop across the structural elements, we have:

$$q = \left(\frac{k}{\sigma_s}\right)\left(\frac{F}{L_s}\right)\Delta T \qquad (23)$$

A first estimate of coil weight is simply $F \approx m_c g V$, where m_c is the mass density of the conductor, and V the total coil volume. Similarly, if the structure supporting the MHD channel must penetrate the dewar, the associated heat leak can be estimated by setting $F \approx (p_i - p_o)A_{ch}$. For a matched load, $P_{gen} \approx Fv/2$, where v is the mean flow velocity in the channel, and an equivalent estimate is $F \approx 2P_{gen}/v$. In any event, such relations can be used to estimate the importance of support heat leak, and therefore, the importance of optimizing support geometry.

Since the MHD channel operates at or considerably above room temperature, the "working area" of a saddle coil is not fully available for the intended application. Some of it must be filled by the type of dewar and support structure described above. Again, "how much" is a strong function of the particular application intended, and is therefore not included in any of the curves generated in this study. To compensate for this factor, one can enter the coil geometry curves of Appendix A with a somewhat greater A_{ch} than is actually required for the anticipated application.

IV. REFRIGERATION

A. Efficiency:

As was mentioned earlier, the cost of refrigeration is the dominant operating cost of ultra-low-temperature cryogenic coils. Such being the case, the time has come to discuss refrigerator efficiencies, before proceeding further.

Brief reference to the Carnot cycle will depict the magnitude of the problem. In order to maintain a liquid nitrogen environment--- that is, to maintain a refrigerated area at 77.4° K, given an ambient temperature of 300° K--- an ideal, Carnot refrigerator would require 2.9 watts of input power for every watt of heat removed from the refrigerated area. To maintain a liquid helium environment (i.e., 4.2° K) under the same conditions would require 70.4 watts of input power for every watt of refrigeration provided. As is hardly surprising, considering the working environment, "real" cryogenic refrigerators require appreciably more power than these "ideal" figures.

Actually, the spread between "real" and "ideal" performance has been reduced significantly, within the last decade. Scott (62) gives a description of the various components used in cryogenic refrigerators, as well as a discussion of many of the factors limiting refrigerator performance. Suffice it to say that though the design of a refrigerator may be simple in theory, the design of a cryogenic refrigerator is extremely complex, in practice. Thus, improved performance has generally been attributable to improved technique--- i.e., "practical engineering"--- rather than any "breakthrough" in basic concepts. Given the law of supply and demand, the effort expended in this field has increased in proportion to the growth of industrial application of cryogenic technology.

Hopefully, further improvement in the performance of cryogenic refrigerators should be expected, under these circumstances.

Fortunately, it is unnecessary to become intimately familiar with the design of cryogenic refrigerators in order to appreciate the two factors which most directly influence their relative efficiency (that is, their performance as compared to the Carnot cycle efficiency).

First, as with many other mechanical devices, small cryogenic refrigerators ($\sim$ 1 watt) tend to be considerably less efficient than comparable large refrigerators (over 100 watts). Of course, the degree of improvement with increased size eventually "tapers off". Bernert and Stekly (103) present curves of relative efficiency vs. size which indicate that relative efficiency "saturates" at a power input of approximately 1000 KW, more or less independently of "cold side" temperature. The significance of this point is that the refrigeration requirements of the coils being analyzed here are sufficiently great that all require "large" refrigerators, by such a standard.

Second, relative efficiency is a function of refrigeration temperature. The engineering problems which must be solved to maintain continuous operation at 4.2^{o} K are obviously more stringent than those confronted in designing for operation at 77.4^{o} K. Thus, not surprisingly, the relative efficiencies which have been attained in helium refrigerators are lower than those which have been attained in nitrogen refrigerators. To be specific, Fig. 18 has been prepared as a working estimate of the input power required, as a function of temperature, for "large", closed loop, continuous-operation cryogenic refrigerators. The "actual" curve is based on an estimate of the present state-of-the-art, with no allowance for anticipated future improvements. The Carnot cycle theoretical limit, as well as a few specific data points, are plotted for comparison.

FIGURE 18

Refrigeration Power vs. Temperature

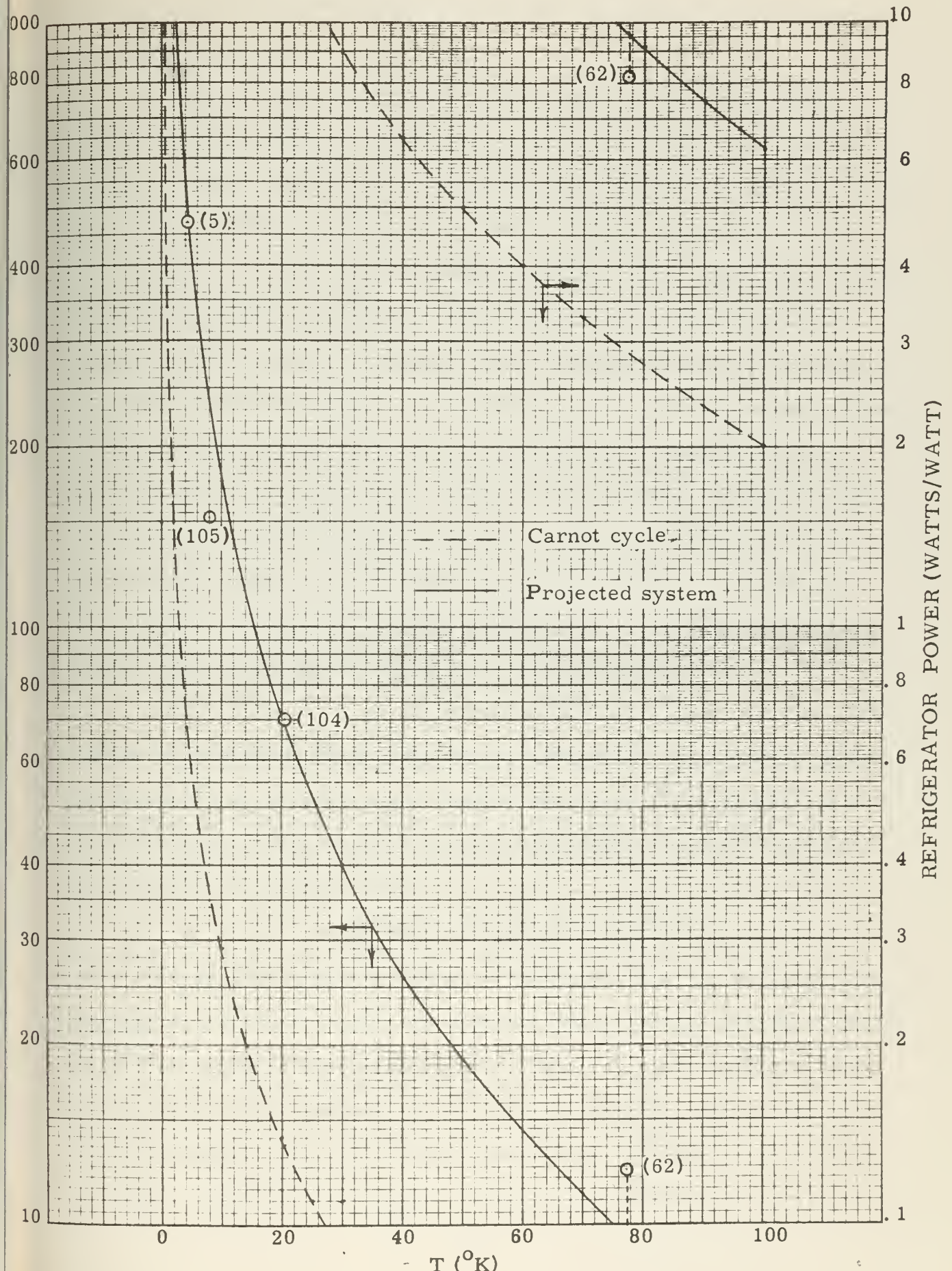

B. Other factors:

The steady-state refrigeration requirements of the saddle coils treated here generally exceed the refrigeration requirements of known cryogenic applications. Again, given the law of supply and demand, refrigerators of sufficient capacity to provide for these needs do not fall into the category of "on-the-shelf hardware". While it is felt that construction of such refrigeration systems is within the capability of existing technology, manufacturers are understandably discrete, regarding the specifications for systems which exist only "on paper". Further, extrapolation of size, weight, and cost figures from the region of current practice would appear to involve a greater degree of uncertainty than was the case with the efficiency figures quoted above. Regrettably, little concrete information regarding such factors is available in the open literature.

In any event, Bernert and Stekly (103) indicate that total refrigeration system mass might be estimated from the relationship:

$$M_s = 15.7 W_I^{0.24}$$

(where M_s is system mass in Kg and W_I refrigerator input power, in KW), for systems with an input power requirement in excess of 10 KW. In a separate article (106), Bernert indicates that capital costs for 4.2° K systems may be estimated from:

$$33\ W_R^{0.52} \leq C_s \leq 20\ W_R^{0.66}$$

(where) C_s is system cost in thousands of dollars, and W_R is refrigeration capacity at 4.2° K, in watts), for systems with a cooling capacity in excess of about 50 watts. Presumably, capital cost for a given cooling capacity should decrease as a function of temperature, probably even more rapidly than does system mass, considering the reduced complexity of the design problem. Certainly, one could scale the above cost estimate in proportion

to total system mass, to obtain a crude "first estimate" of the capital cost of systems operating above 4.2° K. However, for specific information regarding this factor, as well as the other factors mentioned in this section, one would be advised to turn to the various manufacturers' representatives.

V. HEAT TRANSFER

A. Basic concepts:

For various reasons, it is convenient to divide the treatment of heat removal into two separate areas: Heat transfer, discussed in this chapter, deals with the flux of energy from the windings, into the coolant, across a fluid-solid interface. (Here, two factors are of particular importance to the analysis of cryogenic coils: the amount of heat transfer surface required, and the relationship between rate of heat generation, and temperature rise between bulk coolant, and conductor.) Coolant flow, discussed in the next chapter, presupposes a given heat flux into the fluid stream, and explores the influence of this flux on the bulk flow properties of the coolant. (Items of interest will be the bulk temperature profile of the coolant, the relationship between inlet and outlet pressures, and packing factor, etc.)

It is also convenient to categorize the overall heat removal process as "single-phase", or "two-phase". The former term implies that the coolant is a liquid or a vapor, and that energy is removed by sensibly heating that liquid or vapor. The latter term implies that the coolant is a saturated liquid, and that energy is removed in the form of latent heat, by converting a portion of that liquid to vapor.

The analysis of single-phase heat removal is an inherently simpler task than that of two-phase heat removal. For purposes of preliminary analysis, one can characterize a single-phase coolant in terms of "mean" properties: Particularly, by a mean heat transfer coefficient and a mean specific heat. Since energy is removed in the form of sensible heat, the latter, coupled with the bulk flow rate, determines the mean temperature

rise in the bulk fluid. For the present application, there is an obvious interest in keeping this rise as small as practical. Suffice it to say, that coupled with the generally low visosities of cryogenic coolants, this leads to sufficiently high bulk flow rates as to ensure fully developed turbulent flow of the coolant. One can thus determine the mean heat transfer coefficient experimentally, or utilize an appropriate predictive correlation, since such correlations are reasonably accurate under these conditions. (Stevenson, for example, based his design of a gaseous-helium-cooled solenoid (107) on the McAdams correlation:

$$hD/k = 0.023P_r^{0.4}R_e^{0.8}, \qquad (24)$$

where h is the heat transfer coefficent; D, coolant tube diameter; k, thermal conductivity of the coolant; P_r, Prandtl number of the flow, and R_e, Reynolds number of the flow. See Rohsenow and Choi (108) for a discussion of this and other such correlations.) Given the mean heat transfer coefficient, the information required at this point can readily be determined. While it is apparent that considerable search may be necessary to determine the "optimum" operating pressure, etc., the procedure is conceptually straightforward.

By contrast, the analysis of two-phase heat removal is <u>not</u> straightforward: in general, predictive correlations are not sufficiently reliable as to permit accurate computation of the heat transfer coefficient. In fact, it would seem prudent--- if not mandatory--- to construct a precise model of any proposed heat transfer scheme, and obtain experimental confirmation of any theoretical predictions, before entering the final design stage. This would be particularly advisable in the design of large cryogenic saddle coils, as the size and complexity of the over-all system

would render any significant error in the anticipated heat transfer coefficient a most costly mistake.

The above notwithstanding, most of the cryogenic coils which have been built, to date, have utilized some form of two-phase cooling. For this reason, the rest of this chapter, and most of the next, will be devoted to a general discussion of that problem.

B. Pool boiling characteristics:

In a physical sense, the simplest form of two-phase heat transfer is that commonly called "pool boiling", in which a heated specimen is immersed in a large pool of liquid, and cooled by natural-convection boiling, with geometries sufficiently "open" to ensure negligible interference with convective flow. (These conditions can be approximated with small, "jelly-roll" solenoids, which are often cooled by simple immersion.)

The solid line in Fig. 19 is a qualitative representation of the sort of heat transfer curve which one might typically observe under such circumstances. To briefly discuss the regions of this curve:

Region I represents non-boiling convective cooling, and is characterized by low heat flux, and low heat transfer coefficient. (Note, however, that the "ΔT" referred to in Fig. 19 is $T_w - T_{sat}$. As the bulk liquid is subcooled, the wall temperature is only slightly greater than the saturation temperature, and "ΔT" is therefore small.)

Region II is the zone of "nucleate boiling" heat transfer, and is characterized by the formation of bubbles at discrete points distributed across the heat transfer surface: i.e., at surface imperfections, such as scratches, pits, etc. As the bubbles grow and break away from the surface, they are replaced by relatively cool liquid swept in from the

FIGURE 19

"Typical" Saturated Boiling Curves for Cryogenic Liquids

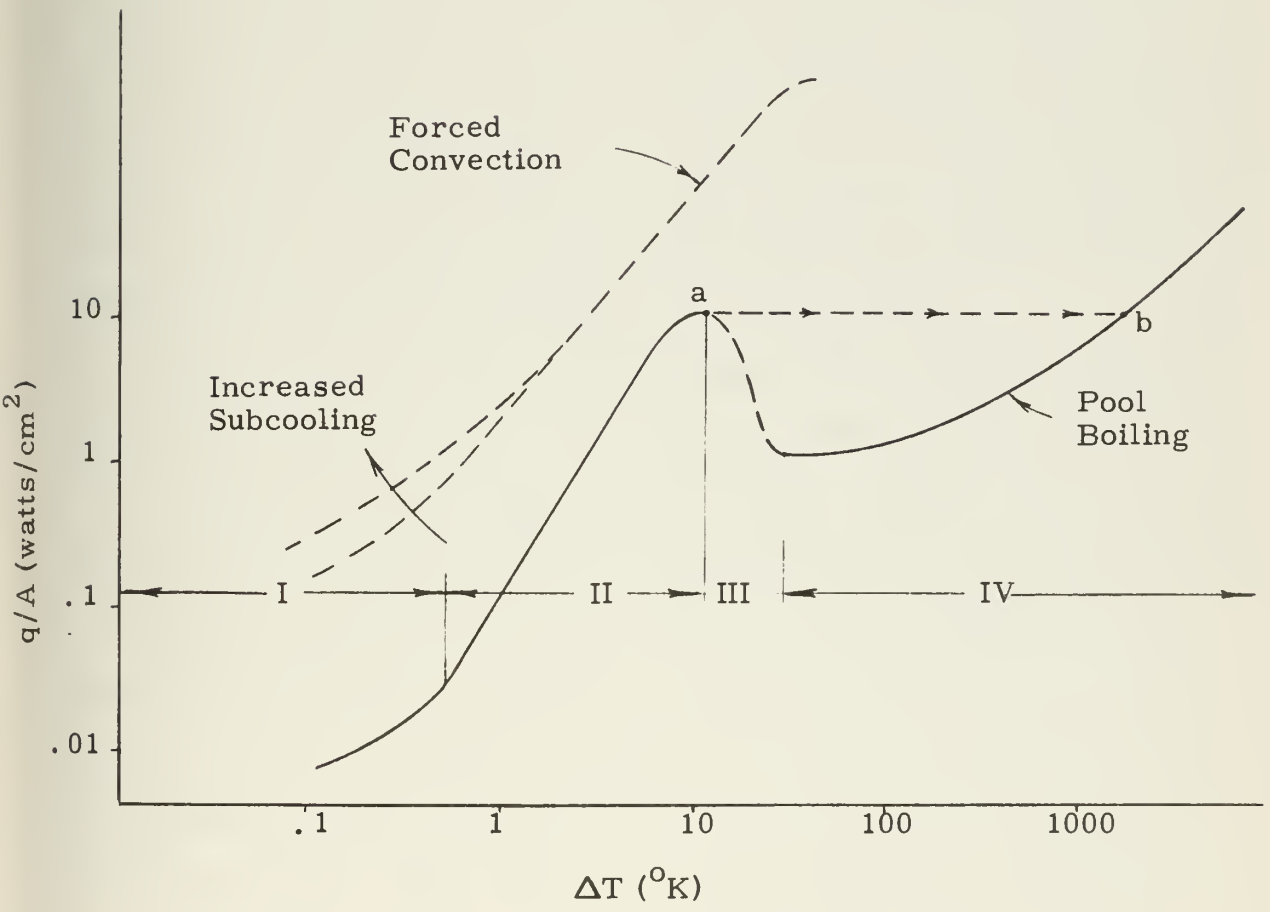

bulk of the fluid. This bubble agitation results in a rapid increase in heat flux with the number of "active" nucleation sites, as the primary flow of heat is across the surface into the relatively cool liquid. Since surface imperfections tend to have a random distribution in size, the number of active sites is a function of ΔT, with "large" sites becoming active before "small" sites.

Region III represents the gradual transition from "nucleate" to "film" boiling. In this region, generally called the "metastable film boiling" region, increasingly greater portions of the surface are blanketed by solid "sheets" of vapor. Under such "sheets", the cool liquid cannot come in contact with the surface. Since the thermal conductivity of the vapor is generally much lower than that of the liquid phase, heat flux actually decreases with increasing ΔT, in this region.

Region IV is the zone of fully developed "film boiling". Here, the entire heat transfer surface is covered by a stable vapor film, and as ΔT increases, heat flux again starts to rise. Finally, at very high ΔT, radiation effects become significant, and heat flux can become quite large.

The heat flux attained at the transition between regions II and III (point "a" in Fig. 19) is variously termed the "peak", "critical", or "burnout" flux. The last term is quite appropriate. If heat is generated at a constantly increasing rate in, say, an electrically heated device, upon reaching this point on the nucleate boiling curve, the operating point must "jump" to the corresponding flux on the film boiling curve (point "b" in Fig. 19), since the characteristics of the device would not permit the decrease in flux required for operation in region III. However, as indicated by the "typical" scale along the abscissa, the ΔT required to maintain the same flux in region IV is generally so large that the device might well melt before the operating point could reach the film boiling

curve.

C. Pool boiling data:

To turn from the general to the specific, four particular cryogenic coolants will be considered in this study: nitrogen, neon, parahydrogen, and helium. All but neon have been widely used by various experimenters, and if current trends continue (e. g., see (109) or (110)), liquid neon is likely to be widely used in the future. As coolants, these liquids effectively span the 0^{o}-100^{o}K temperature range of interest here. (One-atmosphere boiling points are 77.4^{o} K, 27.2^{o} K, 20.3^{o} K, and 4.2^{o} K, respectively. Of course, some control of boiling temperature is possible in each case by variation of operating pressures.)

For basic information regarding boiling heat transfer to liquid nitrogen or hydrogen, one is advised to turn to either of two excellent, recently published works:

Boiling Heat Transfer for Cryogenics, by J. D. Seader, W. S. Miller, and L. A. Kalvinskas (111), is a complete, 171-page survey of the literature on heat transfer to liquid hydrogen, oxygen, and nitrogen. This work discusses and evaluates both predictive correlations and experimental data, for pool boiling, forced-convection subcooled boiling, forced-convection saturated boiling and forced-convection film boiling to these liquids, and includes a twenty-page bibliography, as well as eighteen pages of physical property charts. The work is particularly valuable for its coverage of the largely neglected topic of cryogenic forced convection.

Nucleate and Film Pool Boiling Design Correlations for O_2, N_2, H_2, and He, by E. G. Brentari and R. V. Smith (112), presents an even more detailed survey of pool boiling data for nitrogen and hydrogen, and, as is

apparent, covers helium as well. The authors discuss the various factors which contribute most directly to "scatter" in observed data, and conclude that the general nucleate heat transfer correlation and maximum nucleate heat transfer correlation of Kutateladze (113) provide the best "a priori" design standards, when details of surface condition, orientation, geometry, etc. are not known. Specifically, these correlations state:

$$(q/A) = 8.54 \times 10^{-10}(c_p/h_{lv}\rho_v)^{1.50}(k\,\rho^{1.282}p^{1.750}/t^{.906}\mu^{.626})(\Delta T)^{2.50} \quad (25)$$

and

$$(q/A)_{burnout} = .157\, h_{lv}\rho_v{}^{0.50}(gt\Delta\rho)^{0.25} \quad (26)$$

where all properties pertain to the liquid phase, except those with subscript "v", and q/A is heat flux in watts/cm^2; c_p, specific heat at constant pressure, joules/gm-^oK; h_{lv}, latent heat of vaporization, joules/gm; ρ, density, gm/cm^3; k, thermal conductivity, watts/cm-^oK; p, pressure, dynes/cm^2; t, surface tension between liquid and vapor, dynes/cm; μ, viscosity, gm/cm-sec; ΔT in ^oK, and g is the acceleration due to gravity in cm/sec^2. (The bibliography provided in their work includes a section listing possible sources of information regarding thermodynamic properties.) More conveniently, Brentari and Smith provide a comparative plot of these correlations and available data, and a second plot of predicted q/A vs. ΔT, for various pressures (in atmospheres), for each liquid.

Unfortunately, very little experimental information is available at this time regarding the heat transfer characteristics of liquid neon, probably due to the hitherto limited supply. Hopefully, some data may soon be available as a by-product of the testing of the NASA-Lewis magnet (21, 22), but the only experimental report known to the author at this time is that of Bewilogua and Mahn (114). However, one can estimate the heat transfer characteristics from eqns. (25) and (26), and in fact, Frederking

(115) does present a plot of $q/A_{burnout}$, based on eqn. (26). (The National Bureau of Standards appears to be currently updating its information regarding the thermodynamic properties of neon. See, for example, (116) and (117).)

In any event, based on (112) and (115), one can construct a quick estimate of the nucleate boiling heat transfer characteristics of the four specified coolants, as follows: Assume the one-atmosphere "burnout" flux for nitrogen is 19 watts/cm^2, and that is occurs at a ΔT of 12^o K. Similarly, for neon the figures would be 12 watts/cm^2 at 3^o K; for hydrogen, 8.5 at 3^o K, and for helium, 0.77 at 0.4^o K. Plot these points on a log-log chart, and pass a line downward from each, at a slope of 2.5, to obtain the one-atmosphere characteristic. (Of course, since thermodynamic properties are a function of pressure, both eqns. (25) and (26) are functions of pressure. In general, these characteristic lines shift toward lower ΔT's as pressure is increased. The locus of the burnout point, as a function of pressure, is (roughly) a concave-downward arc. Helium exhibits its maximum burnout flux at about one atmosphere. For the other liquids, the maximum is roughly: nitrogen, 37 watts/cm^2 at $\Delta T = 6.6^oK$ (p = 10 atm.); neon, 18.6 at 1.3^oK ($\sim$8.5 atm.), and hydrogen, 13.2 at 1.6^oK (4 atm.).

Again, it must be stressed that this is a rather crude "first estimate". Equation (25) is a reasonable, slightly conservative "mean", and is probably an excellent guess for "average" conditions. However, conditions may deviate considerably from "average", as evidenced by the fact that results reported by some experimenters lie more than a factor of 5 above or below this correlation. For this reason, it may be worthwhile to briefly discuss a few of the factors which lead to deviation from the norm:

Surface condition: As mentioned above, heat flux varies with the number of active nucleation sites, which among other things is a function of the size distribution of surface imperfections. Thus, a mirror finish would hinder nucleate boiling heat transfer, and data points taken from specimens with such a finish fall well below the norm. Conversely, an artificially roughened surface improves nucleate boiling heat transfer. (See, for example, (118).) Further, the number of active sites is a function of the extent to which a particular liquid "wets" the surface. Any coating or contaminant which decreases "wettability" of the surface will tend to increase heat flux. Cowley, et al. (119) report that artificially greased surfaces can be driven to 50%-100% higher flux levels before burnout, though such surfaces exhibit "below normal" flux levels at subcritical ΔT's. Here, the dominant factor is the poor thermal conductivity of grease. The presence of such an "insulating layer" ($\sim$ 0.2 mm thick) causes a four- to ten-fold increase in total ΔT (between the bulk liquid and the surface) at burnout. The greatest portion of this total ΔT occurs in the insulating layer, and oddly enough, results in a temperature profile which drives a greater heat flux through the insulation, into the liquid, than could be driven directly from the surface into the liquid. The authors state that such use of insulation should increase maximum heat flux in any situation in which heat transfer is initially limited by conditions on the liquid side of the interface.

Surface history: A given surface will generally exhibit greater heat flux when first immersed in coolant, than after repeated measurements under the same conditions. This is partially attributable to the boil-off of surface contaminants, but is probably more dependent upon the initial presence of adsorbed gases. Haselden and Peters (120), having taken pains to ensure an initially clean surface, found that such transients per-

sisted for as long as 2 to 3 hours. Experimenters who do not choose to wait for such an interval, to ensure that consitions have stabilized, may find that their data predict higher heat fluxes than can be maintained for steady-state operation.

Surface orientation and geometry: Although nucleate pool boiling is not particularly sensitive to device geometry, any features which alter the circulation pattern associated with "normal" natural convection (and therefore cause deviation from the strict definition of "pool boiling") will have some influence on nucleate boiling heat transfer. For example, confined channels may tend to become "clogged" with vapor, to such an extent that the churning action associated with nucleate boiling is inhibited. This would sharply reduce attainable heat flux. Similarly, heat transfer from a "bottom" surface may be hampered in a gravity field, since bouyancy may impair the normal motion of bubbles away from the surface. Variations in convective circulation can also cause minor differences between measurements taken near the ends of a test specimen, and those taken near the center. However, by far the most critical of these geometric factors is the marked decrease in attainable heat flux in confined channels. Since this is precisely the type of geometry anticipated in the cooling systems of large coils, natural convection cooling is not an attractive solution for such applications.

D. Qualitative influence of forced convection:

The obvious solution to the problem of "confined geometry" coolant ducts is to turn to forced convection. In addition to the "microscopic" processes discussed above, this adds a new form of turbulent mixing to the heat transfer process: i. e., the "macroscopic" circulation of forced flow. Qualitatively, the effect on the nucleate boiling curve is as depicted

in Fig. 19. In general, the increased heat flux attributable to forced flow can always be made to offset--- or more than offset--- the decrement in attainable flux due to confined geometry. At low qualities, forced convection produces a sharp increase in both heat transfer coefficient, and burnout flux. As quality increases the heat transfer coefficient increases even more (as shown in Fig. 20a), until transition to film boiling occurs, after which the heat transfer coefficient decreases sharply. The forced convection burnout flux decreases more or less linearly with quality, as shown in Fig. 20b. However, even at high qualities, one might reasonably expect the forced convection burnout flux to exceed the pool boiling burnout flux.

The heat flux attained under forced flow conditions is often conceptually divided into its two component parts: one attributable to pool boiling processes, and the other attributable to forced convection. Actually, the physics of the problem are not quite that simple. As the Reynold's number of the flow is increased, nucleation is gradually suppressed. As the quality (mass fraction of vapor) of the flow is increased, the flow of relatively large volumes of vapor along the tube increases the convective turbulence attributed to forced flow. Eventually, a point is reached where the contribution of "microscopic" heat flux is entirely negligible, but by this point, the "macroscopic" heat flux may be much greater than that predicted from eqn. (24). Seader, et al. (111) present a detailed discussion of the predictive correlations which attempt to cope with these interrelated complications, but in general, such correlations have not met with marked success, when applied to "conventional" coolants. Data for forced convection saturated boiling heat transfer to cryogenic coolants is so scarce that one can hardly say the various correlations have been fairly tested, for cryogenic coolants.

FIGURE 20a

Qualitative Variation of Heat Transfer Coefficient with Quality

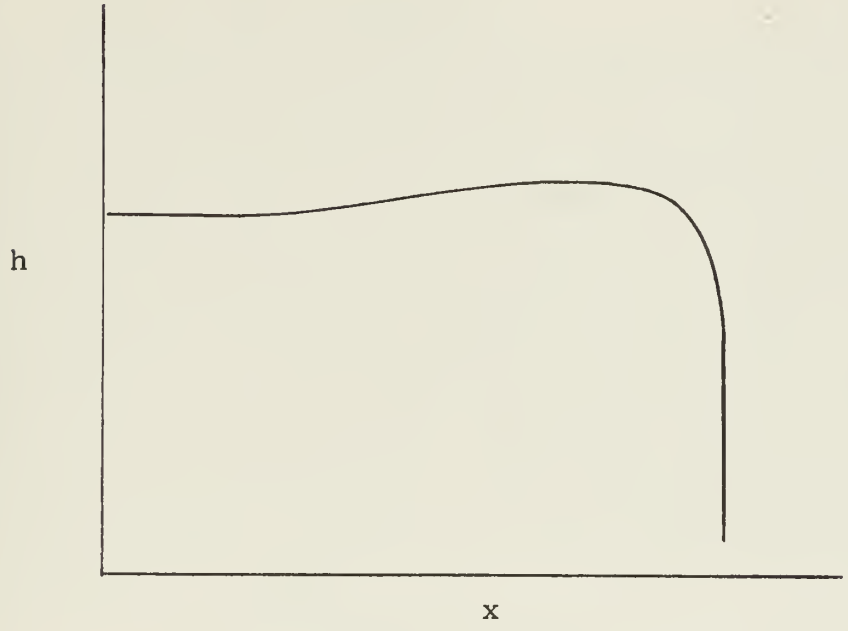

FIGURE 20b

Qualitative Variation of Critical Flux with Quality

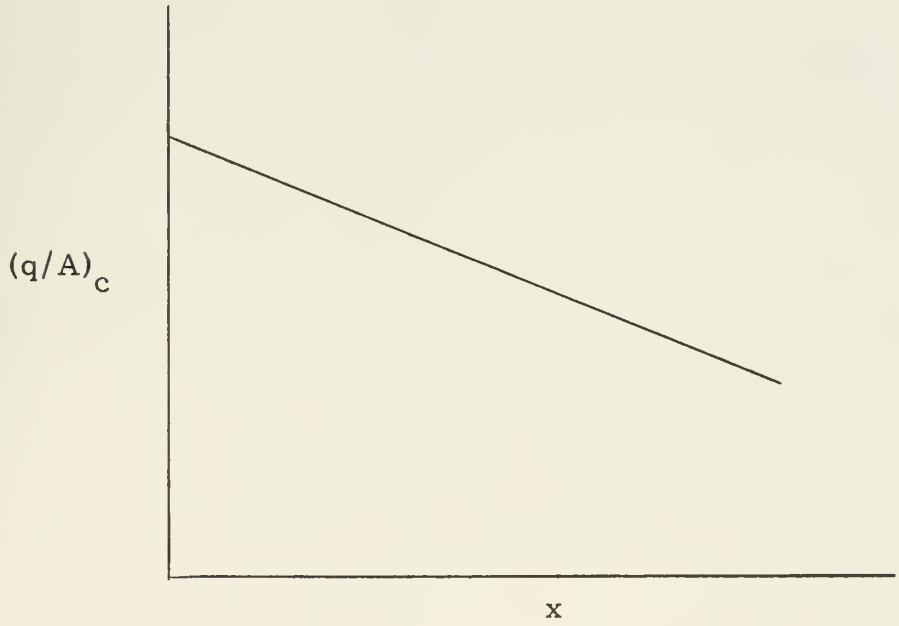

In any event, it would appear that the most successful such correlation, to date, is that developed by Chen (121):

$$q/A = (h_{FC}F + h_{PB}S)\,\Delta T, \qquad (27)$$

where h_{FC} is the forced convection heat transfer coefficient, which could, for example, be computed from eqn. (24); h_{PB} is the pool boiling heat transfer coefficient, which could be computed by dividing eqn. (25) by ΔT; F is an empirical amplification factor which corrects for increased heat flux due to increased convective turbulence at high quality, and S is an empirical attenuation factor, which corrects for the suppression of nucleation at high liquid flow rates. Both (111) and (121) present plots of F as a function of the Martinelli two-phase parameter, X_{tt}, and S as a function of $R_{eL}F^{1.25}$, where

$$X_{tt} = \left(\frac{1-x}{x}\right)^{0.9}\left(\frac{\rho_v}{\rho_L}\right)^{0.5}\left(\frac{\mu_L}{\mu_v}\right)^{0.9} \qquad (28)$$

(here, x is quality, and the other parameters are as defined above), and

$$R_{eL} = DG(1-x)/\mu_L \qquad (29)$$

(where G is the mass flow rate divided by the tube cross sectional area). As a practical matter, the plots provided in (111) are, perhaps, somewhat easier to work with.

It is apparent that the use of this correlation to predict heat flux <u>at a single point</u> along a coolant duct is no minor task, unless the problem has been prepared in advance for computer solution. Further, since both eqn. (28) and eqn. (29) are functions of quality, it is necessary to evaluate eqn. (27) at many points along such a duct, if a "mean" flux is to be determined for purposes of preliminary analysis. Chen has tested this correlation against available data for vertical, axial, stable flow, at heat fluxes below the critical, for water and various hydrocarbons, and found an <u>average</u> deviation of only ± 11 percent, for a quality range of 1 to 71

percent. This achievement is truly remarkable, considering the complexity of the problem! However, individual points may deviate considerably more than the "average", and forced convection heat transfer is more sensitive to geometry and orientation than pool boiling heat transfer. Considering this, and the scarcity of data for two-phase forced convection heat transfer to cryogenic coolants, it should be stressed again that experimental confirmation of heat transfer characteristics should be obtained before proceeding into the detailed design phase.

Under the above circumstances, it is doubtful that the considerable labor involved in the use of Chen's correlation is justifiable for purposes of preliminary analysis. Instead, it is recommended here that the procedure for determining pool boiling heat transfer characteristics, as described in the preceding section, be applied with no correction for forced flow. This procedure has the advantage of being quicker, simpler, and conservative, since the forced convection heat transfer characteristics should be as good as, or better than, this estimate. (It is noted that Frederking (122) specifies that heat flux under conditions of forced convection will always exceed predictions from a pool boiling analysis if quality is low. However, Chen's correlation is less restrictive than this, since fluxes predicted from his model exceed the pool boiling figures up to the limiting quality of 70%.)

VI. COOLANT FLOW

A. Geometric considerations:

While heat flux considerations may determine the amount of heat transfer surface required for a particular coil, the specification of cooling system geometry is far from complete. The required surface area could be provided in a single large coolant duct, or many small ducts, and the choice between these extremes must be based on considerations other than heat flow alone, such as the resulting packing factor, pressure drop across the coil, thermal gradients in the winding, ease of assembly, etc., etc.

To deal with the last item, in particular: The natural tendency would be to assume some specified distribution of circular tubes, of some given L/D. This would be motivated in part by historical precedent, and in part by convenience: Most conventional heat transfer devices utilize circular tubes; we are accustomed to thinking in terms of circular tubes, and the great majority of the correlations used in heat transfer and coolant flow analyses are based on circular tube data. Unfortunately, circular tubes are not likely to be used in "real" cooling systems for coils of the type being considered here, for precisely the same reason that they are used in so many other applications: i.e., ease of manufacture.

Whatever provisions are made for coolant flow must conform to the realities of coil construction. For example, it was shown in Chapter III that the internal support structure required to support the conductors against magnetic stress must run axially down the length of the cylindrical lobes. Thus, it is reasonable to assume that the coolant ducts must run axially: any other geometry would require the ducts to penetrate such structural members, which would be highly undesirable, if not impossible. Further, cooling ducts cannot be run through regions in which they would

be subjected to a heavy stress load. This would require that they have thick walls, for mechanical strength, which would extract a double penalty: reduced heat transfer, and reduced packing factor. Since structure has already been provided to support the conductors, it is reasonable to assume that coolant ducts would be located contiguous to that structure: stress levels are at a maximum on one side of each support shell, but total stress is virtually zero on the other side. A coolant duct, run along the "no-load" side of such a shell, would require a minimum of structural support. This fact is conducive to the use of coolant slots, vice tubes, or pipes. Of course, the model described in Chapter III calls for a greater number of support members in regions of high magnetic fields, since these are the regions of greatest magnetic force density. These are also the regions where magnetoresistance, and therefore heat generation, would be greatest. It is convenient that a greater number of coolant slots would be provided automatically in this region, under the proposed scheme.

Thus, the basic geometry considered here will involve the use of axial slots for coolant flow, with one side of each slot bounded by the internal support structure of the coil. It will be assumed that the height of such slots would be much less than all other significant dimensions (width, length, and radius of curvature), and coolant flow will therefore be handled on a "per unit width" basis. Since the most likely structural material is stainless steel, and since the thermal conductivity of stainless steel is two to four orders of magnitude less than that of the electrical conductors considered here, at the temperatures of interest, it will be assumed that heat enters each coolant slot only across the surface "away from" the support shell. (So far as it involves the results of this analysis, one can treat the possibility of heat input through both surfaces by simply doubling the attainable heat flux which would otherwise be estimated from

the preceding chapter.) Again, the purpose of this analysis will be to determine the relationships between coolant properties, pressure, quality, and heat flux, as "input" variables, and packing factor, coolant pump power, and axial temperature variation, as "output" variables.

B. Properties of coolants:

Since coolant properties are a necessary input to this analysis, it would be well to consider them before proceeding further. In particular, since the primary effort here will be devoted to an analysis of two-phase cooling, the saturation properties (i.e., the thermodynamic properties of a saturated liquid and its vapor, at least nominally under equilibrium conditions) are of especial interest. In fact, an interesting problem exists regarding the processing of this data. Because the coolants considered (helium, parahydrogen, neon and nitrogen) will be examined at pressures approaching their respective critical pressures, such customary and convenient concepts as "incompressible" liquids, and "perfect" gases, are not generally applicable. Further, many pertinent properties exhibit sufficiently non-linear behavior, within the range of interest, as to raise doubts regarding the accuracy of such techniques as linear interpolation between tabulated values. As a convenient means to avoid these complications, a data fitting routine was used to generate a least-square polynomial fit, expressing each such property of interest as an explicit function of pressure, in atmospheres. Specifically, the properties of specific volume of saturated liquid and vapor, saturation temperature, specific enthalpy of the saturated liquid, and heat of vaporization, were expressed as polynomials of the below form:

$$1/\rho_l = a_1 + a_2 p + a_3 p^2 + a_4 p^3$$

$$1/\rho_v = b_1/p + b_2 + b_3 p + b_4 p^2 + b_5 p^3 + b_6 p^4$$

TABLE 6

SATURATION PROPERTY COEFFICIENTS

Property		Helium	Parahydrogen	Neon	Nitrogen
$1/\rho_L$	a_1 =	5.45596	13.3964	0.767861	1.18952
	a_2 =	5.09263	0.796955	0.0675544	0.0559020
	a_3 =	3.69782	-0.0606407	-0.00664262	-0.00437871
	a_4 =	1.15685	0.00500739	0.000224027	0.000195317
Deviation =		0.058%	0.041%	under 0.01%	0.074%
$1/\rho_v$	b_1 =	49.3439	654.454	101.175	195.349
	b_2 =	31.7682	128.968	0.394318	29.5132
	b_3 =	-32.7486	-41.6982	3.23665	-8.96109
	b_4 =	15.3537	6.73209	-0.949753	1.49260
	b_5 =	-4.01758	-0.563735	0.0978116	-0.126834
	b_6 =	0.281743	0.0181262	-0.00343717	0.00420598
Deviation =		under 0.01%	0.100%	0.561%	0.059%
T	c_1 =	2.67907	16.4517	23.1925	67.7503
	c_2 =	2.04654	4.71658	5.04433	11.9973
	c_3 =	-0.461891	-1.00566	-1.25994	-2.66612
	c_4 =	-0.180713	0.144354	0.207938	0.392040
	c_5 =	0.158552	-0.0108406	-0.0176176	-0.0300996
	c_6 =	-0.0309227	0.000323253	0.000582154	0.000918179
Deviation =		under 0.01%	0.049%	0.038%	0.035%
h_L	d_1 =	-28.9212	-293.057	-2.09216	9.57010
	d_2 =	139.468	43.7316	8.43141	24.7498
	d_3 =	-211.281	-7.27746	-1.56955	-5.51273
	d_4 =	163.231	1.05418	0.201394	0.820578
	d_5 =	-61.7927	-0.0791551	-0.0130336	-0.0632501
	d_6 =	9.19968	0.00245513	0.000326842	0.00193276
Deviation =		under 0.01%	0.033%	0.721%	0.134%
h_{LV}	e_1 =	58.3544	462.481	91.6010	214.510
	e_2 =	-137.426	-14.4022	-7.50772	-18.9988
	e_3 =	211.270	-1.53707	1.64718	4.77690
	e_4 =	-163.972	0.159357	-0.200480	-0.789073
	e_5 =	61.7927	-0.00838393	0.0130336	0.0632501
	3_6 =	-9.19968	0.00245513	-0.000326842	-0.00193276
Deviation =		0.035%	0.015%	0.693%	0.148%

$$T = c_1 + c_2 p + c_3 p^2 + c_4 p^3 + c_5 p^4 + c_6 p^5$$
$$h_l = d_1 + d_2 p + d_3 p^2 + d_4 p^3 + d_5 p^4 + d_6 p^5$$
$$h_{lv} = e_1 + e_2 p + e_3 p^2 + e_4 p^3 + e_5 p^4 + e_6 p^5$$

where specific volumes are given in cm^3/gm, temperature in ^oK, and enthalpies in joules/gm. The coefficients a_i, b_i, etc., are tabulated below. The particular functional forms indicated ensure, in all cases, that the accuracy of "fit" exceeds the assumed accuracy of the flow models developed here, within the pressure ranges investigated: i.e., 1-10 atmospheres for saturated nitrogen, neon, and parahydrogen, and 1-2 atmospheres for saturated helium. (The lower limit of 1 atmosphere was set because it was felt that considering the hazard of leakage, no one would care to design a cryogenic cooling system, for a working coil, to operate at sub-atmospheric pressures. The upper limits were set, as a practical matter, considering the decrease in heat of vaporization, and increase in coil operating temperature, at increased operating pressures.) The "deviation" indicated for each set of coefficients is the mean of the absolute value of the difference between "input" property values, and property values generated from the indicated polynomial.

One other general point might be mentioned before turning to the particular: If two-phase cooling is contemplated, one would presumably attempt to operate to a relatively high outlet quality, since pumping "unused" liquid through the cooling loop increases pump capacity, and increases duct size, while contributing nothing to the removal of heat from the coil. In practice, outlet quality must be limited by heat transfer considerations (more on that, later!), but if attainable qualities even approach the range indicated by the upper limit of Chen's correlation, it should be recognized that the outlet stream, from a volumetric viewpoint, will be almost entirely vapor: a "typical" figure would be 99% vapor, for a quality of 50%. As

vapor densities tend to be relatively low, momentum considerations indicate that relatively high vapor outlet velocities may result from relatively low pressure drops: i.e., it is quite possible that the flow could "choke" at, or even before, the outlet. If this is to be avoided, outlet velocities must not be allowed to approach the sonic velocity in the stream. (Note that this would be the so-called "sonic velocity of Mach 1", which Shapiro (123) denotes "c*", not the velocity of sound under stagnation conditions.) The problem here is to determine just what the limiting velocity should be. The only available data are for c_o, the sonic velocity under stagnation conditions. Shapiro shows that for perfect gases:

$$c^*/c_o = \sqrt{2/(\gamma + 1)},$$

where $\gamma = c_p/c_v$ = the ratio of specific heats. However, we are not dealing with perfect gases, and in any event, the sonic velocity in the mixed-phase coolant stream would presumably be lower than that in the vapor, under conditions of 100% quality. Considering these uncertainties, a "limiting velocity" has been defined for each coolant, by using the best available information for c_o and γ at the one atmosphere saturation point, computing c* as above, and multiplying the result by roughly 0.8. In the subsequent analyses, combinations of parameters which would result in flow velocities greater than this limiting velocity will not be considered. The values of γ, c_o, and v_{lim} are presented below, along with other specific information of interest for each coolant.

Helium: (Property values determined form (102, 110) and (124-127). Saturation property polynomials developed from (127).)

one-atmosphere boiling point:	4.22°K
critical point:	5.25°K at 2.26 atm.
ratio of specific heats:	~1.74
sonic velocity:	~145 m/s
limiting velocity:	100 m/s

Considering its low heat of vaporization, and the high cost of 4.2°K

refrigeration, liquid helium is not likely to be used as a two-phase coolant for cryogenic coils, except when cryogenic conductors are used to "stabilize" superconducting coils. (See, e.g., (14).) However, supercritical helium is the logical coolant for coils designed to operate in the vicinity of 10^{o}K (24, 107). The National Bureau of Standards indicates that the optimum operating pressures for such applications lie in the band 15-20 atm. (105). The required coolant volume fraction is not a strong function of pressure, in this range, since the increase in density as pressure is increased from 15 to 20 atm. is largely offset by a decrease in specific heat.

Parahydrogen: (Property values determined from (102, 110, 124-126) and (128-131). Saturation property polynomials developed from (131), except that for liquid specific enthalpy, which was developed from (130).)

one-atmosphere boiling point:	20.27^{o}K
critical point:	32.98^{o}K at 12.76 atm.
ratio of specific heats:	1.803
sonic velocity:	357 m/s
limiting velocity:	250 m/s

Hydrogen gas occurs in two molecular forms, orthohydrogen and parahydrogen, distinguished by the relative direction of nuclear spin of the two component atoms of the molecule. At room temperature, the equilibrium composition is 75 per cent ortho, 25 per cent para. However, at 20.3^{o}K, the equilibrium concentration is about 99% parahydrogen. Since the energy released during conversion is greater than the latent heat of vaporization, this reaction must be catalyzed to completion if liquid hydrogen is to be used continuously in closed-loop cooling systems. Presumably, the composition would not change significantly during the brief period required for the liquid to pass through the coils of a magnet. For these reasons, the properties discussed here are those of liquid parahydrogen.

Basically, liquid hydrogen is a highly promising coolant for cryogenic coils, because of its availability and low boiling point. Although some concern has been expressed regarding the safety of this particular coolant, those who have worked with liquid hydrogen (notably, (19, 20) report "no problems", provided reasonable precautions are observed. (See NBS Report 7253 (132) for a list of safety precautions.) It would seem reasonable to presume that the hazards involved in the use of this coolant in closed-loop systems would be less severe than is the case with open-loop systems, where large volumes of hydrogen gas must be stored or vented.

Neon: (Property values determined from (102, 110, 133) and (116). Saturation property polynomials developed from (116).)

one-atmosphere boiling point:	27.09°K
critical point:	44.40°K at 26.19 atm.
ratio of specific heats:	~1.7
sonic velocity:	134 m/s
limiting velocity:	90 m/s

As has been discussed above, liquid neon has not been widely used as a cryogenic coolant, to date, because of its hitherto limited availability and high cost. Specific advantages attributed to this liquid as a coolant are a relatively high latent heat, on a per-unit-volume basis, and ease of temperature control through pressure regulation. In addition, liquid neon is the only two-phase coolant available which permits maintenance of temperatures near the liquid hydrogen range, without the hazards associated with liquid hydrogen.

Nitrogen: (Property values determined from (102, 124-126, 128, 129) and (134). Saturation property polynomials developed from (134).)

one-atmosphere boiling point:	77.4°K
critical point:	126.1°K
ratio of specific heats:	1.44
sonic velocity:	~167 m/s
limiting velocity:	120 m/s

Nitrogen might be described as the "old standby" cryogenic coolant,

and apparently is used in many applications primarily because its properties are well known, it is readily available in large quantities, and it can be handled with relative ease. However, although various "laboratory" coils have been tested in liquid nitrogen, Tables 1-4 indicate that the temperatures attainable with this coolant are too high to permit realization of the full potential of cryogenic magnets. It is unlikely that large "working" coils would be designed for two-phase liquid nitrogen cooling.

C. Single-phase flow:

Aside from the concepts discussed in the preceding chapter, the only design factor essential to the preliminary analysis of single-phase cooling is the question of pressure drop across the coil. The customary manner of estimating this pressure drop would be to do so in terms of an effective friction factor, f:

$$p = 4 f (L/D)(\rho v^2/2), \qquad (30)$$

where one would again utilize "mean" property values, and where L is the estimated duct length, which would presumably be of the order of the MHD channel length (or, perhaps, the product of that length times the form factor, defined in eqn. (6)). For non-circular cross sections, D would be the "equivalent" or "hydraulic" diameter, given by:

$$D = 4 A/P \qquad (31)$$

where A is the duct cross-sectional area, and P is the wetted perimeter. (For a rectangular slot, of the type discussed previously, $4A \rightarrow 4ws$ and $P \rightarrow 2w$, so $D \cong 2s$, since slot height $s \gg$ slot width w.)

Various estimates are available for the value of f, given fully developed turbulent flow conditions. Rohsenow and Choi (108) suggest:

$$f = 0.0791/R_e^{0.25}, \quad 3 \times 10^3 < R_e \leq 2 \times 10^4 \qquad (32)$$

or (32)

$$f = 0.046/R_e^{0.20}, \quad R_e \geq 2 \times 10^4 .$$

Stevenson (107), on the other hand, uses:

$$f = 0.0014 + 0.125/R_e^{0.32}. \quad (33)$$

(In both eqns. (32) and eqn. (33), $R_e = \rho vD/\mu$.)

Having established an estimated bulk flow rate (from mean temperature rise considerations), the above Δp can be used to determine the power required to pump the coolant through the loop, since

$$P \cong Fv \cong (A\Delta p)v - w\Delta p/\rho \quad (34)$$

where w is now the mass flow rate. Of course, this term represents energy added to the coolant stream, which is converted to heat by friction, and is therefore an added refrigeration load. However, one would anticipate that this load would normally be negligible, compared to I^2R heating. Eqn. (34) can be used to verify this fact, as well as to "size" the pump required for a particular coil. Once again, the procedure is relatively straightforward, and a great deal simpler than the analysis of two-phase flow.

D. Two-phase flow:

Considering the lack of experimental data for forced-convection two-phase cryogenic cooling, the information required for coolant flow calculations must be generated from an analytical model. The problem becomes to select that model which is most likely to correspond to the physical realities of the situation, under these circumstances. Two possibilities will be developed and discussed here, but the ultimate choice must await additional testing.

To turn, first, to background considerations: Sydoriak and Roberts (128) conducted one of the few studies of two-phase cryogenic coolant flow

in confined channels, for both natural and forced convection, and report close correlation between their data and "calculations based on a frictionless flow boiling theory". In essence, the pressure drop due to the always-low viscosity of cryogenic fluids was totally dominated by that attributable to acceleration of the vapor phase (as required to maintain a given flow rate when a quantity of relatively dense liquid is converted to relatively light vapor). The pressure drop associated with any such "inviscid" acceleration can be computed from momentum considerations, provided certain basic information is available regarding flow conditions in the duct.

Chen (121) classifies the possible flow conditions, as depicted in Fig. 21:

Zone 1, at the inlet, represents subcooled conditions, as would be encountered when the saturated liquid, from a heat exchanger, passes through a pump, with resultant increase in pressure, but little increase in temperature. In this region, there is either no generation of vapor, or formation of bubbles, at the duct wall, which decrease in size as they depart the thermal boundary layer.

Zone 2 represents the region of first net generation of vapor. Here, bubbles are formed at the heat transfer surface, break away, and move into the (now saturated) liquid phase. Quality is low, and aside from the convection down the duct, conditions are rather similar to "nucleate pool boiling".

By zone 3, sufficient vapor has been generated that the individual bubbles tend to merge, forming relatively large "blobs" of vapor which accelerate down the duct. Nucleation is gradually suppressed. This flow condition is characterized as "slug flow".

Eventually, the center of the duct becomes filled with an unbroken stream of vapor, as in zone 4, and an effective separation of the phases

FIGURE 21

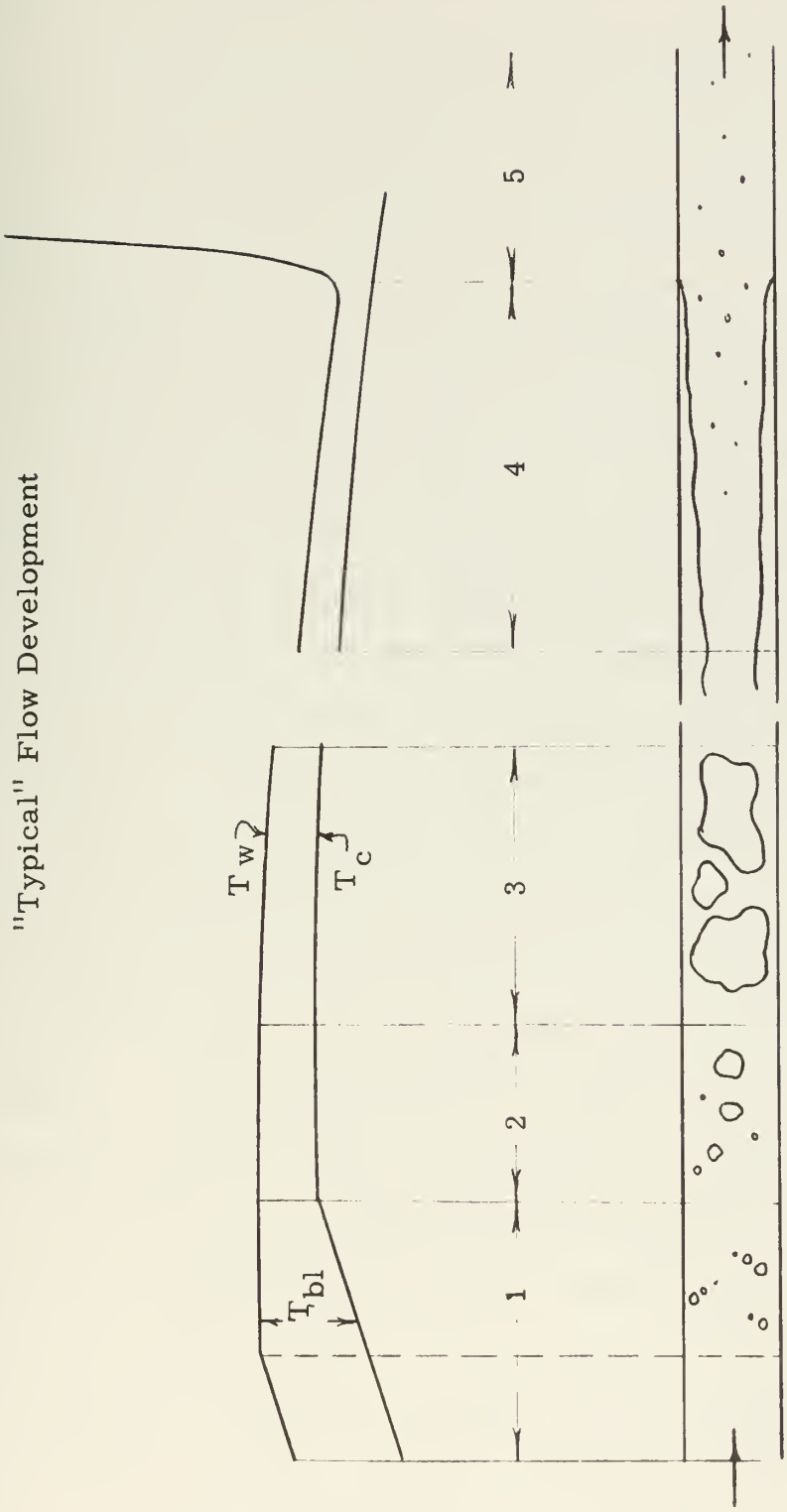

occurs. As Chen's work dealt with circular tubes, he called this the "annular flow" regime. Although some liquid is carried with the vapor in mist-like droplets, the bulk of the liquid phase moves along the walls of the tube.

Finally, as quality increases, the tube walls gradually become dry and zone 5, the "liquid deficient zone", is entered. All the remaining liquid, in this zone, is swept along in the form of droplets, dispersed through the vapor phase.

Actually, the scale of Fig. 21 is distorted. Chen's correlation was based upon the assumption of annular flow conditions, and as mentioned above, is held to be valid, generally, within the range 1 to 71 per cent quality, for the vertical, circular-tube geometry which he investigated. However, the fact that he determined this to be true for one geometry is no assurance that it will be true for other geometries. The various regimes may be less clear-cut, with some zones missing, others enlarged, or mingled. The sequence depicted here is "idealized", and deviations from this sequence are important in two respects: first, flow conditions in zone 4 are most nearly typified by separate, inviscid flow of the liquid and vapor phases, with no mixing between the phases. Zone 5, and perhaps zones 1 and 3, are better typified as inviscid flow, with the boundry condition of "no slip" between the phases. Thus, any shift in the relative importance of these zones would presumably require a shift in the analytical model used to represent flow conditions. Second, when the tube walls become dry, the heat transfer coefficient drops abruptly, due to the low thermal conductivity of the vapor phase, which then contacts the heat transfer surface. If zone 5 is entered at qualities significantly below 70%, for a particular geometry, the outlet quality for a coil cooled by such a system would perforce be limited to such lower qualities. In other words, the fact

that Chen has proven that heat transfer improves with quality if annular flow conditions are maintained, does not, a priori, guarantee that such conditions will be maintained. Again, conditions must be confirmed for the particular application contemplated.

Bearing this in mind, two inviscid flow models will be examined below:

No slip (mist flow) model: Of the two limiting conditions discussed above, the simpler, from an analytical viewpoint, is that assuming no slip between the phases. If either phase is assumed to be dispersed through, and moving with, the other, the resultant two-phase flow can be treated as a hypothetical, homogeneous fluid with properties which are appropriately averaged between those of the liquid and the vapor. Specifically, let us assume steady, inviscid, one-dimensional flow, traversing a slot of constant, but as yet unspecified height, of unit width, and of some length L. The variable z will be used to denote distance from the inlet of the slot (x will refer to quality). It will be assumed that the flow has just reached zero quality at the slot inlet (i. e., $x=0$ at $z=0$), and is subjected to a constant heat flux, q/A, between $z=0$ and $z=L$. (This last is equivalent to the assumption that heat transfer to "real" liquids, which is known to be a function of quality, can be expressed in terms of an effective "mean" q/A.) With an eye toward eventual applications, it will be assumed that outlet pressure, and desired outlet quality, are specified, and that we desire to investigate the relationship between inlet pressure (or, equivalently, pressure drop across the slot), inlet velocity, and slot height. The axial distribution of temperature, velocity, etc. will also be of interest, and in particular, the solution for each combination of parameters must be tested to ensure that the outlet velocity does not exceed the limiting velocity, defined in Section B of this

chapter.

An iterative approach will be used to accomplish these objectives. In order to investigate the influences of inlet pressure, that parameter will be systematically incremented, as:

$$p_i = p_e + n\Delta p \qquad n = 1, 2, 3\text{-----}$$

By use of the saturation property polynomials, all pertinent thermodynamic properties at the inlet and outlet can be determined, once p_i and p_o have been specified. However, the "appropriately averaged" density of the "homogeneous" fluid is required, to relate these variables to flow rate. To quantize this concept: one gram of coolant, in the duct, is by definition comprised of x grams of vapor, and (1-x) grams of liquid. The vapor occupies a volume of x/ρ_v cubic centimeters, and the liquid, $(1-x)/\rho_l$. Since the total volume occupied by this gram of coolant is, by definition, the specific volume of the hypothetical fluid, the "appropriately averaged" density is defined as:

$$\rho = \frac{1}{x/\rho_v + (1-x)/\rho_l} \qquad (35)$$

Since we are considering a slot of unit width, continuity implies:

$$w = \rho vA = \rho vs = \text{const.}, \qquad (36)$$

where w is the mass flow rate, v the common velocity of the two phases (or of the "homogeneous" fluid), and s the still undetermined slot height. However, since s is constant,

$$\rho v = \text{const.} = \rho_i v_i \qquad (37)$$

(here, as elsewhere, subscript "i" refers to inlet properties). Under the stipulated flow conditions, the momentum equation can be integrated directly, between inlet and outlet, to yield :

$$-\Delta p = p_o - p_i = (\rho_i v_i)\Delta v = (\rho_i v_i)^2(1/\rho_o - 1/\rho_i) \qquad (38)$$

Since the only unknown in the above is v_i, we can immediately state:

$$v_i = (1/\rho_i)\sqrt{|\Delta p|/(1/\rho_o - 1/\rho_i)} \qquad (39)$$

The same relationship can also be solved for v_o, which can immediately be checked against the specified limiting velocity:

$$v_o = v_i + \quad p \;/\; {}_i v_i \qquad (40)$$

Assuming $v_o < v_{lim}$, we proceed: Since inlet quality was stipulated to be zero, and the slot is of unit width, at a point infinitesimally removed from the inlet, by a distance dz, we have:

$$x = \frac{(q/A)\ dz}{w\ h_{lv}} \qquad (41)$$

Here, we encounter two problems. First, although h_{lv} is a known function of pressure, the pressure distribution along the slot has not yet been determined, so eqn. (41) cannot be integrated directly to determine x as a function of z. Second, though the ratio (q/A)/w is known to be constant, s is not known in eqn. (36), and the value of this constant is therefore unknown. Letting the unknown constant be K, one additional item is known:

$$\int_o^L \frac{(q/A)\ dz}{w\ h_{lv}} = KL\left(\overline{\frac{1}{h_{lv}}}\right) = x_o \qquad (42)$$

where

$$\left(\overline{\frac{1}{h_{lv}}}\right) = \frac{1}{L}\int_o^L \frac{dz}{h_{lv}}$$

Of course, $(\overline{1/h_{lv}})$ is not known, either, but the problem is now in convenient form for an iterative, numerical solution. Assume

$$\left(\overline{\frac{1}{h_{lv}}}\right) = \frac{1}{2}\left(\frac{1}{h_{lv_i}} + \frac{1}{h_{lv_o}}\right). \qquad (43)$$

By use of eqn. (43), eqn. (42) may be solved for a "first guess" for K. Divide the slot into N segments, of length $\Delta z = L/N$. If N is sufficiently large ($N \geq 10$ yields reasonable results), one may assume $\rho = \rho_i$, $h_{lv} = h_{lv_i}$, etc., throughout the first segment. Eqn. (41) may then be used to determine the quality at the end of the first segment, after which eqn. (35) can be used to increment ρ, then eqn. (37) to increment v, and eqn. (38) to increment p.

With p incremented, new values may be determined for the thermodynamic properties, and these used to advance the solution through the next segment, etc. When the outlet is reached, computed outlet quality can be compared to desired outlet quality, and the estimate for K corrected accordingly. A simple, linear correction was found to yield rapid convergence:

$$K_2 = K_1(x_{desd}/x_{compt}), \text{ etc.}$$

Of course, when suitable convergence is obtained, the desired temperature, pressure, and velocity profiles have also been obtained, and eqn. (42) may be solved directly for the hitherto unknown relationship between (q/A) and s.

No mixing (annular flow) model: Essentially, the assumptions made regarding flow conditions for the no-slip model pertain as well to the no-mixing case, except that concerning the distribution of the phases. Here, we shall assume that the liquid phase remains adjacent to the walls of the slot, while the vapor phase flows along the center of the slot. With neither phase entrained in the other, the assumption of inviscid flow implies that liquid and vapor can (and indeed, must!) proceed at different velocities. Instead, if the pressure profile is to be one-dimensional in character, the bulk velocity of each phase must adjust (considering density differences) so that the pressure drop along, say, a streamline in the center of the duct --- which lies entirely in the vapor phase--- is equal, at any z, to the pressure drop along a streamline adjacent to the wall, lying entirely in the liquid phase. Thus, we now have two separate momentum equations to deal with, and therefore two different phase velocities, which precludes treating the two-phase flow as a simple "homogeneous" fluid. (At the inlet, assuming quality is exactly zero, the first infinitesimal quantity of vapor generated causes no finite change in flow conditions. Therefore, at the

inlet, and only at the inlet, the two phase velocities are equal.)

The concept of "quality" becomes somewhat more complex, given that liquid and vapor velocities are generally unequal. Actually, quality is a static concept, which was easily extended to the preceding dynamic case, because the phases moved together. To avoid confusion, the term will here be taken to mean:

$$x = \frac{\rho_v s_v dz}{\rho_v s_v dz + \rho_l s_l dz} = \frac{\rho_v s_v}{\rho_v s_v + \rho_l s_l}, \qquad (44)$$

where we again speak in terms of unit width, and s_v is that portion of the slot height occupied by the vapor phase ($s_v + s_l = s$, as defined above). For convenience, the variable ξ will be defined as:

$$\xi = \frac{A_l}{A_v} = \frac{s_l}{s_v} = \frac{1-x}{x}\frac{\rho_v}{\rho_l} \qquad (45)$$

In terms of ξ, the continuity equation, written between inlet and outlet, now becomes:

$$\rho_{l_i} v_i (1 + \xi) = \rho_{l_o} v_{l_o} \xi + \rho_{v_o} v_{v_o} \qquad (46)$$

Because specific volume is a known function of pressure, the two momentum equations can be integrated directly between inlet and outlet:

$$\Delta p_l = \frac{1}{2}\left[\frac{1}{(1/\rho_l)}\right](v_{l_o}^2 - v_i^2) \qquad (47)$$

$$\Delta p_v = \frac{1}{2}\left[\frac{1}{(1/\rho_v)}\right](v_{v_o}^2 - v_i^2) \qquad (48)$$

where $\left(\overline{\frac{1}{\rho}}\right) = \frac{\int dp/\rho}{p_e - p_i}$,

which can be evaluated by direct integration of the appropriate saturation property polynominals. Of course, as was stated above, we require

$$\Delta p_l = \Delta p_v \qquad (49)$$

In principle, eqns. (45-49) can be reduced to three equations with the three unknowns v_i, v_{v_o}, and could therefore be solved explicitly for the

inlet and outlet velocities. In practice, this is messy, and an iterative approach was employed here. This problem was solved in tandem with the no-slip problem, preceding. The inlet velocity determined for the former problem was inserted in eqns. (47) and (48), which were then solved for v_{l_o} and v_{v_o}. These values were inserted in eqn. (46), which was solved for a corrected "guess" for v_i, etc. Convergence was found to be quite rapid: generally, the value of v_{v_o} converged in a single iteration, and v_{l_o} and v_i in two or three.

Of course, once determined, v_{v_o} can be checked against v_{lim}, and assuming $v_{v_o} < v_{lim}$, we again proceed. With inlet and outlet variables completely determined, it is again convenient to adopt an iterative, numerical solution. In this case, the energy relationship becomes:

$$(q/A)\, dz = h_{lv}\, \delta w_v, \tag{50}$$

where δw_v is the change in the vapor mass flow rate while traversing the distance dz. For an incremental analysis, let

$$K = \frac{(q/A)\ L}{Ns} \tag{51}$$

Again, s is unknown, but if the two problems are solved in tandem, we can use the slot height determined from the no-slip model for the same set of thermodynamic parameters. Using an approach similar to that of the preceding problem, at the k^{th} section:

$$w_{v_k}/s = w_{v_{k-1}}/s + K/h_{k-1}$$

Specifically, at the inlet, w_v is defined to be zero. Further, $w_v + w_l = w$, which is still constant. To advance the solution from one station to the next, let $s_v' = s_v/s$ and $s_l' = s_l/s$ ($s_v' + s_l' = 1$). Then,

$$v_{v_k} s_{v_k} = (1/\rho_{v_{k-1}})(w_{v_{k-1}}/s + K/h_{lv_{k-1}}) = v_{v_k}(1-s_{l_k}') \tag{52}$$

$$v_{l_k} s_{l_k}' = (1/\rho_{l_{k-1}})(w_{l_{k-1}}/s - K/h_{lv_{k-1}}) \tag{53}$$

and, to keep $\Delta p_l = \Delta p_v$ between stations:

$$\rho_{l_{k-1}} (v_{l_k}^2 - v_{l_{k-1}}^2) = \rho_{v_{l-1}} (v_{v_k}^2 - v_{v_{k-1}}^2) \qquad (54)$$

At the inlet, $s_v = 0$, $s_l = 1$, $w_v =$), and $w_1/s = \rho_{l_i} v_i$. Eqns. (52-54) can be used to advance the solution consecutively from one section to the next, although an iterative solution is again convenient. Here, eqn. (53) was solved for s_{l_k}', under the assumption that

$$v_{l_k} \cong v_{l_{k-1}} + \frac{v_{l_o} - v_{l_{k-1}}}{N - (k-1)} ,$$

eqn. (52) was then solved for v_{v_k}, after which eqn. (54) was used to derive a correction for the assumed value of v_{l_k}.

At the outlet, computed and desired outlet qualities should be compared, and the process repeated with a new value of K, until desired convergence is obtained. As was the case previously (when eqn. (42) was used to compute s), eqn. (51) can be solved for that variable, after the solution has converged.

Utilization of the above models: actually, both these problems were programmed for computer solution, but in terms of the parameter S, which is defined by the relationship:

$$S = s/(q/A)L \qquad (55)$$

The reason for this shift of variables is that the slot factor, S, is the more convenient parameter for the contemplated application: for a specified p_o and x_o, a single curve can be developed, giving S as a function of Δp. A family of such curves, for various x_o, concisely displays the general relationship between inlet and outlet pressure, quality, and slot height, for any (q/A) and L.

Further, while the incremental models give access to a temperature profile, through application of the saturation temperature polynomial to the

computed pressure at each station, a more useful figure for preliminary analysis would be the mean coolant temperature, or better still, the mean temperature increment. The former is defined as:

$$\overline{T}_c = \frac{1}{L}\int T\, dz \cong \frac{1}{N}\sum_{k=1}^{N} T_k \qquad (56)$$

The latter might be defined as $\Delta T_c = \overline{T}_c - T_o$, but as a matter of convenience, will be defined instead as:

$$\Delta T_c = \overline{T}_c - T_{sat,\ 1\ atm.} \qquad (57)$$

under the assumption that the one-atmosphere saturation temperature may be more readily available than the outlet temperature, if outlet pressure differs from one atmosphere.

The primary advantage of dealing with the temperature increment, defined by eqn. (57), rather than the mean temperature, is that the magnitude of the increment clearly underlines the added "cost" of operating at elevated pressures. In computing mean coil resistivity, the first estimate for mean coil temperature would be given by:

$$\overline{T} \cong T_w = T_{s,1} + \Delta T_c + \Delta T_{bl} \qquad (58)$$

Here, T_w is actually the wall temperature of the cooling duct, and ΔT_{bl} is the temperature increment across the thermal boundary layer, which would presumably be determined from the same source as the figure used for mean (q/A): either a predictive correlation, as discussed in the preceding chapter, or experimental data. This is classed as a "first estimate", since if the coolant ducts are widely spaced, an additional correction might be necessary to account for thermal gradients in the conductor material. However, this factor is again best left for the detailed design phase. In general, the $\overline{T}$ defined in eqn. (58) would be the temperature used to enter the mean coil resistivity curves of Appendix B.

Correction for subcooling at inlet: Either of the above models could be applied to the problem at hand--- e. g., to predict coolant volume fraction for a cryogenic coil--- depending upon which was most representative of flow conditions realized in the type of slot geometry contemplated. Again, it is to be regretted that experimental data are simply not available for forced flow, two-phase cryogenic cooling with this type of slot geometry. Presumably, all efforts would be made to maintain operation in the "annular flow" regime, in which case the no-mixing model would seem most pertinent. However, in the absence of experimental data, the no-slip model has the advantage of producing a more conservative prediction: Since the relatively dense liquid must accelerate with the vapor phase in that case, flow velocities tend to be lower for a given Δp. This, in turn, requires larger slots to pass the same bulk rate of flow, as would be required to maintain the same specified outlet quality. Until experimental data confirm that viscous effects are truly negligible, throughout the range considered here, this "built-in conservatism" might well be used as "advance compensation" for possible viscous effects.

In any event, before either model can be applied to predict flow relationships in "real" coolant ducts, one additional correction should be introduced. Both models assumed zero quality at the slot inlet, but as was mentioned above, the zero-quality saturation point would not, in fact, be reached until the subcooled liquid coolant, coming from the pump(s), had been heated to its saturation temperature. Particularly at high pressures, where h_{lv} tends to be relatively small, the energy absorbed before reaching the saturation point might be significant. (Note, however, that it should not be predominant, or this could not properly be classed as "two-phase cooling". However, the pressure ranges selected for the various coolants

in effect constrain the problem to avoid that possibility.)

What the above models actually predict is the relationship between pressure, slot factor, etc., and the length of that portion of the slot devoted to two-phase flow. Suppose zero quality is reached at the point z_o, rather than at the inlet. The liquid at the inlet would presumably be subcooled by an amount δh, where

$$\delta h = h_{sat,\ p_i} - h_{sat,\ p_o} - \delta h_{pump} \qquad (59)$$

"Ideal" pumps are isentropic, but "real" pumps are not. Assuming that the efficiency of a "real" pump would be of the order of 50%, we have:

$$\delta h_{pump} \cong \frac{2(p_i - p_o)}{\rho l_o} \qquad (60)$$

Then, assuming constant (q/A), as before,

$$\delta h(\rho_i v_i s) = (q/A)z_o .$$

Let the distance $(L-z_o)$ be designated L', and the slot factor computed with L' be S'. Then,

$$z_o/L' = \delta h(\rho_i v_i) \frac{s}{(q/A)L} = \delta h \rho_i v_i S'$$

Actually, the slot factor derived from the previous models is, correctly, S'. If S' were multiplied by L, vice L', too large a value would be computed for s. Presuming L would be known, while L' might not be, the previously computed slot factor must be corrected:

$$S = \frac{L'S'}{L} = \frac{L'S'}{L' + z_o} = \frac{S'}{1 + \delta h \rho_i v_i S'} \qquad (61)$$

Eqns. (59-61) can be applied to correct the slot factor predicted from either flow model.

Next, the mean temperature increment predicted from the preceding models must be re-examined. The original $\bar{T}_c$, which will now be called $\bar{T}_c'$, was based on the nonlinear, monotonically decreasing temperature profile between $z = z_o$ and $z = L$. By contrast, as discussed previously,

conditions in the subcooled flow can be approximated as a linear temperature increase between $z=0$ and $z=z_o$. (Note that the "hot spot" in the windings of a coil cooled by such a system would occur just at $z=z_o$, where coolant temperature would roughly equal the coolant saturation temperature, at the inlet pressure.) Since a pump efficiency of 50% would imply relatively little temperature increase for the coolants considered, even when pumped through the maximum pressure increment investigated, the corrected ΔT_c can be approximated as:

$$\Delta T_c \cong \frac{L'\overline{T}_c' + z_o(T_{s,p_i} + T_{s,p_o})/2}{L} - T_{s,1}$$

$$= \frac{\overline{T}_c' + \delta h \rho_i v_i S'(T_{s,p_i} + T_{s,p_e})/2}{1 + \delta h \rho_i v_i S'} - T_{s,1} \qquad (62)$$

Finally, it was originally stated that "inlet pressure will be systematically incremented" by assuming $p_i = p_o + n\,\Delta p$. Again, the pressures so specified correspond to conditions at $z=z_o$, vice $z=0$. With single-phase flow to $z=z_o$, Δp could be corrected by deriving an additive term from eqn. (30). However, in general $z_o << L$, and we choose to remain with an inviscid model. One correction can be applied, though, even to an inviscid model: The liquid density decreases between $z=0$ and $z=z_o$, since liquid density is a significant function of temperature, if not pressure. This requires a slight flow acceleration, which results in a pressure decrement of the order:

$$\Delta p_{inlet} \cong (\rho_i v_i)^2 (1/\rho_{s,p_i} - 1/\rho_{s,p_o}) \qquad (63)$$

thus, a "corrected" Δp can be determined by adding eqn. (63) to the Δp specified in the incremental analyses. This has been done, though in most cases, the correction is insignificant.

The details of the calculations performed, in applying the no-slip and no-mixing models, corrected for subcooling at the inlet, to the analysis of

the two-phase cryogenic cooling problem, are discussed in the next chapter. The results of these calculations are presented in Appendix D.

E. Other coolant flow considerations:

In closing this chapter, two factors which cannot be discussed quantitatively deserve qualitative mention:

The first is the problem of inlet and outlet connections to the coolant ducts: although the slot geometry discussed herein probably corresponds reasonably well to such geometries as might be employed throughout the greater portion of "real" cryogenic saddle coils, the applicability obviously terminates at coolant inlet and outlet connections. In fact, no simple solution is seen to the problem of compatability with coil geometry at these points. Presumably, ducts would not be "spiraled" through several axial passes, to emerge at the surface of the coil, since the analysis indicates that increased duct length requires increased slot height, and therefore decreased coil packing factor. Further, the geometry of the "end turns" of the coil is not particularly compatible with conventional use of inlet and outlet headers. The problem is a moot one, and regretably beyond the scope of this study.

The second problem has to do with the possibility of a parallel flow instability in two-phase cooling systems. It is probable that whatever connection scheme were devised would feed several ducts "in parallel". Let us assume that steady-state operation has been established, and investigate what might happen if some local phenomenon perturbs the flow rate through a particular duct.

Fig. 21a depicts two curves of flow rate vs. Δp, such as might be characteristic for a particular coolant and a particular geometry at constant (q/A). Basically, characteristics of class I are "safe", but those

FIGURE 22a

"TYPICAL" FLOW CHARACTERISTICS

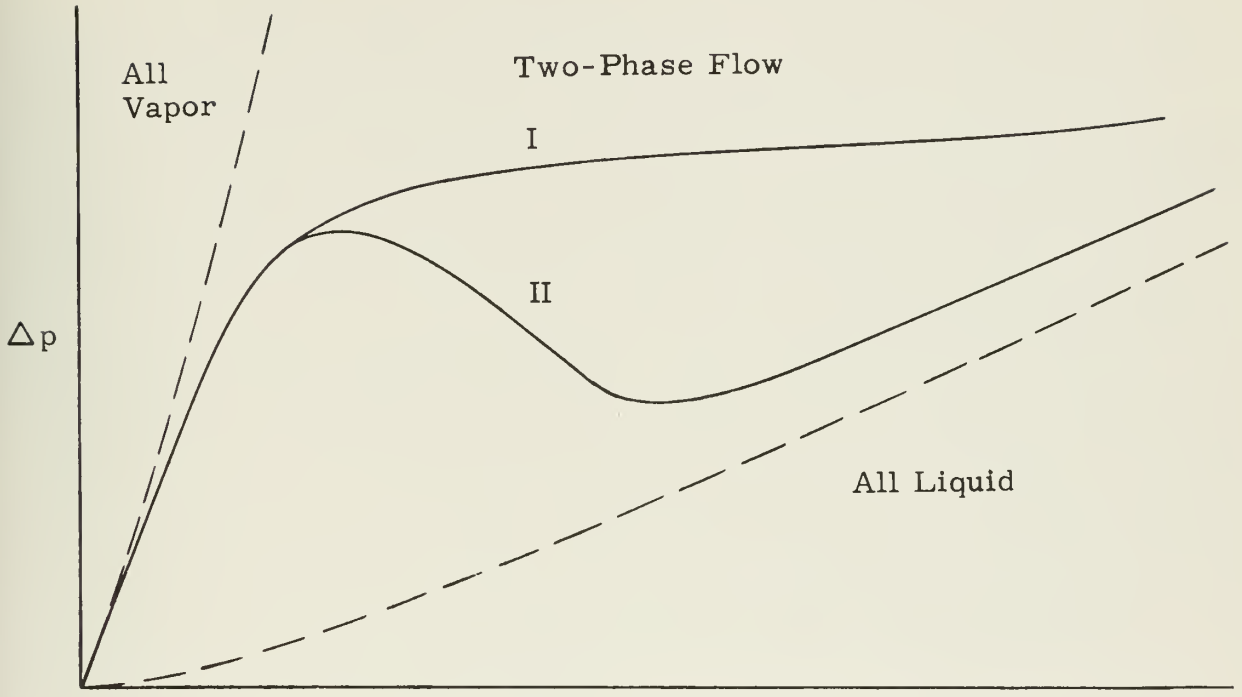

FIGURE 22b

POSSIBLE FLOW INSTABILITY

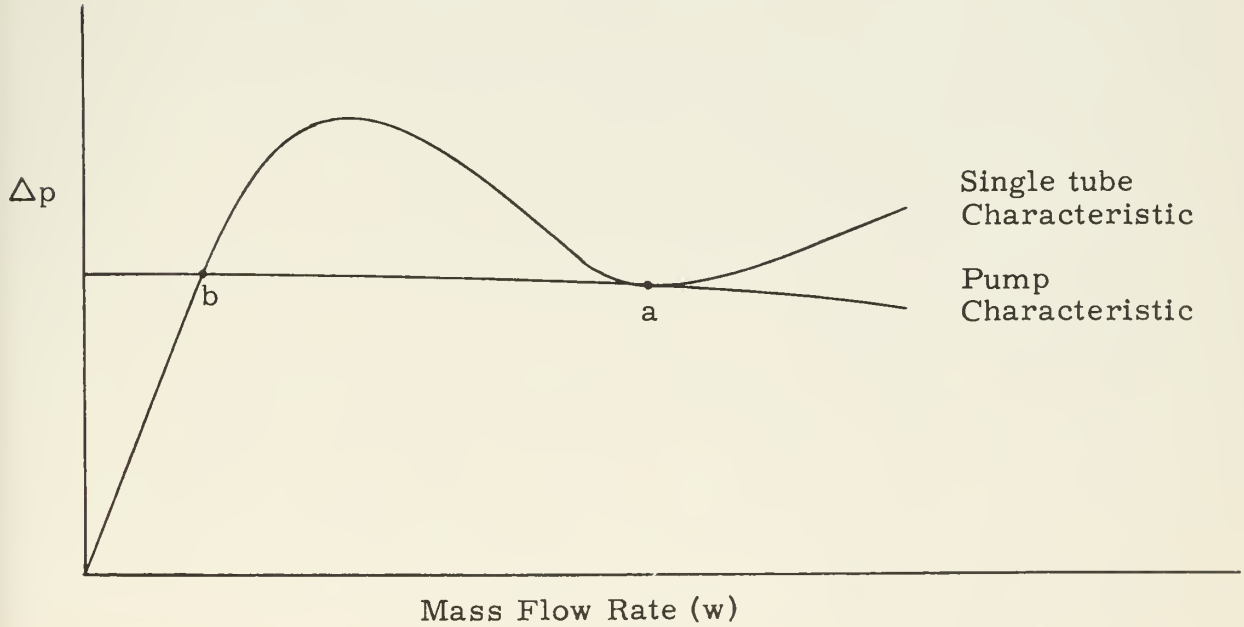

of class II may lead to problems:

If a high-capacity pump is supplying several ducts in parallel, the pump characteristic might imply essentially constant Δp, regardless of flow conditions in any one duct. Such a characteristic is shown superimposed on a class II characteristic in Fig. 21b. If steady-state operation had been established at point a, and a sudden fluctuation caused a momentary decrease in mass flow rate in a particular duct, the operating point for that duct might "jump" to point b. If the quality at point b were so high that flow conditions entered the "liquid deficient" regime, heat transfer to that duct would then drop abruptly, leading to the creation of a "hot spot" extending the axial length of the coil. The problem is obvious; the situation can be avoided or ameliorated by careful design; but that is also beyond the scope of this study.

VII. GENERATION AND USE OF CHARACTERISTIC CURVES

A. Curves of coil geometry:

Generation: The curves of coil geometry, presented in Appendix A, and those of mean coil resistivity, in Appendix B, were generated from a single computer program, consisting of a calling sequence (main program), and several functional subroutines. A brief resume will be given here of the logic used in these routines, and of the numerical ranges investigated during the processing of data. The programs themselves are presented in Appendix E. All are written in Fortran, for use with the M. I. T. Computation Center version of the Fortran Moniter System, and were run on the Computation Center's I. B. M. 7090 digital computer.

MAIN, as mentioned above, is primarily a calling sequence. As pertains to the coil geometry problem, MAIN reads an input data card, to determine the desired channel area (in square meters), desired channel flux density (in kilogauss), and effective coil current density (in amps/square meter). The calling sequence is "looped", so that data from one card are processed completely, then another card read, etc. As processed here, channel area was varied through the specific values of 10, 1, 0.1, and 0.01 m^2, flux density through 25, 50, 75, and 100 kilogauss, and current density varied as necessary to investigate form factors in the approximate range $1.3 \leqq F \leqq 5$ (e.g., 10^5 to 10^7 a/m^2 for $A_{ch} = 10$, and 5×10^6 to 10^8 a/m^2 for $A_{ch} = 0.01$). Customarily, B was varied through all its values, for a fixed J_e and A_{ch}, then J_e incremented, and the process repeated, until all coils suitable for a particular channel size had been investigated.

SIZE performs the actual calculation of coil geometry for a specified set of input parameters. Eqns. (1-6) have been programmed in the ration-

alized MKS system of units; thus, the specified B is divided by ten to convert to a consistent set of units. SIZE uses an iterative approach to determine the required cylinder radius for a particular coil: eqn. (1) is solved for cylinder offset, and a "first guess" is made that

$$R \cong a + \sqrt{A_{ch}}/2 \quad .$$

This value is inserted in eqns. (2) and (3), and the resulting computed channel area compared to the specified channel area. Based on this comparison, the estimated R is varied systematically, until the deviation between specified and computed A_{ch} is less than 0.01%, or until the process has been repeated 50 times. (The latter option was found to be an unnecessary precaution, within the range investigated.) The subroutine then computes the width, height, and area of the "optimum" channel for the resultant coil, the coil length, total cross section (both lobes), total surface area, and total volume (uncorrected for end turns), and finally, the coil form factor. This information is stored until MAIN calls the output routine, PRINT.

Use of coil geometry curves: The output of the above subroutine is presented in Figs. A-1 to A-3, as an explicit function of the form factor, F, defined in eqn. (6). F has been chosen as the independent variable, for two reasons: It provides a convenient, quantitative index to the "shape" of a saddle coil, and more importantly, provides an immediate indication of design optimization. (This latter point will be discussed in Chapter VIII.) To utilize the information presented in these curves:

1. Specify desired A_{ch}, B, and F.
2. Enter Fig. A-1 with F, and determine J_e required to attain that F.
3. Enter Fig. A-2 with F. Compute w_{ch}, a, and R by multiplying plotted values by $10\sqrt{A_{ch}}$.
4. Enter Fig. A-3 with F. Compute A_s and A_{cl} by multiplying plotted values by 100 A_{ch}. Compute V by multiplying plotted value by $1000(A_{ch})^{3/2}$.

5. Correct for end turns by multiplying A_s and V by F.

As stated in Chapter I, the above assumes that the coil length, L, is equal to $10\sqrt{A_{ch}}$. However, the information plotted in these curves can be corrected for $L \neq 10\sqrt{A_{ch}}$:

1. Carry out steps 1-4, as above.
2. Correct A_s and V by multiplying by $L/10\ \ A_{ch}$.
3. Correct F: $F' = 1 + (F - 1)(10\sqrt{A_{ch}}/L)$.
4. Correct for end turns by multiplying A_s and V by F'.

Note that the optimization procedure discussed in the next chapter pertains to F', vice F, when L is not equal to $10\sqrt{A_{ch}}$. However, all parameters plotted as functions of F must be "looked up" as functions of F. Of the geometric parameters, only A_s and V need be corrected for the "new" length.

B. Mean coil resistivity curves:

Generation: Mean coil resistivity was computed as a function of temperature, at ten degree increments, from 5° to 95° K, for each coil processed by MAIN. To reduce input-output time, the necessary field-free and magnetoresistance data for a particular metal were "read in" only once, at the start of each run, by having MAIN call READ before entering the computing loop.

READ is strictly an input routine, designed to read, in sequence:

1. Ten specified temperatures, from a single card;
2. The field-free resistance corresponding to each specified temperature (see Tables 1-4), from two data cards;
3. The magnetoresistance for the particular metal, as tabulated in Table 5, from ten data cards.

FIELD determines the field distribution within the upper-right-hand

quadrant of the coil, to permit calculation of magnetoresistance. (A modified version of FIELD was also used to compute the vector diagrams presented in Figs. 12-16.) The upper-right-hand quadrant was selected, since the symmetry of the field distribution indicates that the mean resistivity of any quadrant is equal to the mean resistivity of the entire coil.

FIELD positions a "grid" of 5000 squares over the upper-right-hand quadrant of the coil. The overall size of the grid is 2R wide by R high, with the lower left corner of the grid positioned at the center of the MHD channel. Each component square has sides of dimension R/50.

FIELD first scans the left-most vertical column of squares, working from bottom to top, and determines which squares have centers which fall within the coil quadrant. FIELD computes and saves the value of the field intensity at the center of these squares, using the equations:

$$B_x = \frac{\mu_o J_e}{2} \left[1 - \frac{R^2}{(x+a)^2 + y^2} \right] y \qquad (64)$$

$$B_y = \frac{\mu_o J_e}{2} \left\{ (a+x) \left[\frac{R^2}{(x+a)^2 + y^2} \right] + (a-x) \right\} \qquad (65)$$

$$|B| = \sqrt{B_x^2 + B_y^2} \ , \qquad (66)$$

where the x-y origin is the lower left corner of the grid. After locating the uppermost square which falls within the coil quadrant, FIELD shifts to the next vertical column to the right, etc., until locating the first such column which lies entirely outside the coil. The field intensity at the center of each square which fell within the coil is saved in an array, with the location of the data corresponding to the location of the square in the grid. Locations corresponding to squares which fell outside the coil are set to zero. FIELD also saves the location of the first column which fell entirely outside the coil.

RHO next computes mean coil resistivity, using the field distribution generated by FIELD, and the resistance data supplied by READ. RHO sequentially examines each specified temperature. For each temperature, RHO determines the field-free resistivity, then scans the array of field intensities for non-zero entries (examining only those columns which were previously scanned by FIELD). RHO divides each non-zero entry by the field-free resistivity, and used the result as an index to find the "nearest" corresponding entry in the magnetoresistance table. RHO then computes "total" resistivity at the center of the corresponding square, and assumes this to be representative of the total resistivity of the entire square. Finally, RHO computes mean coil resistivity, for the particular temperature, from the relation:

$$\overline{\rho} = \frac{1}{N} \sum_{i=1}^{N} \rho_i \qquad (67)$$

N being the number of locations found to have non-zero entries.

In this incremental analysis (as with all other incremental analyses conducted herein!), the "fineness" of the grid was selected through successive reduction of the increment used, so that the degree of approximation associated with a particular increment size could be estimated. The increment specified ensures that the accuracy of the computational technique is consistent with the accuracy of the physical model.

Use of resistivity curves: The data in Tables 1-5 indicate that indium coils would not be competitive with coils wound from the other conductor materials investigated, except at temperatures below 4^{o} K. As it seems unlikely that cryogenic coils would be designed for operation below 4^{o} K, indium was dropped from the list of potential conductor materials, and no mean coil resistivity curves are presented for that metal. However, curves of mean resistivity vs. temperature for coils wound of sodium, copper, and

aluminum, are presented in Figs. B-1 to B-16. These curves have been normalized to the 1.7715 micro-ohm-centimeter standard, to permit direct comparison with "conventional" copper coils. Further, resistivity curves for all three metals are superimposed in each figure, to permit direct comparison between these metals as cryogenic conductors. Figs. B-1 to B-4 are for 25 kg coils, B-5 to B-8 for 50 kg coils, etc., with each figure presenting data for a particular form factor. (F and B together determine the geometric distribution of magnetoresistance, and therefore define mean resistivity, for a particular metal. However, the variation is sufficiently slow--- except for copper below 30° K--- that interpolation is generally unnecessary: to determine mean resistivity, simply enter that figure which most nearly corresponds to the contemplated application.

While these curves were computed from the data presented in Tables 1-5, approximate adjustment can be made, should it be desired to assume some value for any one of the three components of "total" resistivity, other than those used here: the plotted "mean" resistivity can be compared to the tabulated "field-free" resistivity, to determine the percentage contribution of each component to total resistance. (Note that the 0° K entry in each of Tables 1-4 is the assumed residual resistance ratio for the various metals.) Once the percentage contribution of a component is known, the net effect of changing that component can readily be estimated.

C. Structural curves:

Generation: The curves of structural volume fraction, presented in Appendix C, were generated by a second computer program, consisting of a calling sequence (main program), and the subroutines SIZE, CSHELL, and TSHELL.

MAIN is again "looped"; uses the same input data as the previous program (A_{ch}, B, and J_e), and again calls SIZE to evaluate the geometric parameters of each saddle coil so specified. MAIN then systematically varies the specified conductor stress limit (σ_c) through the values 3,000, 6,000, 9,000, and 12,000 p. s. i., and the structural stress limit (σ_d) through the values 120,000, 90,000, 60,000 and 30,000 p. s. i. (All values of σ_d are "matched" with a single value of σ_c, before the latter is incremented.) CSHELL and TSHELL are called for each combination of σ_c and σ_d, to compute the compressive and tensile volume fractions, respectively.

To explain this particular sequencing: The required number of structural shells decreases as σ_c increases. Thus, if no shells are required for a particular σ_c, none will be required for higher σ_c. Accordingly, if total computed volume fraction is found to be identically zero for any value of σ_c, MAIN does not search to higher values, but concludes that the problem has been "solved", for that particular coil, and calls for new input data.

Similarly, shell thickness increases with decreasing σ_d. Thus, if the structural volume fraction is unreasonably high, for a given σ_d, MAIN does not search to lower σ_d, but increments σ_c immediately, to reduce the number of shells. "Unreasonably high" is defined, in the program, as a volume fraction of 0.8 or greater.

SIZE, aside from a minor reduction in the number of "output" parameters computed, is the same subroutine as described above.

CSHELL computes the compressive volume fraction by the procedure described in Section D of Chapter III. Since electrical variables and coil geometry data are expressed in metric units, while Windenburg's equations (and most available strength data) are in English units, considerable conversion of units occurs during the computational process.

TSHELL computes the tensile volume fraction by the process described in Section E of Chapter III. Specifically, TSHELL slices the coil lobe into shells of thickness dr = a/10, where a is the offset between the center of the cylinder and the center of the channel. Per unit length, the volume of each such shell is assumed to be $2r\Theta$ dr, where r is the inner radius of the shell, and Θ is defined by eqn. (20), in terms of that radius. TSHELL integrates eqn. (18) numerically, by "piling up" such shells until the effective pressure exceeds σ_c. TSHELL then "shaves" the last shell, reducing its thickness so that $p_e = \sigma_c$ at the outer radius of the stack. A structural support shell is inserted at this radius, and its volume determined as indicated in eqn. (22). TSHELL continues this process until the outer edge of the coil is reached, then divides the accumulated volume by the volume of a unit length of coil lobe.

When the above computation has been completed, TSHELL prints σ_c, σ_d, the number of compressive and tensile shells, the compressive and tensile volume fractions, and the total structural volume fraction. Control is then returned to MAIN, which specifies a new combination of σ_c and σ_d, or begins work on the next coil, as appropriate.

Use of structural curves: Curves of structural volume fraction as a function of form factor are presented in Figs. C-1 to C-4, with each figure presenting the data for a particular σ_d. Interestingly enough, for a given σ_d, structural volume fraction was found to be much more sensitive to F and B, than to σ_c. Accordingly, curves are presented for each value of B investigated, but only for σ_c = 3,000 and 12,000 p. s. i. The structural volume fraction for intermediated values of σ_c can be estimated, to within the probable accuracy of the model, by simple linear interpolation between these two families of curves.

D. Coolant curves:

Generation: The coolant curves, presented in Appendix D, were generated in two stages: First, curve fitting routines were utilized to develope the saturation property polynomials, and then, using these polynomials, curves of slot factor (S), mean coolant temperature increment (ΔT_c), and coolant inlet velocity (v_{in}) were generated by the techniques discussed in Chapter VI.

The curve fitting routines were executive programs built around an M. I. T. Computation Center SHARE program, GLSQ. Briefly, GLSQ determines a least-square solution to an overspecified problem (M equations in N unknowns, with M > N), or the exact solution to a "properly set" problem (M equations in M unknowns), by matrix inversion techniques.

Both GLSQ, and an example of the type of data fitting routine used in conjunction with it, are presented in Appendix E. The data fitting routine specifies the functional form to which the data are to be reduced--- e. g., $y = a_1 + a_2x + - - - - + a_nx^{N-1}$--- and for each data point (x, y), computes the various powers of x. (Actually, the functional form need not be constrained to a simple power series in x: it could as well involve terms in e^x, sin x, etc.) These factors are sent to GLSQ in an array, with each row of the array corresponding to one data point. (Obviously, there must be at least as many data points as there are coefficients to be evaluated in the set $\{a_i\}$.) GLSQ solves the matrix for the unknown coefficients $\{a_i\}$. The example program prints these coefficients, the resultant minimum mean square deviation, and lists x, $y_{observed}$, $y_{generated}$, $y_{obs} - y_{gen}$, and $100(y_{obs}-y_{gen})/y_{gen}$ (% deviation) for each data point. (Input required: one card, listing the number of data points (M), and M cards, each listing the coordinates of a single data point.) Of the two figures which appear repeatedly in the DIMENSION statement, 200 is the maximum number of

data points which can be processed, and 7 is the number of terms in one row of the matrix. Both of these figures may be adjusted, as desired.

The coolant flow program consists of a main program, the subroutines READS, NOSLIP, NOMIX, INLET, and PRINTS, and the functions SVOLL, SVOLV, TEMP, HLIQ, HTVP, AVSVL, and AVSVV:

READS determines the saturation property coefficients (as listed in Table 6) for the coolant to be investigated, the three values of outlet quality to be examined, and the limiting velocity to be applied to the flow.

NOSLIP reads in the outlet pressure to be assumed, the "step size" to be utilized in incrementing the inlet pressure, and the number of increments to be examined. NOSLIP then solves the no-slip flow model, exactly as discussed in the preceding chapter, using a 25-station incremental model. Iterative solutions are cycled until the one-cycle change in the control variable is less than 0.1%. For a given p_i and p_o, flow conditions are solved for each specified x_o. After this, p_i is incremented, and the process repeated until all specified inlet pressures have been investigated.

NOMIX solves the no-mixing flow model in the same manner. One additional point should be noted: Statements 9 and 10 of this subroutine generate a corrected estimate for the constant K, which appears in eqns. (51-53), in order to obtain convergence between computed and desired outlet qualities. Actually, the "loop gain" in this particular iterative solution is a strong function of the degree to which specified operating pressures approach the critical pressure of the coolant being investigated. The attenuation factors of 10.0 and 5.0, which appear in statements 9 and 10, as listed in Appendix E, provide suitable convergence for nearly all runs covered here. However, if specified pressures lie quite close to the critical pressure--- e.g., above about 7.5 atmospheres for liquid hydrogen, or

one atmosphere and above for liquid helium--- loop gain is so small that the solution converges too slowly if these factors are used. They should be replaced by the factors 3.0 and 1.5, respectively. (Conversely, if the latter values were used for, say, liquid nitrogen in the pressure range of 1 to 10 atmospheres, the resultant correction would be excessive, and the solution would oscillate, or diverge.)

INLET corrects the flow solution for subcooling at the inlet, as indicated in eqns. (61-63).

PRINTS can be used to list the output data from all three of the preceding analytical subroutines, or, by omission of statements 1-25, can be used to obtain only the "corrected" data, generated by INLET. The latter option is obviously less time consuming.

The functions SVOLL and SVOLV utilize the saturation property coefficients, obtained from READS, to compute, respectively, the specific volume of the saturated liquid, and specific volume of the saturated vapor, in accord with the functional forms listed in Section B of Chapter VI. Similarly, TEMP computes saturation temperature, HLIQ the specific enthalpy of the saturated liquid, and HTVP the heat of vaporization, for a specified pressure. AVSVL and AVSVV respectively compute the mean specific volume of liquid and vapor, for use in eqns. (47) and (48), for a specified p_i and p_o.

Use of coolant curves: Curves of S, ΔT_c, and v_{in} vs. Δp for each of the various coolants studied are presented in Figs. D-1a to D-12c: D-1 to D-3 pertaining to liquid nitrogen, D-4 to D-6 to neon, D-7 to D-9 to parahydrogen, and D-10 to D-12 to helium.

Each figure presents a family of curves, showing variation of a particular property with Δp, for various outlet pressures, at a specified quality: e.g., D-1a presents data for x_o = 30%, D-1b for x_o = 50%, and D-1c for x_o = 70%. The "a-b-c" sequence is similarly repeated in all other fig-

ures. Similarly, the D-1 set are curves of S vs. Δp, D-2, ΔT_c vs. Δp, and D-3, v_{in} vs. Δp. This sequence is also repeated for each coolant. Finally, the data generated by the no-slip and no-mixing flow models are displayed side-by-side, in each figure, for ease of comparison.

In general, the plotted curves should not be extrapolated to higher values of Δp. Each curve is terminated, either because v_{out} would exceed the specified limiting velocity, or because p_{in} would exceed the specified limiting pressure, were Δp increased further. However, the curves could certainly be extrapolated to lower values of Δp than those plotted.

For a specified p_o and Δp, the inlet velocity curves permit estimation of the required coolant pump power, as indicated by eqn. (34). Similarly, the ΔT_c curves permit estimation of that parameter, for insertion into eqn. (58), and the slot factor curves permit estimation of the coolant volume fraction: given a preliminary estimate of q (total I^2R loss), q/A, and L,

$$\text{coolant volume} = V_c = As = \left[q/(a/A)\right]\left[S(q/A)L\right] = qSL \qquad (68)$$

and

$$\text{C.V.F.} = V_c/V\,, \qquad (69)$$

where V is as given by eqn. (7).

Thus, these curves supply the final link in the chain of information required for preliminary analysis of cryogenic saddle coils. A suggested procedure for conducting such an analysis is discussed in the next chapter.

VIII. DESIGN OF CRYOGENIC SADDLE COILS

A. General design characteristics:

Presumably, the first parameters which would be specified in the design of an MHD saddle coil would be the desired channel size, and desired field intensity: these requirements are set by the intended MHD application, and could not conveniently be altered to suit the whim of the coil designer. Since we have assumed $L = 10\sqrt{A_{ch}}$, in line with Sutton's work (28, 29), this implies specification of B and A_{ch}, as the first step in the design process.

Assuming this has been done, the next step in the design of cryogenic saddle coils would be the selection of a particular metal for the coil conductors, and the selection of a particular coolant (and, by implication, specification of the approximate range of possible operating temperatures). "Next", because the selection is obviously limited; the choice can be simply and directly related to the overall design philosophy, and will have a profound influence on subsequent development of the design.

Figure 23 depicts the total electric and refrigeration power requirement (neglecting heat leak and coolant pump power) as a function of coil operating temperature, for a "typical" cryogenic saddle coil (B= 50 kg, $A_{ch} = 0.1\ m^2$, F = 2), assuming unity packing factor. The approximate range of operating temperatures attainable, with each of the liquid coolants examined here, is indicated at the bottom of the figure. Although the specified assumptions indicate these curves to be a "rough" approximation to the characteristics of "real" coils, several conclusions nevertheless appear valid:

1. Under the same assumptions, a conventional, copper saddle coil would dissipate 16.7 Mw. Comparing this to the curves in Fig. 23, it is apparent that liquid nitrogen would not be used to cool "working" saddle coils.

FIGURE 23

Electrical plus Refrigeration Power for 50 kg Saddle Coils with $A_{ch} = 0.1$, $F = 2$, $\lambda = 1$

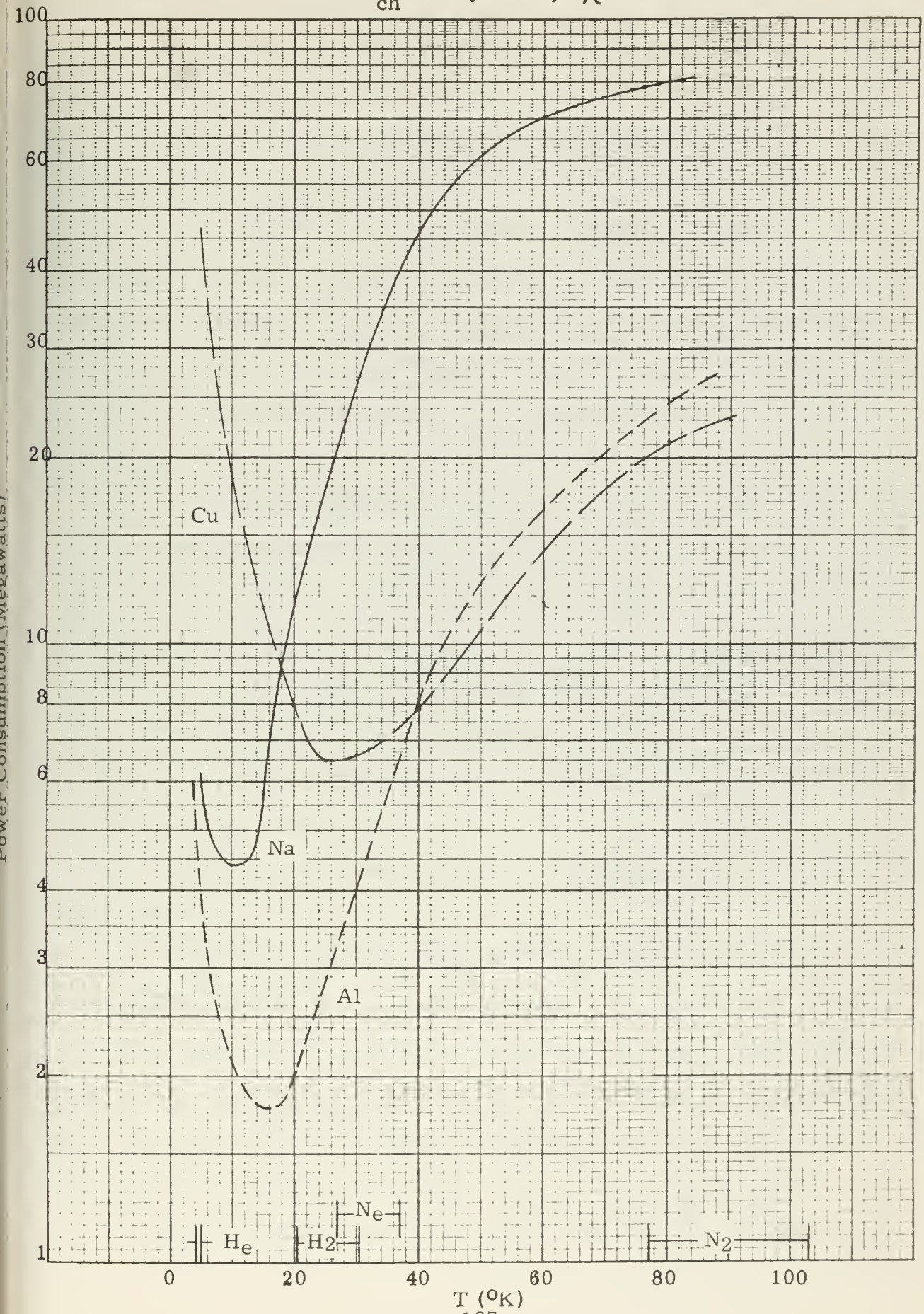

2. If liquid nitrogen were used to cool an experimental coil, copper conductors would yield lowest power consumption. If coil weight were an important factor, aluminum conductors would seem the best compromise between weight and power consumption.

3. In the liquid neon range and below, aluminum appears to be the "optimum" conductor material. Optimum operating temperature for aluminum saddle coils is about 16^{o} K--- i. e., about the same temperature recommended by Taylor and Post (26) for aluminum solenoids--- and the optimum is fairly sharp: a 10^{o} temperature shift in either direction increases losses by more than 50%.

4. Based on this crude model, operation at liquid neon or liquid helium temperatures would appear roughly equivalent, from the viewpoint of power consumption. However, a comparison of the slot factors presented in Figs. D-4 and D-10 indicates that use of the latter coolant would result in lower packing factors, and thus greater losses. Again, liquid helium probably would not be used as a coolant for cryogenic saddle coils, except when cryogenic conductors are used to "stabilize" superconductors, as discussed by Kantrowitz and Stekly (14).

5. If a two-phase coolant is to be used, liquid hydrogen would seem the best choice.

6. Supercritical helium is the only coolant which could maintain the "optimum" temperature for aluminum coils.

Thus, assuming the motivation for utilizing cryogenic saddle coils is that of reduced operating power requirements, one would normally select aluminum for the coil conductors, and liquid hydrogen or supercritical helium for the coolant, based on these data.

The next fundamental variable to be considered, after the specification

of B, A_{ch}, the conductor metal, and the coolant, is the general "shape" of the contemplated coil. While the specified saddle coil model seemingly determines this, a glance at Figs. 12-16 will indicate the wide variation of form still possible within this family of coils. Of course, "shape" can be quantitatively described by the value of the form factor, F, and Fig. 24 displays relative power consumption as a function of F (under the same assumptions that applied to Fig. 23). Here, the minimum occurs at F = 2.0. Power consumption rises gradually as F is increased above this value: loss density (ρJ_e^2) varies inversely with F, but a comparison of Figs. A-1 and A-3 indicates that Je decreases relatively slowly with F, above F = 2, while coil volume increases quite rapidly. As a result, total power consumption and coil size both increase if F increases above 2.0. One can therefore immediately class form factors above that value as "not of interest". Conversely, total power consumption rises if F is decreased below 2, because the sharp rise in J_e more than offsets the decrease in total volume. However, though Fig. 24 indicates that a coil with F = 1.34 would have twice the power consumption of one with F = 2, Fig. A-3 indicates that its volume would be smaller by more than an order of magnitude. Thus, for some applications, form factors less than 2 might be desirable.

As defined here, the minimum attainable F is theoretically 1.22: this corresponds to a sinusoidally distributed current sheet (infinite current density), flowing axially in a cylindrical shell of zero thickness. Realistically, Figs. C-1 and C-4 indicate that structural requirements alone would constrain "real" coils to form factors above about 1.3-1.6, depending upon the specified flux density, and allowable stress levels. Thus, we can define the "range of interest" of coil shapes at those corresponding to form factors between 1.3 and 2.0, with the lower end of the attainable range corresponding

FIGURE 24

Relative Power Consumption vs. F for $\lambda = 1$

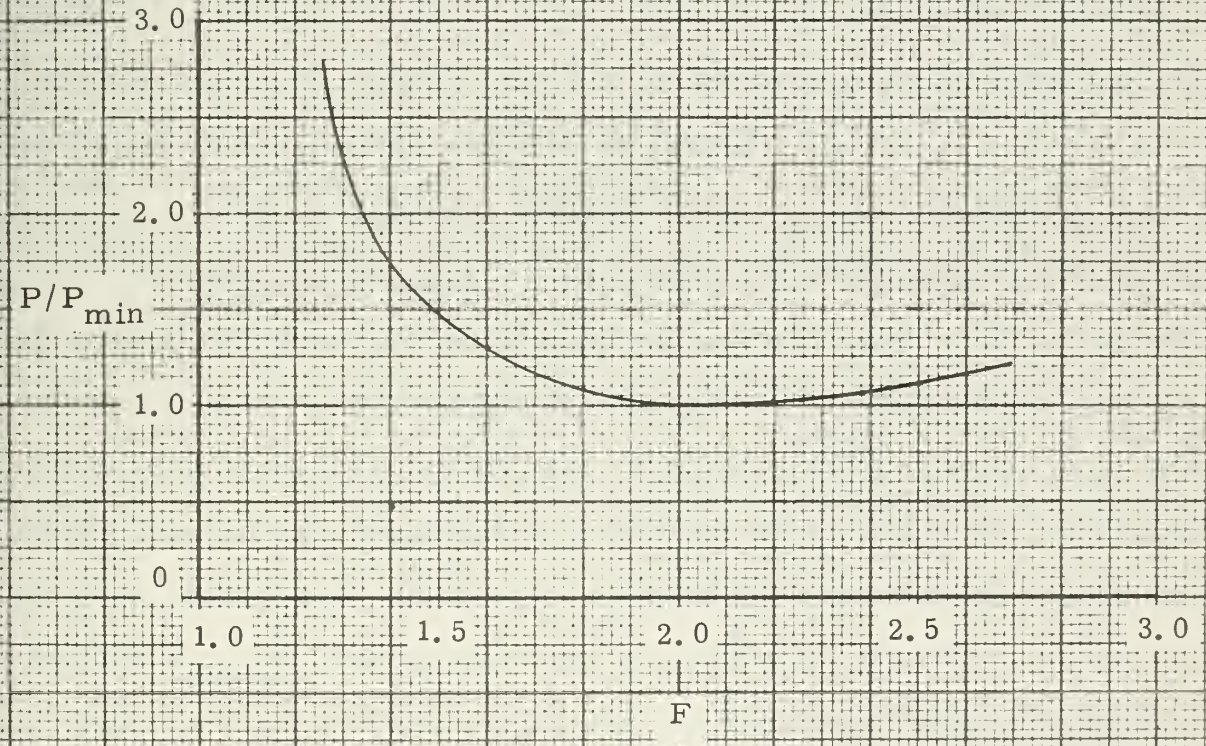

to minimum power consumption.

B. Simplified design procedure:

Bearing the above in mind, Fig. 25 presents a flow diagram of the recommended design procedure for cryogenic saddle coils. Although the motivation for much of the sequencing is obvious, some explanation of various points might be useful:

The design cycle begins with F=2, since both coolant and structural volume fractions are lowest at this point, within the range of forms defined above. The design process entails an iterative search on these factors, to estimate maximum attainable packing factor for a given F. Packing factor, of course, is determined from the relationship:

$$\lambda = 1 - (\text{S. V. F.} + \text{C. V. F.}). \qquad (70)$$

As F is decreased, the point will be reached where the sum of the coolant and structural volume fractions equals or exceeds unity: i. e., where no physical solution exists. However, if a physical solution exists at all--- that is, if it is possible to build any "real" coil, for a given B, A_{ch}, conductor, and coolant combination--- the form factor of 2.0 will correspond to a "realizable" coil. Successive reduction of F can then be used to determine the smallest "realizable" coil, should that be desired.

Once B and F have been specified, the structural volume fraction can be determined immediately (from Appendix C), since it is not a function of resistivity, temperature, coolant pressure, etc. However, to determine the required coolant volume fraction, total power dissipation must be known, and to determine power dissipation, packing factor must be known. For non-unity packing factors, loss density becomes $\rho J^2 = \rho(J_e/\lambda)^2$, and total conductor volume becomes λFV. Thus,

FIGURE 25

SIMPLIFIED FLOW DIAGRAM FOR SADDLE COIL DESIGN

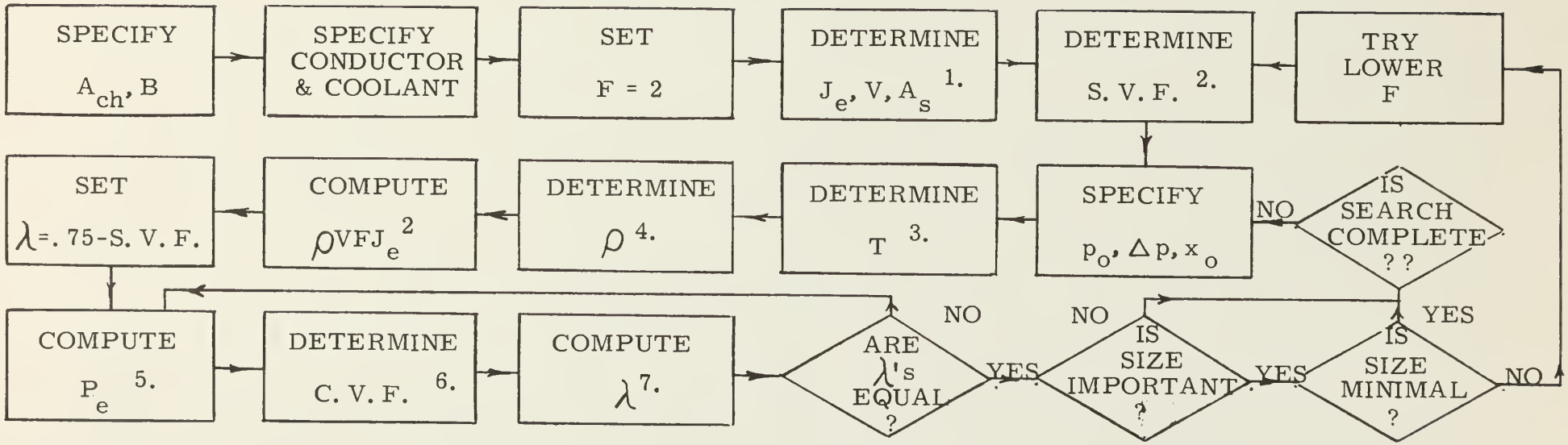

1. From Appendix A
2. From Appendix C
3. Use eqn. (58), Chapter 5, and Appendix D
4. From Appendix B
5. Use eqn. (71)
6. Use eqns. (68) and (69)
7. Use eqn. (70)

$$P_e(\lambda) = \rho VFJ_e^2/\lambda = P_e(\lambda=1)/\lambda \qquad (71)$$

It is suggested that a "first guess" be made that $\lambda = 0.75 - S.V.F.$ For the smaller F=2 coils, this is reasonably accurate, and for the larger F=2 coils, it will be found to be conservative. P_e can then be estimated, the corresponding coolant volume fraction computed, and λ recomputed from eqn. (70). Note that if the "recomputed" λ equals or exceeds the "assumed" λ, the "assumed" λ is physically realizable. However, unless the two are equal, the "realizable" coil has not been optimized, in the sense of obtaining minimum power consumption for the specified form factor. Thus, the design should be recycled until maximum attainable packing factor has been determined. (The solution can be made to converge rapidly. In fact, after some practice manipulating Appendices C and D, a better "first guess" can generally be made than that suggested.)

In order to determine coolant volume fraction (and, for that matter, mean coil operating temperature) for a two-phase coolant, one must specify a particular combination of x_o, p_o, and Δp. Presumably, the simplest procedure here would be to estimate the highest outlet quality which can safely be maintained (since coolant volume fraction decreases as quality increases), select a "reasonable" Δp (which can be related to coolant pump power through eqn. (34)), and "search" on p_o, starting at one atmosphere and working upward. Coolant volume fraction generally (but not always) decreases with increased outlet pressure, due to increased vapor density in the coolant stream. The question here is whether or not the increased packing factor presumably attainable with higher outlet pressures decreases power consumption more than the higher coil operating temperature (due to higher ΔT_c) increases power consumption. (Or, if not, and minimum size is being sought, if the higher loss may be tolerable, in exchange for smaller

size.) Thus, the flow chart indicates that once the "optimum" design (minimum power consumption, minimum size, or some compromise between these) has been determined for a particular x_o, p_o, and Δp, one should specify a new combination of these parameters, and recycle the design.

C. Example problem: minimum power consumption:

As an example of the above design procedure, let us determine the total power consumption for an F=2, liquid-hydrogen-cooled, aluminum saddle coil for use with an MHD channel requiring B=50 kg, and $A_{ch} = 0.1\ m^2$:

1. From Fig. A-1, $J_e = 5.81 \times 10^4\ B/\sqrt{A_{ch}} = 5.81 \times 10^4\ (50/\sqrt{.1})$ = $\underline{9.2 \times 10^6}$ a/m^2.

2. $L = 10\sqrt{A_{ch}} = 3.16$ m: therefore, from Fig. A-3, $V = .176L^3$ = 5.56 m^3, and $A_s = 2.31\ L^2 = \underline{23.1}\ m^2$.

3. Assume σ_c = 4500 p.s.i. and σ_d = 60,000 p.s.i.: from Fig. C-2, S.V.F. = $\underline{.033}$.

4. Assume p_o = 1 atm., Δp = 0.5 atm., and x_o = 50%. From Fig. D-8b (no-slip model), $\Delta T_c = 0.9\ ^oK$.

5. Kutateladze's correlation for peak heat flux for liquid hydrogen indicates that the critical pool boiling heat flux, for a pressure of $\sim$ 1.25 atm., is about 10 watts/cm^2 at $\Delta T_{bl} = 2.8\ ^oK$. (See (112).) Presumably, forced convection cooling would at least equal this. In keeping with the discussion in Chapter V, we shall assume these figures apply here.

6. Using the above, $\overline{T}$ = 20.3 + 0.9 + 2.8 = $\underline{24}^oK$.

7. From Fig. B-7, $\rho = 2.69 \times 10^{-3}\ \rho_s = (2.69 \times 10^{-3})(1.772 \times 10^{-8})$ = $\underline{4.76 \times 10^{-11}}$ ohm-meters.

8. The total electrical power loss for λ = 1 would be $\rho VFJ_e^2 = \underline{44.9}$ Kw.

9. Assume λ = .75 - S.V.F. = .75 - .03 = .72. Corrected power loss

becomes 44.9/.72 = 62.3 Kw.

10. From Fig. D-7b (no-slip model), $S = 1.16 \times 10^{-4}$. From eqn. (58), coolant volume is therefore: $V_c = qS(FL) = (6.23 \times 10^4)(1.16 \times 10^{-4})$ (632) $cm^3 = 4.56 \times 10^{-3}\ m^3$, and C.V.F. is of the order of .005/5, which is negligible.

11. At this point, it would be well to re-examine the applicability of the "inviscid flow" model. The fact that the model calls for such a minute coolant volume fraction in this case is related to the fact that loss density scales with resistivity, and the resistivity of aluminum at this temperature is about three orders of magnitude less than that of copper at 300^o K. assuming q = 46.3 Kw and q/A = 10, the required total heat transfer surface would be 4630 cm^2. Thus, the inviscid flow model indicates that a slot height of about (3390/4630) = 0.732 cm is required, from energy balance considerations. However, this would result in an "equivalent" L/D of (632/1.464) = 432, which leads to the possibility that viscous effects may not be negligible, in this case.

To a first approximation, pressure drop due to viscous effects may be considered directly additive to that attributed to the inviscid flow model. We can establish an upper and lower bound on the influence of viscosity by asking what additional Δp would be required to move the specified flow if a) the coolant were entirely liquid, and b) the coolant were entirely vapor.

The viscosity of saturated liquid hydrogen, for $p \sim 1$ atm., is about 126 micropoise, and the "equivalent diameter" of the slot is 2(0.732) = 1.464 cm. From Fig. D-9b, the inlet velocity under the specified conditions is 5.30 m/s. Thus, the Reynold's number for "all liquid" flow would be:

$$\rho VD/\mu = (.0707)(530)(1.464)/(1.26 \times 10^{-4}) = 5.86 \times 10^5$$

and the corresponding friction factor (from (108)) would be 3.20×10^{-3}.

From eqn. (30), $\Delta p = 4f(L/D)(\rho v)^2/(2\rho)$. Here, $\rho v = .0707(530) = 37.5$, and 1 atm. $= 1.013 \times 10^6$ dynes/cm^2. Thus,

$$\Delta p_{min} = 4(.00320)(432)(37.5)^2/(2)(.0707)(1.013 \times 10^6) = .054 \text{ atm.}$$

Similarly, the viscosity of the saturated vapor would be about 11 micropoise; the Reynold's number for "all vapor" flow would be 6.71×10^6 (since ρv = const for the specified flow), and the corresponding friction factor would be 2.25×10^{-3}. Thus,

$$\Delta p_{max} = 4(.00225)(432)(37.5)^2/(2)(1.34 \times 10^{-3})(1.013 \times 10^6) = 3.24 \text{ atm.}$$

Obviously, this flow is not "inviscid"! However, we can adjust our model, by demanding that the total pressure drop be of the order originally specified. Very approximately, viscous pressure drop scales as $(L/D)^3$: Let us try increasing D by a factor of 4. To maintain roughly the same outlet quality, we shall maintain constant mass flow rate by decreasing (ρv) by the same factor. The "new" bounds become:

$$\Delta p_{min} = 4(.00320)(108)(9.38)^2/(2)(.0707)(1.013 \times 10^6) = .000845 \text{ atm.}$$

$$\Delta p_{max} = 4(.00225)(108)(9.38)^2/(2)(1.34 \times 10^{-3})(1.013 \times 10^6) = .0506 \text{ atm.}$$

This more acceptable! (Ironically, coolant volume fraction now becomes .0135/5.56 = .002, which is still negligible!) With the corrected figures, maximum attainable packing factor is of the order of 0.96, and corresponding electric power consumption would be 46.8 Kw.

12. Assuming surface heat leak is of the order of .05 watts/m^2, total heat leak from this source is .05(23.1) 1 watt, which is negligible.

13. Assume that the thermal conductivity of the support structure is about 0.1 watts/cm-$^\circ$K, and that the length of support elements is of the order of the coil radius (which, from Fig. A-2, is .186 L = 0.588 m). Let the specified stress limit in the supports be 30,000 p.s.i. The net cross section required to support the coil mass would be of the order of:

$$A = \frac{Mg}{\sigma} = \frac{2700(5.56)(2.205)}{30,000} = 1.1 \text{ in}^2 = 7.1 \text{ cm}^2.$$

Since the coil would presumably be supported in all three directions, let us increase this figure to ~ 25 cm^2. Then, the net structural heat leak would be of the order of .1(25/58.8)(276) = 11.68 watts, which is negligible.

14. The flow energy supplied by the pump represents hydraulic dissipation, and presumably is removed as heat by the refrigerator. Assuming a pump efficiency of 50%, this is of the order of $2(\vec{F}.\vec{v}) - 2(V_c \Delta p/L)v_{in}$. Using the adjusted flow figures, dissipation from this source is of the order of $2(.0135)(.5 \times 1.013 \times 10^5)(1.325)/6.32 = 287$ watts.

15. Although the coil windings are at about 24° K, the refrigerator must remove heat from the coolant at 20.3° K. From Fig. 18, refrigerator power is about 70 watts/watt. Total operating power required is thus $71(4.71 \times 10^4) = 3.34$ Mw.

16. If the hypothesized MHD channel were utilized for a seeded-gas MHD generator, one might assume a density of power generation in the channel of ~ 150 Mw/m^3. Since channel volume is 0.316 m^3, such a generator would produce about 47.4 Mw of electrical power. Thus, the total operating power consumption of this coil would amount to about 7% of the generator output. Similar calculations indicate that at this temperature, all 50 kg, F=2 saddle coils share the basic characteristics discussed above: i.e., coolant volume fraction, heat leak, and hydraulic dissipation do not significantly influence the design, within the range of sizes covered by this investigation. Further, since structural volume fraction has been found to be a function of B, F, σ_c, and σ_d only, packing factor is virtually independent of coil size. Thus, since coil volume and channel volume scale together for constant F, and J_e scales as $1/\sqrt{A_{ch}}$ for constant B, the percentage of generator output consumed by such coils would scale as $1/A_{ch}$,

for B=50 kg, F=2 saddle coils, in the range $.01 \leq A_{ch} \leq 10$ square meters.

Several factors bear discussion at this point. The first is that one might, or might not, ever realize the theoretically attainable packing factor of 0.96. Probably, insulation requirements, and simple engineering convenience, would reduce this to about 0.7. However, it was previously indicated that for coils of the same packing factor, the power consumption of a cryogenic aluminum coil would be about an order of magnitude less than that of a comparable "conventional" coil. With loss densities running three orders higher, it does not appear likely that "conventional" coils could approach the packing factors attainable with near-optimum-temperature cryogenic coils. Thus, whether or not the theoretical limit of 0.96 were attained, one might expect that a relative assessment of "attainable" cryogenic and conventional coils would favor the former, even more than might be assumed from Fig. 23.

Next, even if the packing factor realized in an "as built" coil were appreciably lower than that predicted by the theoretical model, the underlying physical characteristics of the design should remain roughly as described here. Most specifically, one would expect the percentage power consumption of "minimum loss" MHD generator coils to scale inversely with channel cross section, under the geometric assumptions made here. Under these circumstances, it appears that such coils would be suitable for MHD power generation, with generators of 50 Mw output, or larger. Since MHD generators must probably produce well over 50 Mw to be commercially competitive, due to other considerations, such coils would appear highly attractive for power generation applications.

Finally, since coolant volume proved to be such an insignificant item in this example problem, it is apparent that one need not strive for maximum attainable q/A in cooling system design. Our "conservative" estimate was

that we could obtain a heat flux of 10 watts/cm^2, at a ΔT_{bl} of 2.8 ^oK. Suppose this ΔT_{bl} could be reduced to, say, 1 ^oK, either through achievement of an improved heat transfer coefficient (through forced convection), or through the luxury of providing additional heat transfer surface, to reduce q/A. Presumably, we would have two choices: either to operate the refrigerator 1.8^o "hotter", or to operate the coil 1.8^o "colder". Assuming that attainable refrigerator efficiencies do, in fact, conform to some smooth curve, and are not a "step function", Fig. 18 indicates that the former option would reduce refrigeration power to about 61.6 watts/watt, and therefore reduce total power consumption by about 12%. The latter option would reduce mean coil resistivity to about 3.6 x 10^{-11} ohm-centimeters, and therefore reduce total power consumption by about 20%. This again reflects the marked temperature sensitivity of the optimum operating point, and indicates that one would do well to experiment with different heat transfer solutions. It also indicates the importance of obtaining realiable heat transfer data for the particular surface and geometry contemplated.

D. Example problem: "lightweight" coil:

For comparison with the above, it might be interesting to determine the characteristics of an F=1.3, liquid-hydrogen-cooled, aluminum saddle coil for the same application:

1. From Appendix A, J_e now becomes 7.3 x 10^7 a/m^2, and V becomes 0.316 m^3. From Fig. B-5, mean coil resistivity is 5.11 x 10^{-11} ohm-meters, and from Fig. C-2, the structural volume fraction becomes .145. Other significant "input" parameters are unchanged.

2. Electrical power consumption for λ =1 becomes 111.7 Kw.

3. Slot factor is unchanged, but assumed slot length now becomes FL=1.3(3.16) = 4.11 m. Coolant volume becomes 6230 cm^3, and C.V.F. becomes .02, for a net packing factor of .835, and resultant electrical loss of 134 Kw.

4. Checking slot height, L/D=445. We again must enlarge the slots by a factor of 4, to reduce L/D to about 110. Adjusted coolant volume fraction becomes .08, for a net packing factor of .829, and an electrical loss of 135 Kw.

5. Assuming the same refrigerator efficiency, total power consumption would be 9.58 Mw.

To compare this coil with that preceding: the volume of the "minimum loss" (F=2) coil was 17.6 times as great as that of the MHD channel. By contrast, the volume of the "lightweight" (F=1.3) coil is equal to that of the MHD channel. The former coil would weigh approximately 16.5 tons, the latter, about 0.93 tons. This reduction in size and mass (and presumably, initial capital cost) has been purchased at the expense of an increase in power consumption (and therefore, operating cost) by a factor of 2.9.

IX. CONCLUSIONS

1. "Minimum loss" cryogenic saddle coils appear economically feasible for use with MHD generating channels with an output of 50 Mw or greater. The total power requirement of such coils comprises less than 10% of generator output at 50 Mw, and the percentage of output power consumed by the coil scales approximately as $1/A_{ch}$, for the specified geometric model.

2. The optimum conductor for such saddle coils is aluminum. The optimum operating temperature (to minimize total power consumption) is about 16 ^{o}K. At this temperature, total power consumption of cryogenic aluminum saddle coils would be about one order of magnitude less than that of comparable "conventional" copper saddle coils, with the same packing factor. However, reduced loss density (the resistivity of aluminum at this temperature is about three orders less than that of "standard" copper at 300 ^{o}K), and the increased strength of structural materials at cryogenic temperatures, should permit realization of much higher packing factors in the cryogenic coils. Since total loss varies inversely with packing factor, the comparison between attainable cryogenic and "conventional" coils favors the former, even more strongly.

3. Temperature optimization is fairly critical: a shift of 10^{o} K in either direction will cause, roughly, a 50% increase in total operating power requirements. Therefore, supercritical helium or liquid hydrogen would be the preferred coolants. (A recent NBS study (105) indicates that optimum operating pressures for the former coolant fall in the range of 15 to 20 atm.) At constant packing factor, liquid-helium and liquid-neon-cooled coils would be about equally remote from the optimum, in terms of total

power consumption. However, the low heat of vaporization and low heat flux attainable with the former might lead to lower packing factors. Whatever the coolant used, geometric considerations and coil size indicate that a forced convection cooling system would be required. The advantage most frequently cited for the use of liquid neon for immersion-cooled coils--- i. e., better packing factors, because of higher latent heat of vaporization, on a volumetric basis--- is inapplicable to forced-convection cooling systems. The low sonic velocity reported for neon sharply restricts attainable flow rates, due to choking considerations. Thus, for forced-convection cooling systems, given the same heat flux, outlet quality, etc., liquid hydrogen permits higher packing factors than liquid neon.

4. The "shape" of the saddle coil model has been quantized in terms of the form factor, $F = 1 + L_e/L$, which compares the mean length of the end turns (assumed to contribute nothing to the "useful" field) to the "working" length of the coil. Forms of interest fall in the range $1.3 \leqq F \leqq 2.0$. The "minimum loss" coil is that corresponding to F=2, at which point coil volume is nearly 18 times the volume of the associated MHD channel. If F is increased above 2, both coil size and total loss increase. Obviously, such shapes are not of interest. If F is decreased below 2, total loss increases, but coil size decreases: at F=1. 3, coil volume equals the volume of the associated MHD channel, and losses are higher by about a factor of 3 (for 50 kg, liquid-hydrogen-cooled, aluminum saddle coils). Minimum attainable F is largely determined by structural considerations and falls roughly in the range $1.3 \leqq F_{min} \leqq 1.6$, depending upon the application. Mean coil resistivity is a very weak function of F, except for copper coils below 60 ^{o}K.

5. Structural Volume fraction has been found to be a function of the

desired channel flux density, the coil form factor, the specified structural stress limit, and the specified conductor stress limit, only. It is a fairly strong function of the first three, and a weak function of the fourth. Basically, the conductor stress limit determines the number of structural elements required, and the structural stress limit, their thickness. Since the resistivity of aluminum is sensitive to "cold work", it is essential that stress levels in aluminum cryogenic conductors be kept below the proportional limit for that material. Since yield strength is generally decreased by the same metallurgical processing used to minimize the resistivity of cryogenic conductors, considerable thought must be given to the design of structural supports for aluminum coils. If possible, aluminum coils should be designed to permit final anneal after assembly, or at least, anneal of individual conductor "bundles" after final shaping.

6. At or near optimum temperature, heat removal from cryogenic aluminum coils is not a significant problem. For example, for a liquid-hydrogen-cooled aluminum coil, the heat transfer surface and coolant volume required from an energy-balance viewpoint are insignificant. However, coolant ducts must be distributed through the windings, in sufficient number of ensure reasonable temperature homogeneity. Analysis of coil geometry and stress distribution indicates that the most likely coolant duct geometry would involve the use of slots (vice tubes, pipes, etc.), located adjacent to structural support members. Assuming the support structure would be stainless steel, the thermal conductivity of that structure would be two to four orders of magnitude less than that of the coil conductors, at the temperatures investigated here. Therefore, it seems reasonable to assume that heat flux into the coolant would occur only across the slot surface "away from" the support structure.

7. At or near optimum temperature, heat generation may be so low that the coolant slot height must be "sized" by consideration of viscous effects, rather than by use of the inviscid-flow, energy-balance models presented herein. However, when such is the case, coolant volume fraction tends to be so small that the choice between these alternatives does not strongly influence the ultimate outcome of the design analysis.

8. At or near optimum temperature, the performance of aluminum cryogenic coils is dominated by refrigeration costs. In this study, it was estimated that currently, 70 watts of refrigerator power would be required to remove each watt of heat generated at 20.3 ^{o}K. Of the various heat sources, electrical losses dominate. (For a 50 kg, F=2, liquid-hydrogen-cooled aluminum coil, suitable for use with a 47 Mw MHD generator, electrical losses were computed to be 46.8 Kw, surface heat leak, 1 watt, structural heat leak, $\sim$ 6 watts, and hydraulic dissipation, $\sim$ 300 watts. Heat leak through the electrical input connections was not estimated, but presumably, proper design of these leads can ensure that this leak is negligible, compared to I^2R heating.) An ideal, Carnot refrigerator would require only 13.8 watts of power for every watt of heat "pumped" from 20.3^{o} to 300^{o} K. There is obviously "room for improvement", and past trends indicate that further improvement in refrigerator efficiency may be expected. Any improvement in refrigerator efficiency would obviously be reflected in reduced operating costs.

9. Due to the strong coupling between the residual resistivity of aluminum, and the other components of "total" resistivity, improved metallurgical techniques might yield a significant reduction in the resistivity of that metal, at 16^{o} K. (In particular, the process which Post and Taylor have utilized to reduce the residual resistivity of sodium (63) may hold some promise.) If the Bloch-Gruneisen curve does, in fact, serve as a

lower-bound for the resistivity of aluminum, a net reduction of about a factor of two may be possible.

10. Considering 8. and 9. above, one might reasonably hope for an eventual reduction in the minimum power requirements of cryogenic saddle coils, by as much as a factor of 4 below that currently attainable.

11. This study has been limited to "air-core" coils, in keeping with the model defined in Chapter I. However, it is possible that the basic saddle coil configuration, for a smaller F=2 coils investigated here, could feasibly be modified for use with an iron core. In a sense, this might buy the first 20 kg "for free". By such means, 50 kg saddle coils might be made attractive for use with smaller MHD generators than the 50 Mw minimum established here.

X. RECOMMENDATIONS

Every effort has been made to ensure mutual independence between the various sections of this work, in order that the value of the whole need not depend upon complete acceptance of each component part. Specifically, there are several areas where existing data are scanty, or controversial, or where the "state-of-the-art" is in a process of apparent change:

1. Magnetoresistance is known to be sensitive to size effects, and one might be advised to obtain experimental data for the conductor geometry contemplated. If this is done, the possible inaccuracies inherent in "pulsed" measurements should be weighed carefully, before proceeding. If possible, such data should be obtained before entering the detailed design phase.

2. Cryogenic refrigerators have been improved significantly within the last several years. Since the early 1960's, the projected power consumption of large, liquid-helium refrigerators has dropped from 1000 watts per watt to 500 watts per watt, and further improvement seems likely. Here, the best source of information would be the various manufacturers' representatives.

3. Heat transfer is probably the greatest point of uncertainty in this work. While the heat transfer problem does not dominate "optimum" saddle coil design, both resistivity and refrigerator efficiency are sufficiently strong functions of temperature that ΔT_{bl} and ΔT_c should be established with some accuracy, if possible. Presumably, one could afford the luxury of designing for low heat flux and low pressure drop, to minimize these temperature increments. With two-phase coolants, it would be valuable to know the maximum heat flux which could be tolerated, without risking burnout.

Again, experiments to obtain these data, for the coolant and duct geometry contemplated, should be conducted as early in the design process as possible. In particular, experimental data for forced-convection, two-phase cryogenic boiling, with the type of slot goemetry discussed here, are nonexistant at the present time.

In short, if better information can be obtained, in any of these areas, it can readily be substituted for the pertinent section of this work, and the analysis modified accordingly.

Finally, one point might bear repeating, in closing. The only justification for the added cost and complexity of cryogenic coils, as compared to "conventional" coils, is that of reduced operating power requirements. Even if an optimum-temperature, F=2 coil is considered undesirable for a particular application, the basic motivation for using some other cryogenic coil, rather than a "conventional" coil, is still the same. Logically, then, the design analysis should sieze every opportunity to ensure that the cryogenic coil specified delivers its full potential. For example, the use of metal foils is convenient in the construction of "tape-wound" solenoids. However, if preliminary experiments indicate that the magnetoresistance of such foils lies appreciably above the bulk of amassed experimental data, then that concept should be discarded, and some other conductor geometry investigated, before proceeding to the construction stage. Considering the extreme penalty paid for every watt of heat dissipated within the coil, the expenditure of additional time, effort, and capital before building the coil should be easily justifiable on the basis of reduced operating cost!

APPENDICES

A COMPREHENSIVE ANALYSIS OF CRYOGENIC MAGNETS SUITABLE FOR MAGNETOHYDRODYNAMIC APPLICATIONS

by

JOHN ALLEN McMORRIS II, LIEUTENANT, U.S. NAVY

B.S., U.S. Naval Academy
(1957)

S.M., Nav. Eng., Massachusetts Institute of Technology
(1963)

SUBMITTED IN PARTIAL FULFILLMENT OF THE
REQUIREMENTS FOR THE DEGREE OF
DOCTOR OF SCIENCE
at the
MASSACHUSETTS INSTITUTE OF TECHNOLOGY
June, 1965

THESIS SUPERVISOR: HERBERT H. WOODSON, SC.D.
Professor of Electrical Engineering

Library
U. S. Naval Postgraduate School
Monterey, California

APPENDICES

A COMPREHENSIVE ANALYSIS OF CRYOGENIC MAGNETS SUITABLE FOR MAGNETOHYDRODYNAMIC APPLICATIONS

by

JOHN ALLEN McMORRIS II, LIEUTENANT, U.S. NAVY

B.S., U.S. Naval Academy
(1957)

S.M., Nav. Eng., Massachusetts Institute of Technology
(1963)

SUBMITTED IN PARTIAL FULFILLMENT OF THE
REQUIREMENTS FOR THE DEGREE OF
DOCTOR OF SCIENCE
at the
MASSACHUSETTS INSTITUTE OF TECHNOLOGY
June, 1965

THESIS SUPERVISOR: HERBERT H. WOODSON, SC.D.
Professor of Electrical Engineering

Library
U. S. Naval Postgraduate School
Monterey, California

APPENDICES

A. Coil geometry curves.....158
B. Mean coil resistivity curves.....162
25 KG coils.....163
50 KG coils.....167
75 KG coils.....171
100 KG coils.....175
C. Structural curves.....179
D. Coolant curves.....184
Nitrogen.....185
Neon.....194
Parahydrogen.....203
Helium.....212
E. Computer programs.....221
Coil geometry / resistivity.....222
Structural analysis.....228
Data fitting.....232
Coolant flow analysis.....235
F. Bibliography.....249

APPENDIX A

Coil Geometry Curves

List of Symbols

a	Offset between center of channel and center of either coil cylinder (m)
A_{ch}	MHD channel cross-sectional area (m^2)
A_{cl}	Total coil cross-sectional area (both lobes) (m^2)
A_s	Total coil surface area (m^2)
B	Channel flux density (KG)
J_e	Effective current density (amps/m^2)
L	Channel (or coil) length (m)
R	Coil cylinder radius (m)
V	Total coil volume (m^3)
W_{ch}	MHD channel width (m)

FIGURE A-1

Effective Current Density for given Form Factor

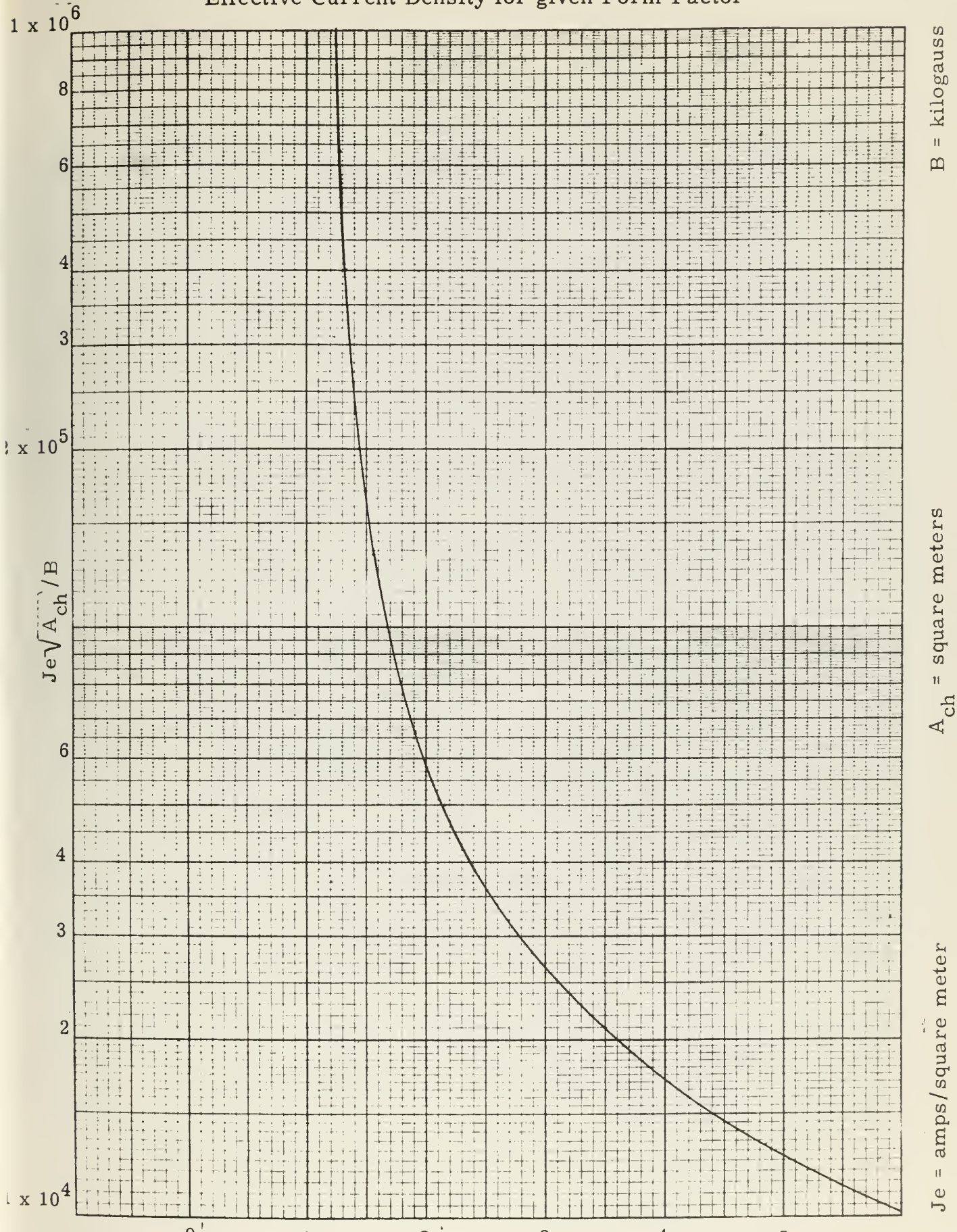

FIGURE A - 2

R, a, and W_{ch} for given Form Factor

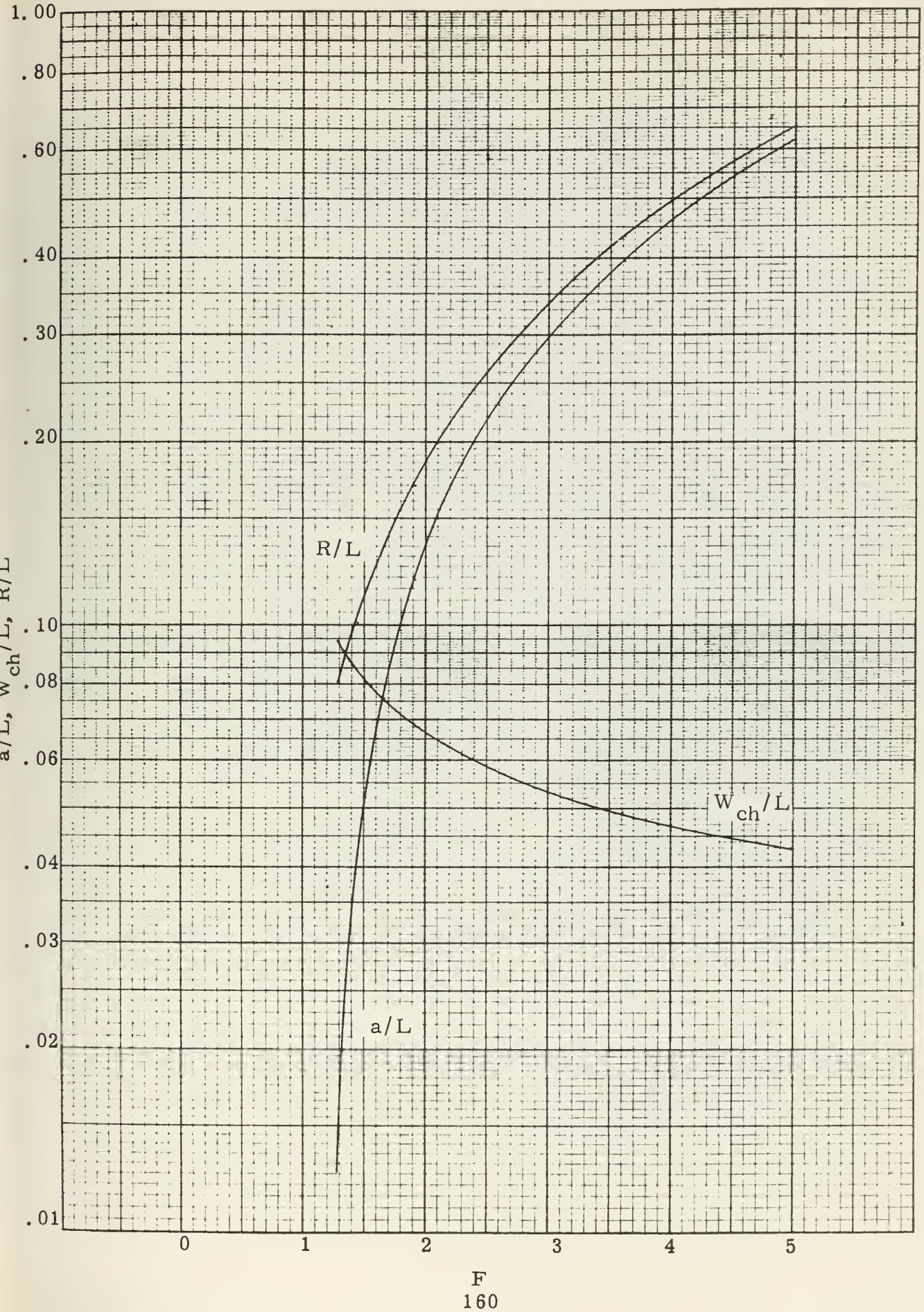

FIGURE A -3

A_s, A_{cl}, and V for given Form Factor

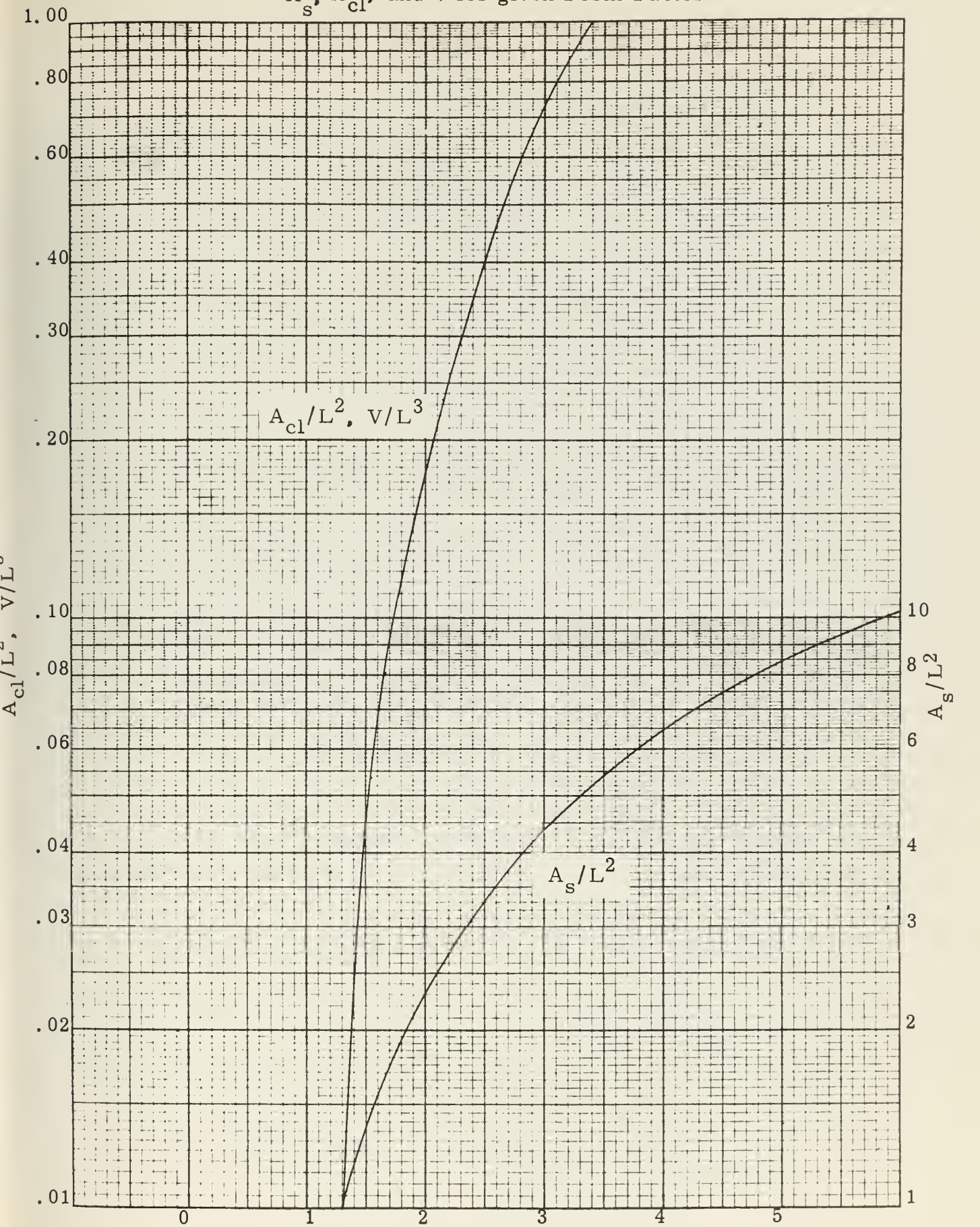

APPENDIX B

Resistivity Curves

List of Symbols

B	Channel flux density (KG)
F	Coil form factor (dimensionless)
R	Mean coil resistivity (ohm-meters)
R_s	Standard resistance: 1.7715×10^{-8} ohm-meters
T	Mean coil temperature (^{o}K)

FIGURE B-1

R/R_s for B = 25 kg F = 1.3

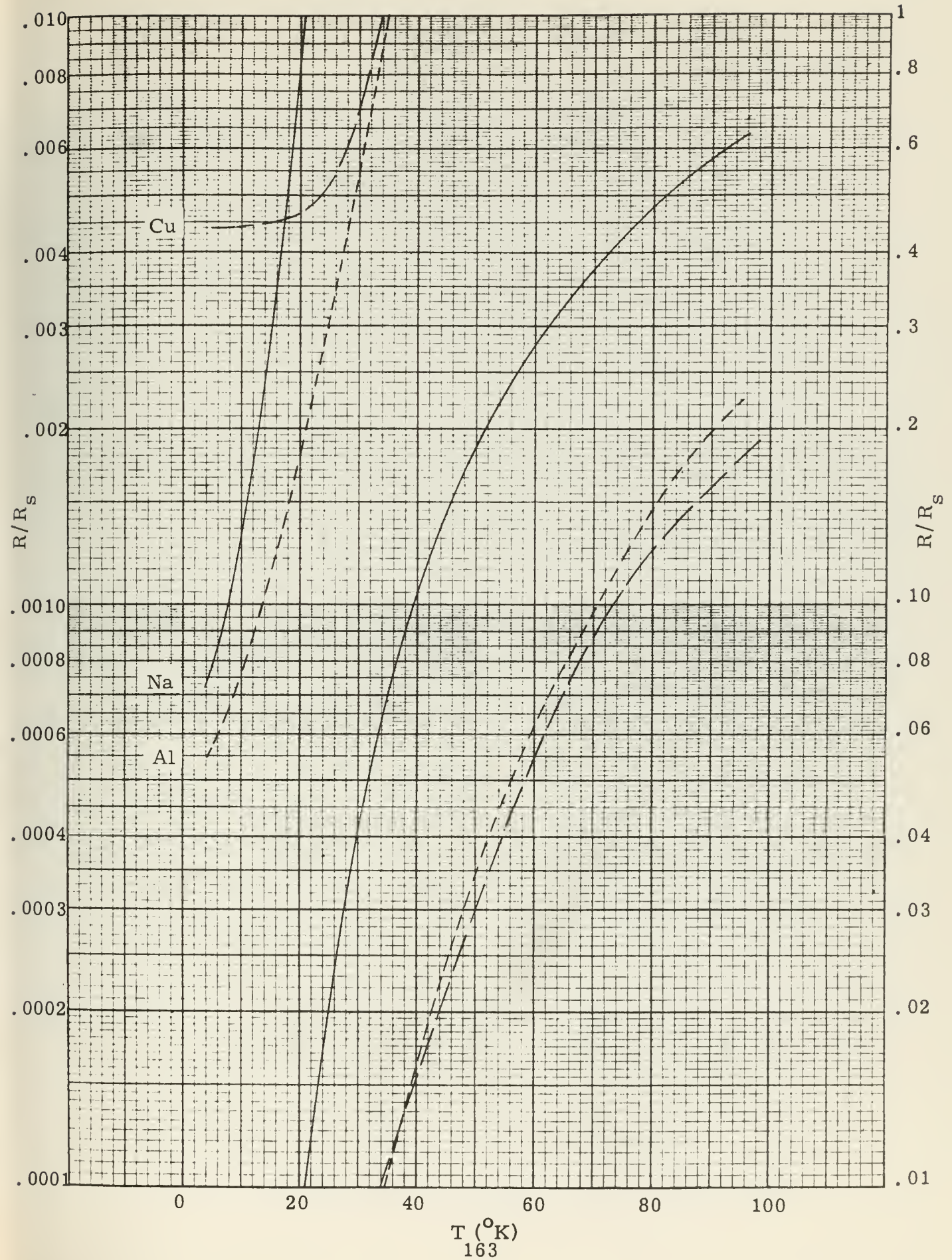

FIGURE B-2

R/R_s for B = 25 kg, F = 1.6

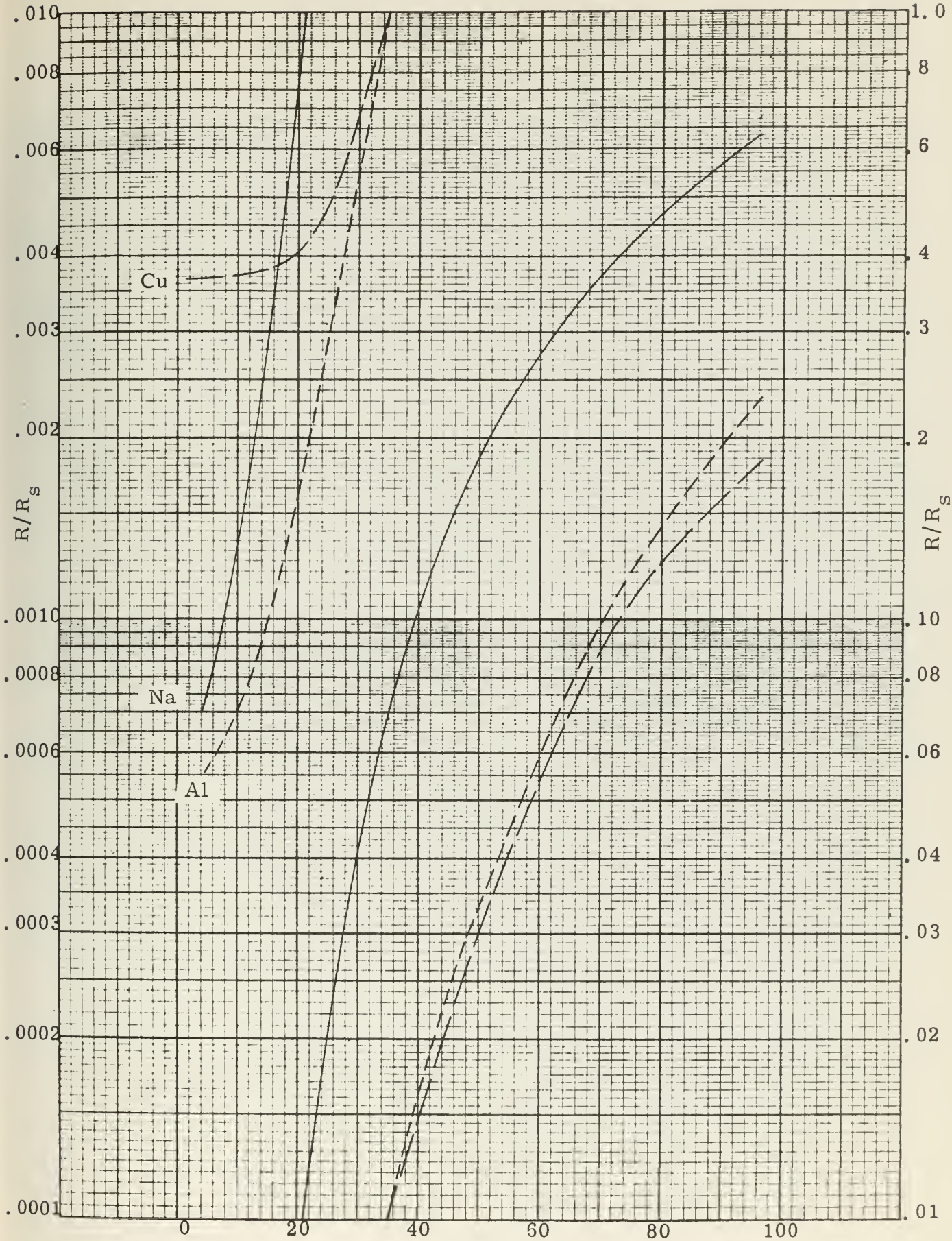

FIGURE B-3

R/R_S for B = 25 kg, F = 2.0

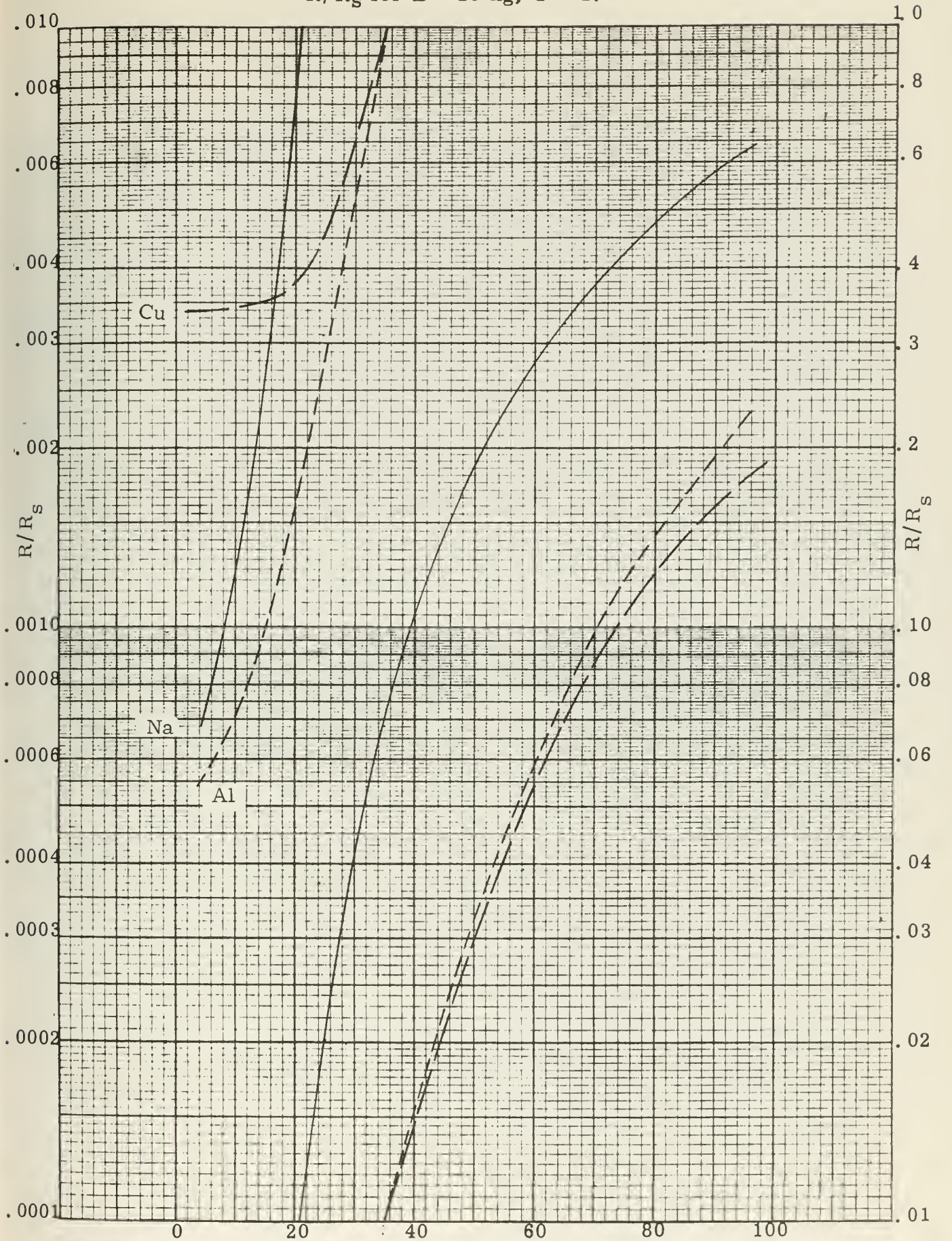

FIGURE B-4

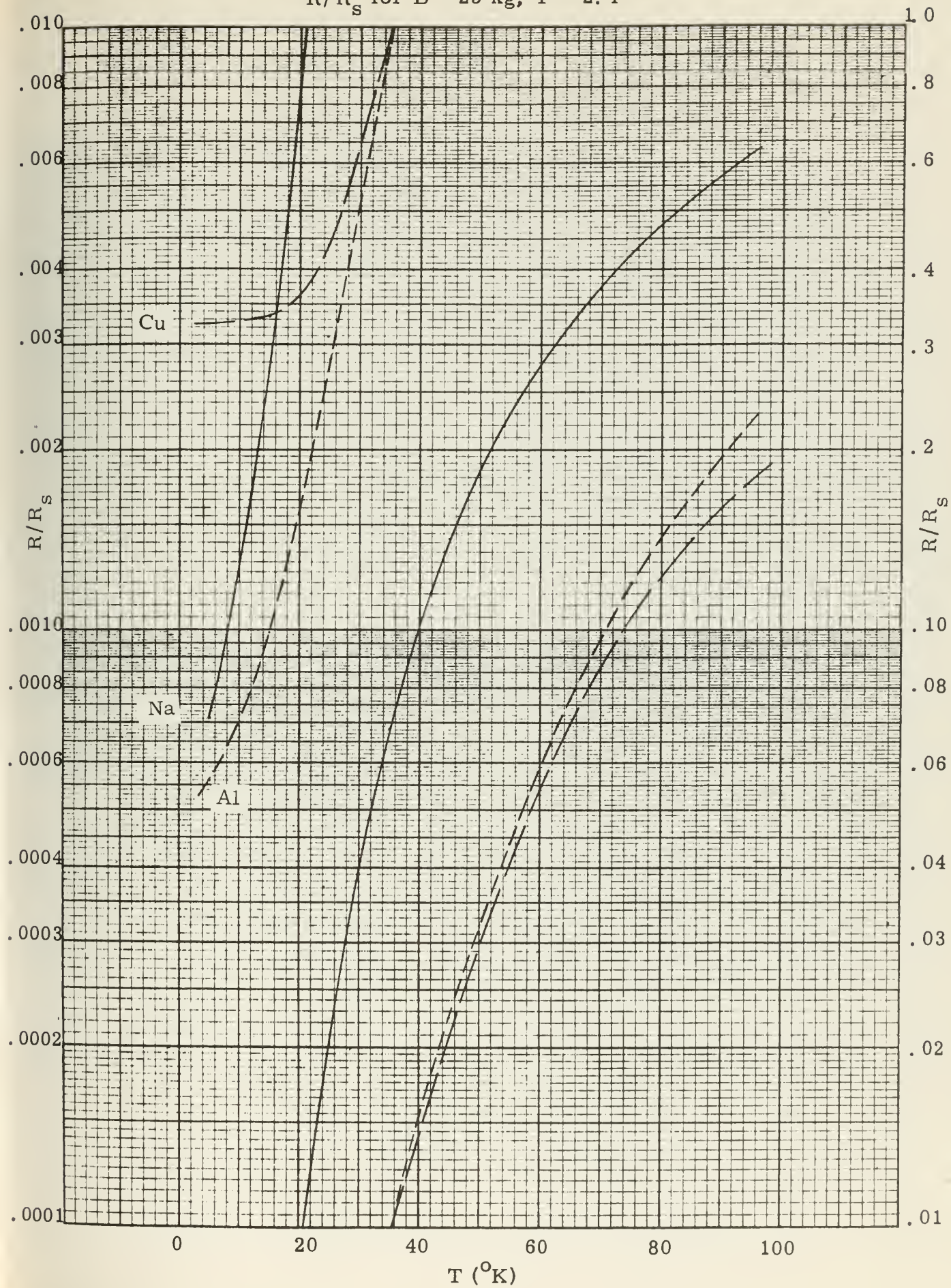
R/R_s for B = 25 kg, F = 2.4
.010
.008
.006
.004
.003
.002
.0010
.0008
.0006
.0004
.0003
.0002
.0001
1.0
.8
.6
.4
.3
.2
.10
.08
.06
.04
.03
.02
.01
R/R_s
R/R_s
Cu
Na
Al
0
20
40
60
80
100
T (°K)

FIGURE B - 5

R/R_s for B = 50 kg, F = 1.3

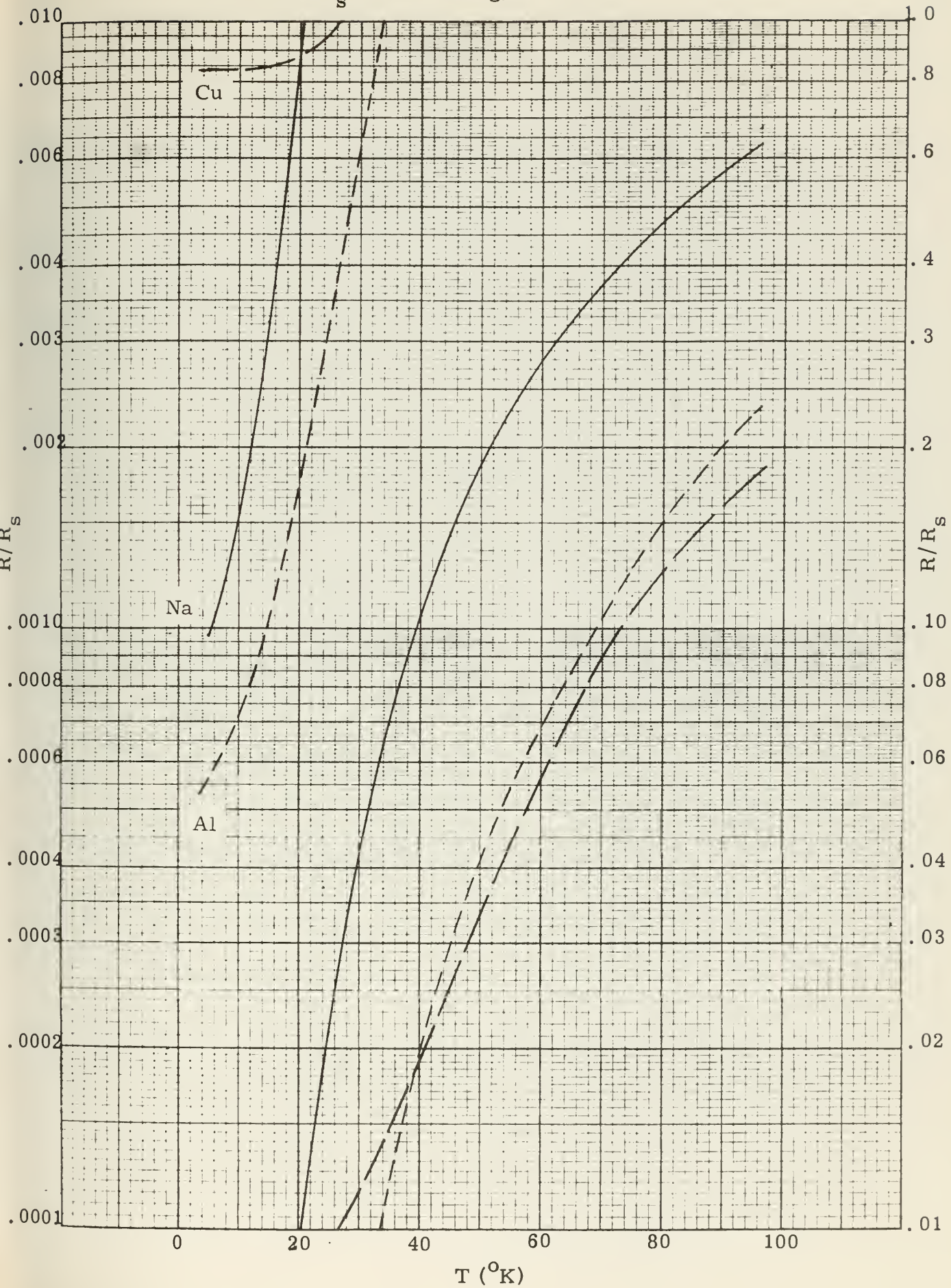

FIGURE B - 6

R/R_s for B = 50 kg, F = 1.7

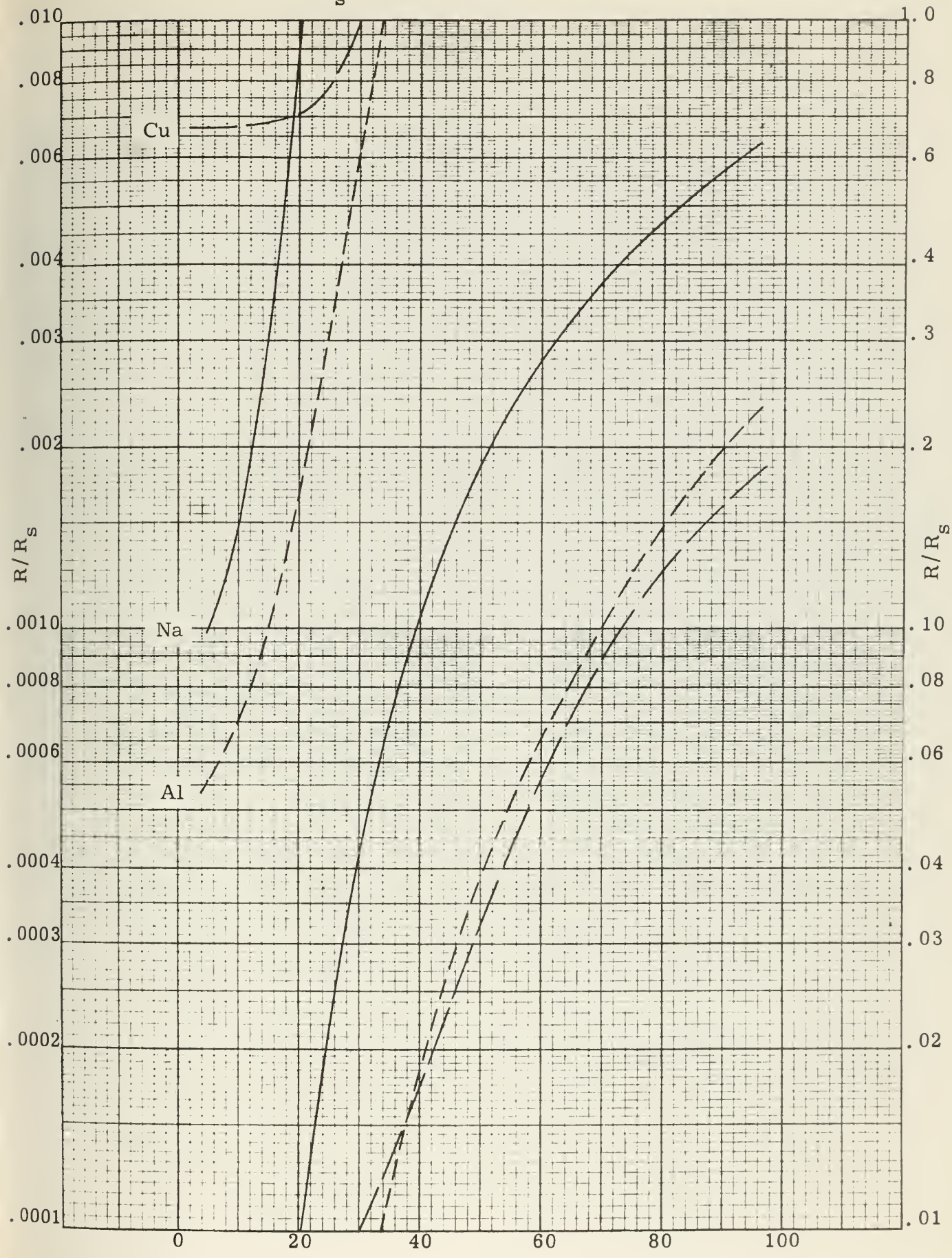

FIGURE B - 7

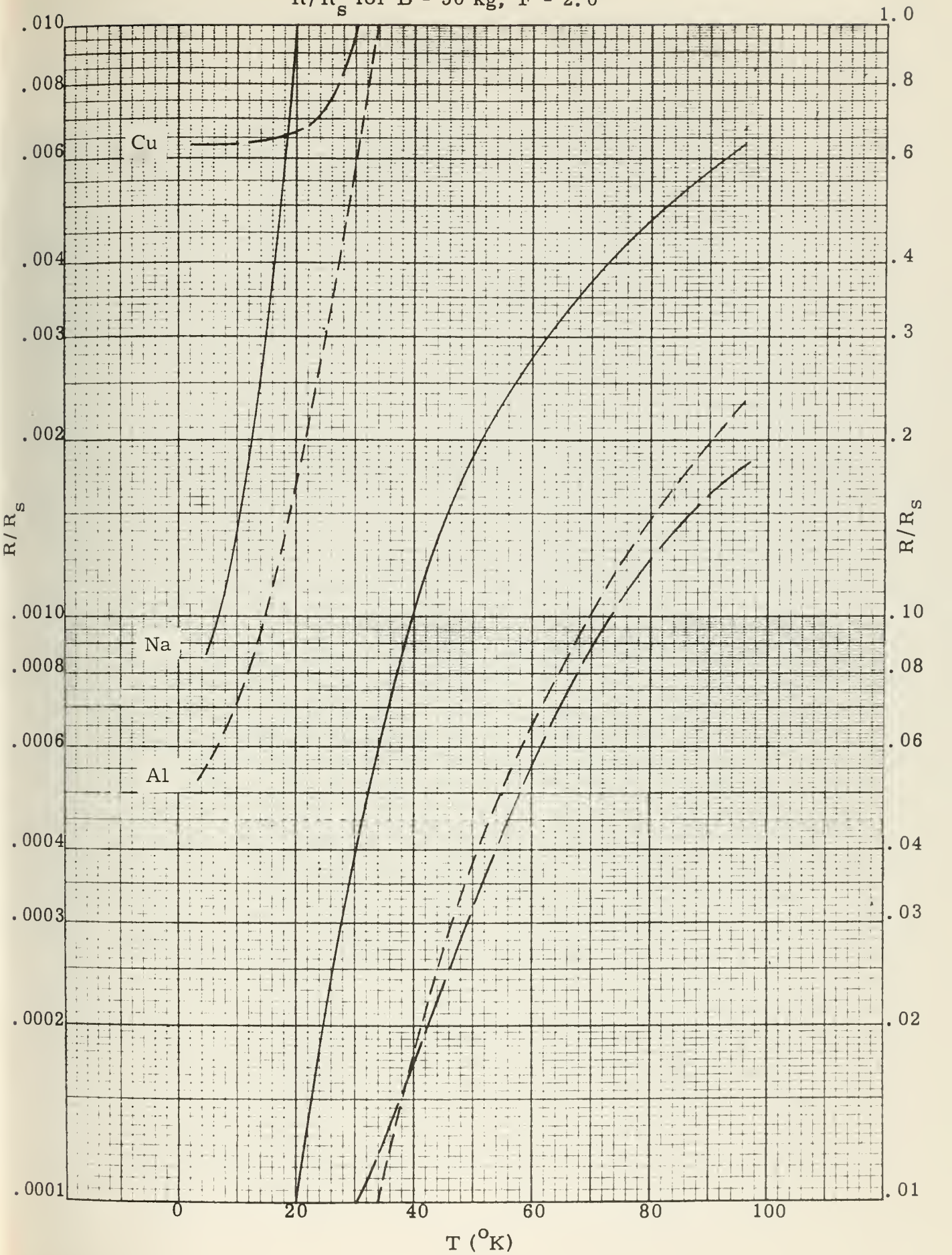
R/R_s for B = 50 kg, F = 2.0
.010
.008
.006
.004
.003
.002
.0010
.0008
.0006
.0004
.0003
.0002
.0001
1.0
.8
.6
.4
.3
.2
.10
.08
.06
.04
.03
.02
.01
R/R_s
R/R_s
Cu
Na
Al
0
20
40
60
80
100
T (°K)

FIGURE B-8

R/R_s for B = 50 kg, F = 2.7

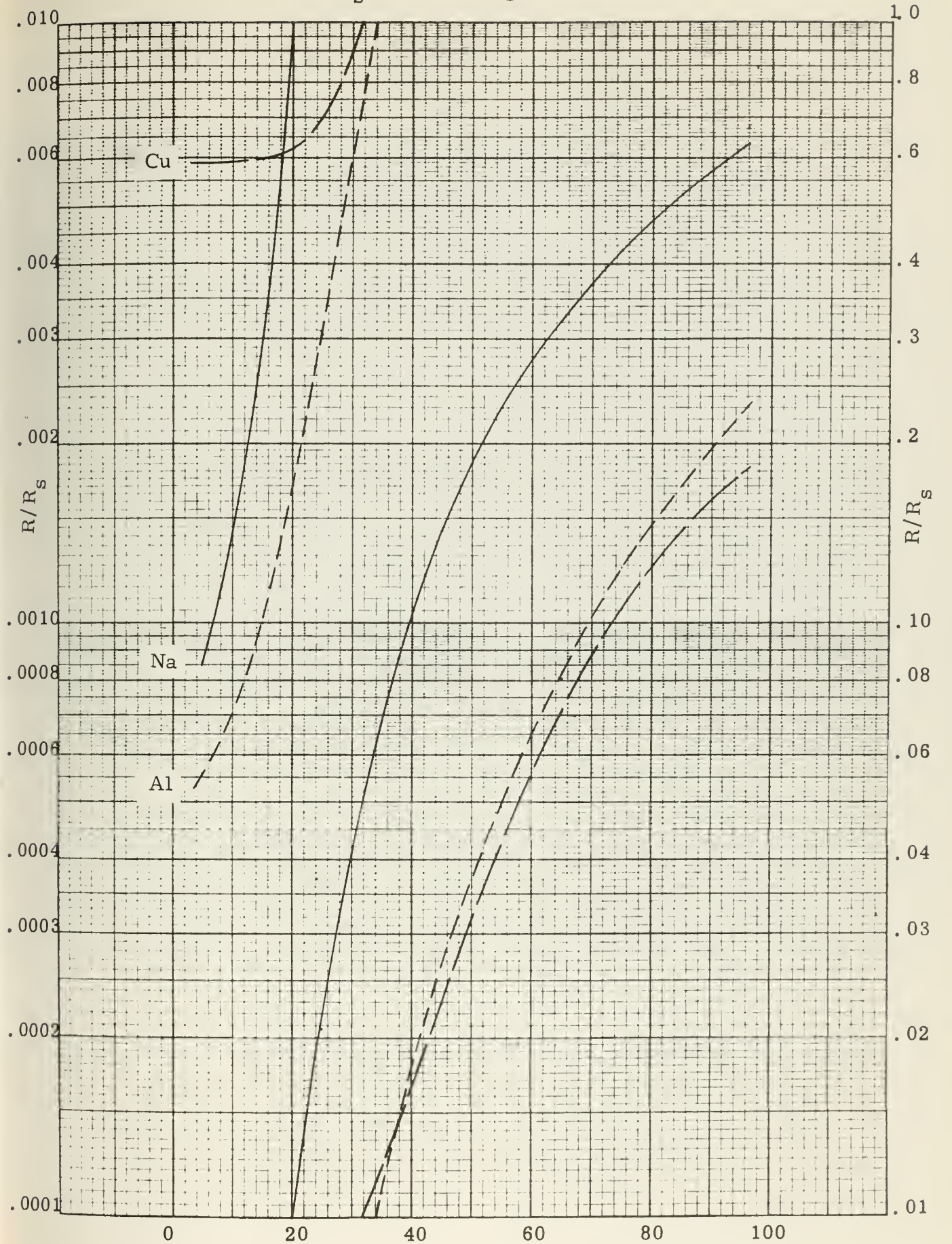

FIGURE B-9

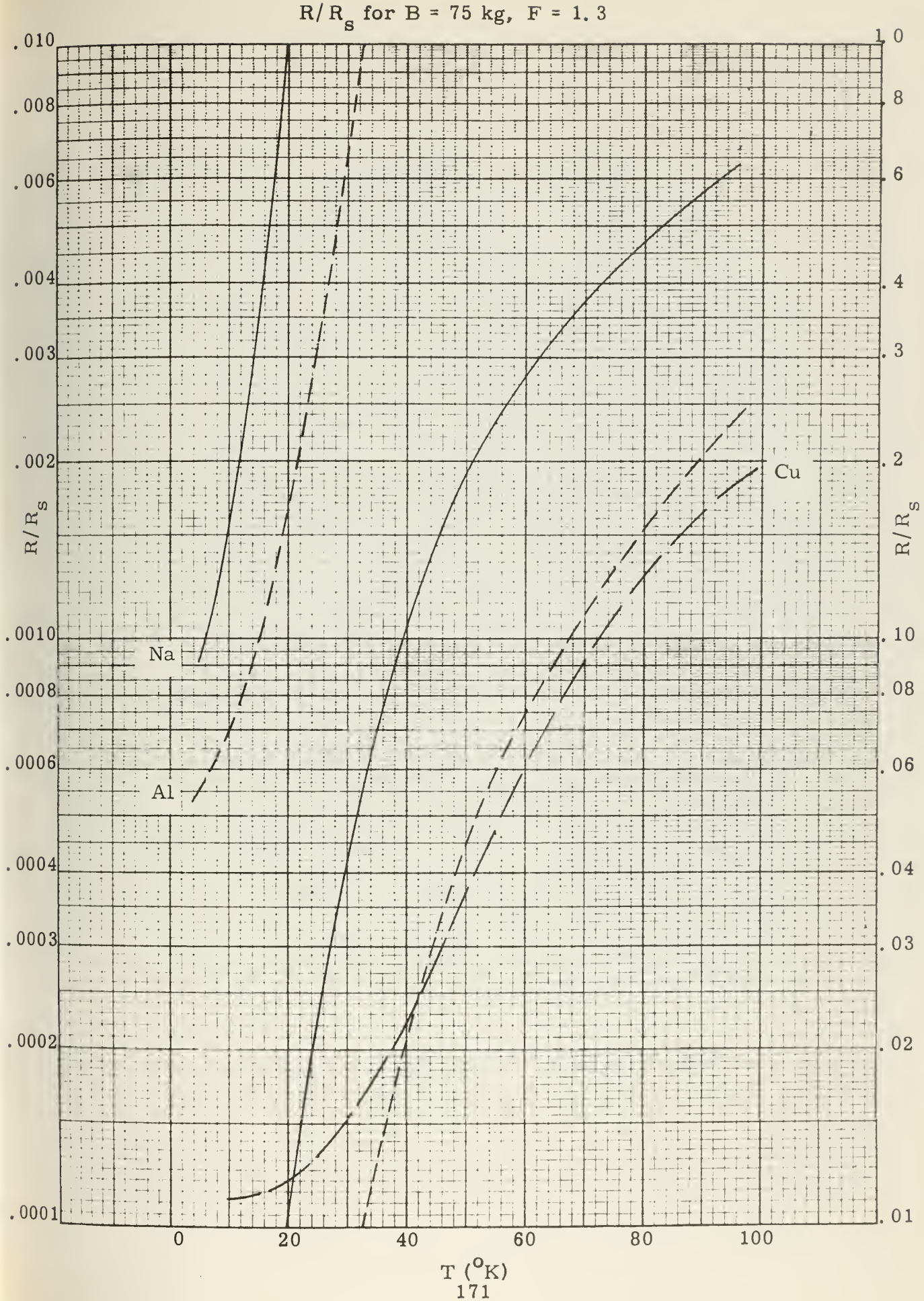
R/R_s for B = 75 kg, F = 1.3
.010
.008
.006
.004
.003
.002
.0010
.0008
.0006
.0004
.0003
.0002
.0001
R/R_s
1.0
.8
.6
.4
.3
.2
.10
.08
.06
.04
.03
.02
.01
R/R_s
Na
Al
Cu
0
20
40
60
80
100
T (°K)

FIGURE B-10

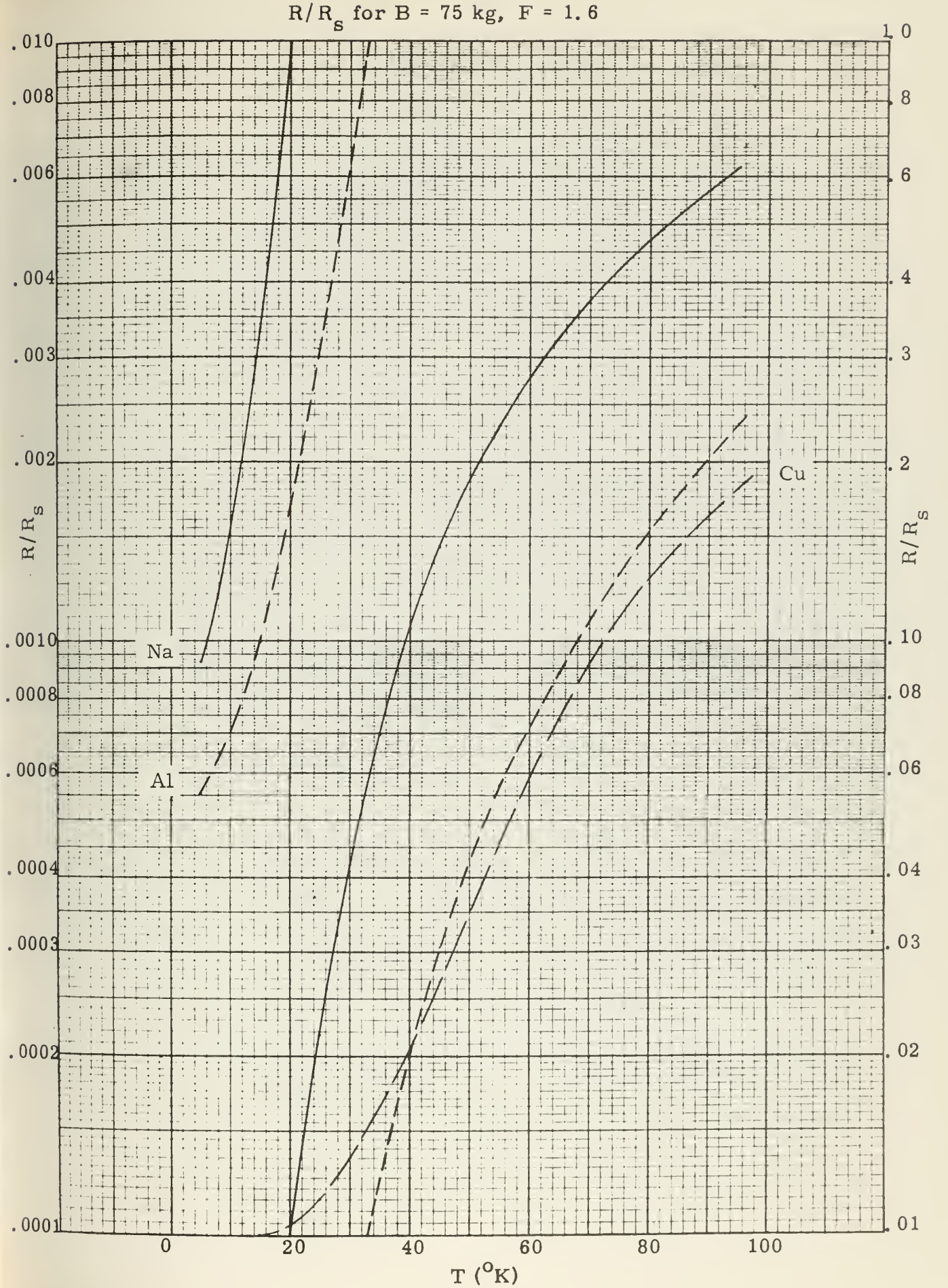
R/R_s for B = 75 kg, F = 1.6
.010
.008
.006
.004
.003
.002
.0010
.0008
.0006
.0004
.0003
.0002
.0001
R/R_s
Na
Al
Cu
1.0
8
6
4
3
2
10
08
06
04
03
02
01
R/R_s
0
20
40
60
80
100
T (°K)

FIGURE B-11

R/R_s for B = 75 kg, F = 2.0

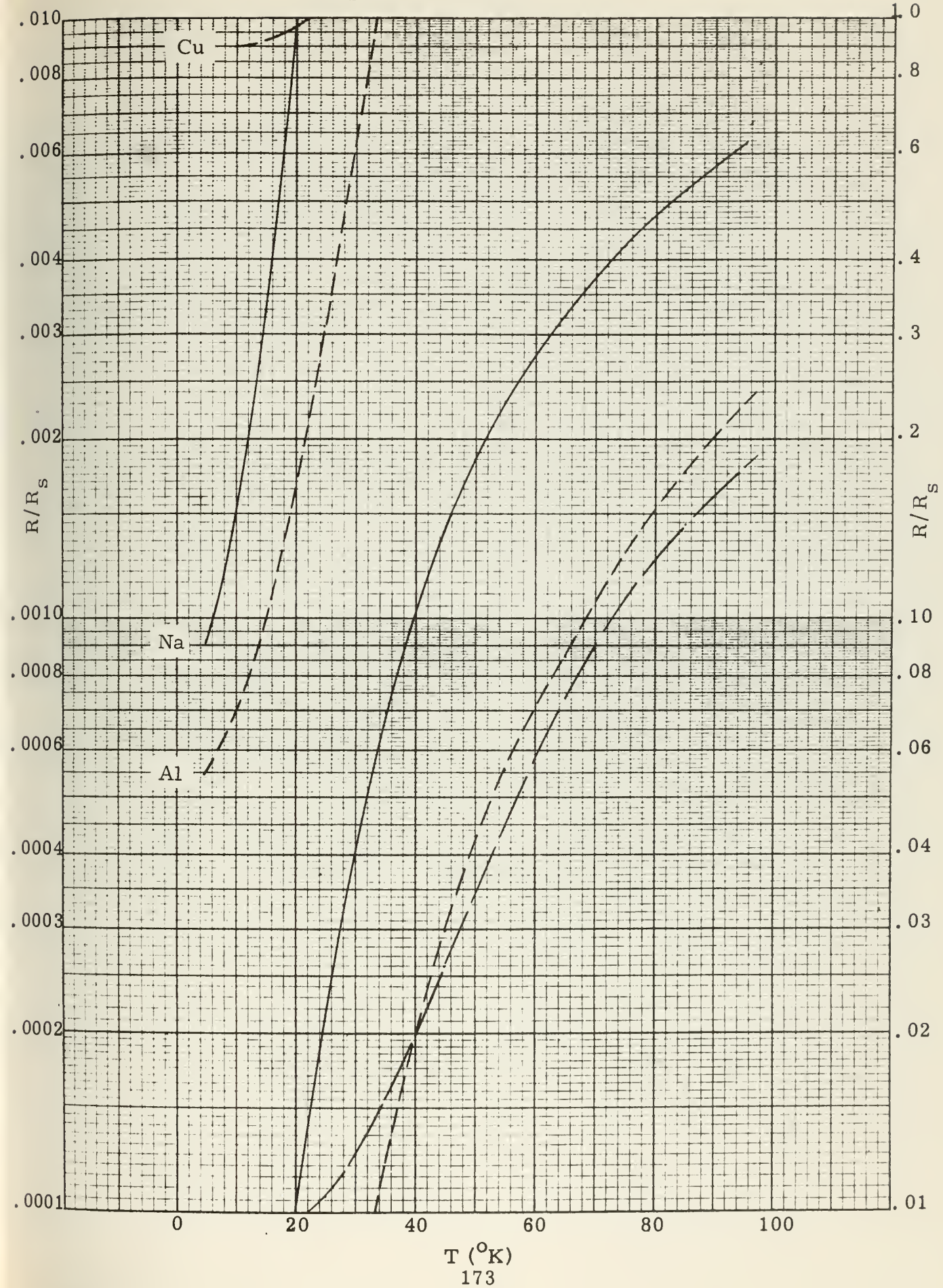

FIGURE B-12

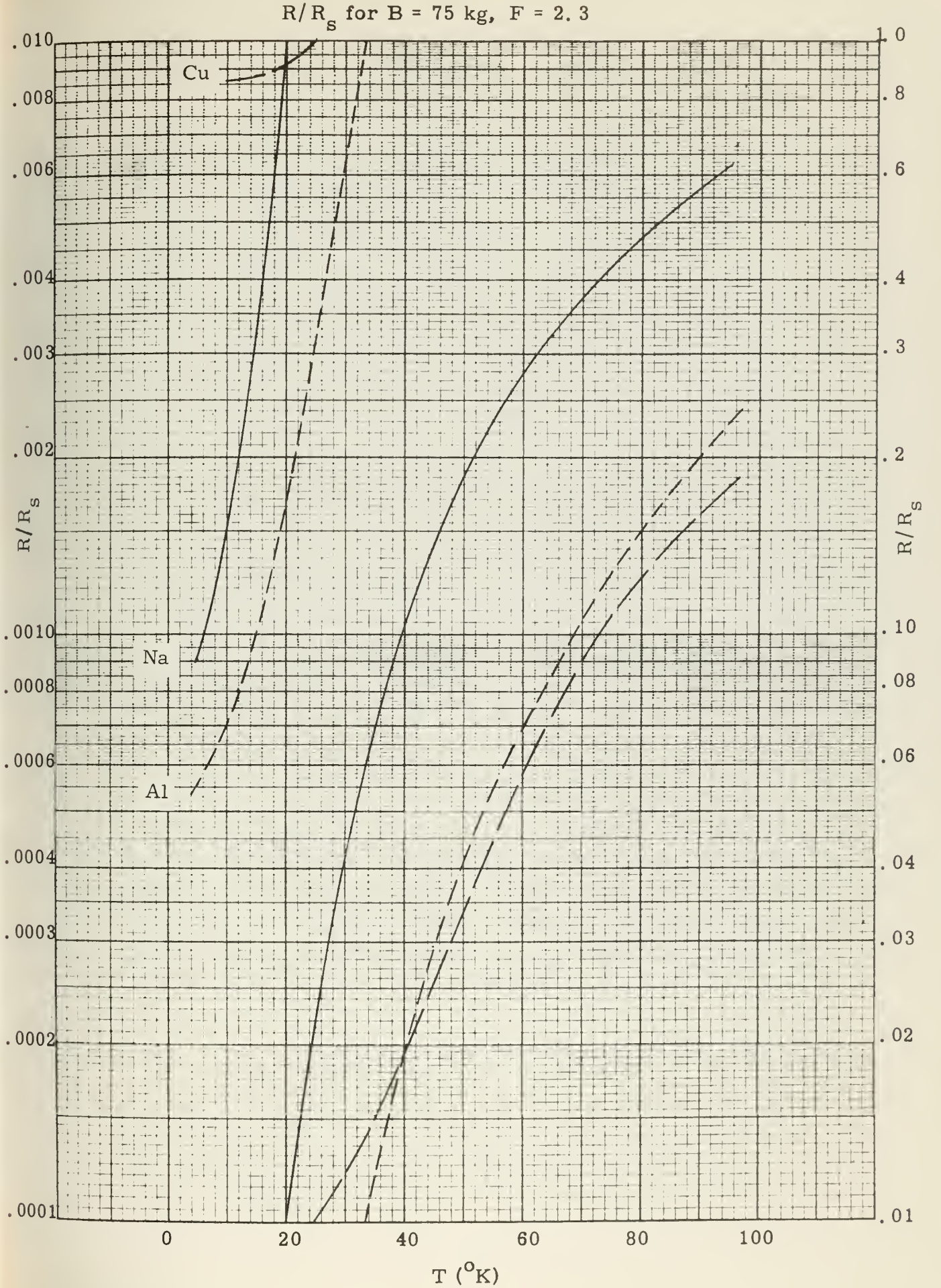
R/R_s for B = 75 kg, F = 2.3
Cu
Na
Al
.010
.008
.006
.004
.003
.002
.0010
.0008
.0006
.0004
.0003
.0002
.0001
1.0
.8
.6
.4
.3
.2
.10
.08
.06
.04
.03
.02
.01
R/R_s
R/R_s
0
20
40
60
80
100
T (°K)

FIGURE B-13

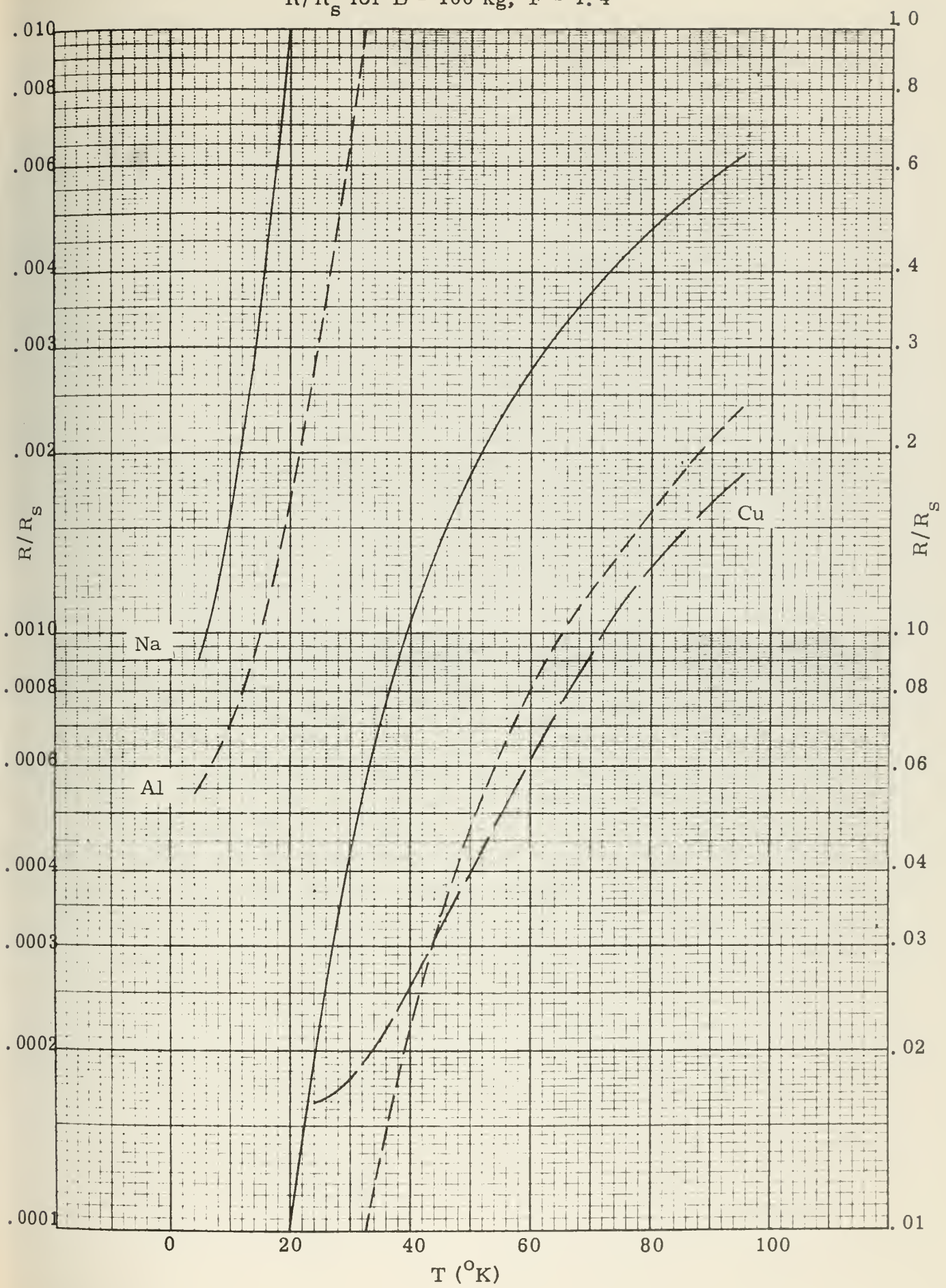
R/R_s for B = 100 kg, F = 1.4
.010
.008
.006
.004
.003
.002
.0010
.0008
.0006
.0004
.0003
.0002
.0001
R/R_s
1.0
.8
.6
.4
.3
.2
.10
.08
.06
.04
.03
.02
.01
R/R_s
Na
Al
Cu
0
20
40
60
80
100
T (°K)

FIGURE B-14

R/R_s for B = 100 kg, F = 1.7

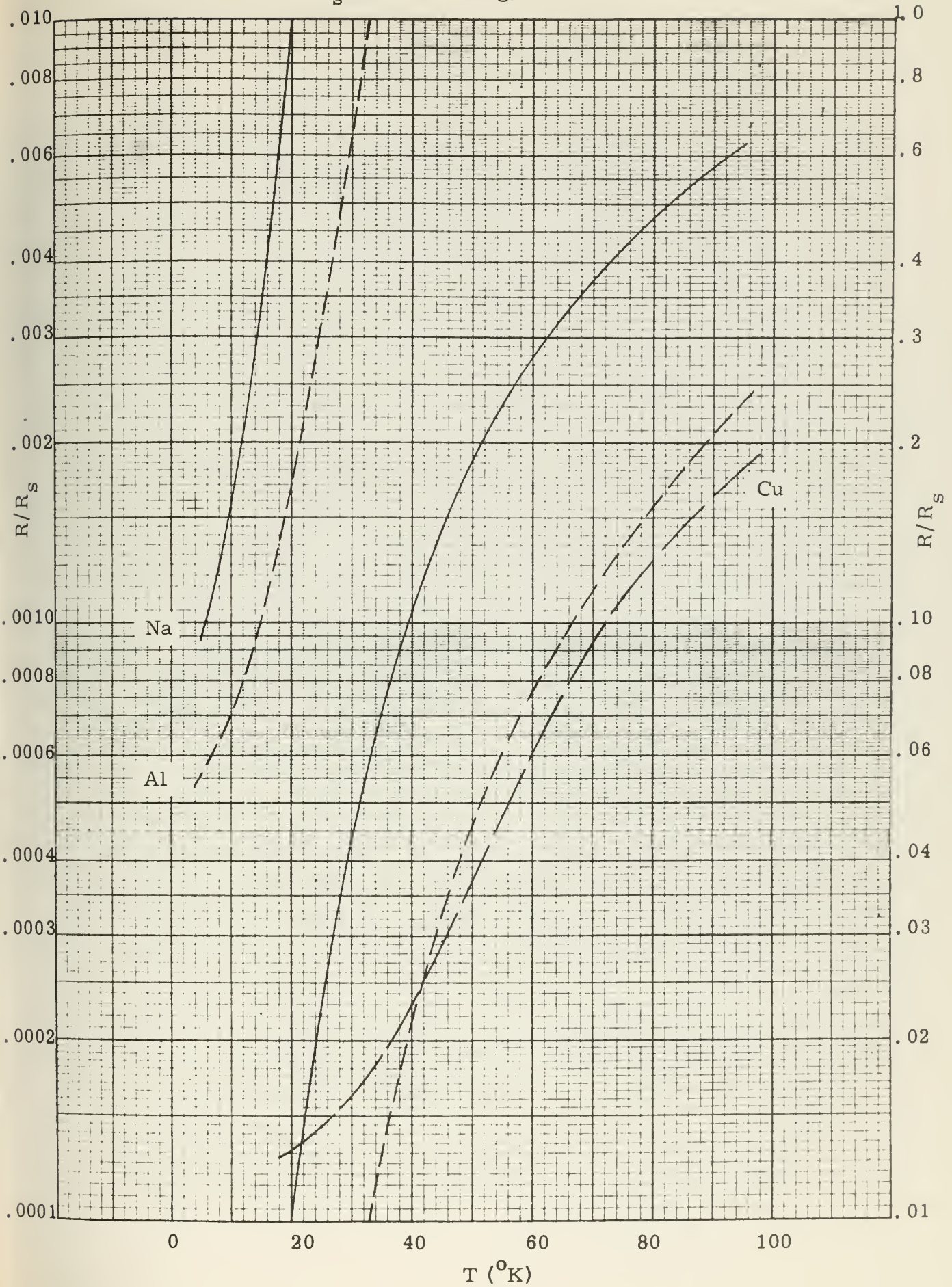

FIGURE B-15

R/R_s for B = 100 kg, F = 2.1

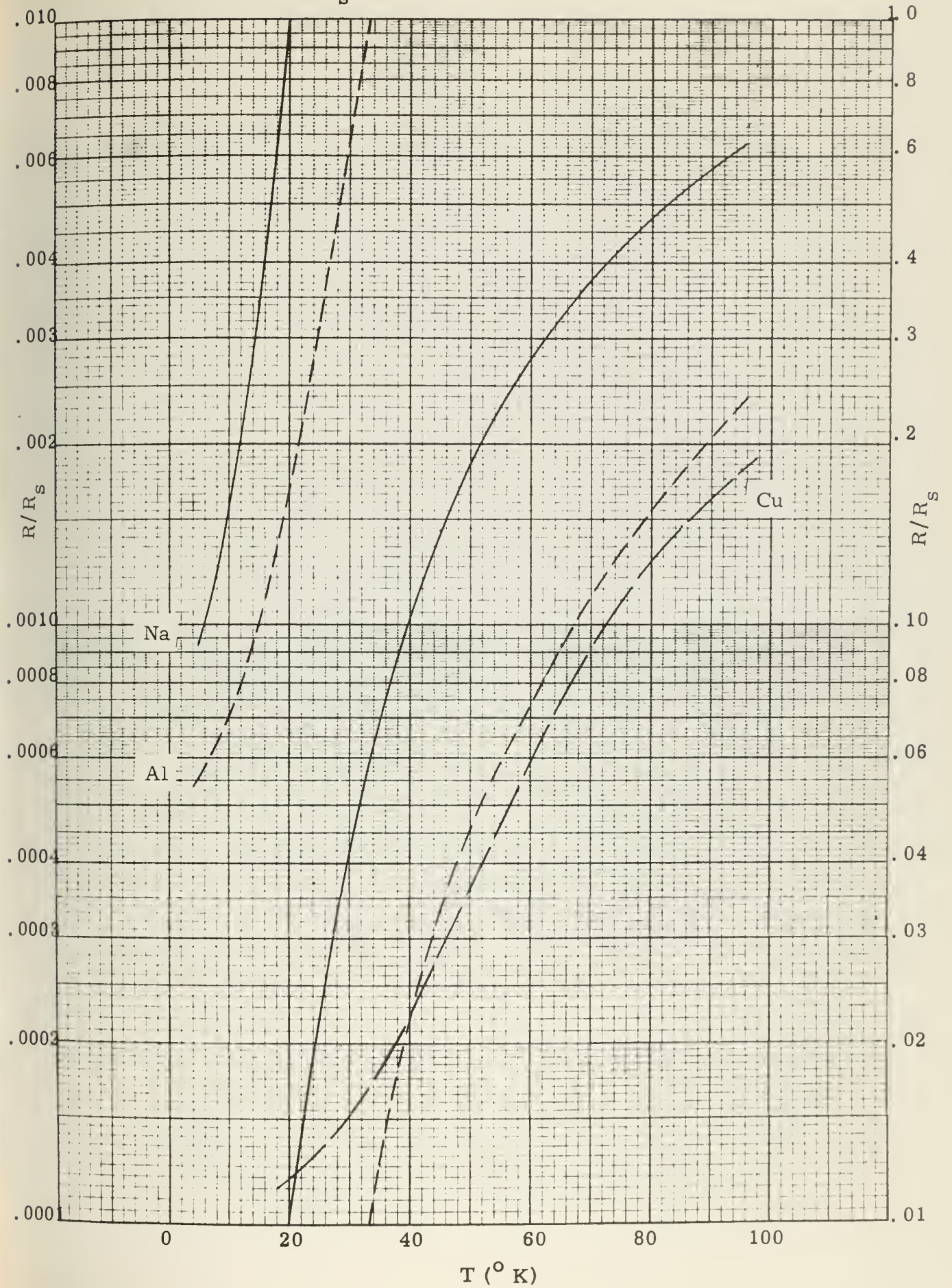

FIGURE B-16

R/R_s for B = 100 kg, F = 2.7

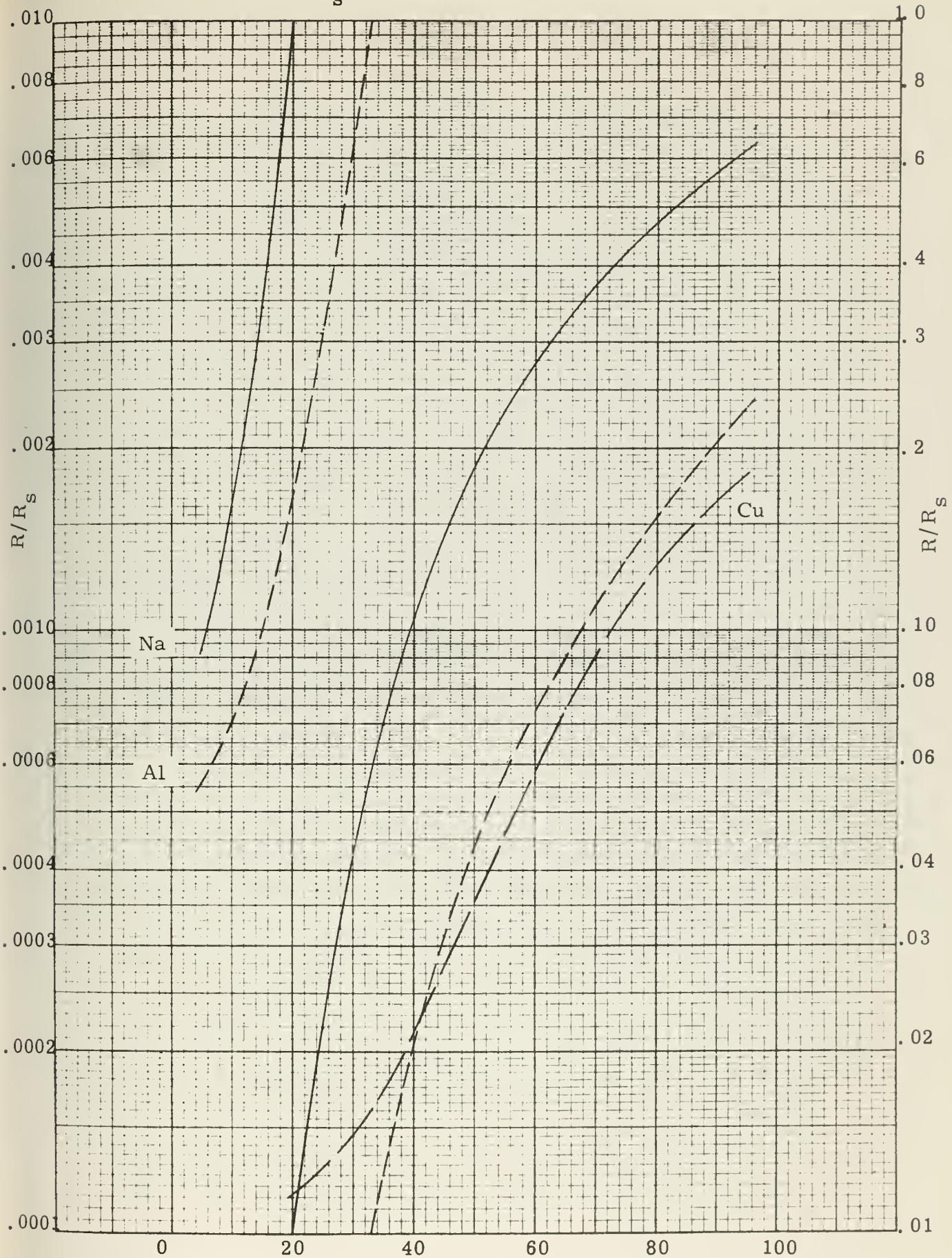

APPENDIX C

Structural Curves

List of Symbols

B Channel flux density (KG)

F Coil form factor (dimensionless)

S. V. F. Structural volume fraction (dimensionless)

σ_c Specified stress limit for coil conductors (kpsi)

σ_d Design stress limit for coil structure (kpsi)

FIGURE C - 1

Structural Volume Fraction vs. F for σ_D = 30 kpsi

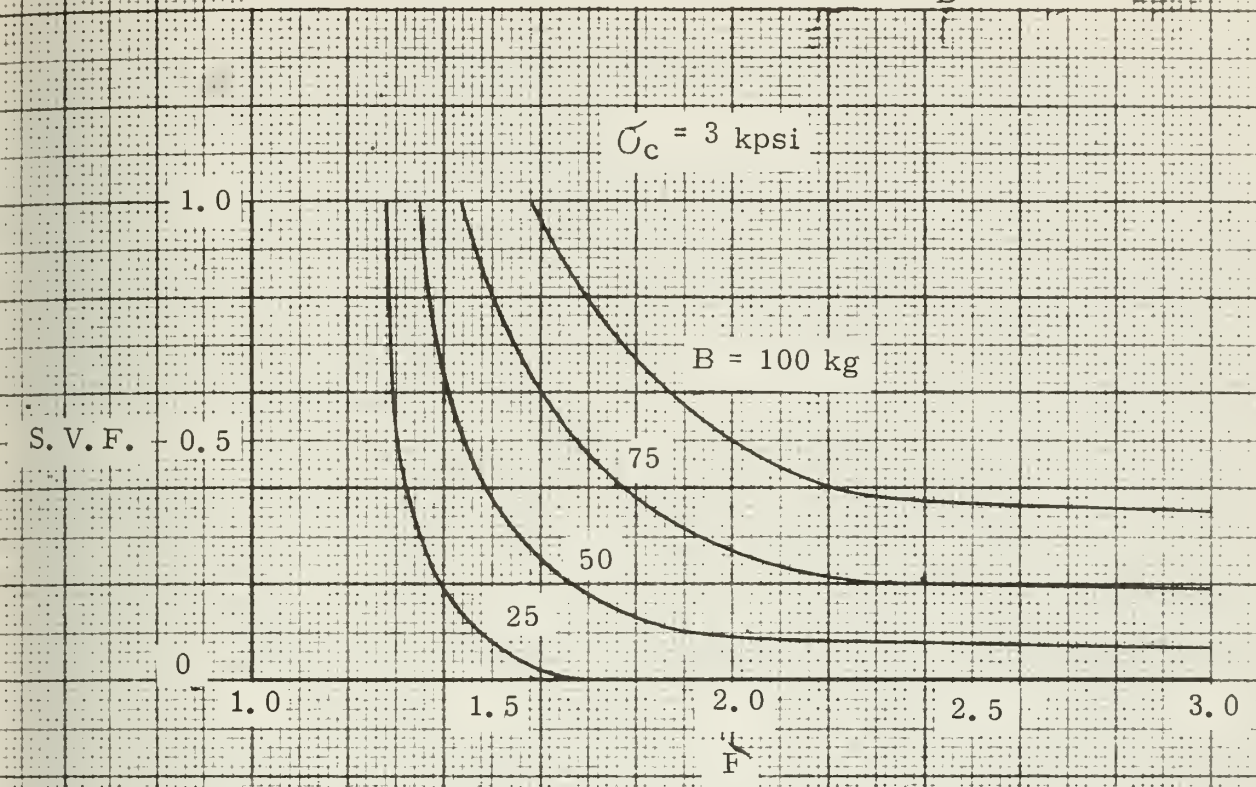

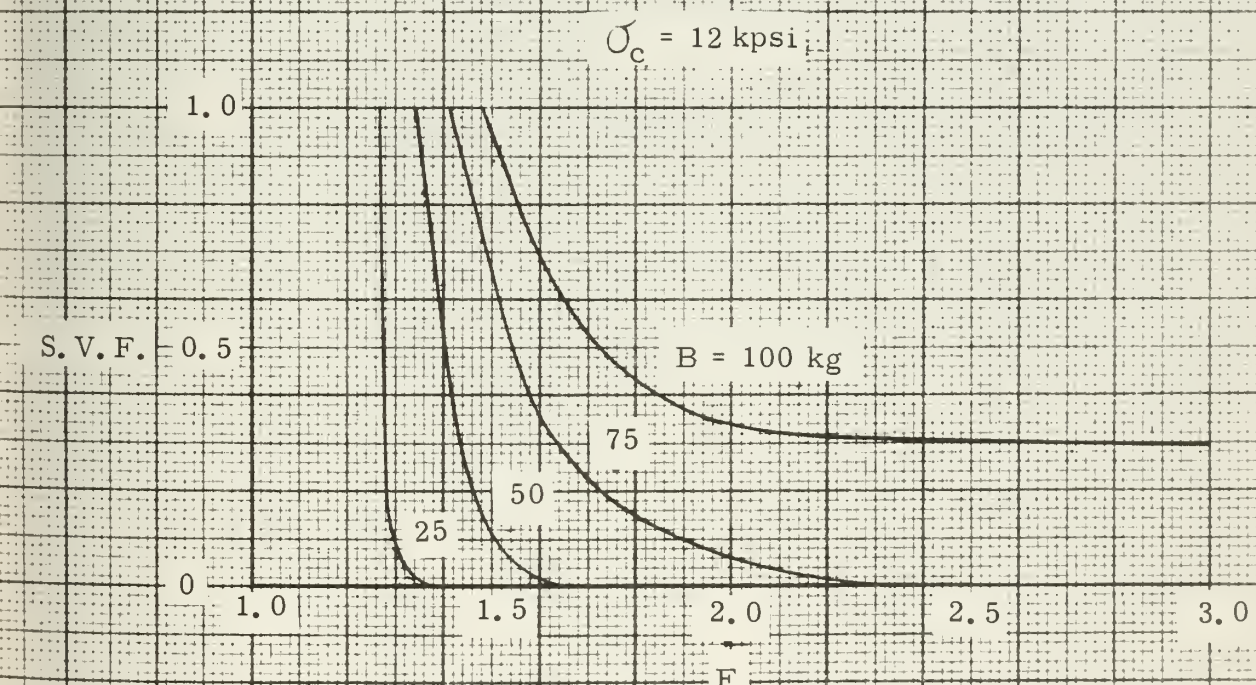

FIGURE C - 2

Structural Volume Fraction vs. F for σ_D = 60 kpsi

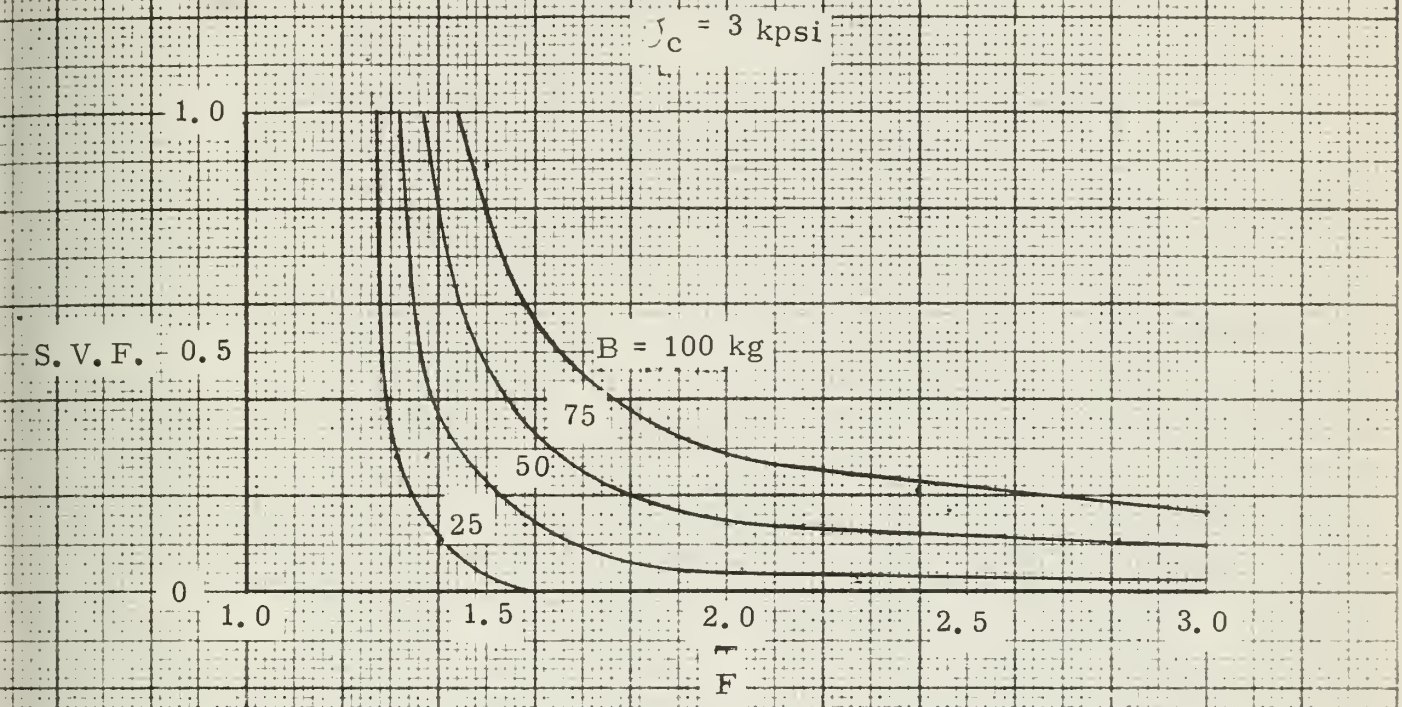

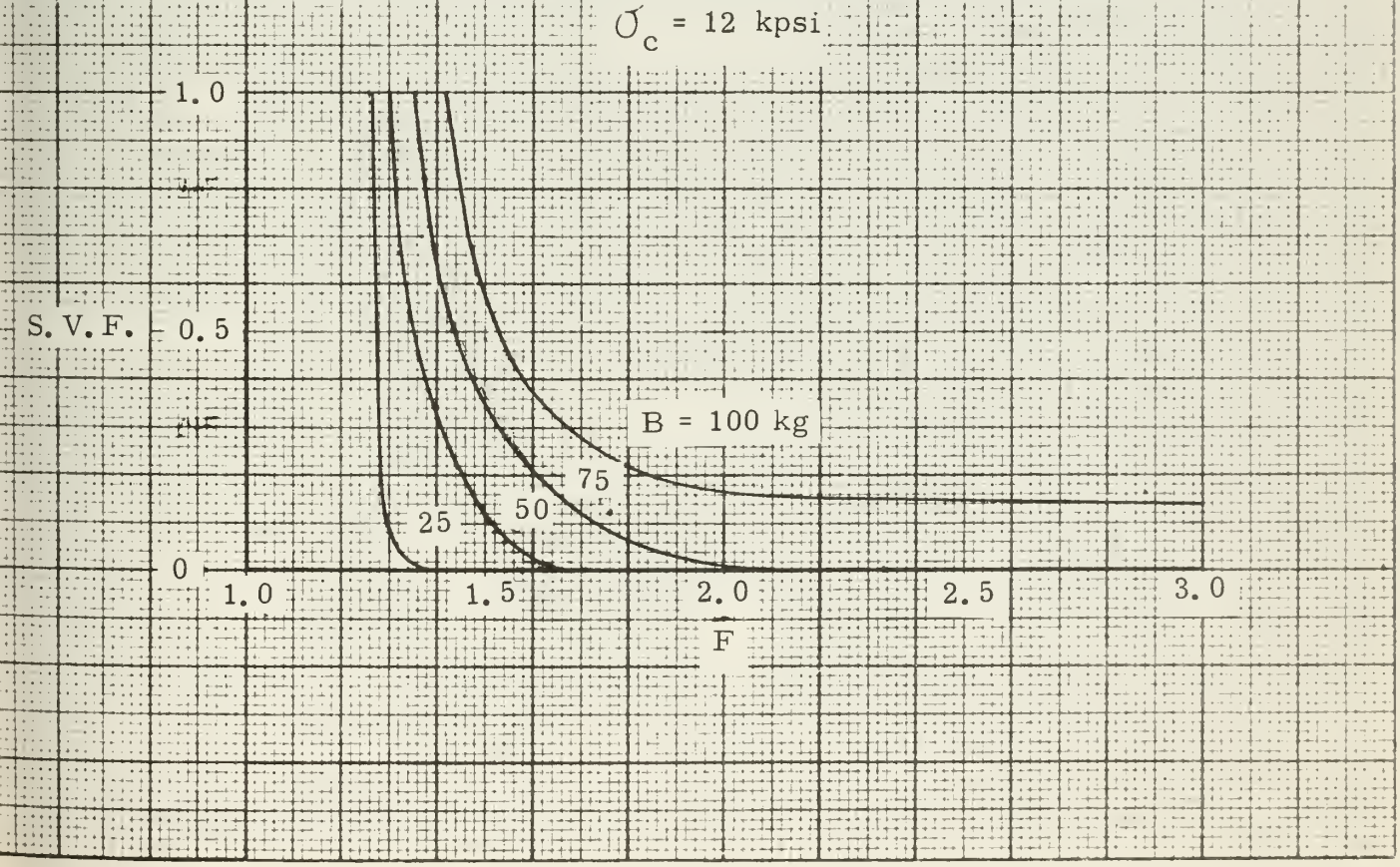

FIGURE C - 3

Structural Volume Fraction vs. F for σ_D = 90 kpsi

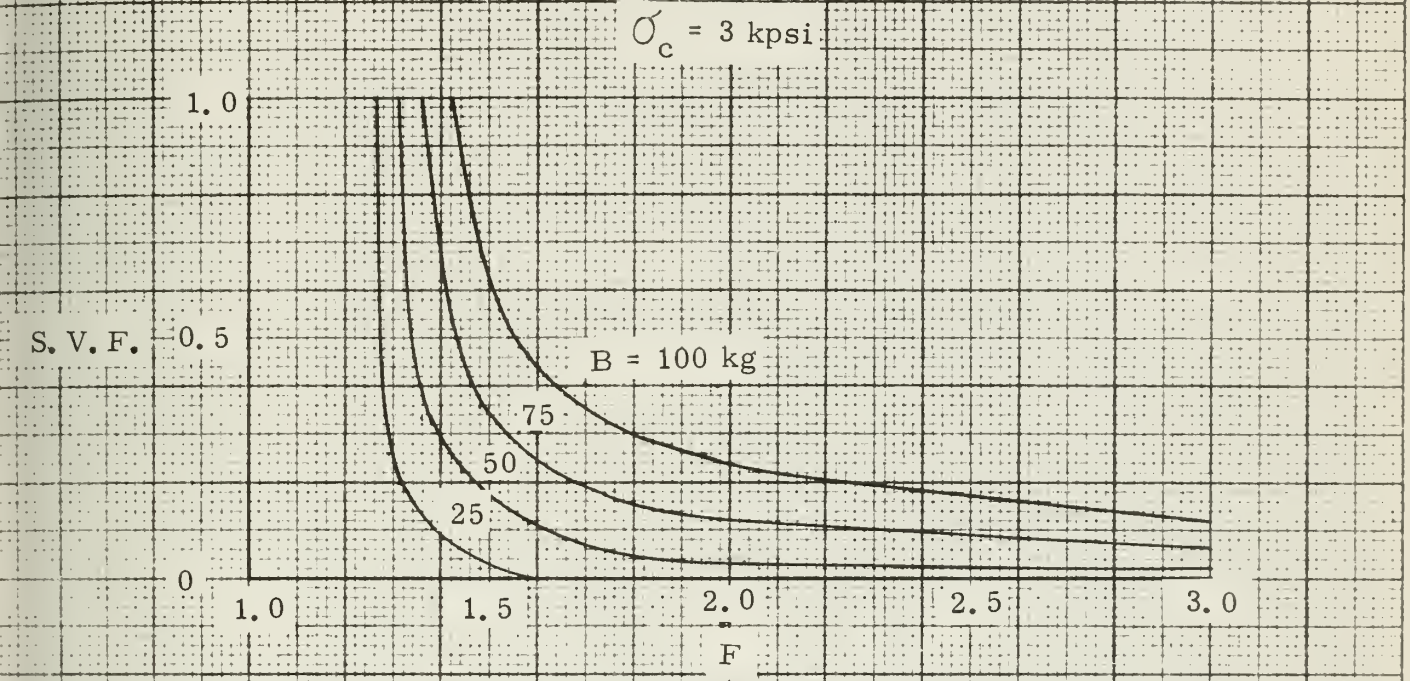

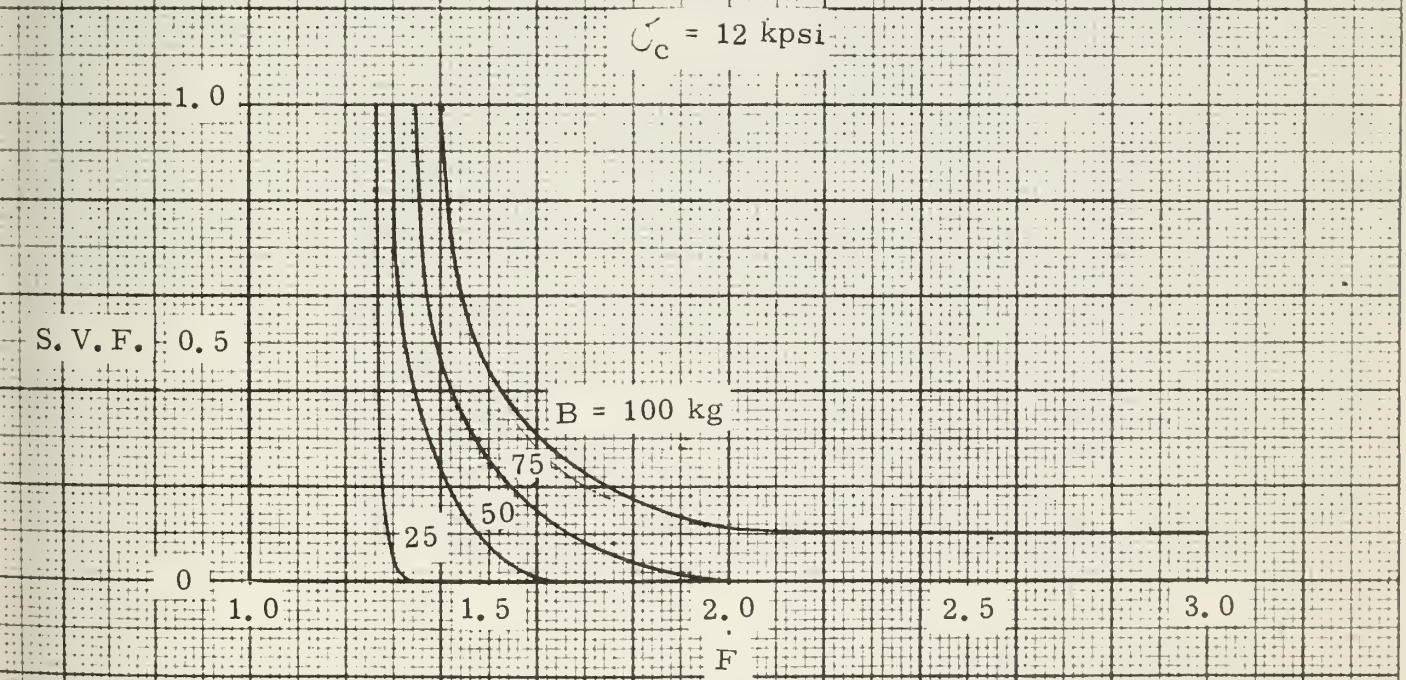

FIGURE C - 4

Structural Volume Fraction vs. F for σ_D = 120 kpsi

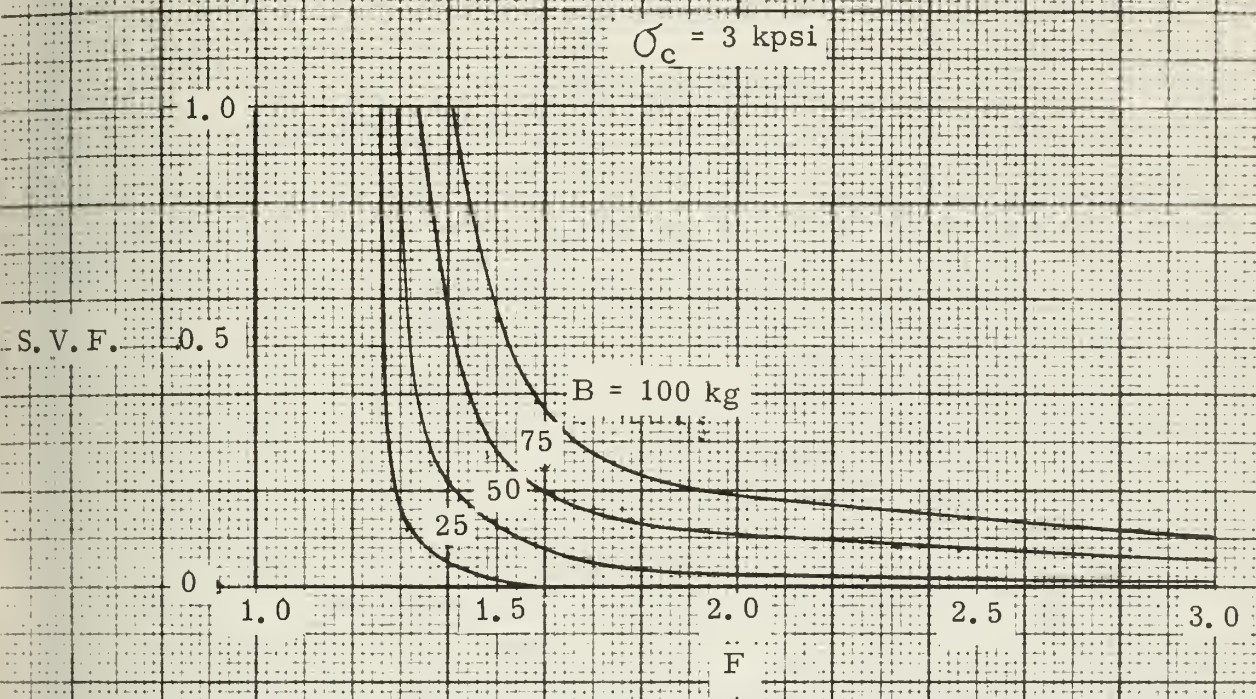

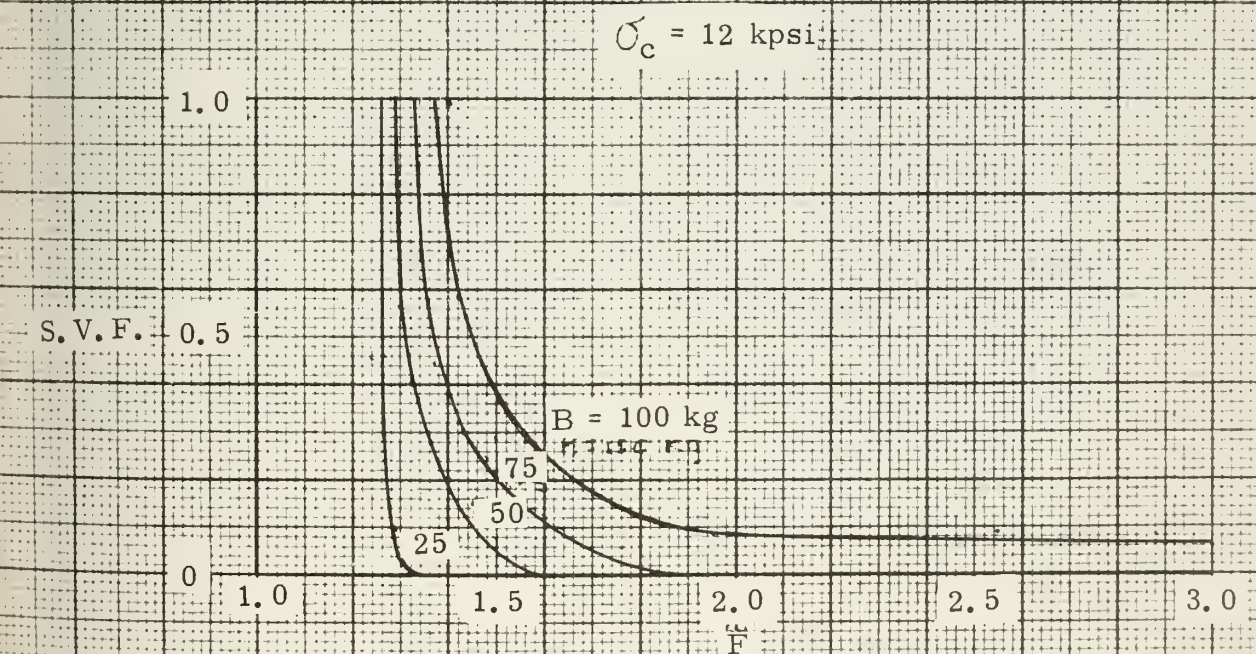

APPENDIX D

Coolant Curves

List of Symbols

p_o Coolant outlet pressure (atm.)

Δp Coolant pressure drop (inlet to outlet) (atm.)

S Slot factor (cm^2/watt)

ΔT_c Mean temperature increment to correct for deviation of temperature of bulk liquid from 1-atm. saturation temperature (^oK)

v_{in} Coolant inlet velocity (m/s)

FIGURE D - 1a

Nitrogen: S vs. Δp for x_o = 30%

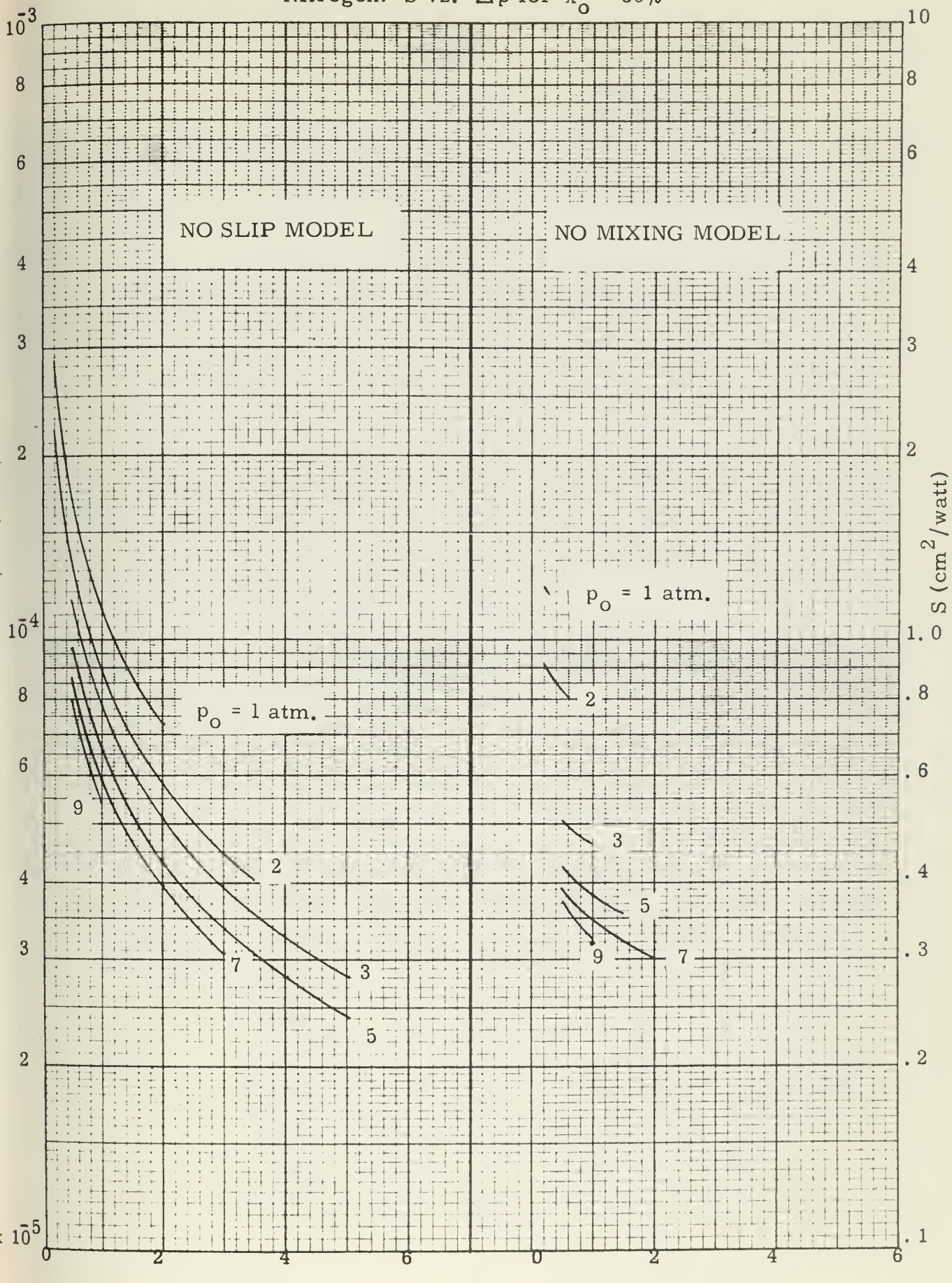

FIGURE D - 1b

Nitrogen: S vs. Δp for x_o = 50%

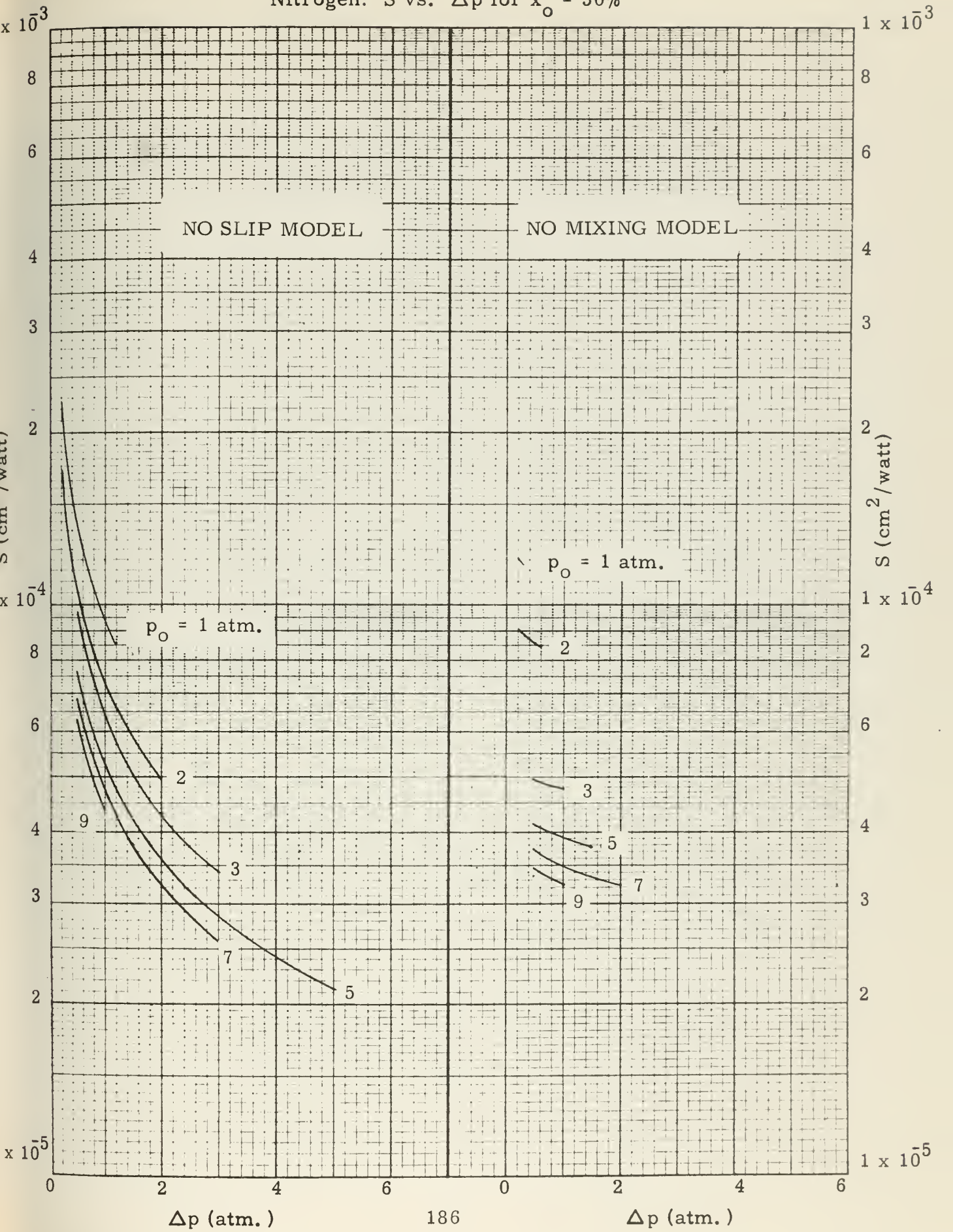

FIGURE D - 1c

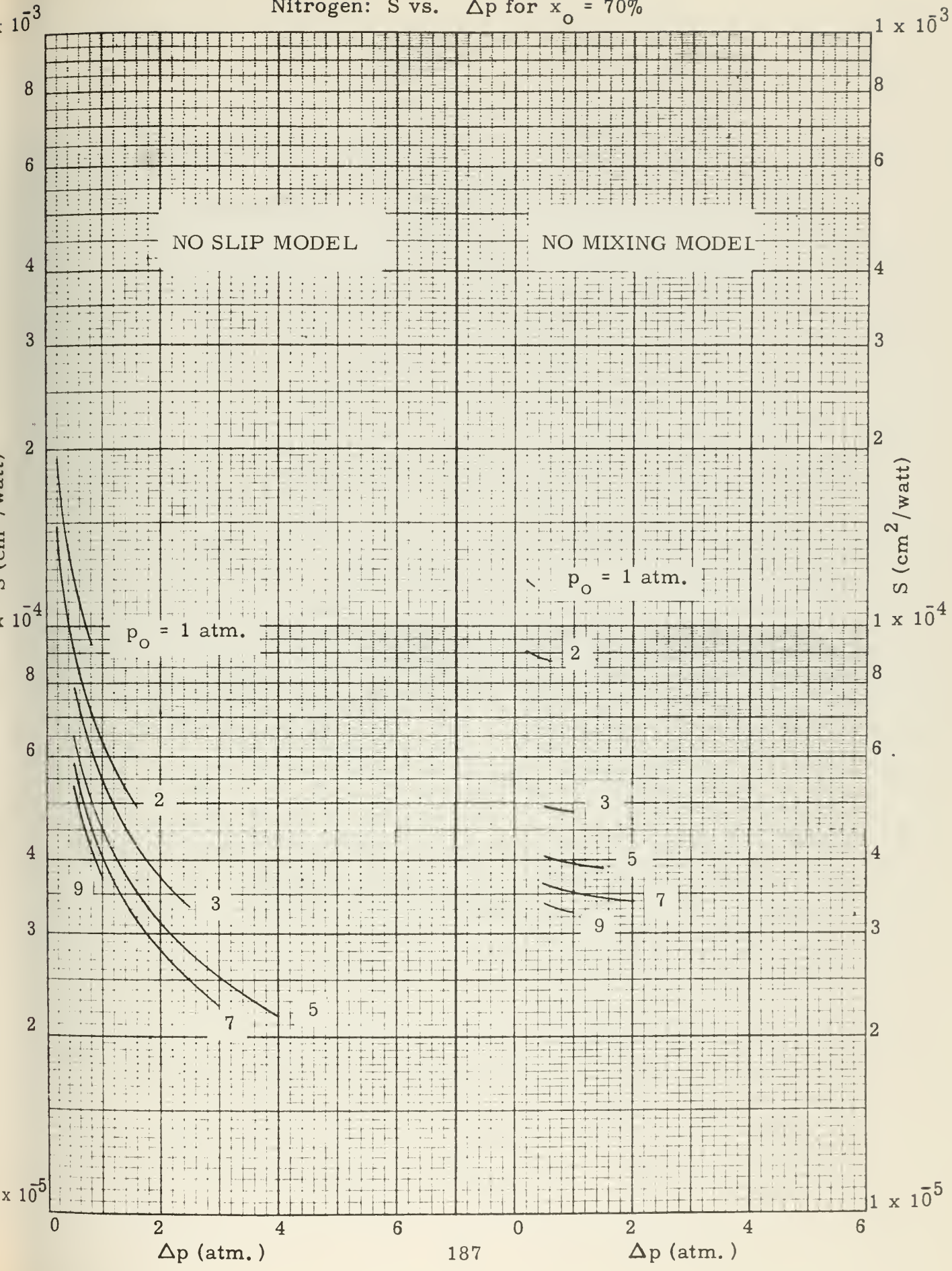
Nitrogen: S vs. Δp for x_o = 70%
NO SLIP MODEL
NO MIXING MODEL
p_o = 1 atm.
2
3
5
7
9
S (cm²/watt)
Δp (atm.)
0
2
4
6
1 x 10⁻³
1 x 10⁻⁴
1 x 10⁻⁵

FIGURE D - 2a

Nitrogen: ΔT_c vs. Δp for x_o = 30%

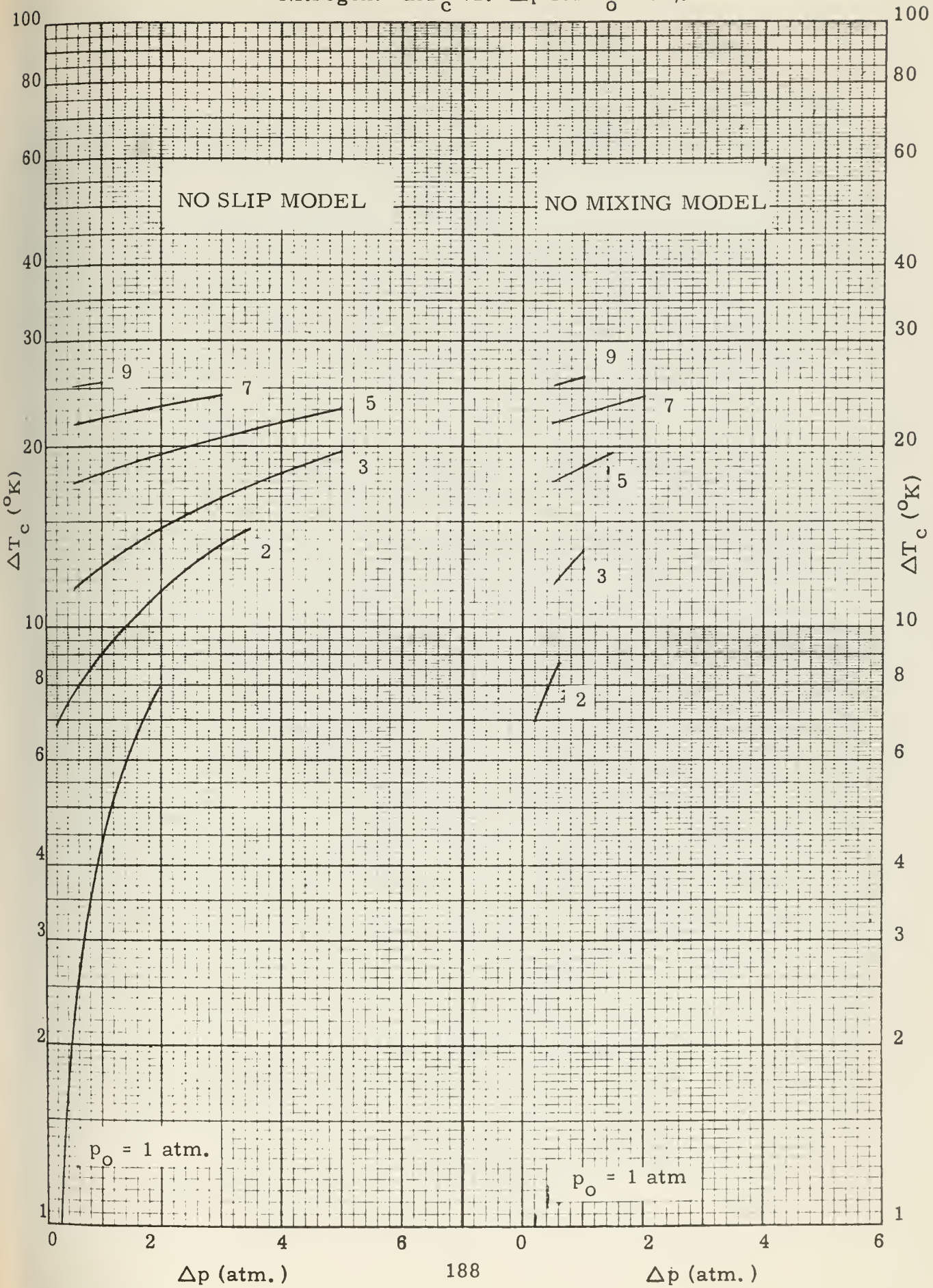

FIGURE D - 2b

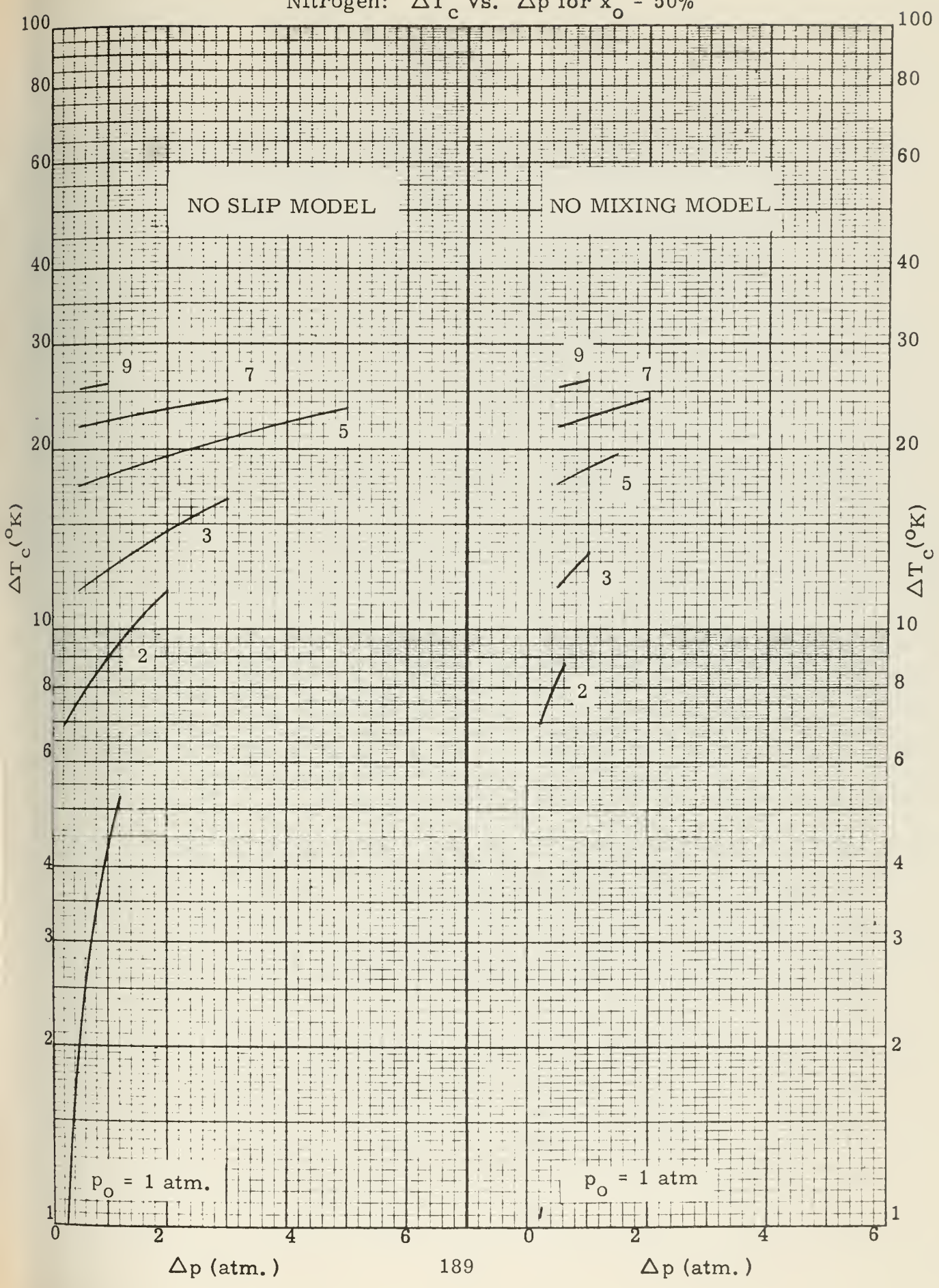
Nitrogen: ΔT_c vs. Δp for x_o = 50%
NO SLIP MODEL
NO MIXING MODEL
9
7
5
3
2
p_o = 1 atm.
p_o = 1 atm
ΔT_c (°K)
Δp (atm.)
Δp (atm.)

FIGURE D - 2c

Nitrogen: ΔT_c vs. Δp for x_o = 70%

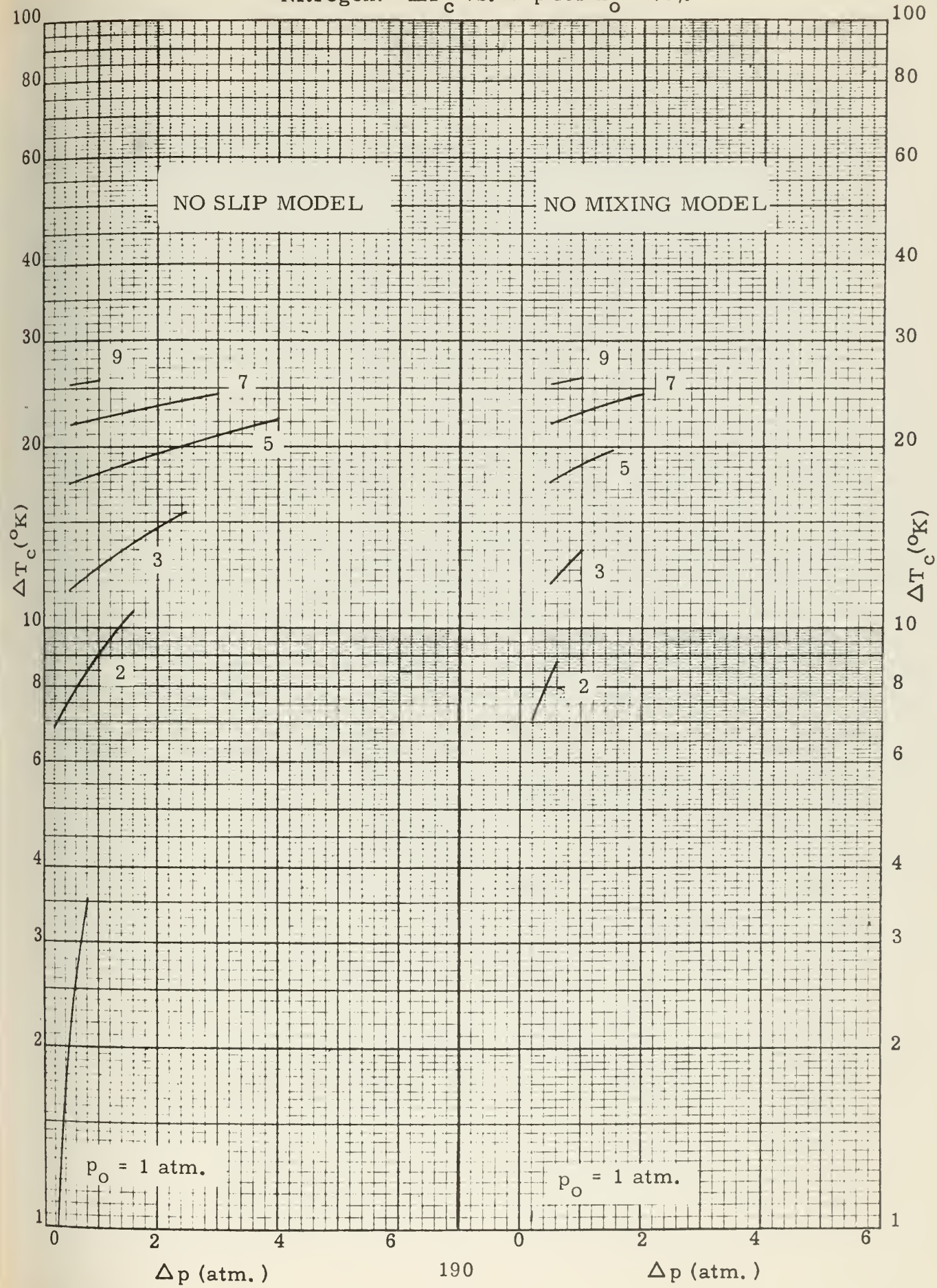

FIGURE D - 3a

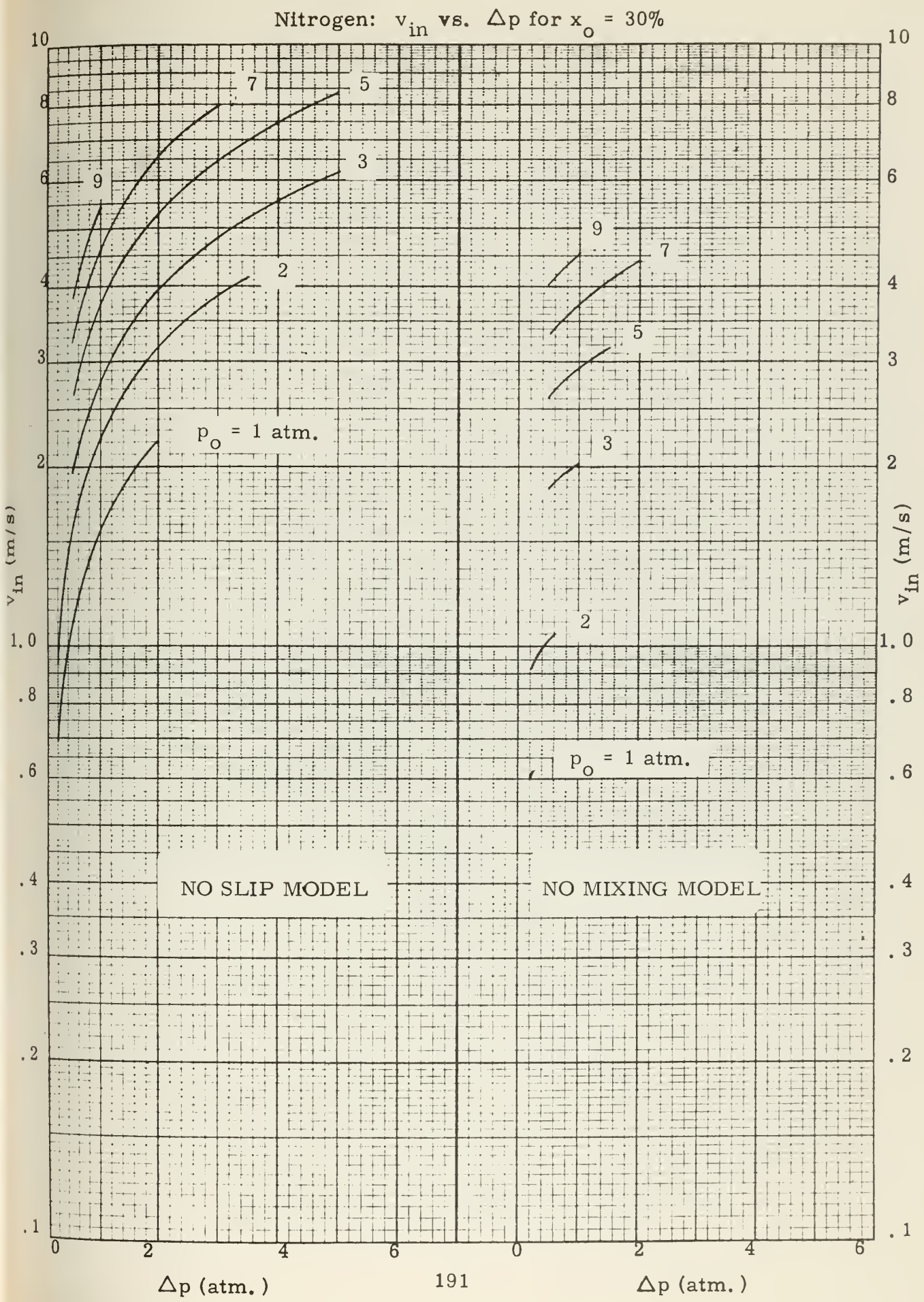
Nitrogen: v_{in} vs. Δp for x_o = 30%
v_{in} (m/s)
Δp (atm.)
p_o = 1 atm.
NO SLIP MODEL
NO MIXING MODEL
9
7
5
3
2
10
8
6
4
3
2
1.0
.8
.6
.4
.3
.2
.1
0
2
4
6

FIGURE D - 3b

Nitrogen: v_{in} vs. Δp for x_o = 50%

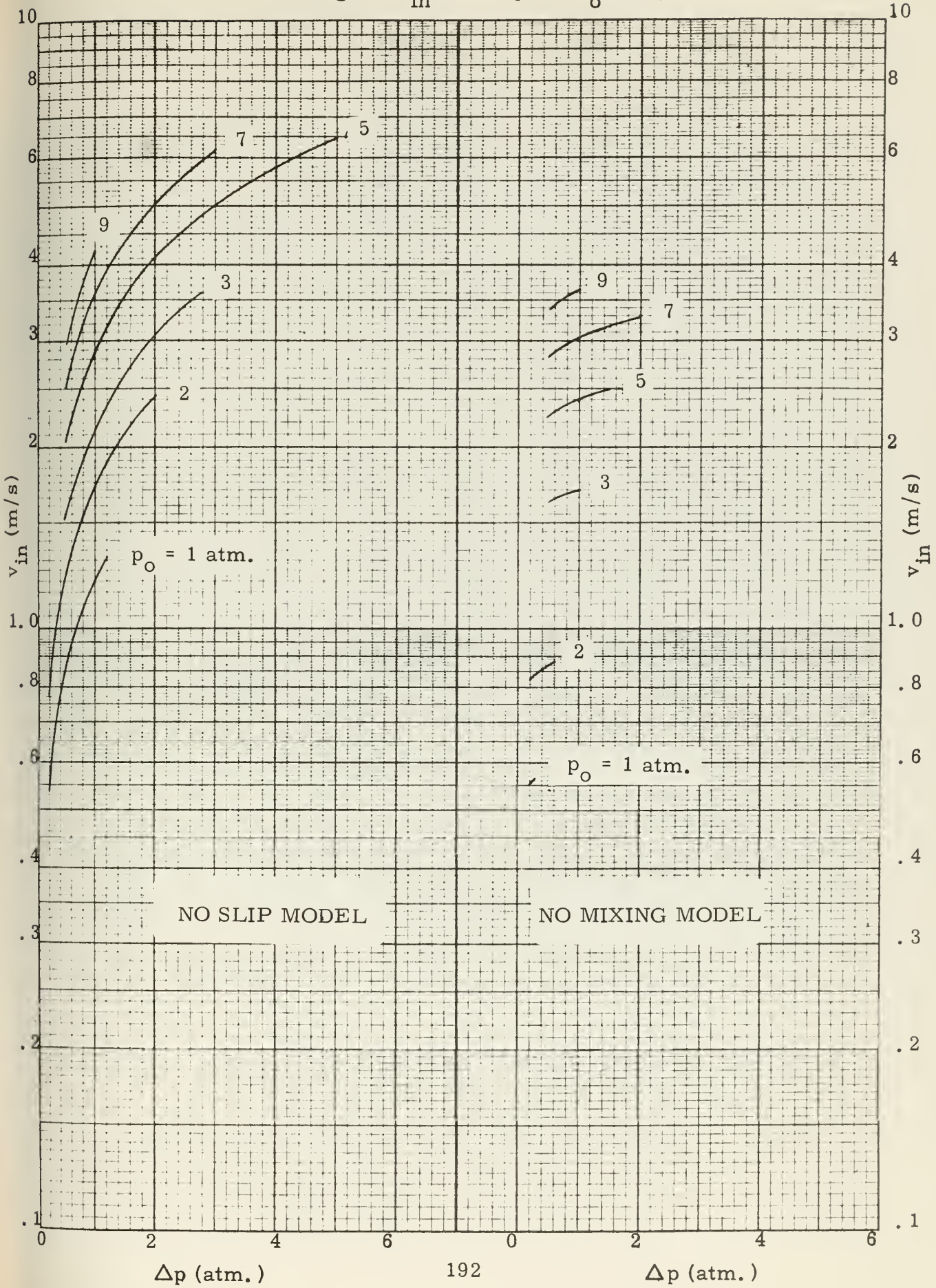

FIGURE D - 3c

Nitrogen: v_{in} vs. Δp for x_o = 70%

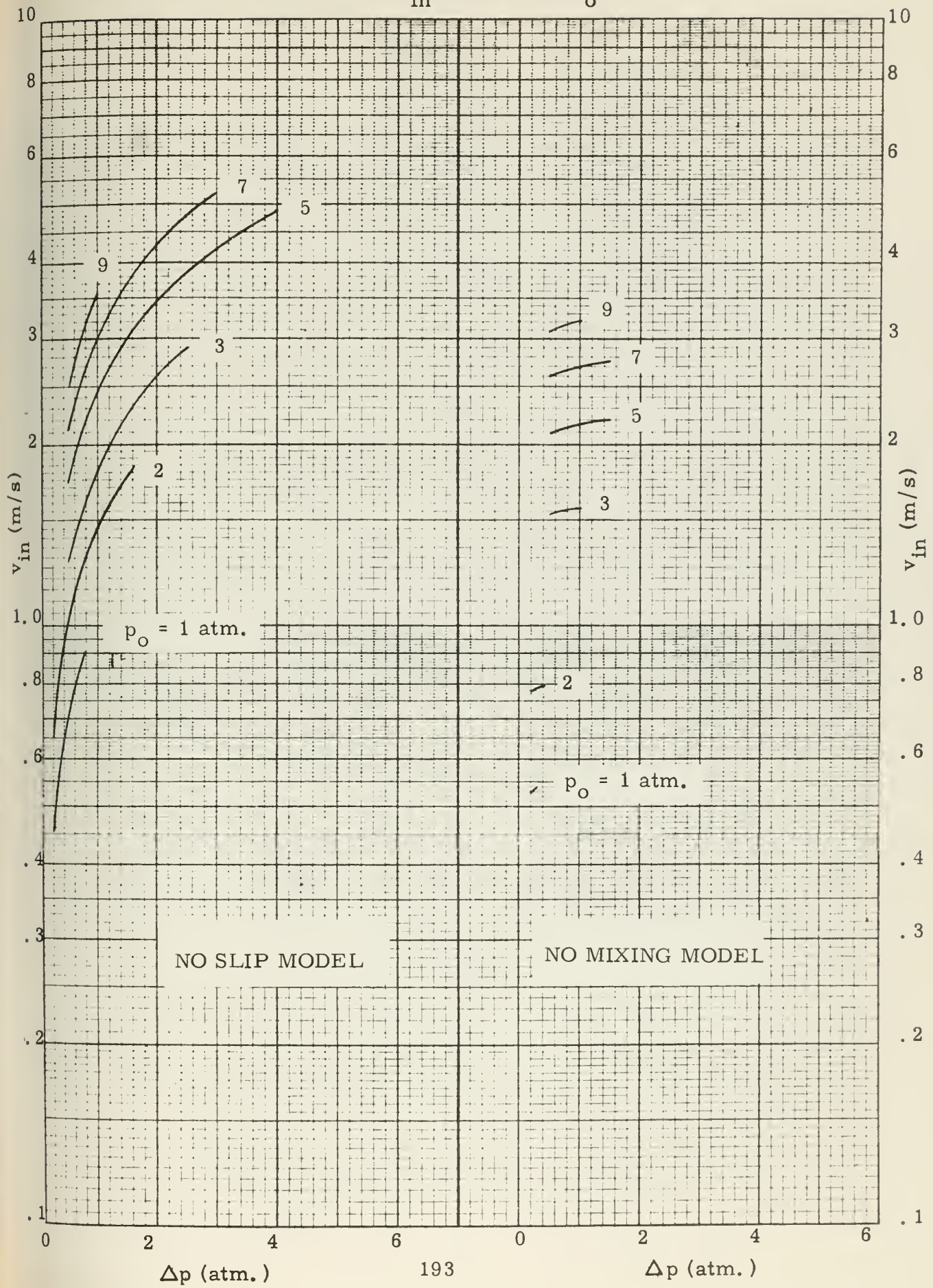

FIGURE D - 4a

Neon: S vs. Δp for x_o = 30%

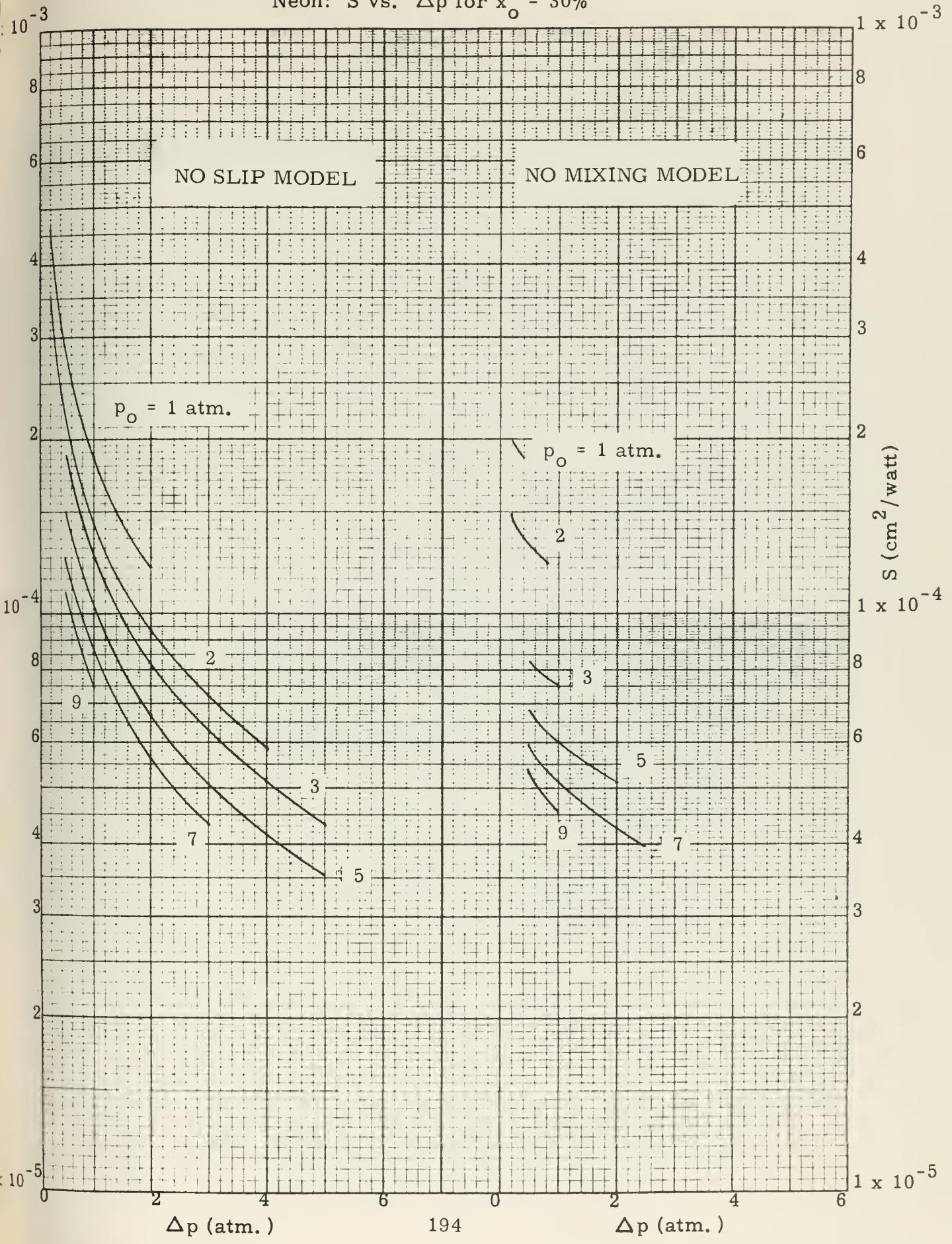

FIGURE D - 4b

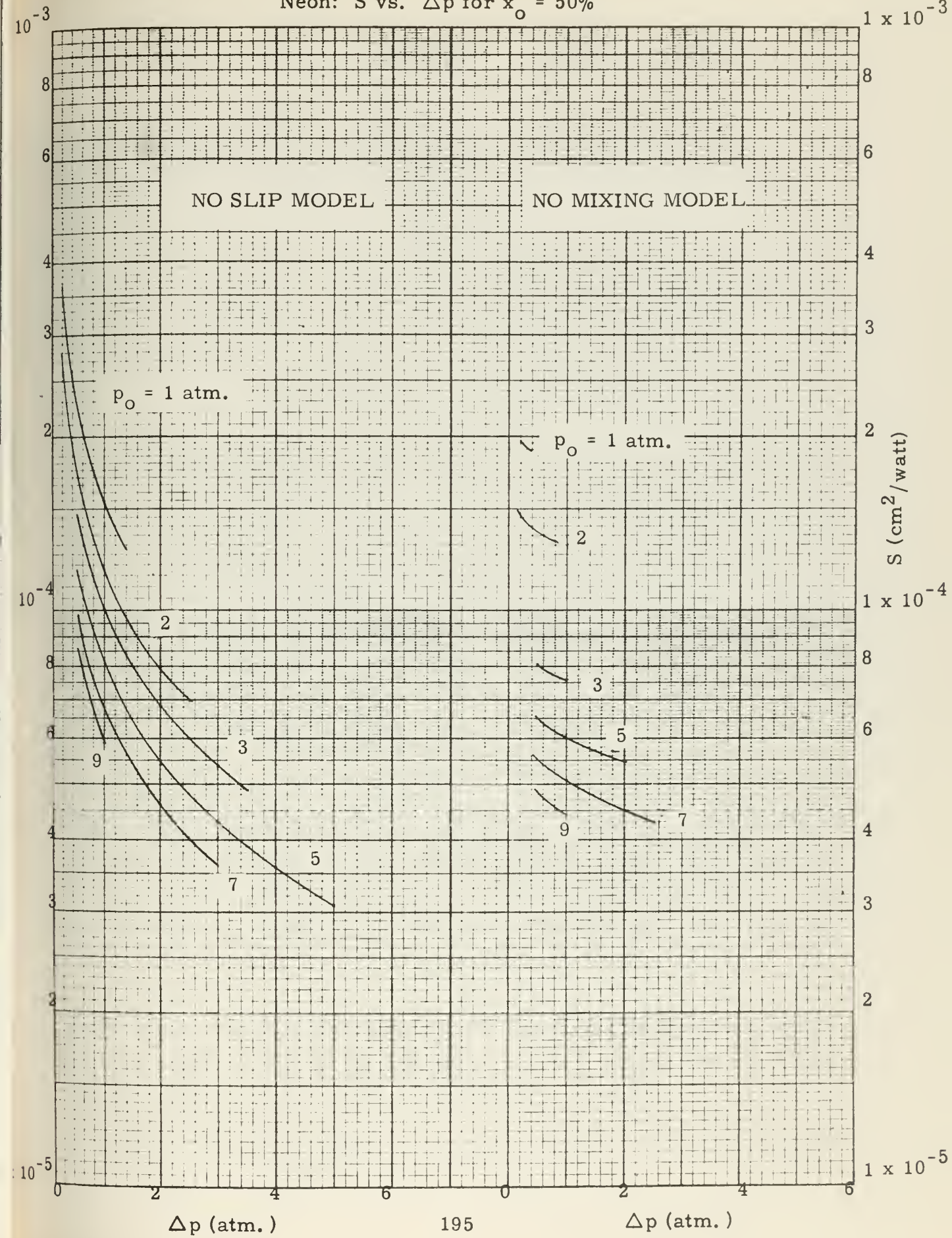
Neon: S vs. Δp for x_o = 50%
NO SLIP MODEL
NO MIXING MODEL
p_o = 1 atm.
p_o = 1 atm.
2
3
5
7
9
2
3
5
7
9
S (cm^2/watt)
Δp (atm.)
Δp (atm.)
10^{-3}
10^{-4}
10^{-5}
1 x 10^{-3}
1 x 10^{-4}
1 x 10^{-5}
0
2
4
6

FIGURE D - 4c

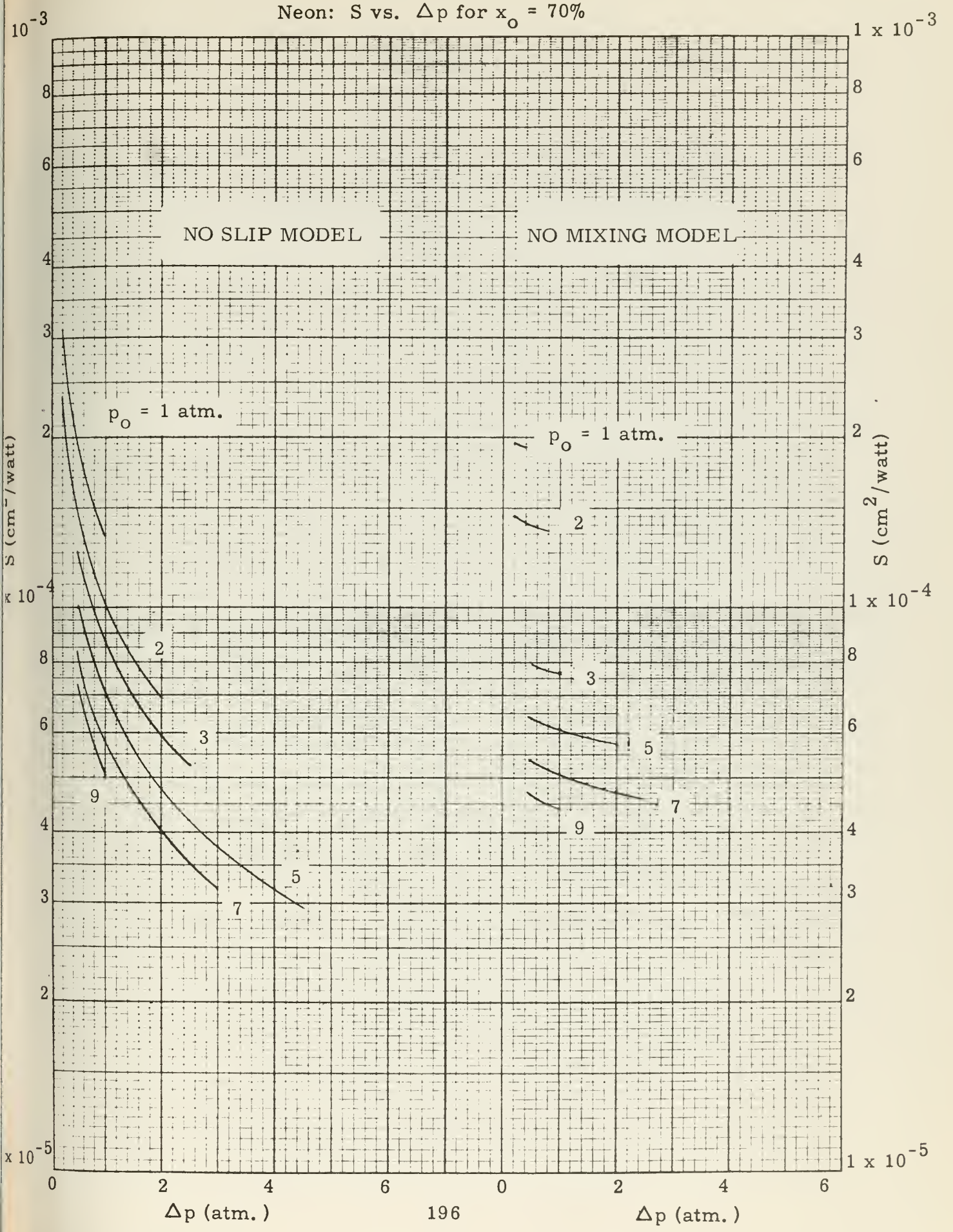
Neon: S vs. Δp for x_o = 70%
NO SLIP MODEL
NO MIXING MODEL
p_o = 1 atm.
p_o = 1 atm.
2
3
5
7
9
2
3
5
7
9
S (cm²/watt)
S (cm²/watt)
Δp (atm.)
Δp (atm.)
0
2
4
6
10^{-3}
1×10^{-3}
1×10^{-4}
1×10^{-5}

FIGURE D - 5a

Neon: ΔT_c vs. Δp for x_o = 30%

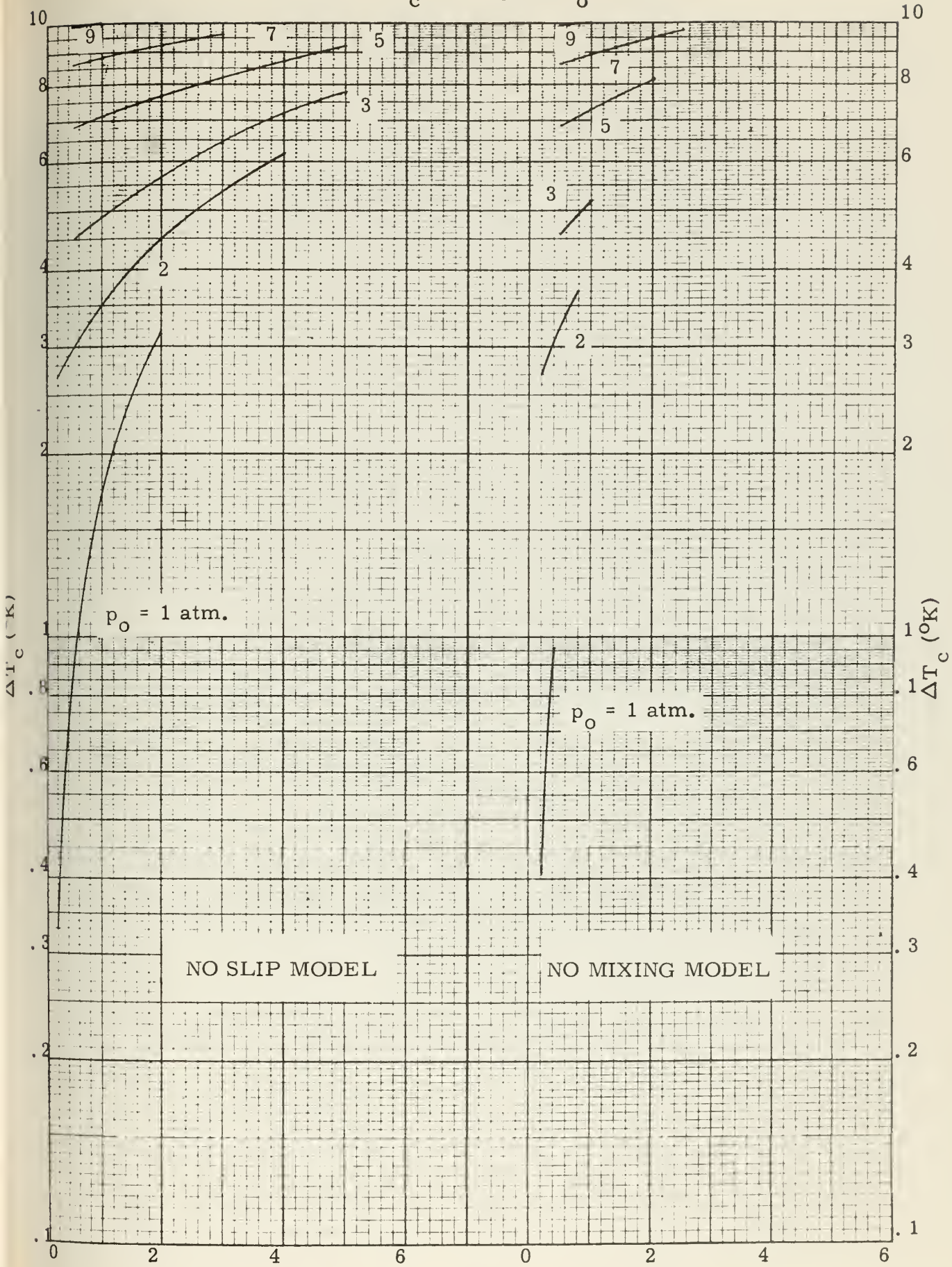

FIGURE D - 5b

Neon: ΔT_c vs. Δp for x_o = 50%

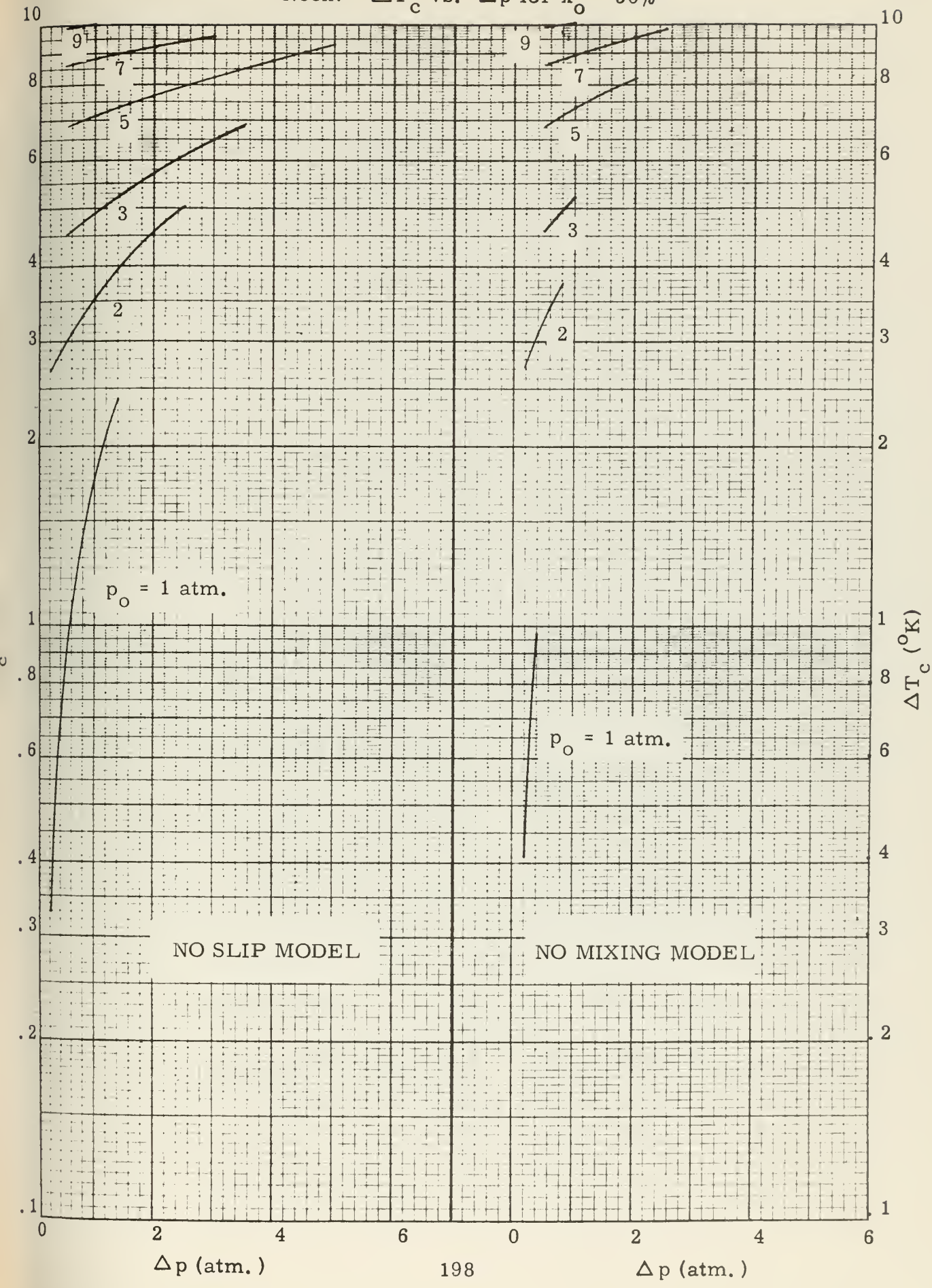

FIGURE D - 5c

Neon: ΔT_c vs. Δp for x_o = 70%

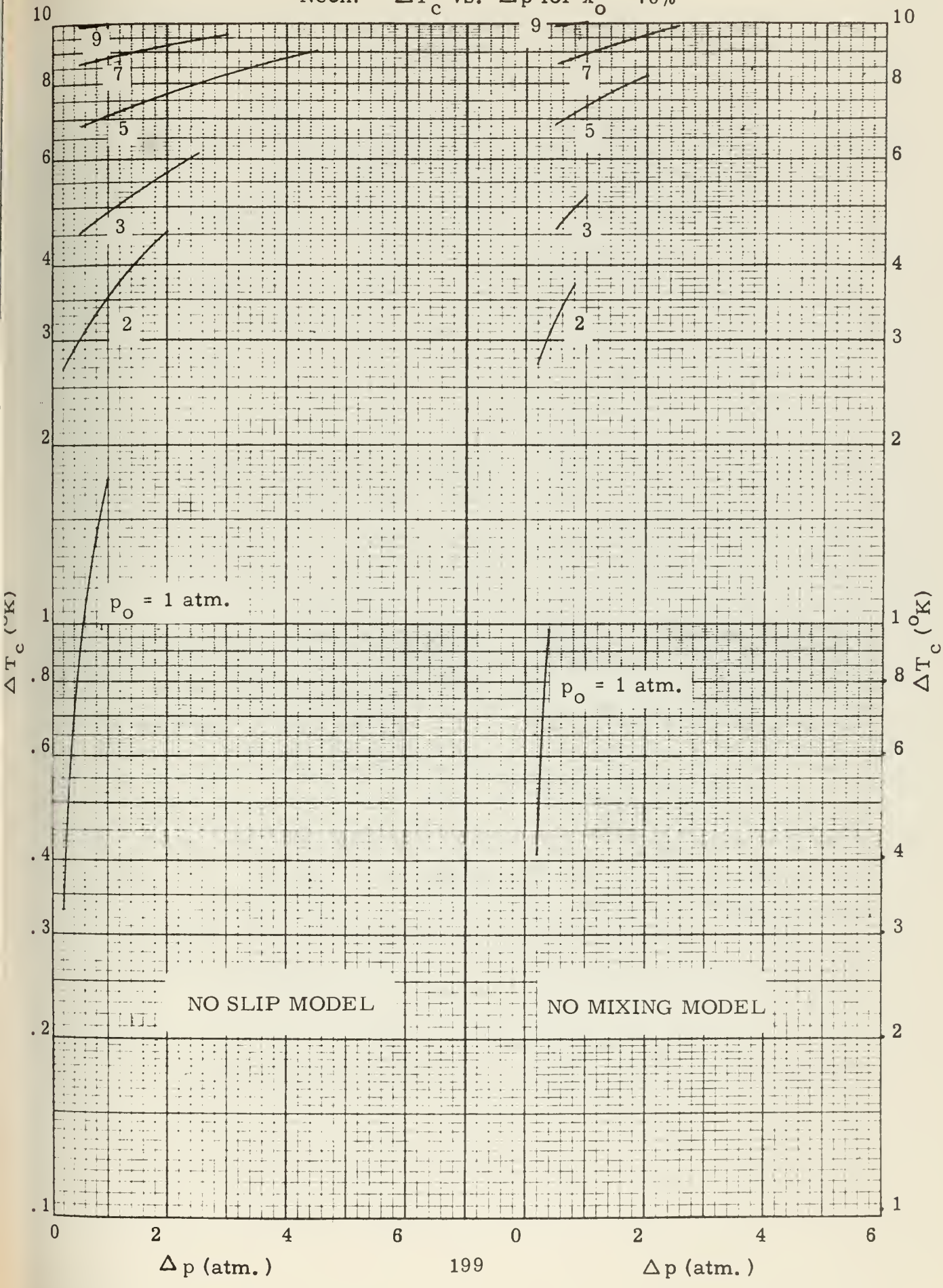

FIGURE D - 6a

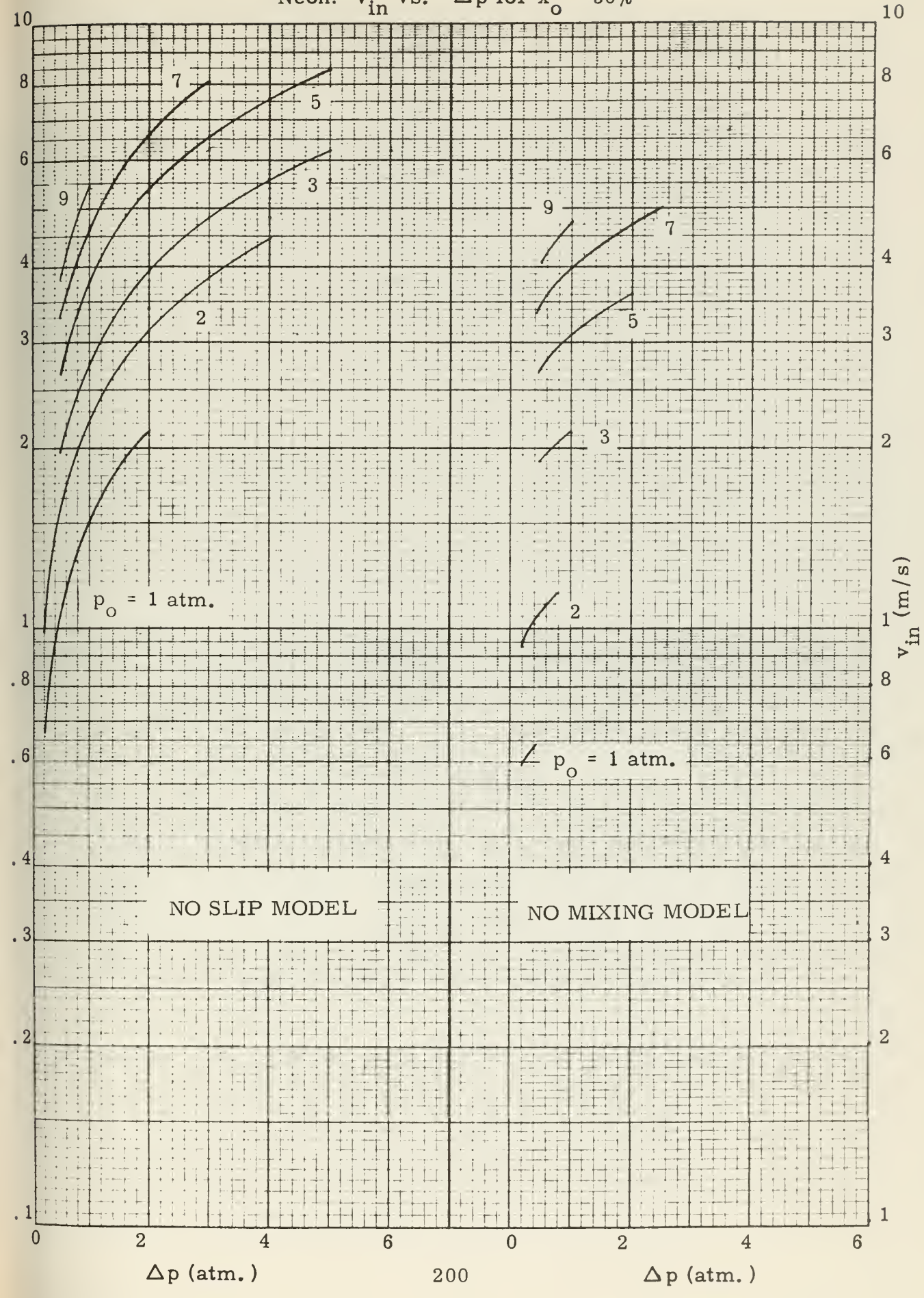
Neon: v_{in} vs. Δp for x_o = 30%
10
8
6
4
3
2
1
.8
.6
.4
.3
.2
.1
7
5
3
9
2
p_o = 1 atm.
NO SLIP MODEL
9
7
5
3
2
p_o = 1 atm.
NO MIXING MODEL
0
2
4
6
Δp (atm.)
v_{in} (m/s)

FIGURE D - 6b

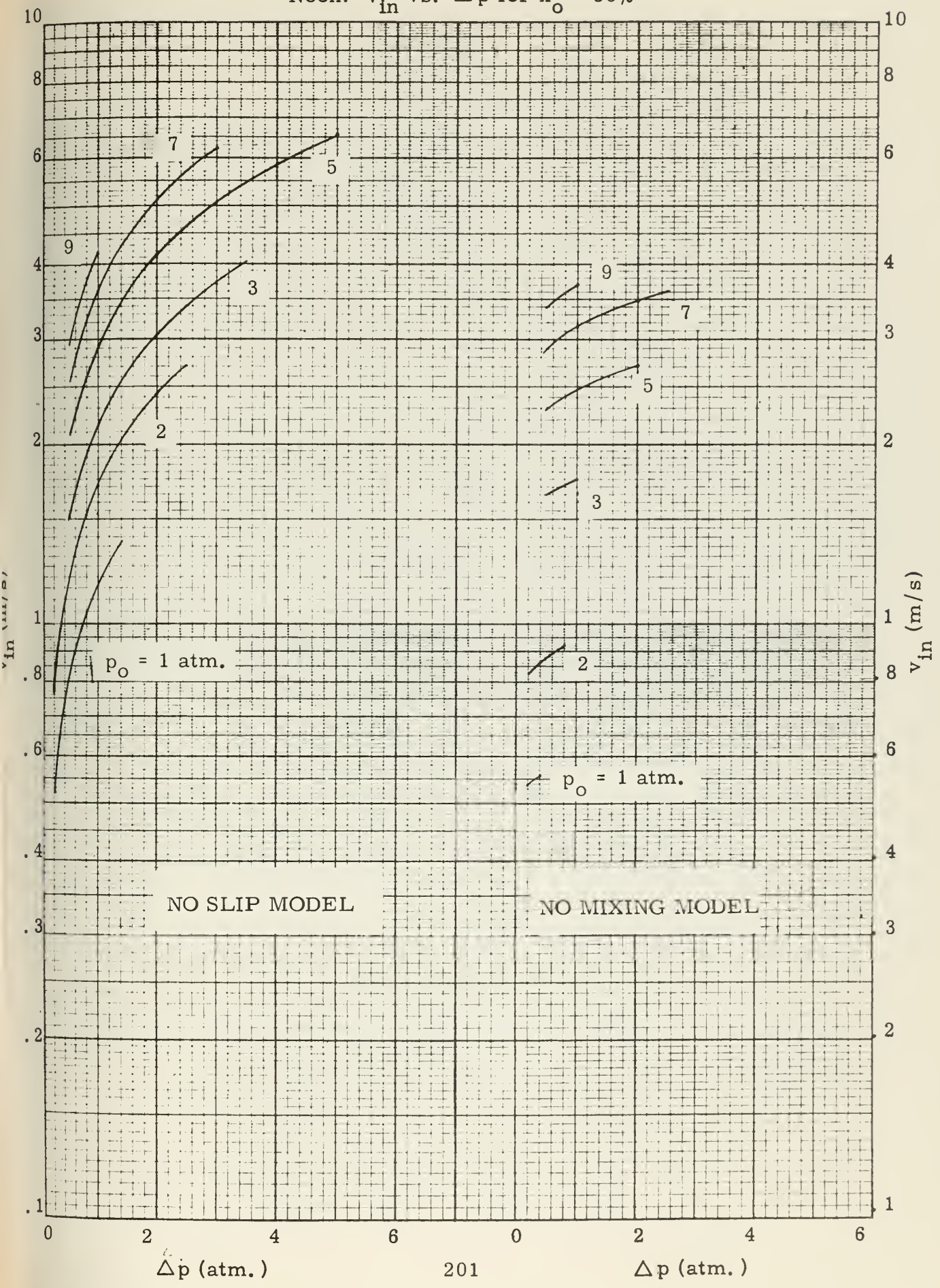
Neon: v_{in} vs. Δp for x_o = 50%
10
8
6
4
3
2
1
.8
.6
.4
.3
.2
.1
7
5
9
3
2
p_o = 1 atm.
NO SLIP MODEL
9
7
5
3
2
p_o = 1 atm.
NO MIXING MODEL
0
2
4
6
Δp (atm.)
v_{in} (m/s)

FIGURE D-6c

Neon: v_{in} vs. Δp for x_o = 70%

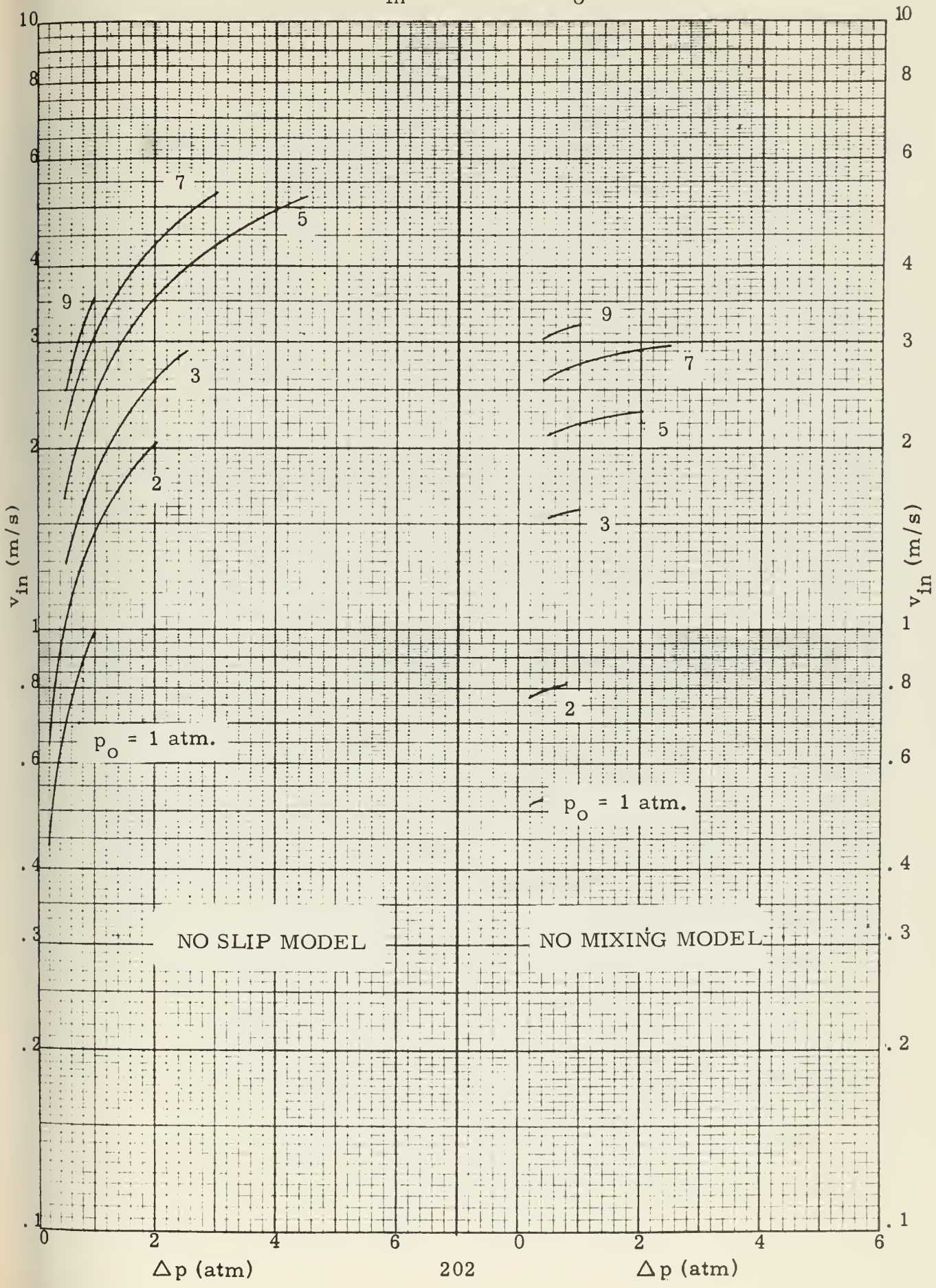

FIGURE D - 7a

Parahydrogen: S vs. Δp for x_o = 30%

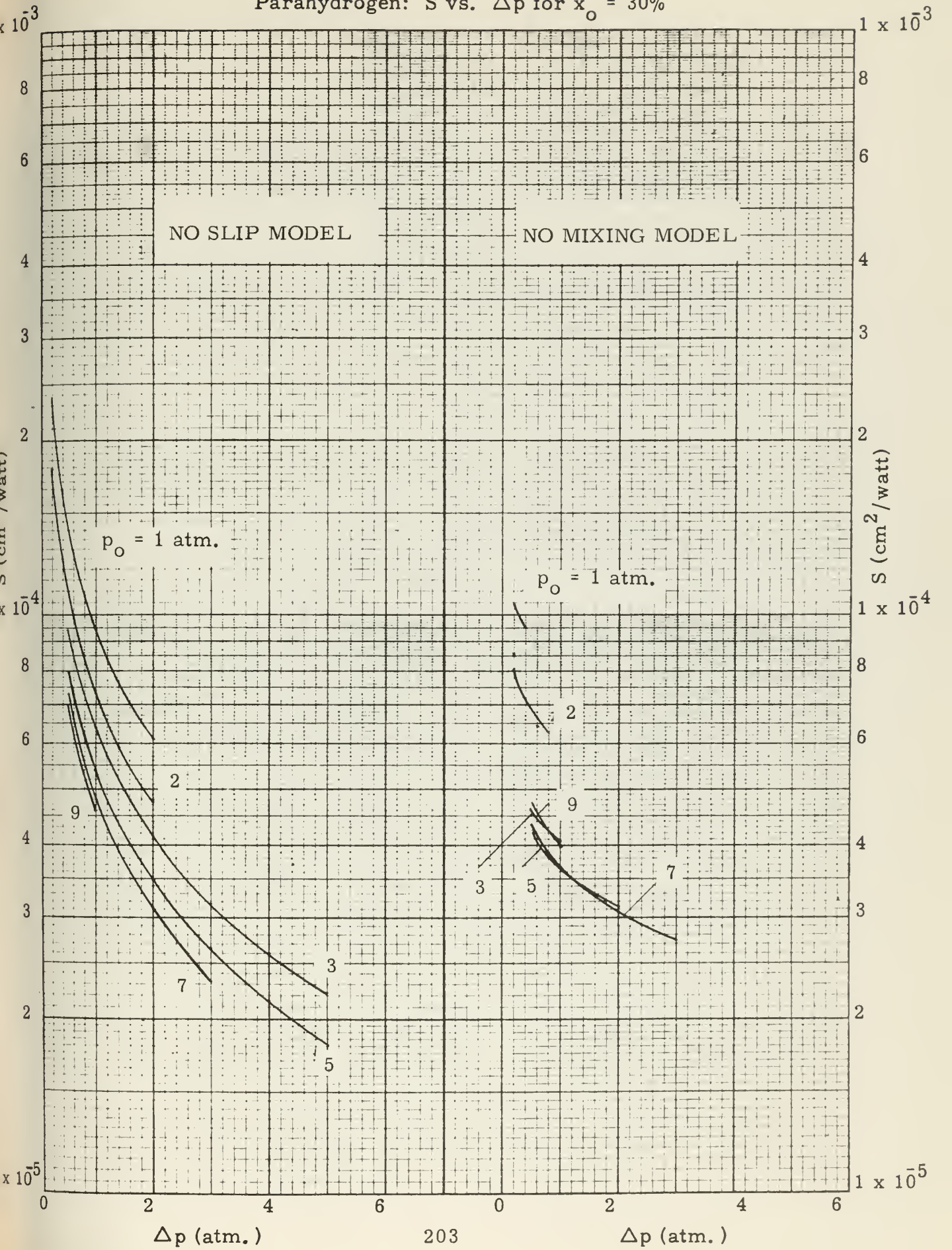

FIGURE D - 7b

Parahydrogen: S vs. Δp for x_o = 50%

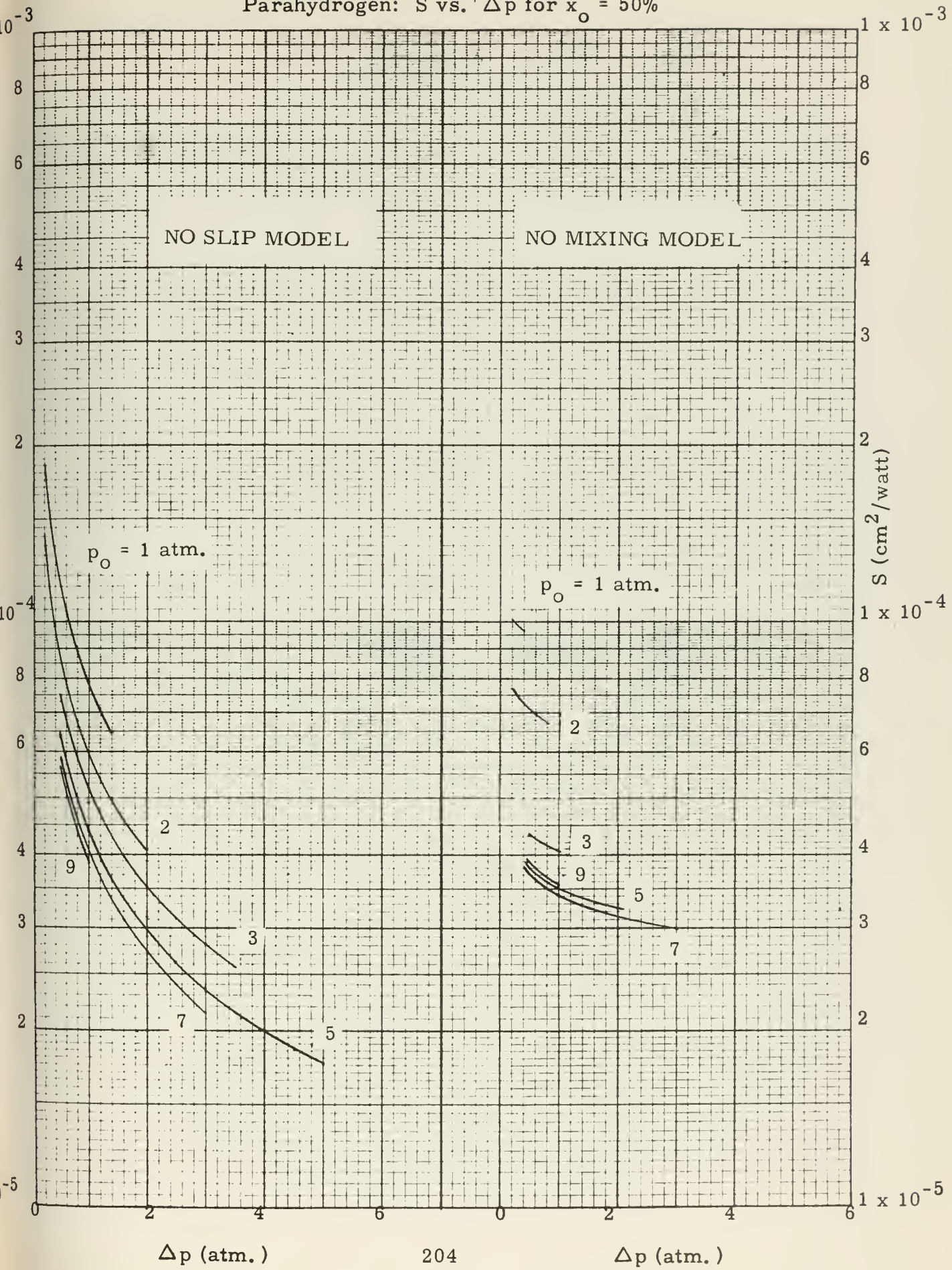

FIGURE D - 7c

Parahydrogen: S vs. Δp for x_o = 70%

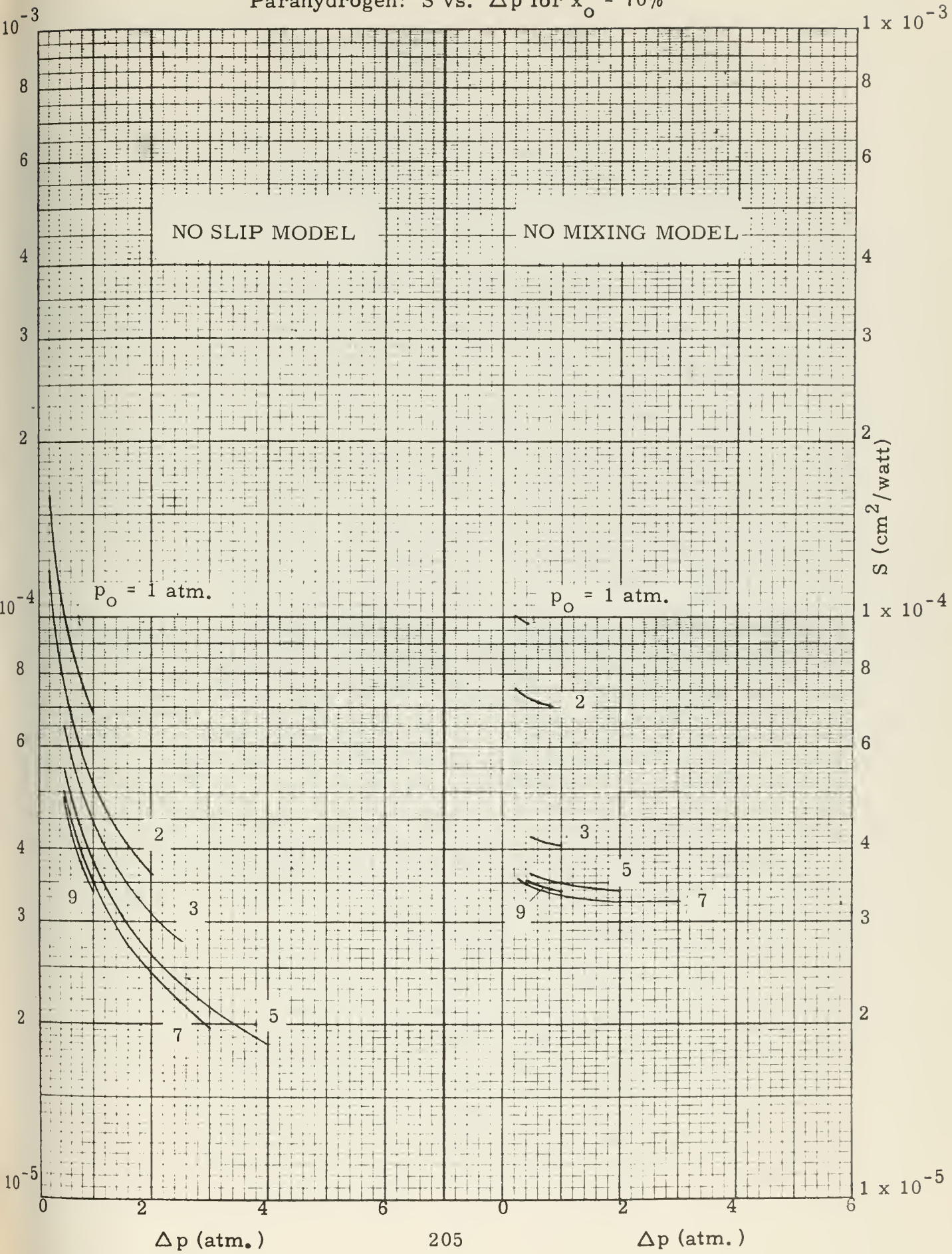

FIGURE D - 8a

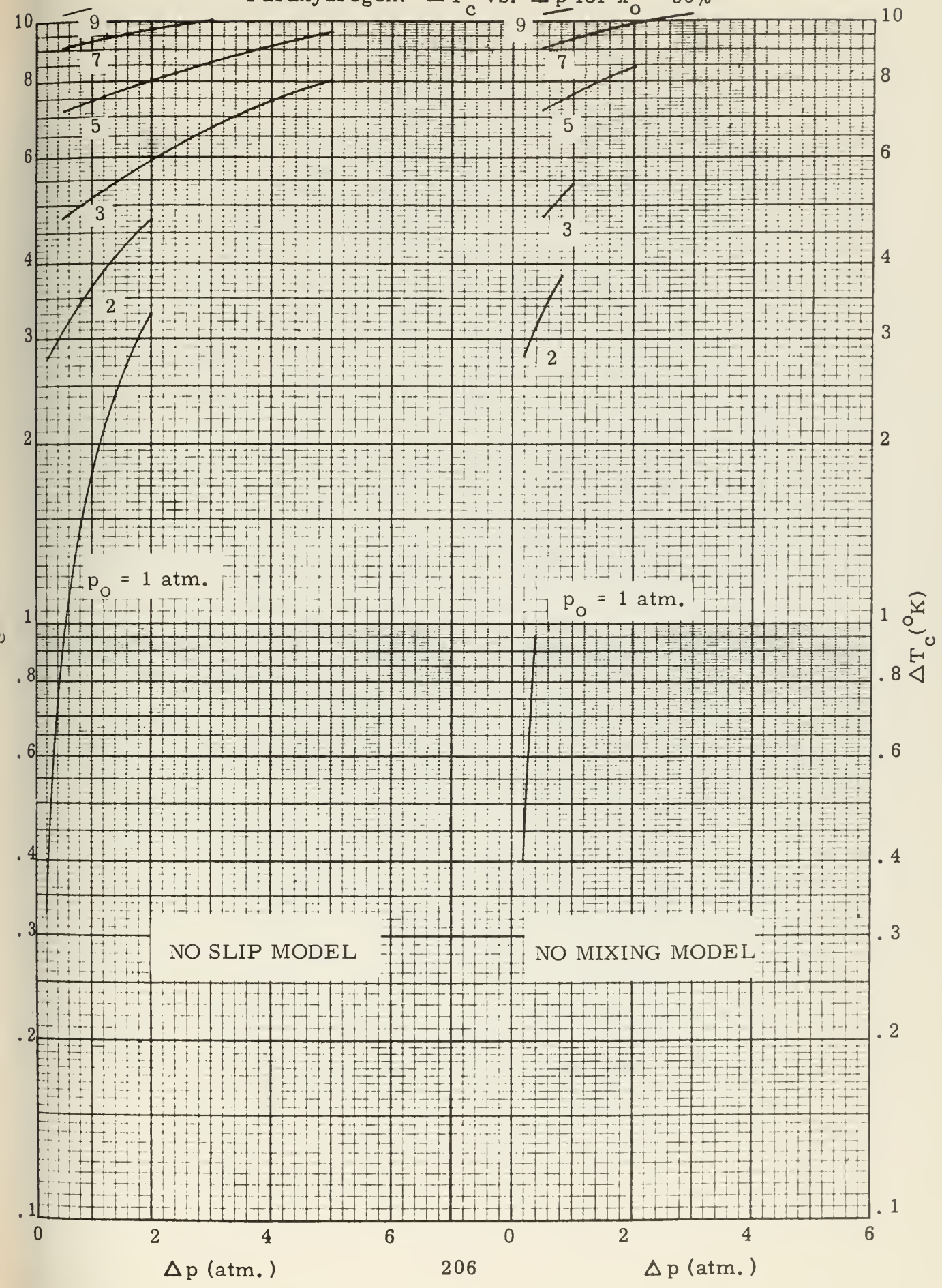
Parahydrogen: ΔT_c vs. Δp for x_o = 30%
9
7
5
3
2
p_o = 1 atm.
NO SLIP MODEL
NO MIXING MODEL
ΔT_c (°K)
Δp (atm.)
Δp (atm.)
0
2
4
6
10
8
1
.8
.6
.4
.3
.2
.1

FIGURE D - 8b

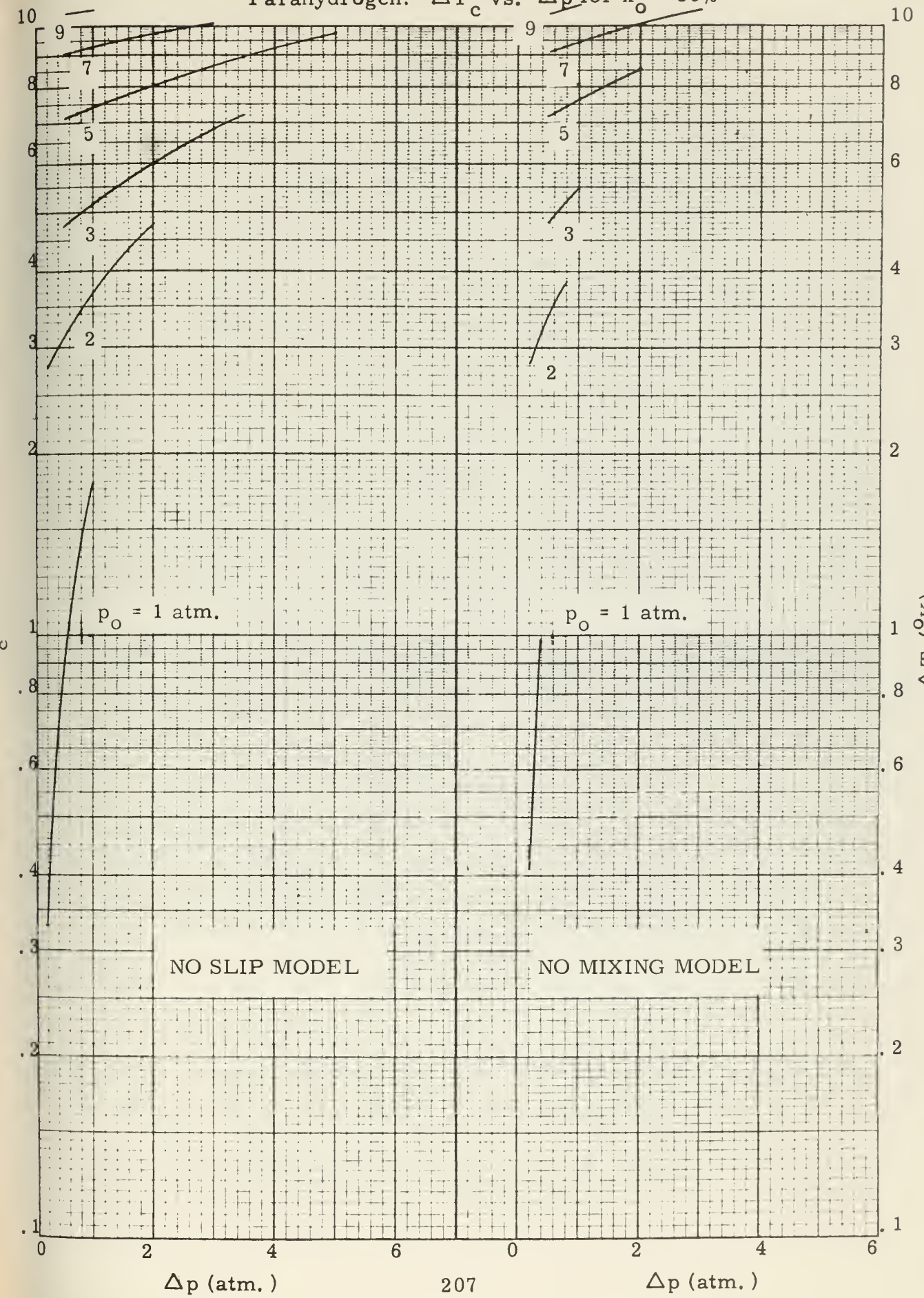
Parahydrogen: ΔT_c vs. Δp for x_o = 50%
9
7
5
3
2
p_o = 1 atm.
NO SLIP MODEL
NO MIXING MODEL
ΔT_c (°K)
Δp (atm.)
Δp (atm.)
0
2
4
6
10
8
1
.8
.6
.4
.3
.2
.1

FIGURE D - 8c

Parahydrogen: ΔT_c vs. Δp for x_o = 70%

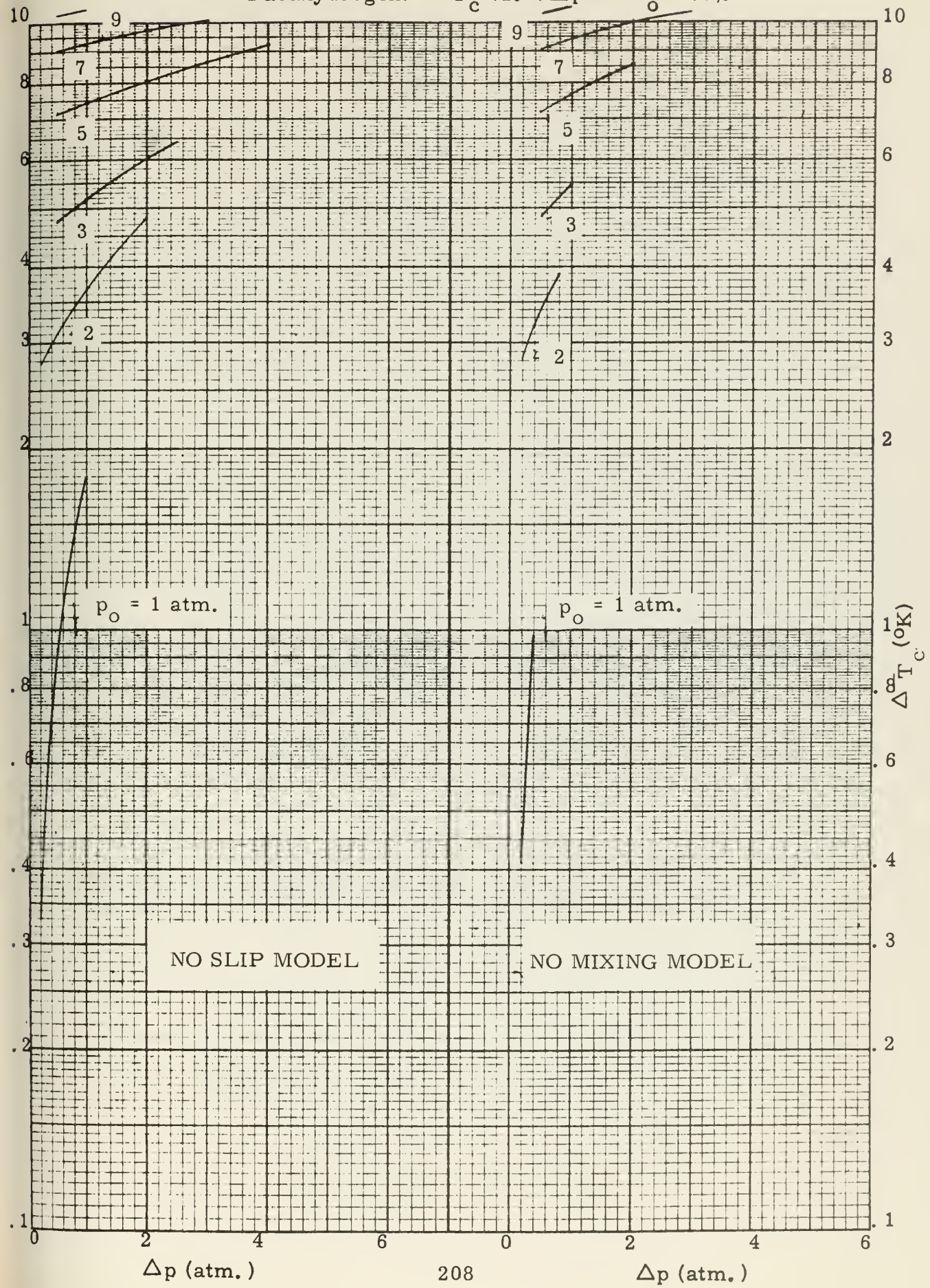

FIGURE D - 9a

Parahydrogen: v_{in} vs. Δp for x_o = 30%

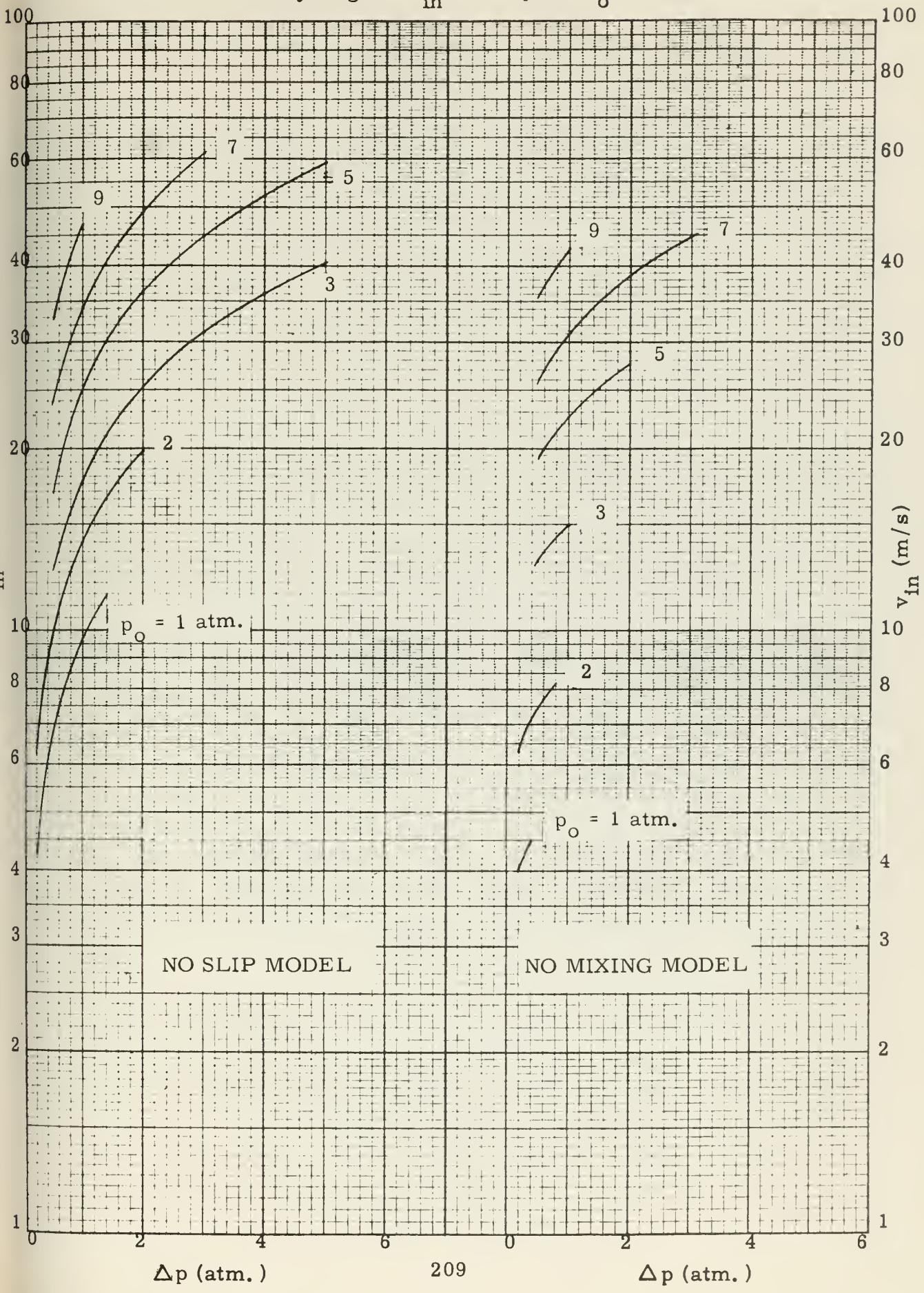

FIGURE D - 9b

Parahydrogen: v_{in} vs. Δp for x_o = 50%

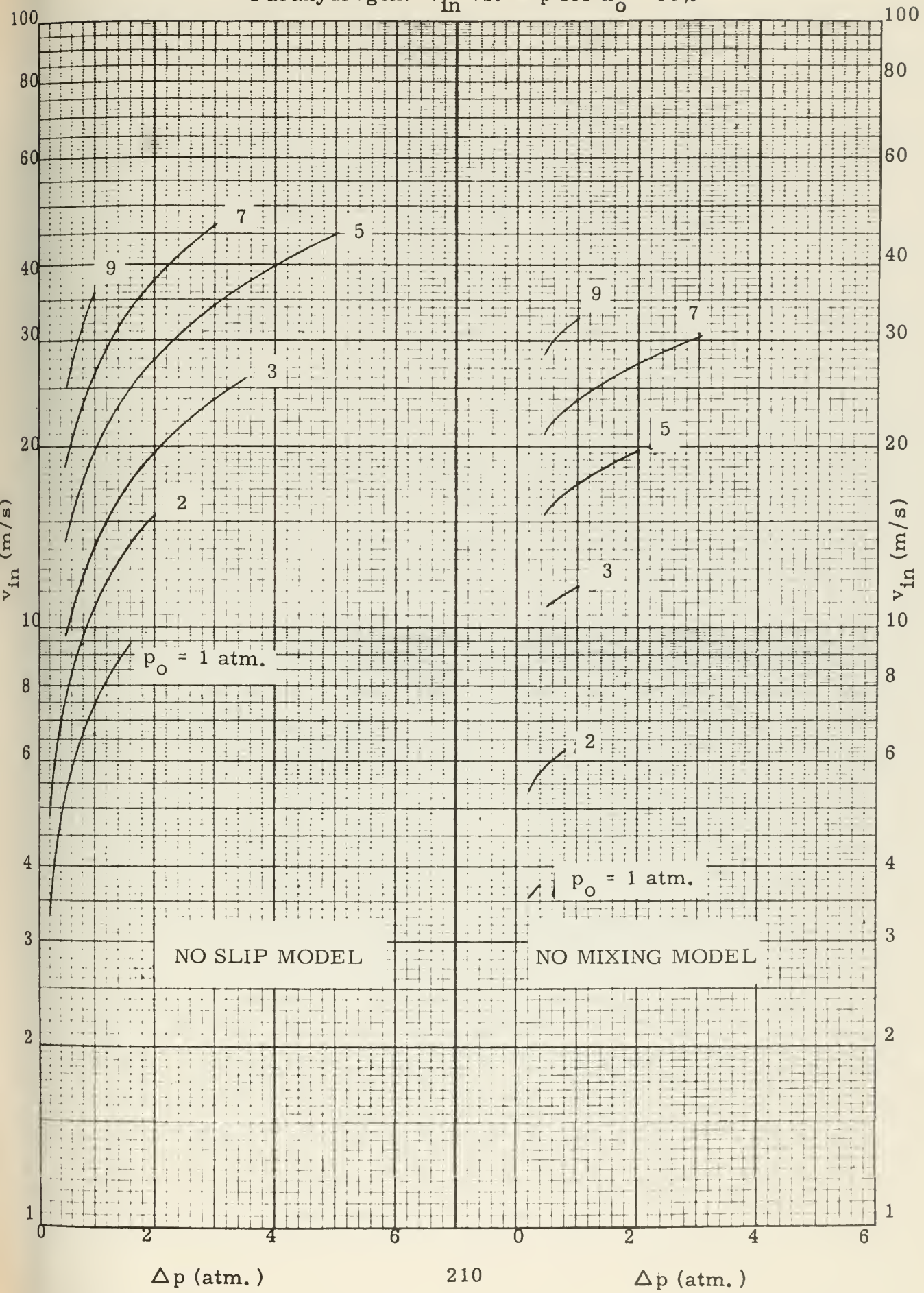

FIGURE D - 9c

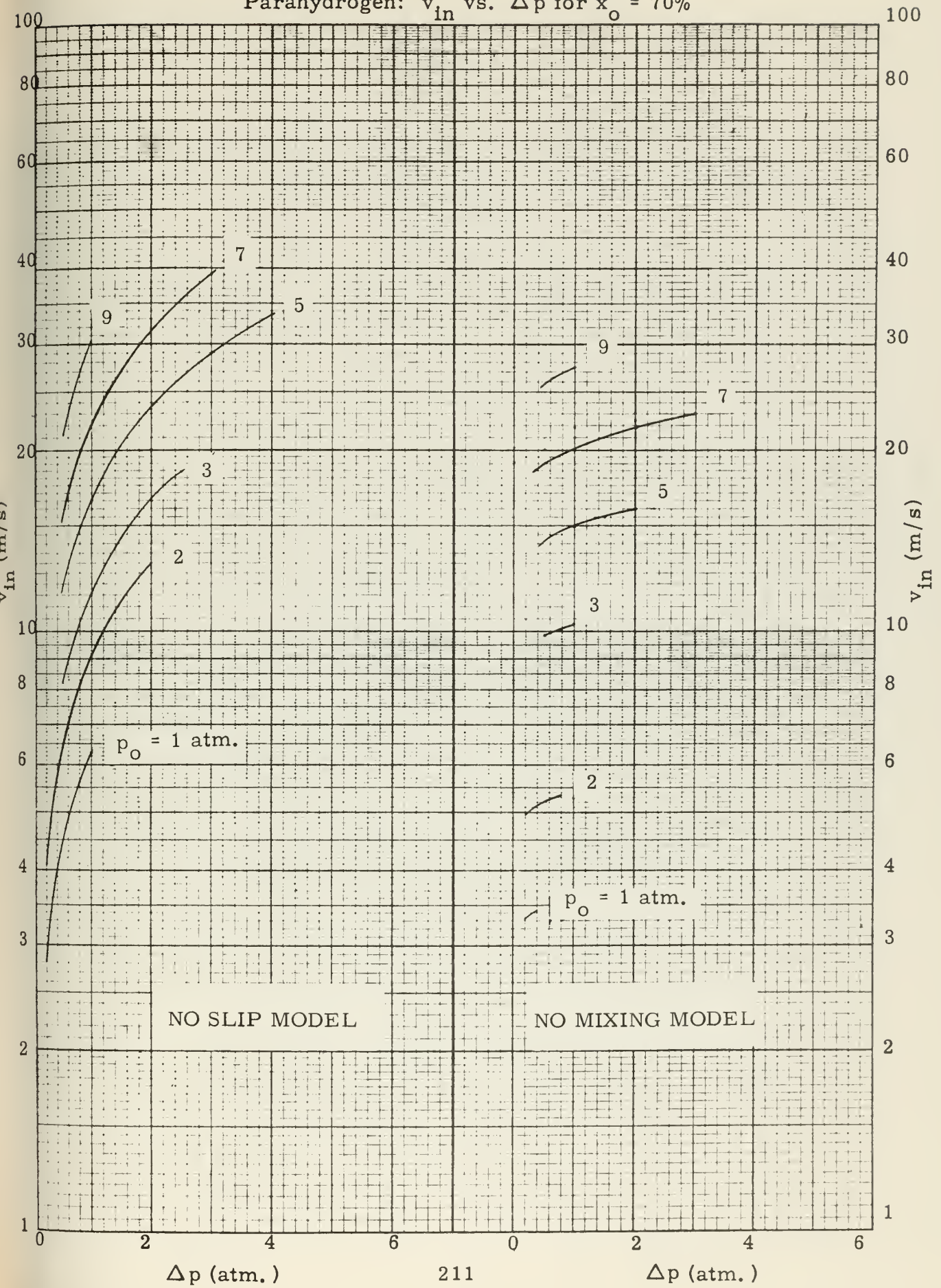
Parahydrogen: v_{in} vs. Δp for x_o = 70%
v_{in} (m/s)
Δp (atm.)
p_o = 1 atm.
NO SLIP MODEL
NO MIXING MODEL
9
7
5
3
2

FIGURE D - 10a

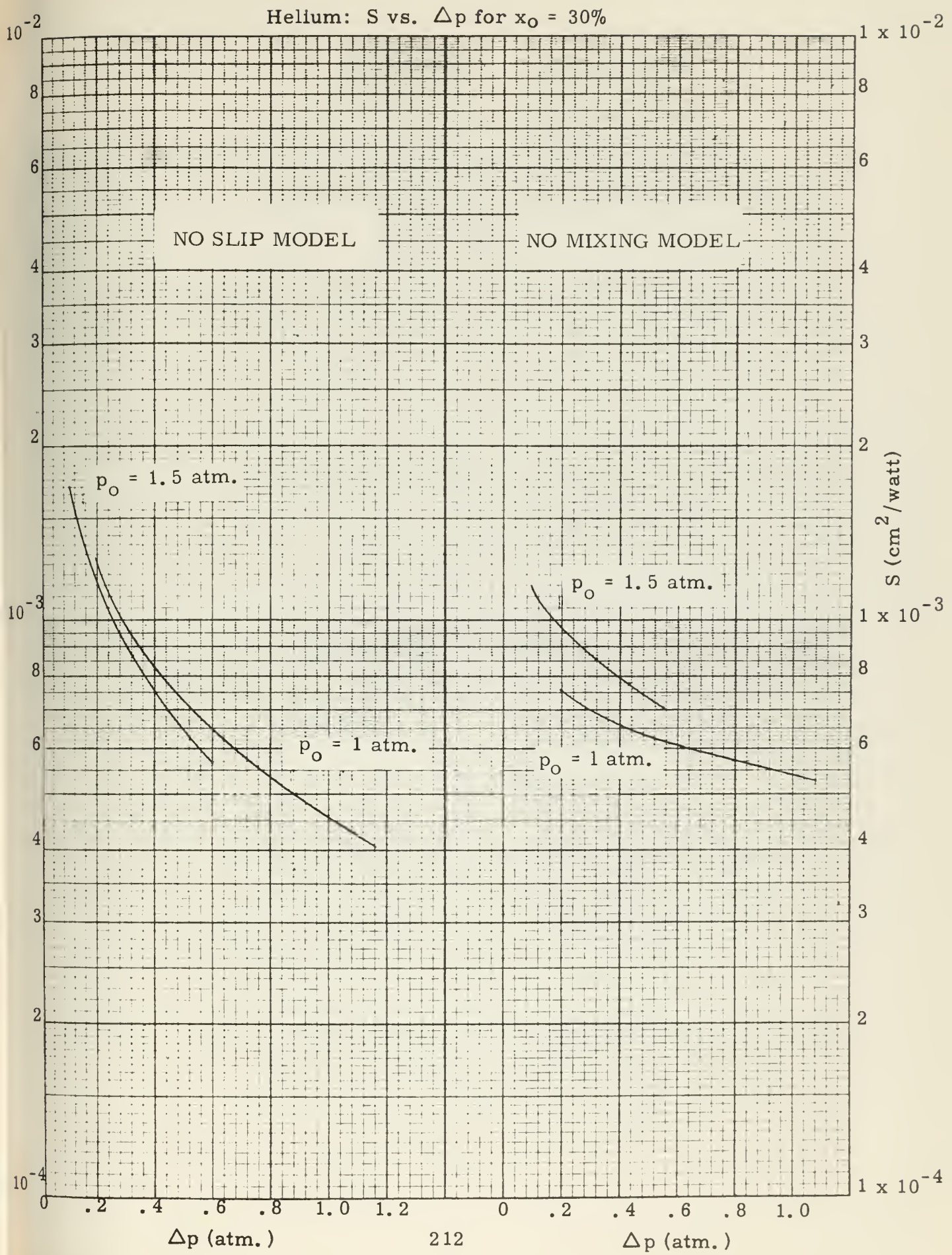
Helium: S vs. Δp for x_o = 30%
NO SLIP MODEL
NO MIXING MODEL
p_o = 1.5 atm.
p_o = 1 atm.
p_o = 1.5 atm.
p_o = 1 atm.
S (cm^2/watt)
Δp (atm.)
Δp (atm.)
10^{-2}
10^{-3}
10^{-4}
1 x 10^{-2}
1 x 10^{-3}
1 x 10^{-4}
0 .2 .4 .6 .8 1.0 1.2
0 .2 .4 .6 .8 1.0

FIGURE D - 10b

Helium: S vs. Δp for x_o = 50%

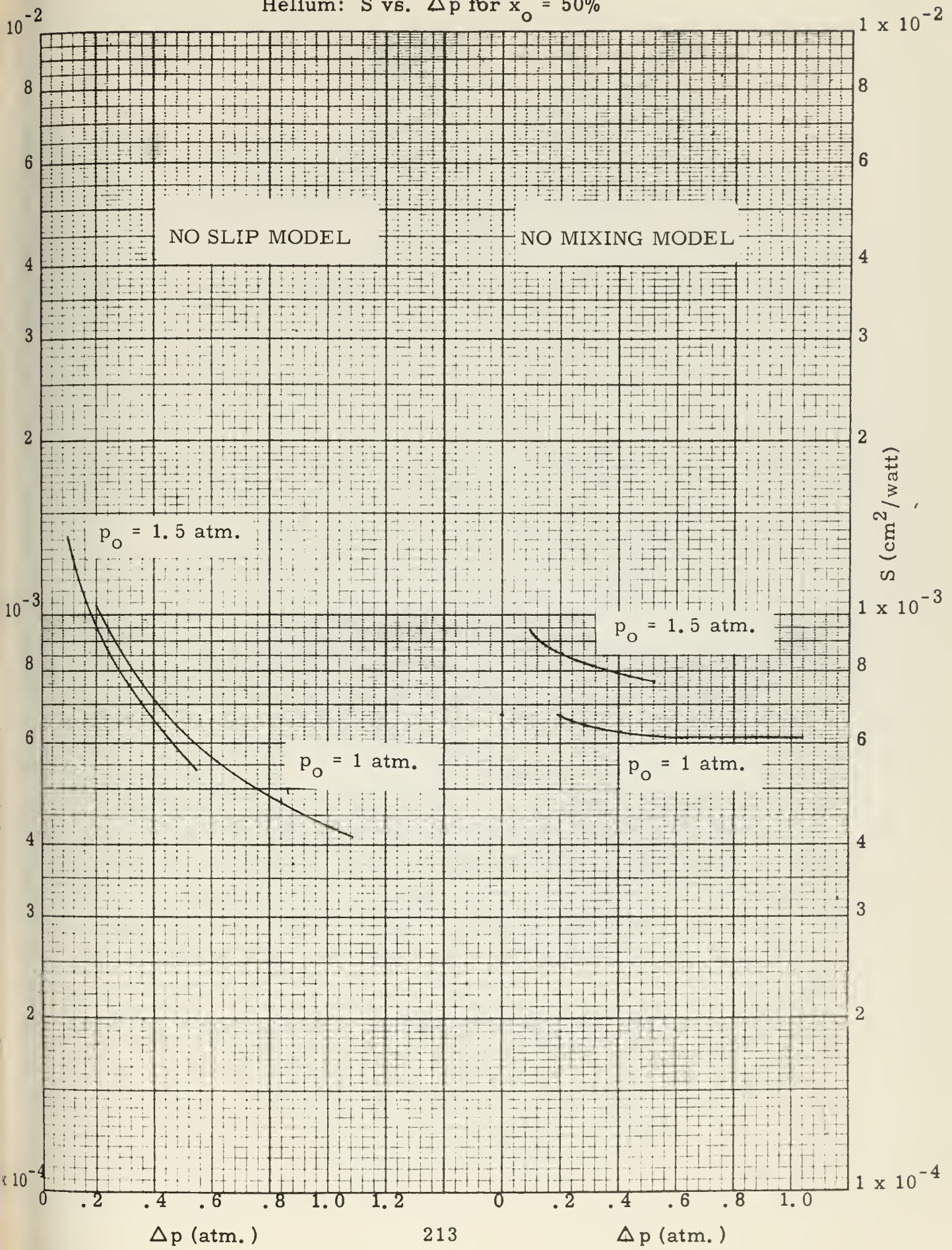

FIGURE D - 10c

Helium: S vs. Δp for x_o = 70%

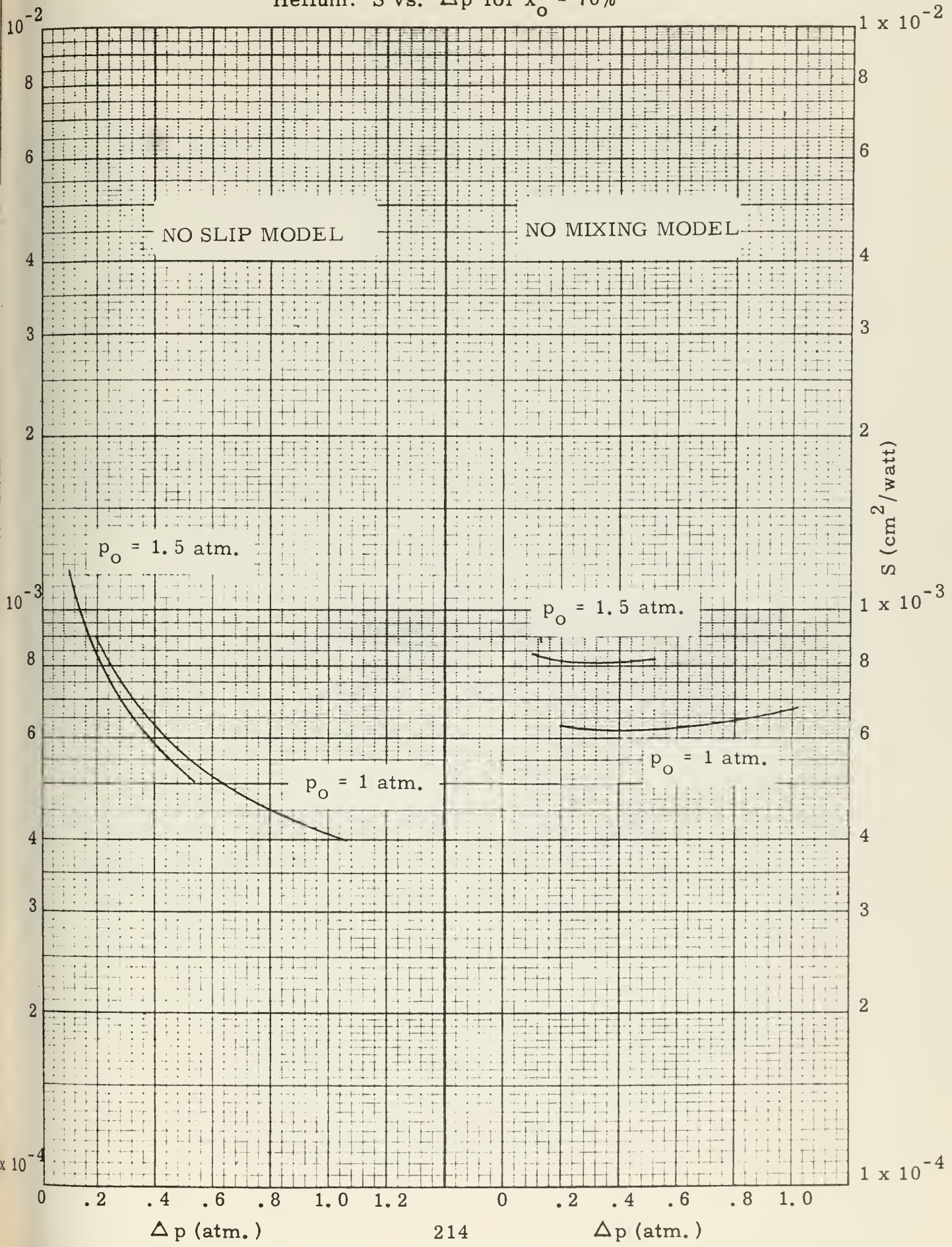

FIGURE D - 11a

Helium: ΔT_c vs. Δp for x_o = 30%

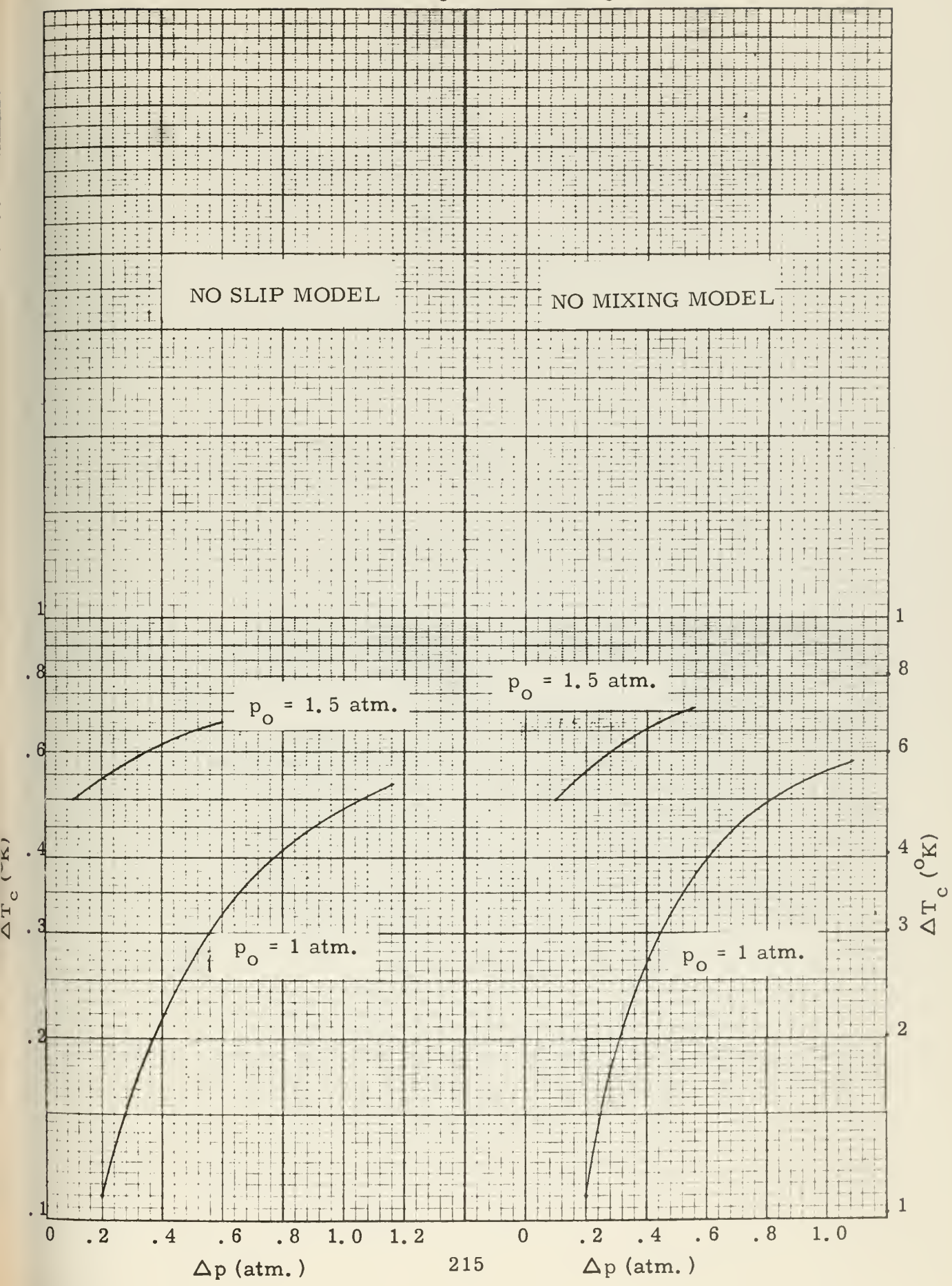

FIGURE D - 11b

Helium: ΔT_c vs. Δp for x_o = 50%

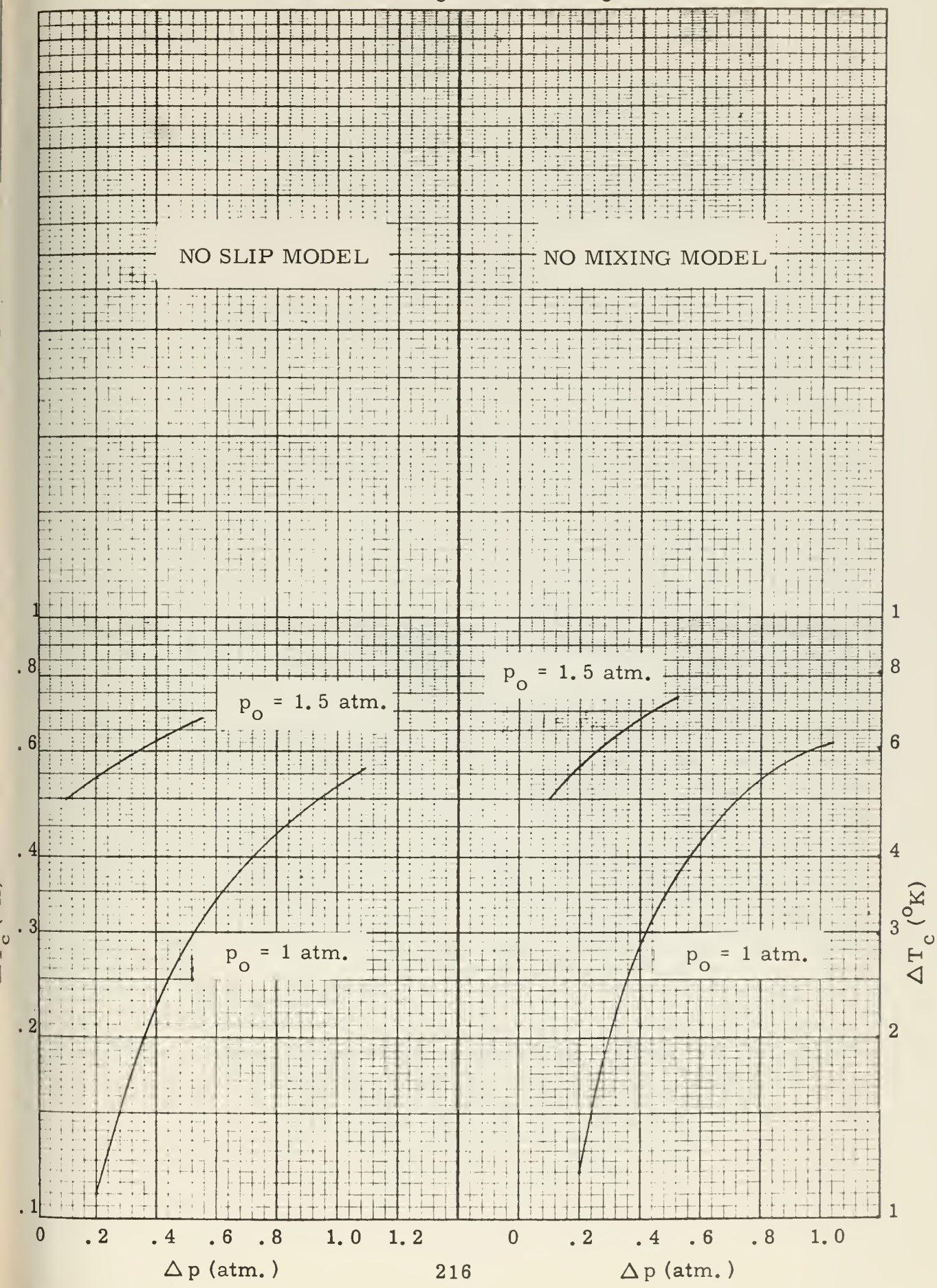

FIGURE D - 11c

Helium: ΔT_c vs. Δp for x_o = 70%

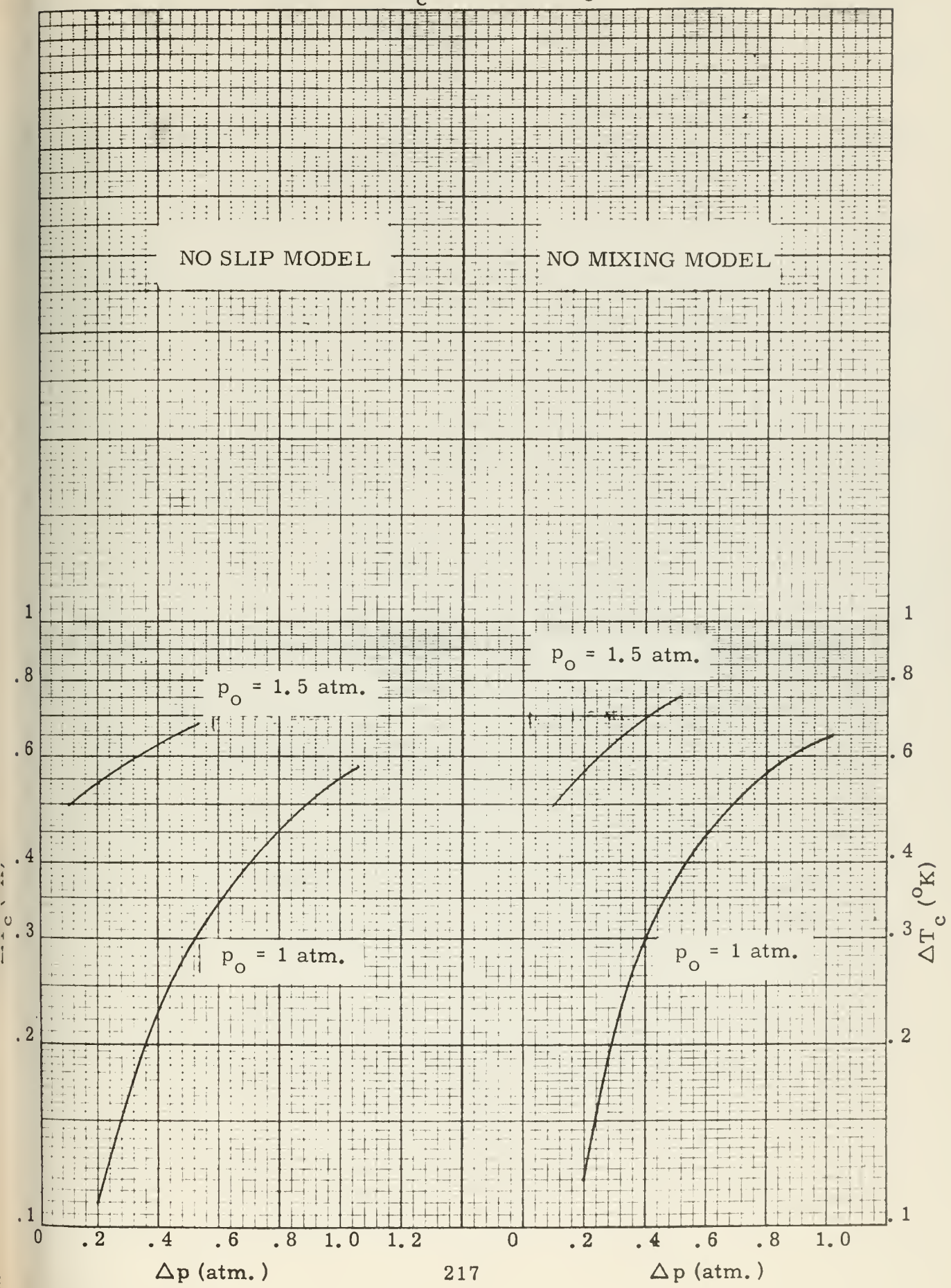

FIGURE D - 12a

Helium: v_{in} vs. Δp for x_o = 30%

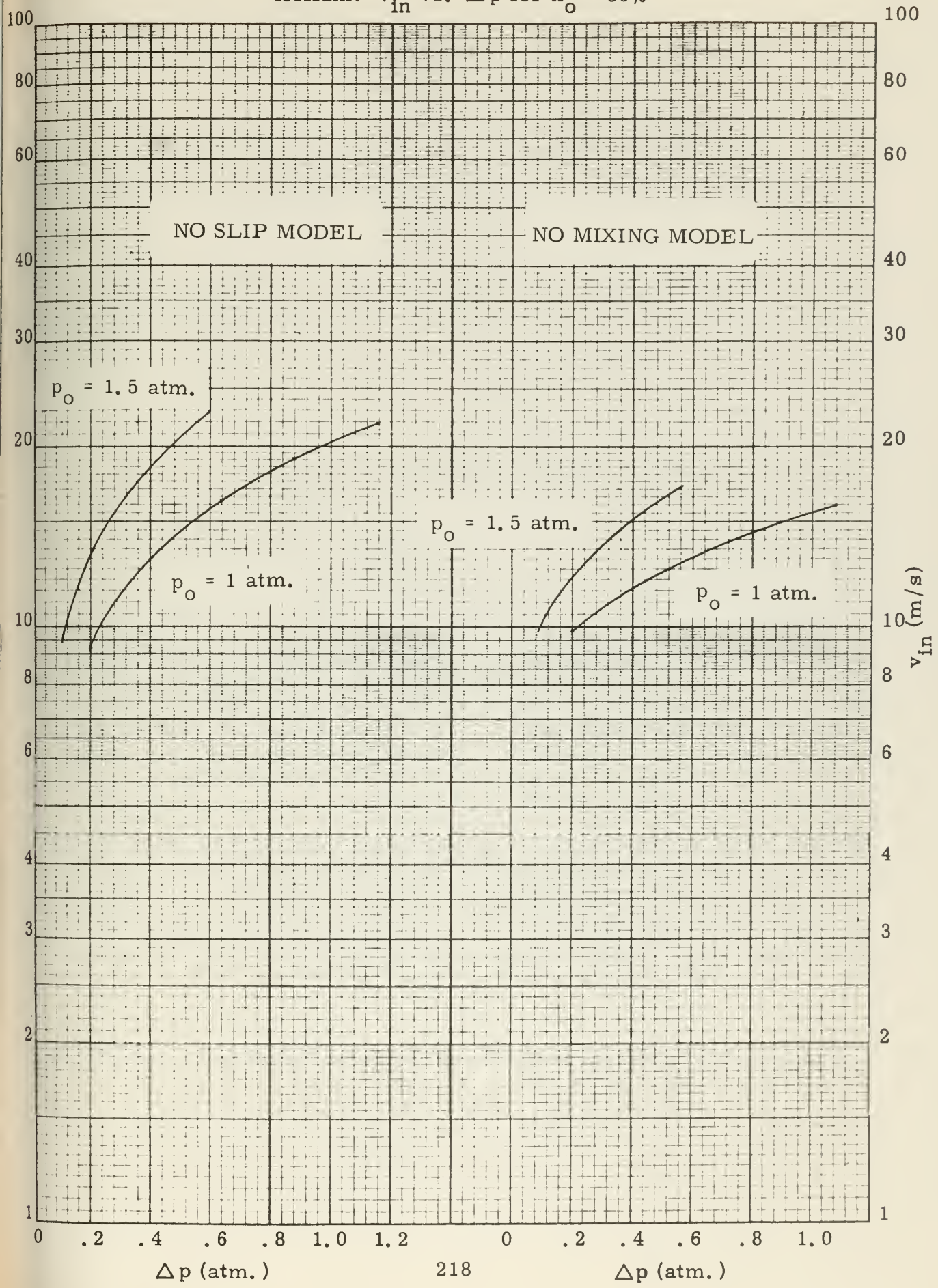

FIGURE D - 12b

Helium: v_{in} vs. Δp for x_o = 50%

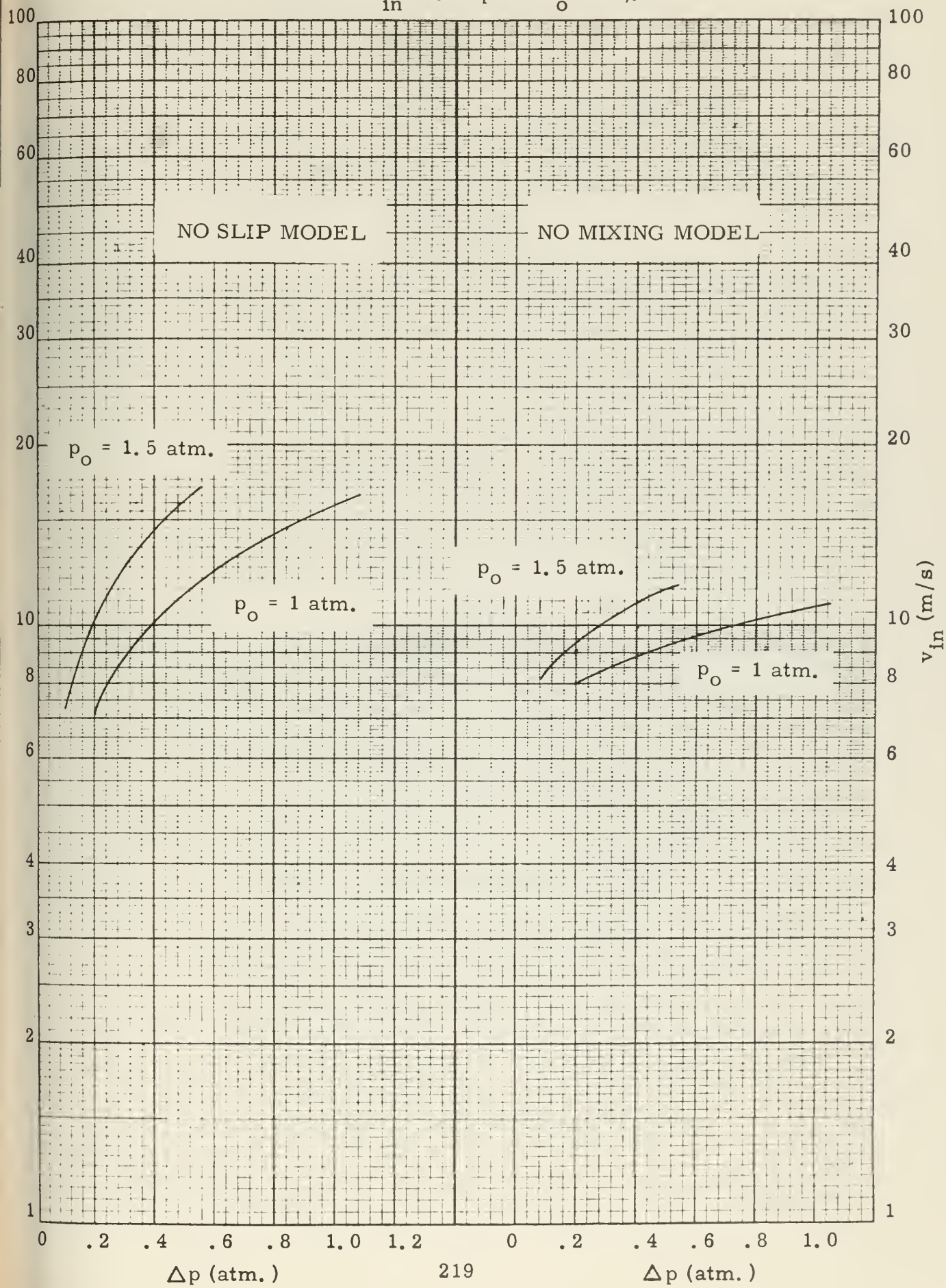

FIGURE D - 12c

Helium: v_{in} vs. Δp for x_o = 70%

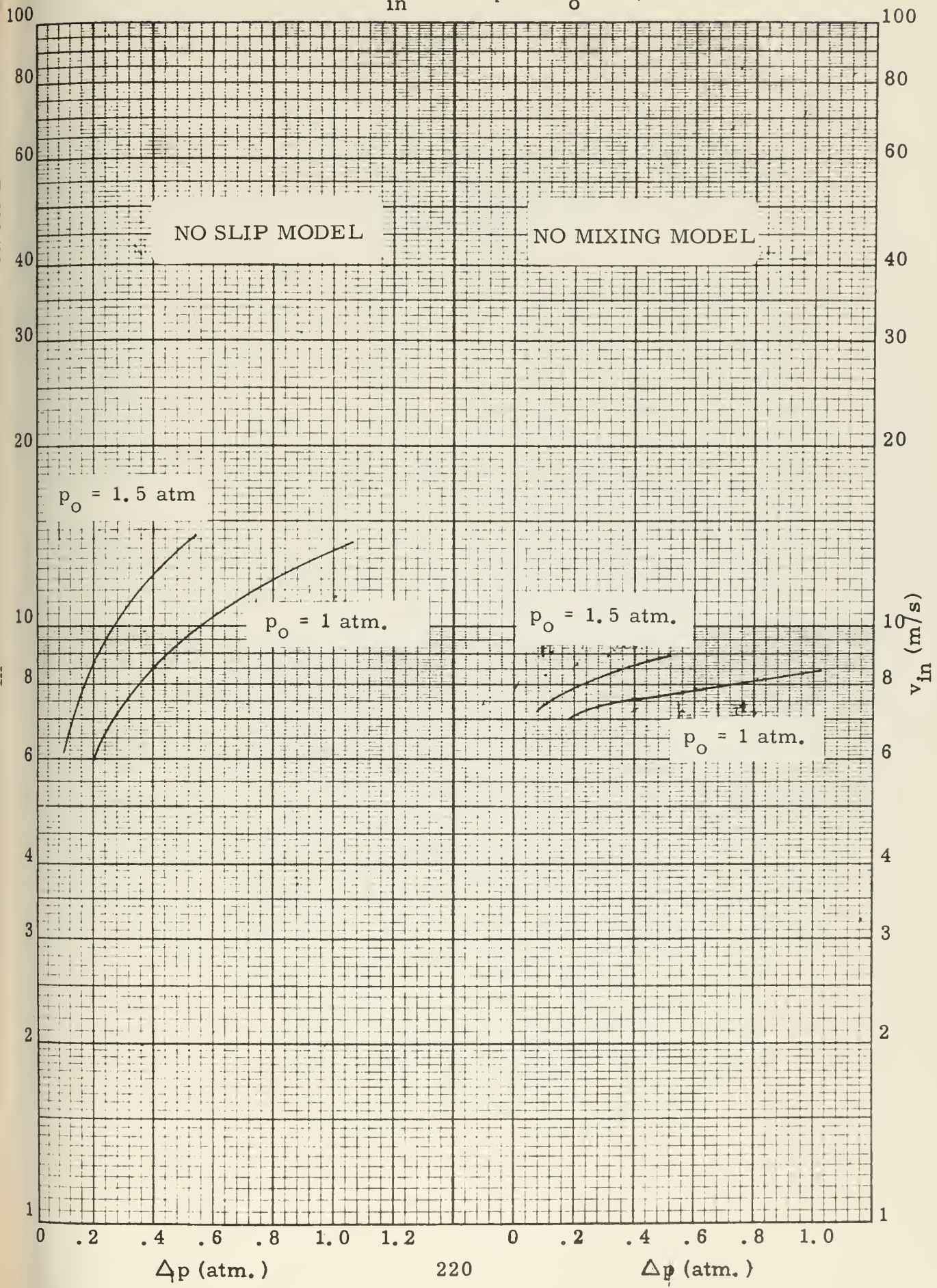

APPENDIX E

Computer Programs

```
MAIN PROGRAM  (COIL GEOMETRY/RESISTIVITY ANALYSIS)


 DIMENSION TEMP(10),RTEMP(10),RMAG(9,5),BTAB(100,50),AVRHO(10)
 COMMON ACHAN, WCHAN, HCHAN, ALTH, ACOIL, RADIUS, OFFSET, TEMP,
1RTEMP, RMAG, BTAB, AVRHO, RSQ, LBTAB, VCOIL, SCOIL, ENDFAC
 CALL READ
 READ 2, A1, B, CUR
 FORMAT(2F13.5, E13.4)
 CALL SIZE (A1, B, CUR)
 CALL FIELD (CUR)
 CALL RHO
 CALL PRINT (A1,B,CUR)
 GO TO 1
 END
```

```
      SUBROUTINE READ


      DIMENSION TEMP(10),RTEMP(10),RMAG(9,5),BTAB(100,50),AVRHO(10)
      COMMON ACHAN, WCHAN, HCHAN, ALTH, ACOIL, RADIUS, OFFSET, TEMP,
     1RTEMP, RMAG, BTAB, AVRHO, RSQ, LBTAB, VCOIL, SCOIL, ENDFAC
      READ 1, (TEMP(I),I=1,10)
      FORMAT(10I4)
      READ 2, (RTEMP(I),I=1,10)
      FORMAT(5E11.4)
      READ 3, ((RMAG(I,J),I=1,9),J=1,5)
      FORMAT (5E11.4/4E11.4)
      RETURN
      END
```

```
      SUBROUTINE SIZE (A1, B, CUR)


      DIMENSION TEMP(10),RTEMP(10),RMAG(9,5),BTAB(100,50),AVRHO(10)
      COMMON ACHAN, WCHAN, HCHAN, ALTH, ACOIL, RADIUS, OFFSET, TEMP,
     1RTEMP, RMAG, BTAB, AVRHO, RSQ, LBTAB, VCOIL, SCOIL, ENDFAC
      A=A1
      OFFSET=B/(1.25664E-5*CUR)
      DO 4 I=1,50
      RADIUS=OFFSET+SQRTF(A)/2.
      RSQ=RADIUS*RADIUS
      S=SQRTF(OFFSET*OFFSET+8.*RSQ)-3.*OFFSET
      ACHAN=S*SQRTF(RSQ-(OFFSET+S/4.)*(OFFSET+S/4.))
      DELTA=A1-ACHAN
      IF(A1/10000.-ABSF(DELTA)) 2,5,5
      IF (DELTA) 3,5,4
    4 A=A-0.9*DELTA
      A=A+DELTA
      WCHAN=S/2.
      HCHAN=ACHAN/WCHAN
      ALTH=10.*SQRTF(ACHAN)
      GAMMA=ACOSF(OFFSET/RADIUS)
      ACOIL=2.*RSQ*(3.14159-(2.*GAMMA-SINF(2.*GAMMA)))
      VCOIL=ACOIL*ALTH
      SCOIL=12.56637*RADIUS*ALTH
      ENDFAC=3.14159*(RADIUS+OFFSET)/ALTH + 1.
      RETURN
      END
```

```
      SUBROUTINE FIELD (CUR)


      DIMENSION TEMP(10),RTEMP(10),RMAG(9,5),BTAB(100,50),AVRHO(10)
      COMMON ACHAN, WCHAN, HCHAN, ALTH, ACOIL, RADIUS, OFFSET, TEMP,
     1RTEMP, RMAG, BTAB, AVRHO, RSQ, LBTAB, VCOIL, SCOIL, ENDFAC
      DO 1 I=1,100
      DO 1 J=1,50
      BTAB(I,J)=0.
      X1=RADIUS-OFFSET
      X2=RADIUS+OFFSET
      DELTA=RADIUS/50.
      SET=DELTA/2.
      BMAG=6.28318E-7*CUR
      DO 10 I=1,100
      AI=I
      X=AI*DELTA-SET
      IF(X2-X) 11,2,2
      XMO=X-OFFSET
      XMOSQ=XMO*XMO
      XPO=X+OFFSET
      XPOSQ=XPO*XPO
      Y2=SQRTF(RSQ-XMOSQ)
      IF(X-X1) 3,7,7
      Y1=SQRTF(RSQ-XPOSQ)
      DO 6 J=1,50
      AJ=J
      Y=AJ*DELTA-SET
      IF(Y-Y1) 6,4,4
      IF(Y2-Y) 10,5,5
      RATIO=RSQ/(XPOSQ+Y*Y)
      BX=BMAG*(1.-RATIO)*Y
      BY=BMAG*(XPO*RATIO-XMO)
      BTAB(I,J)=SQRTF(BX*BX+BY*BY)
      CONTINUE
      GO TO 10
      DO 9 J=1,50
      AJ=J
      Y=AJ*DELTA-SET
      IF(Y2-Y) 10,8,8
      RATIO=RSQ/(XPOSQ+Y*Y)
      BX=BMAG*(1.-RATIO)*Y
      BY=BMAG*(XPO*RATIO-XMO)
      BTAB(I,J)=SQRTF(BX*BX+BY*BY)
      LBTAB=I
      RETURN
      END
```

```
      SUBROUTINE RHO


      DIMENSION TEMP(10),RTEMP(10),RMAG(9,5),BTAB(100,50),AVRHO(10)
      COMMON ACHAN, WCHAN, HCHAN, ALTH, ACOIL, RADIUS, OFFSET, TEMP,
     1RTEMP, RMAG, BTAB, AVRHO, RSQ, LBTAB, VCOIL, SCOIL, ENDFAC
      DA=RSQ/2500.
      DO 8 I=1,10
      DASUM=0.
      RDASUM=0.
      DO 7 J=1,LBTAB
      DO 7 K=1,50
      IF(BTAB(J,K)) 7,7,1
      L=0
      M=1
      IN=10.*BTAB(J,K)/RTEMP(I)
      IF(IN-10) 2,4,4
      RDASUM=RDASUM+RTEMP(I)*DA
      GO TO 6
      IN=IN/10
      M=M+1
      IF(100-IN) 3,3,5
      L=(IN+5)/10
      RDASUM=RDASUM+RTEMP(I)*(RMAG(L,M)+1.)*DA
      DASUM=DASUM+DA
      CONTINUE
      AVRHO(I)=RDASUM/DASUM
      RETURN
      END
```

```
      SUBROUTINE PRINT (A1,B,CUR)


      DIMENSION TEMP(10),RTEMP(10),RMAG(9,5),BTAB(100,50),AVRHO(10)
      COMMON ACHAN, WCHAN, HCHAN, ALTH, ACOIL, RADIUS, OFFSET, TEMP,
     1RTEMP, RMAG, BTAB, AVRHO, RSQ, LBTAB, VCOIL, SCOIL, ENDFAC
      IF (LIST) 1,1,3
    1 LIST=4
      PRINT 2
    2 FORMAT(1H1)
      PRINT 4, A1,B,CUR
    4 FORMAT(1H0/34H0       DESIRED CHANNEL AREA (M2) =,F9.4,6X,26HDESIRE
     1D FLUX DENSITY (KG)=,F5.1,6X,32HDESIRED CURRENT DENSITY (A/M2) =,
     2F9.3)
      PRINT 5, ACHAN,WCHAN,HCHAN
    5 FORMAT(35H        COMPUTED CHANNEL AREA (M2) =,F8.4,6X,23HOPT CHANN
     1EL WIDTH (M) =,F8.4,6X,28HOPTIMUM CHANNEL HEIGHT (M) =,F13.4)
      PRINT 6, ALTH,RADIUS,OFFSET
    6 FORMAT(33H        COMPUTED COIL LENGTH (M) =,F10.4,6X,21HCYLINDER R
     1ADIUS (M) =,F10.4,6X,21HCYLINDER OFFSET (M) =,F20.4)
      PRINT 7, ACOIL,VCOIL,SCOIL
    7 FORMAT(33H        TOTAL CROSS SECTION (M2) =,F10.4,6X,19HTOTAL VOLU
     1ME (M3) =,F12.4,6X,25HTOTAL SURFACE AREA (M2) =,F16.4)
      PRINT 8, ENDFAC
    8 FORMAT(1H0,48X,19HCORRECTION FACTOR =,F12.4)
      PRINT 9
    9 FORMAT(1H0,30X,72HMEAN COIL RESISTIVITY AS A FUNCTION OF TEMPERATU
     1RE FOR ALUMINUM WINDINGS)
      PRINT 10,(TEMP(I),I=1,10)
   10 FORMAT(12H0  T (DEG K),10I12)
      PRINT 11, (AVRHO(I),I=1,10)
   11 FORMAT(12H   RHO RATIO,10E12.4)
      LIST=LIST-1
      RETURN
      END
```

MAIN PROGRAM (STRUCTURAL ANALYSIS)

```
 COMMON A1,B,CUR,SIGMAC,SIGMAD,ALTH,ACOIL,RADIUS,RSQ,OFFSET,ENDFAC,
1NCOMP,VCOMP,CFRACT,NTENS,VTENS,TFRACT,VFRACT
 PRINT 1
 FORMAT(1H1)
 READ 3, A1,B,CUR
 FORMAT(2F13.5,E13.4)
 CALL SIZE
 PRINT 4, A1,B,CUR,RADIUS,ENDFAC
 FORMAT(1H0/7H ACHAN=,F6.2,3H M2,10X,2HB=,F6.1,3H KG,10X,2HJ=,E9.3,
15H A/M2,10X,2HR=,F8.4,2H M,10X,7HENDFAC=,F7.4/1H )
 DO 7 I=1,4
 AI=I
 SIGMAC=AI*3000.
 DO 6 J=1,4
 AJ=5-J
 SIGMAD=AJ*30000.
 CALL CSHELL
 CALL TSHELL
 IF (VFRACT-.8) 5,7,7
 IF (VFRACT) 8,8,6
 CONTINUE
 CONTINUE
 GO TO 2
 END
```

```
      SUBROUTINE SIZE


      COMMON A1,B,CUR,SIGMAC,SIGMAD,ALTH,ACOIL,RADIUS,RSQ,OFFSET,ENDFAC,
     1NCOMP,VCOMP,CFRACT,NTENS,VTENS,TFRACT,VFRACT
      A=A1
      OFFSET=B/(1.25664E-5*CUR)
      DO 4 I=1,50
      RADIUS=OFFSET+SQRTF(A)/2.
      RSQ=RADIUS*RADIUS
      S=SQRTF(OFFSET*OFFSET+8.*RSQ)-3.*OFFSET
      ACHAN=S*SQRTF(RSQ-(OFFSET+S/4.)*(OFFSET+S/4.))
      DELTA=A1-ACHAN
      IF(A1/10000.-ABSF(DELTA)) 2,5,5
      IF(DELTA) 3,5,4
      A=A-.9*DELTA
      A=A+DELTA
      ALTH=10.*SQRTF(ACHAN)
      GAMMA=ACOSF(OFFSET/RADIUS)
      ACOIL=2.*RSQ*(3.14159-(2.*GAMMA-SINF(2.*GAMMA)))
      ENDFAC=3.14159*(RADIUS+OFFSET)/ALTH + 1.
      RETURN
      END
```

```
      SUBROUTINE CSHELL


      COMMON A1,B,CUR,SIGMAC,SIGMAD,ALTH,ACOIL,RADIUS,RSQ,OFFSET,ENDFAC,
     1NCOMP,VCOMP,CFRACT,NTENS,VTENS,TFRACT,VFRACT
      VCOMP=0.
      NCOMP=0
      RLIM=SQRTF(2.*SIGMAC*1.01325E+05/(14.696*1.25664E-06))/CUR
      IF (RLIM-RADIUS) 1,16,16
    1 RIN=RLIM
      ROUT=RIN*((1.+6.*SIGMAC*1.01325E+05/(14.696*1.25664E-06*CUR*CUR*RI
     1N*RIN))**(1./3.))
      IF (ROUT-RADIUS) 3,3,4
    3 PRESS=SIGMAC
      GO TO 5
    4 PRESS=14.696*1.25664E-06*CUR*CUR*(RSQ*RADIUS-RIN*RIN*RIN)/(1.01325
     1E+05*6.*RIN)
    5 X=(SIGMAD/37500.)*(ALTH/(2.*RIN))
      IF (X-20.) 6,10,10
    6 TN1=.525*PRESS/SIGMAD
      PCRIT=7.532E+07*(TN1**2.5)/(ALTH/(2.*RIN)-.045*SQRTF(TN1))
      IF (PCRIT-PRESS) 8,9,9
    8 TN1=TN1*((PRESS/PCRIT)**.4)
    9 GO TO 7
   10 IF (5.-X) 10,13,13
   13 TN2=(PRESS/50.186E+06)**(1./3.)
      PLIM=.96386*SIGMAD*TN2
      IF (PLIM-PRESS) 11,12,12
   11 TNLIM=(PLIM/50.186E+06)**(1./3.)
      SLOPE=150.558E+06*TNLIM*TNLIM
      TINT=TNLIM-PLIM/SLOPE
      PINT=-SLOPE*TINT
      TN2=(PRESS-PINT)/SLOPE
   12 IF (X-20.) 12,14,14
   14 IF (TN1-TN2) 13,14,14
   13 TCOMP=(2.*RIN)*TN1
      GO TO 15
   14 TCOMP=(2.*RIN)*TN2
   15 VCOMP=VCOMP+3.14159*(2.*RIN)*TCOMP
      NCOMP=NCOMP+1
      RIN=ROUT
      IF (RIN-RADIUS) 2,16,16
   16 CFRACT=VCOMP/(3.14159*RSQ)
      RETURN
      END
```

```
      SUBROUTINE TSHELL


      COMMON A1,B,CUR,SIGMAC,SIGMAD,ALTH,ACOIL,RADIUS,RSQ,OFFSET,ENDFAC,
     1NCOMP,VCOMP,CFRACT,NTENS,VTENS,TFRACT,VFRACT
      VTENS=0.
      NTENS=0
      R=RADIUS
      DR=.1*OFFSET
      RLIM=RADIUS+2.*OFFSET
      FCONST=1.25664E-06*RSQ*CUR*CUR
      FSUM=0.
      X=(R*R-RSQ+4.*OFFSET*OFFSET)/(4.*OFFSET)
      ANGLE=ACOSF(X/R)
      DF=FCONST*ANGLE*DR
      FSUM=FSUM+DF
      R=R+DR
      IF (R-RLIM) 3,6,6
      PRESS=14.696*FSUM/(1.01325E+05*2.*R*ANGLE)
      IF (PRESS-SIGMAC) 2,5,4
      R=R-(FSUM-2.*R*ANGLE*SIGMAC*1.01325E+05/14.696)/(FCONST*ANGLE)
      TTENS=R*SIGMAC/SIGMAD
      VTENS=VTENS+2.*R*ANGLE*TTENS
      NTENS=NTENS+1
      GO TO 1
      TFRACT=2.*VTENS/ACOIL
      VFRACT=CFRACT+TFRACT
      PRINT 7, SIGMAC,SIGMAD,VFRACT,NCOMP,CFRACT,NTENS,TFRACT
      FORMAT(8H SIGMAC=,F8.1,4H PSI,8X,7HSIGMAD=,F9.1,4H PSI,8X,7HVFRACT
     1=,F6.3,8X,3HNC=,I3,8X,3HVC=,F6.3,8X,3HNT=,I3,8X,3HVT=,F6.3)
      RETURN
      END
```

SAMPLE MAIN PROGRAM (DATA FITTING)

```
 DIMENSION X(200),Y(200),YGEN(200),DELTA(200),PRCENT(200),A(200,7),
1Z(7),IL(7)
 READ 1, L
 FORMAT(I3)
 READ 2, (X(I), Y(I), I=1,L)
 FORMAT(2F10.4)
 DO 3 I=1,L
 A(I,1)=1.0
 A(I,2)=X(I)
 A(I,3)=A(I,2)*X(I)
 A(I,4)=A(I,3)*X(I)
 A(I,5)=A(I,4)*X(I)
 A(I,6)=A(I,5)*X(I)
 A(I,7)=Y(I)
 M=6
 N=L
 E1=.1E-5
 CALL GLSQ(A,Z,IL,N,M,ALPHA,E1,E1)
 DO 4 I=1,L
 X2=X(I)*X(I)
 YGEN(I)=Z(1)+Z(2)*X(I)+Z(3)*X2+Z(4)*X2*X(I)+Z(5)*X2*X2+Z(6)*X2*X2*
1X(I)
 DELTA(I)=Y(I)-YGEN(I)
 PRCENT(I)=100.*DELTA(I)/YGEN(I)
 SUM=L
 RMS=SQRTF(ALPHA*ALPHA/SUM)
 PRINT 5, RMS
 FORMAT(1H1,6X,120HASSUMING Y = A(0) + A(1)X + A(2)X2 + A(3)X3 + A(
14)X4 + A(5)X5, THE BELOW COEFFICIENTS MINIMIZE RMS DEVIATION TO A
2VALUE /1H ,6X,3HOF ,E14.6,1H.)
 PRINT 6, (Z(I),I=1,4)
 FORMAT(1H0,6X,7HA(0) = ,E14.6,10X,7HA(1) = ,E14.6,10X,7HA(2) = ,E1
14.6,10X,7HA(3) = ,E14.6)
 PRINT 7, Z(5), Z(6)
 FORMAT(1H ,37X,7HA(4) = ,E14.6,10X,7HA(5) = ,E14.6)
 PRINT 8
 FORMAT(1H0/1H0,42X,47HGENERATED AND OBSERVED DATA ARE COMPARED BEL
10W.)
 PRINT 9
 FORMAT(1H0,22X,1HX,18X,10HY OBSERVED,14X,11HY GENERATED,14X,9HDEVI
1ATION,10X,7HPERCENT/1H0)
 PRINT 10, (X(I), Y(I), YGEN(I), DELTA(I), PRCENT(I), I=1,L)
 FORMAT(1H ,14X,E14.6,10X,E14.6,10X,E14.6,10X,E14.6,10X,F7.2)
 GO TO 100
 END
```

```
      SUBROUTINE GLSQ(A,X,IL,N,M,ALPHA,E1,E2)


      DIMENSION A(200,7),X(7),IL(7)
      MM=M+1
      LL = 1
      DO 60 J=1,MM
   60 IL(J)=0
      I=1
      DO 3 K=1,MM
      II=I+1
      DO 4 J=II,N
      IF(ABSF(A(J,K))-E1)4,4,6
    6 T1=SQRTF((A(J,K))**2+(A(I,K))**2)
      S=A(J,K)/T1
      C=A(I,K)/T1
      DO 5 L=K,MM
      T2=C*A(I,L)+S*A(J,L)
      A(J,L)=-S*A(I,L)+C*A(J,L)
    5 A(I,L)=T2
      LL=LL+1
    4 CONTINUE
      IF(ABSF(A(I,K))-E2)3,3,8
    8 IL(K)=I
      I=I+1
    3 CONTINUE
      X(MM)=-1.0
      II=M
      DO 35 I=1,M
   35 X(I)=0.0
      DO 30 J=1,M
      IF(IL(II))30,30,31
   31 S=0.0
      LL=II+1
      I=IL(II)
      DO 32 K=LL,MM
   32 S=S+A(I,K)*X(K)
      X(II)=-S/A(I,II)
   30 II=II-1
      IF(IL(MM))50,51,50
   51 ALPHA=0.0
      GO TO 52
   50 I=IL(MM)
      ALPHA=A(I,MM)
   52 RETURN
      END
```

MAIN PROGRAM (COOLANT FLOW ANALYSIS)

```
 DIMENSION A(4),B(6),C(6),D(6),E(6),QUAL(3),PIN(10),DPNS(10,3),DPNM
1(10,3),TIN(10),TAVNS(10,3),TAVNM(10,3),DTNS(10,3),DTNM(10,3),DENSI
2N(10),VINNS(10,3),VINNM(10,3),CVINNS(10,3),CVINNM(10,3),VOUTNS(10,
33),VLONM(10,3),VVONM(10,3),HVAVNS(10,3),HVAVNM(10,3),SLOTNS(10,3),
4SLOTNM(10,3),CSLTNS(10,3),CSLTNM(10,3)
 COMMON A,B,C,D,E,QUAL,VLIM,POUT,DELTAP,NOPINC,PIN,DPNS,DPNM,TIN,TA
1VNS,TAVNM,DTNS,DTNM,TOUT,DENSIN,DNLOUT,DNVOUT,VINNS,VINNM,CVINNS,C
2VINNM,VOUTNS,VLONM,VVONM,HVAVNS,HVAVNM,SLOTNS,SLOTNM,CSLTNS,CSLTNM
 CALL READS
 CALL NOSLIP
 CALL NOMIX
 CALL INLET
 CALL PRINTS
 GO TO 1
 END
```

```
SUBROUTINE READS


 DIMENSION A(4),B(6),C(6),D(6),E(6),QUAL(3),PIN(10),DPNS(10,3),DPNM
1(10,3),TIN(10),TAVNS(10,3),TAVNM(10,3),DTNS(10,3),DTNM(10,3),DENSI
2N(10),VINNS(10,3),VINNM(10,3),CVINNS(10,3),CVINNM(10,3),VOUTNS(10,
33),VLONM(10,3),VVONM(10,3),HVAVNS(10,3),HVAVNM(10,3),SLOTNS(10,3),
4SLOTNM(10,3),CSLTNS(10,3),CSLTNM(10,3)
 COMMON A,B,C,D,E,QUAL,VLIM,POUT,DELTAP,NOPINC,PIN,DPNS,DPNM,TIN,TA
1VNS,TAVNM,DTNS,DTNM,TOUT,DENSIN,DNLOUT,DNVOUT,VINNS,VINNM,CVINNS,C
2VINNM,VOUTNS,VLONM,VVONM,HVAVNS,HVAVNM,SLOTNS,SLOTNM,CSLTNS,CSLTNM
 READ 1, (A(I),I=1,4)
 READ 1, (B(I),I=1,6)
 READ 1, (C(I),I=1,6)
 READ 1, (D(I),I=1,6)
 READ 1, (E(I),I=1,6)
 FORMAT(5F14.6)
 READ 2, (QUAL(I),I=1,3)
 FORMAT(3F10.4)
 READ 3, VLIM
 FORMAT(F10.4)
 RETURN
 END
```

```
      SUBROUTINE NOSLIP


      DIMENSION A(4),B(6),C(6),D(6),E(6),QUAL(3),PIN(10),DPNS(10,3),DPNM
     1(10,3),TIN(10),TAVNS(10,3),TAVNM(10,3),DTNS(10,3),DTNM(10,3),DENSI
     2N(10),VINNS(10,3),VINNM(10,3),CVINNS(10,3),CVINNM(10,3),VOUTNS(10,
     33),VLONM(10,3),VVONM(10,3),HVAVNS(10,3),HVAVNM(10,3),SLOTNS(10,3),
     4SLOTNM(10,3),CSLTNS(10,3),CSLTNM(10,3)
      COMMON A,B,C,D,E,QUAL,VLIM,POUT,DELTAP,NOPINC,PIN,DPNS,DPNM,TIN,TA
     1VNS,TAVNM,DTNS,DTNM,TOUT,DENSIN,DNLOUT,DNVOUT,VINNS,VINNM,CVINNS,C
     2VINNM,VOUTNS,VLONM,VVONM,HVAVNS,HVAVNM,SLOTNS,SLOTNM,CSLTNS,CSLTNM
      READ 100, POUT,DELTAP,NOPINC
  100 FORMAT(2F10.4,I10)
      TOUT=TEMP(POUT)
      DNLOUT=1./SVOLL(POUT)
      DNVOUT=1./SVOLV(POUT)
      DO 7 I=1,NOPINC
      AI=I
      PINC=AI*DELTAP
      PIN(I)=POUT+PINC
      TIN(I)=TEMP(PIN(I))
      SVOLIN=SVOLL(PIN(I))
      DENSIN(I)=1./SVOLIN
      DO 6 M=1,3
      SPVOUT=QUAL(M)/DNVOUT+(1.-QUAL(M))/DNLOUT
      VINNS(I,M)=SVOLIN*SQRTF(1.01325E+06*PINC/(SPVOUT-SVOLIN))
      VOUTNS(I,M)=VINNS(I,M)+1.01325E+06*PINC*SVOLIN/VINNS(I,M)
      IF (VLIM-VOUTNS(I,M)) 1,2,2
    1 SLOTNS(I,M)=0.
      GO TO 6
    2 CONST=.08*QUAL(M)/(1./HTVP(PIN(I))+1./HTVP(POUT))
      G=VINNS(I,M)/SVOLIN
      X=0.
      TSUM=0.
      HNVSUM=0.
      PRESS=PIN(I)
      DO 4 J=1,25
      TSUM=TSUM+TEMP(PRESS)
      HINV=1./HTVP(PRESS)
      HNVSUM=HNVSUM+HINV
      X=X+CONST*HINV
      SPVOL=X*SVOLV(PRESS)+(1.-X)*SVOLL(PRESS)
      PRESS=PIN(I)-G*(SPVOL*G-VINNS(I,M))/1.01325E+06
      CONST=CONST*QUAL(M)/X
      QCHECK=ABSF((X-QUAL(M))/QUAL(M))
      IF(.001-QCHECK) 3,5,5
    3 TAVNS(I,M)=TSUM/25.
      HVAVNS(I,M)=HNVSUM/25.
      SLOTNS(I,M)=HVAVNS(I,M)/(QUAL(M)*G)
    4 CONTINUE
    5 CONTINUE
      RETURN
      END
```

```
SUBROUTINE NOMIX


 DIMENSION A(4),B(6),C(6),D(6),E(6),QUAL(3),PIN(10),DPNS(10,3),DPNM
1(10,3),TIN(10),TAVNS(10,3),TAVNM(10,3),DTNS(10,3),DTNM(10,3),DENSI
2N(10),VINNS(10,3),VINNM(10,3),CVINNS(10,3),CVINNM(10,3),VOUTNS(10,
33),VLONM(10,3),VVONM(10,3),HVAVNS(10,3),HVAVNM(10,3),SLOTNS(10,3),
4SLOTNM(10,3),CSLTNS(10,3),CSLTNM(10,3)
 COMMON A,B,C,D,E,QUAL,VLIM,POUT,DELTAP,NOPINC,PIN,DPNS,DPNM,TIN,TA
1VNS,TAVNM,DTNS,DTNM,TOUT,DENSIN,DNLOUT,DNVOUT,VINNS,VINNM,CVINNS,C
2VINNM,VOUTNS,VLONM,VVONM,HVAVNS,HVAVNM,SLOTNS,SLOTNM,CSLTNS,CSLTNM
 DO 13 I=1,NOPINC
 FV=2.0265E+06*(PIN(I)-POUT)*AVSVV(PIN(I),POUT)
 FL=2.0265E+06*(PIN(I)-POUT)*AVSVL(PIN(I),POUT)
 DO 12 M=1,3
 VIN=VINNS(I,M)
 ARATIO=(1.-QUAL(M))*DNVOUT/(QUAL(M)*DNLOUT)
 FIN=1./(DENSIN(I)*(1.+ARATIO))
 DA=DNLOUT*ARATIO
 VVONM(I,M)=SQRTF(FV+VIN*VIN)
 VLONM(I,M)=SQRTF(FL+VIN*VIN)
 VINNM(I,M)=FIN*(VLONM(I,M)*DA+VVONM*DNVOUT)
 DELTA=VINNM(I,M)-VIN
 VCHECK=ABSF(DELTA)/VINNM(I,M)
 VIN=VINNM(I,M)
 IF(.001-VCHECK) 1,2,2
 IF (VLIM-VVONM(I,M)) 3,4,4
 SLOTNM(I,M)=0.
 GO TO 12
 CONST=.04/SLOTNS(I,M)
 G=VINNM(I,M)*DENSIN(I)
 WFV=0.
 WFL=G
 TSUM=0.
 PRESS=PIN(I)
 VL1=VINNM(I,M)
 VV1=VINNM(I,M)
 DO 8 J=1,25
 TSUM=TSUM+TEMP(PRESS)
 DL=1./SVOLL(PRESS)
 DV=1./SVOLV(PRESS)
 H=HTVP(PRESS)
 WFL=WFL-CONST/H
 WFV=WFV+CONST/H
 AJ=26-J
 VL=VL1+(VLONM(I,M)-VL1)/AJ
 AL=WFL/(DL*VL)
 VV2=WFV/((1.-AL)*DV)
 VL2=SQRTF(DV*(VV2*VV2-VV1*VV1)/DL+VL1*VL1)
 VLCHEK=VL2-VL
 IF(VLCHEK) 61,7,62
 VL=VL+VLCHEK/5.0
 GO TO 63
 VL=VL+VLCHEK/10.0
```

```
IF(.001-ABSF(VLCHEK)/VL2) 6,7,7
DP=DV*(VV2*VV2-VV1*VV1)/2.
PRESS=PRESS-DP/1.01325E+06
VL1=VL2
VV1=VV2
X=DV*(1.-AL)/(DV*(1.-AL)+DL*AL)
QCHECK=X/QUAL(M)-1.
IF(QCHECK) 10,11,9
CONST=CONST*(1.-QCHECK/10.)/(1.-QCHECK/5.)
CONST=CONST*(1.-QCHECK/5.)
IF(.001-ABSF(QCHECK)) 5,11,11
TAVNM(I,M)=TSUM/25.
SLOTNM(I,M)=.04/CONST
CONTINUE
CONTINUE
RETURN
END
```

```
 SUBROUTINE INLET


 DIMENSION A(4),B(6),C(6),D(6),E(6),QUAL(3),PIN(10),DPNS(10,3),DPNM
1(10,3),TIN(10),TAVNS(10,3),TAVNM(10,3),DTNS(10,3),DTNM(10,3),DENSI
2N(10),VINNS(10,3),VINNM(10,3),CVINNS(10,3),CVINNM(10,3),VOUTNS(10,
33),VLONM(10,3),VVONM(10,3),HVAVNS(10,3),HVAVNM(10,3),SLOTNS(10,3),
4SLOTNM(10,3),CSLTNS(10,3),CSLTNM(10,3)
 COMMON A,B,C,D,E,QUAL,VLIM,POUT,DELTAP,NOPINC,PIN,DPNS,DPNM,TIN,TA
1VNS,TAVNM,DTNS,DTNM,TOUT,DENSIN,DNLOUT,DNVOUT,VINNS,VINNM,CVINNS,C
2VINNM,VOUTNS,VLONM,VVONM,HVAVNS,HVAVNM,SLOTNS,SLOTNM,CSLTNS,CSLTNM
 PSTD=1.
 TSTD=TEMP(PSTD)
 DO 1 I=1,NOPINC
 DH=HLIQ(PIN(I))-HLIQ(POUT)-.20265*(PIN(I)-POUT)/DNLOUT
 TAVIN=(TEMP(PIN(I))+TEMP(POUT))/2.
 DO 1 M=1,3
 DLNS=DH*DENSIN(I)*VINNS(I,M)*SLOTNS(I,M)
 CSLTNS(I,M)=SLOTNS(I,M)/(1.+DLNS)
 CVINNS(I,M)=VINNS(I,M)*DENSIN(I)/DNLOUT
 DPNS(I,M)=PIN(I)-POUT+DENSIN(I)*VINNS(I,M)*(VINNS(I,M)-CVINNS(I,M)
1)/1.01325E+06
 DTNS(I,M)=(TAVNS(I,M)+DLNS*TAVIN)/(1.+DLNS)-TSTD
 DLNM=DH*DENSIN(I)*VINNM(I,M)*SLOTNM(I,M)
 CSLTNM(I,M)=SLOTNM(I,M)/(1.+DLNM)
 CVINNM(I,M)=VINNM(I,M)*DENSIN(I)/DNLOUT
 DPNM(I,M)=PIN(I)-POUT+DENSIN(I)*VINNM(I,M)*(VINNM(I,M)-CVINNM(I,M)
1)/1.01325E+06
 DTNM(I,M)=(TAVNM(I,M)+DLNM*TAVIN)/(1.+DLNM)-TSTD
 DO 5 I=1,NOPINC
 DO 5 M=1,3
 IF(CSLTNS(I,M)) 3,2,3
 CVINNS(I,M)=0.
 DPNS(I,M)=0.
 DTNS(I,M)=0.
 IF(CSLTNM(I,M)) 5,4,5
 CVINNM(I,M)=0.
 DPNM(I,M)=0.
 DTNM(I,M)=0.
 CONTINUE
 RETURN
 END
```

```
FUNCTION SVOLL(P)


 DIMENSION A(4),B(6),C(6),D(6),E(6),QUAL(3),PIN(10),DPNS(10,3),DPNM
1(10,3),TIN(10),TAVNS(10,3),TAVNM(10,3),DTNS(10,3),DTNM(10,3),DENSI
2N(10),VINNS(10,3),VINNM(10,3),CVINNS(10,3),CVINNM(10,3),VOUTNS(10,
33),VLONM(10,3),VVONM(10,3),HVAVNS(10,3),HVAVNM(10,3),SLOTNS(10,3),
4SLOTNM(10,3),CSLTNS(10,3),CSLTNM(10,3)
 COMMON A,B,C,D,E,QUAL,VLIM,POUT,DELTAP,NOPINC,PIN,DPNS,DPNM,TIN,TA
1VNS,TAVNM,DTNS,DTNM,TOUT,DENSIN,DNLOUT,DNVOUT,VINNS,VINNM,CVINNS,C
2VINNM,VOUTNS,VLONM,VVONM,HVAVNS,HVAVNM,SLOTNS,SLOTNM,CSLTNS,CSLTNM
 P2=P*P
 P3=P2*P
 SVOLL=A(1)+A(2)*P+A(3)*P2+A(4)*P3
 RETURN
 END
```

```
FUNCTION SVOLV(P)


 DIMENSION A(4),B(6),C(6),D(6),E(6),QUAL(3),PIN(10),DPNS(10,3),DPNM
1(10,3),TIN(10),TAVNS(10,3),TAVNM(10,3),DTNS(10,3),DTNM(10,3),DENSI
2N(10),VINNS(10,3),VINNM(10,3),CVINNS(10,3),CVINNM(10,3),VOUTNS(10,
33),VLONM(10,3),VVONM(10,3),HVAVNS(10,3),HVAVNM(10,3),SLOTNS(10,3),
4SLOTNM(10,3),CSLTNS(10,3),CSLTNM(10,3)
 COMMON A,B,C,D,E,QUAL,VLIM,POUT,DELTAP,NOPINC,PIN,DPNS,DPNM,TIN,TA
1VNS,TAVNM,DTNS,DTNM,TOUT,DENSIN,DNLOUT,DNVOUT,VINNS,VINNM,CVINNS,C
2VINNM,VOUTNS,VLONM,VVONM,HVAVNS,HVAVNM,SLOTNS,SLOTNM,CSLTNS,CSLTNM
 P2=P*P
 P3=P2*P
 SVOLV=B(1)/P+B(2)+B(3)*P+B(4)*P2+B(5)*P3+B(6)*P2*P2
 RETURN
 END
```

```
      FUNCTION TEMP(P)


      DIMENSION A(4),B(6),C(6),D(6),E(6),QUAL(3),PIN(10),DPNS(10,3),DPNM
     1(10,3),TIN(10),TAVNS(10,3),TAVNM(10,3),DTNS(10,3),DTNM(10,3),DENSI
     2N(10),VINNS(10,3),VINNM(10,3),CVINNS(10,3),CVINNM(10,3),VOUTNS(10,
     33),VLONM(10,3),VVONM(10,3),HVAVNS(10,3),HVAVNM(10,3),SLOTNS(10,3),
     4SLOTNM(10,3),CSLTNS(10,3),CSLTNM(10,3)
      COMMON A,B,C,D,E,QUAL,VLIM,POUT,DELTAP,NOPINC,PIN,DPNS,DPNM,TIN,TA
     1VNS,TAVNM,DTNS,DTNM,TOUT,DENSIN,DNLOUT,DNVOUT,VINNS,VINNM,CVINNS,C
     2VINNM,VOUTNS,VLONM,VVONM,HVAVNS,HVAVNM,SLOTNS,SLOTNM,CSLTNS,CSLTNM
      P2=P*P
      P3=P2*P
      TEMP=C(1)+C(2)*P+C(3)*P2+C(4)*P3+C(5)*P2*P2+C(6)*P3*P2
      RETURN
      END
```

```
FUNCTION HLIQ(P)


 DIMENSION A(4),B(6),C(6),D(6),E(6),QUAL(3),PIN(10),DPNS(10,3),DPNM
1(10,3),TIN(10),TAVNS(10,3),TAVNM(10,3),DTNS(10,3),DTNM(10,3),DENSI
2N(10),VINNS(10,3),VINNM(10,3),CVINNS(10,3),CVINNM(10,3),VOUTNS(10,
33),VLONM(10,3),VVONM(10,3),HVAVNS(10,3),HVAVNM(10,3),SLOTNS(10,3),
4SLOTNM(10,3),CSLTNS(10,3),CSLTNM(10,3)
 COMMON A,B,C,D,E,QUAL,VLIM,POUT,DELTAP,NOPINC,PIN,DPNS,DPNM,TIN,TA
1VNS,TAVNM,DTNS,DTNM,TOUT,DENSIN,DNLOUT,DNVOUT,VINNS,VINNM,CVINNS,C
2VINNM,VOUTNS,VLONM,VVONM,HVAVNS,HVAVNM,SLOTNS,SLOTNM,CSLTNS,CSLTNM
 P2=P*P
 P3=P2*P
 HLIQ=D(1)+D(2)*P+D(3)*P2+D(4)*P3+D(5)*P2*P2+D(6)*P3*P2
 RETURN
 END
```

```
FUNCTION HTVP(P)


 DIMENSION A(4),B(6),C(6),D(6),E(6),QUAL(3),PIN(10),DPNS(10,3),DPNM
1(10,3),TIN(10),TAVNS(10,3),TAVNM(10,3),DTNS(10,3),DTNM(10,3),DENSI
2N(10),VINNS(10,3),VINNM(10,3),CVINNS(10,3),CVINNM(10,3),VOUTNS(10,
33),VLONM(10,3),VVONM(10,3),HVAVNS(10,3),HVAVNM(10,3),SLOTNS(10,3),
4SLOTNM(10,3),CSLTNS(10,3),CSLTNM(10,3)
 COMMON A,B,C,D,E,QUAL,VLIM,POUT,DELTAP,NOPINC,PIN,DPNS,DPNM,TIN,TA
1VNS,TAVNM,DTNS,DTNM,TOUT,DENSIN,DNLOUT,DNVOUT,VINNS,VINNM,CVINNS,C
2VINNM,VOUTNS,VLONM,VVONM,HVAVNS,HVAVNM,SLOTNS,SLOTNM,CSLTNS,CSLTNM
 P2=P*P
 P3=P2*P
 HTVP=E(1)+E(2)*P+E(3)*P2+E(4)*P3+E(5)*P2*P2+E(6)*P3*P2
 RETURN
 END
```

```
      FUNCTION AVSVL(PH,PL)


      DIMENSION A(4),B(6),C(6),D(6),E(6),QUAL(3),PIN(10),DPNS(10,3),DPNM
     1(10,3),TIN(10),TAVNS(10,3),TAVNM(10,3),DTNS(10,3),DTNM(10,3),DENSI
     2N(10),VINNS(10,3),VINNM(10,3),CVINNS(10,3),CVINNM(10,3),VOUTNS(10,
     33),VLONM(10,3),VVONM(10,3),HVAVNS(10,3),HVAVNM(10,3),SLOTNS(10,3),
     4SLOTNM(10,3),CSLTNS(10,3),CSLTNM(10,3)
      COMMON A,B,C,D,E,QUAL,VLIM,POUT,DELTAP,NOPINC,PIN,DPNS,DPNM,TIN,TA
     1VNS,TAVNM,DTNS,DTNM,TOUT,DENSIN,DNLOUT,DNVOUT,VINNS,VINNM,CVINNS,C
     2VINNM,VOUTNS,VLONM,VVONM,HVAVNS,HVAVNM,SLOTNS,SLOTNM,CSLTNS,CSLTNM
      PH2=PH*PH
      PH3=PH2*PH
      PL2=PL*PL
      PL3=PL2*PL
      AVSVL=(A(1)*(PH-PL)+A(2)*(PH2-PL2)/2.+A(3)*(PH3-PL3)/3.+A(4)*(PH2*
     1PH2-PL2*PL2)/4.)/(PH-PL)
      RETURN
      END
```

```
      FUNCTION AVSVV(PH,PL)


      DIMENSION A(4),B(6),C(6),D(6),E(6),QUAL(3),PIN(10),DPNS(10,3),DPNM
     1(10,3),TIN(10),TAVNS(10,3),TAVNM(10,3),DTNS(10,3),DTNM(10,3),DENSI
     2N(10),VINNS(10,3),VINNM(10,3),CVINNS(10,3),CVINNM(10,3),VOUTNS(10,
     33),VLONM(10,3),VVONM(10,3),HVAVNS(10,3),HVAVNM(10,3),SLOTNS(10,3),
     4SLOTNM(10,3),CSLTNS(10,3),CSLTNM(10,3)
      COMMON A,B,C,D,E,QUAL,VLIM,POUT,DELTAP,NOPINC,PIN,DPNS,DPNM,TIN,TA
     1VNS,TAVNM,DTNS,DTNM,TOUT,DENSIN,DNLOUT,DNVOUT,VINNS,VINNM,CVINNS,C
     2VINNM,VOUTNS,VLONM,VVONM,HVAVNS,HVAVNM,SLOTNS,SLOTNM,CSLTNS,CSLTNM
      PH2=PH*PH
      PH3=PH2*PH
      PL2=PL*PL
      PL3=PL2*PL
      AVSVV=(B(1)*LOGF(PH/PL)+B(2)*(PH-PL)+B(3)*(PH2-PL2)/2.+B(4)*(PH3-P
     1L3)/3.+B(5)*(PH2*PH2-PL2*PL2)/4.+B(6)*(PH3*PH2-PL3*PL2)/5.)/(PH-PL
     2)
      RETURN
      END
```

```
      SUBROUTINE PRINTS


      DIMENSION A(4),B(6),C(6),D(6),E(6),QUAL(3),PIN(10),DPNS(10,3),DPNM
     1(10,3),TIN(10),TAVNS(10,3),TAVNM(10,3),DTNS(10,3),DTNM(10,3),DENSI
     2N(10),VINNS(10,3),VINNM(10,3),CVINNS(10,3),CVINNM(10,3),VOUTNS(10,
     33),VLONM(10,3),VVONM(10,3),HVAVNS(10,3),HVAVNM(10,3),SLOTNS(10,3),
     4SLOTNM(10,3),CSLTNS(10,3),CSLTNM(10,3)
      COMMON A,B,C,D,E,QUAL,VLIM,POUT,DELTAP,NOPINC,PIN,DPNS,DPNM,TIN,TA
     1VNS,TAVNM,DTNS,DTNM,TOUT,DENSIN,DNLOUT,DNVOUT,VINNS,VINNM,CVINNS,C
     2VINNM,VOUTNS,VLONM,VVONM,HVAVNS,HVAVNM,SLOTNS,SLOTNM,CSLTNS,CSLTNM
      PRINT 1
    1 FORMAT(1H1,57X,17HOUTLET PARAMETERS)
      PRINT 2, POUT,TOUT,DNVOUT,DNLOUT
    2 FORMAT(1H0,16HPRESSURE (ATM) =,F6.3,7X,21HTEMPERATURE (DEG K) =,F6
     1.2,7X,22HVAPOR DENSITY (G/CC) =,F8.6,7X,23HLIQUID DENSITY (G/CC) =
     2,F8.5)
      PRINT 3
    3 FORMAT(1H0/1H ,36X,59HFLOW PARAMETERS BASED ON NO-SLIP MODEL ARE T
     1ABULATED BELOW.)
      DO 15 M=1,3
      PRINT 4, QUAL(M)
    4 FORMAT(1H0/1H ,52X,16HOUTLET QUALITY =,F4.2)
      PRINT 5
    5 FORMAT(1H0,20X,5HINLET,9X,5HINLET,12X,4HMEAN,9X,5HINLET,8X,5HINLET
     1,9X,6HOUTLET,6X,10HNORMALIZED)
      PRINT 6
    6 FORMAT(1H ,18X,8HPRESSURE,5X,11HTEMPERATURE,5X,11HTEMPERATURE,5X,7
     1HDENSITY,6X,8HVELOCITY,6X,8HVELOCITY,8X,4HSLOT)
      PRINT 7
    7 FORMAT(1H ,20X,5H(ATM),8X,7H(DEG K),9X,7H(DEG K),8X,6H(G/CC),6X,8H
     1(CM/SEC),6X,8H(CM/SEC),7X,6HHEIGHT/1H )
      DO 12 I=1,NOPINC
      IF(SLOTNS(I,M)) 10,13,8
    8 PRINT 9, PIN(I),TIN(I),TAVNS(I,M),DENSIN(I),VINNS(I,M),VOUTNS(I,M)
     1,SLOTNS(I,M)
    9 FORMAT(1H ,19X,F6.3,8X,F6.2,10X,F6.2,8X,F7.5,4X,E10.4,4X,E10.4,5X,
     1F10.4)
      GO TO 12
   10 PRINT 11, PIN(I)
   11 FORMAT(1H ,19X,F6.3,38X,49H---PROGRAM ERROR--- COMPUTED SLOT HEIGH
     1T NEGATIVE)
   12 CONTINUE
      GO TO 15
   13 PRINT 14
   14 FORMAT(1H ,37X,58HHIGHER INLET PRESSURE RESULTS IN EXCESSIVE OUTLE
     1T VELOCITY)
   15 CONTINUE
      PRINT 1
      PRINT 2, POUT,TOUT,DNVOUT,DNLOUT
      PRINT 16
   16 FORMAT(1H0/1H ,35X,61HFLOW PARAMETERS BASED ON NO-MIXING MODEL ARE
     1 TABULATED BELOW.)
      DO 25 M=1,3
```

```
 PRINT 4, QUAL(M)
 PRINT 17
 FORMAT(1H0,11X,5HINLET,9X,5HINLET,12X,4HMEAN,9X,5HINLET,8X,5HINLET
1,9X,6HLIQUID,11X,5HVAPOR,8X,10HNORMALIZED)
 PRINT 18
 FORMAT(1H , 9X,8HPRESSURE,5X,11HTEMPERATURE,5X,11HTEMPERATURE,5X,7
1HDENSITY,6X,8HVELOCITY,5X,11HOUTLET VEL.,5X,11HOUTLET VEL.,8X,4HSL
2OT)
 PRINT 19
 FORMAT(1H ,11X,5H(ATM),8X,7H(DEG K),9X,7H(DEG K),8X,6H(G/CC),6X,8H
1(CM/SEC),6X,8H(CM/SEC),8X,8H(CM/SEC),9X,6HHEIGHT/1H )
 DO 23 I=1,NOPINC
 IF(SLOTNM(I,M)) 22,24,20
 PRINT 21, PIN(I),TIN(I),TAVNM(I,M),DENSIN(I),VINNM(I,M),VLONM(I,M)
1,VVONM(I,M),SLOTNM(I,M)
 FORMAT(1H ,10X,F6.3,8X,F6.2,10X,F6.2,8X,F7.5,4X,E10.4,5X,E10.4,6X,
1E10.4,6X,E10.4)
 GO TO 23
 PRINT 11, PIN(I)
 CONTINUE
 GO TO 25
 PRINT 14
 CONTINUE
 PRINT 26
 FORMAT(1H1,42X,48HFLOW PARAMETERS ADJUSTED FOR SUBCOOLING AT INLET
1)
 DO 31 M=1,3
 PRINT 27,POUT,QUAL(M),DNLOUT
 FORMAT(1H0/1H ,12X,17HOUTLET PRESSURE =,F6.3,5H ATM.,11X,16HOUTLET
1 QUALITY =,F4.2,11X,24HLIQUID DENSITY AT PUMP =,F7.5,5H G/CC)
 PRINT 28
 FORMAT(1H0,10X,51H----------------     NO SLIP MODEL ----------
1---,10X,51H----------------- NO MIXING MODEL ----------     )
 PRINT 29
 FORMAT(1H0,10X,9HDELTA (P),5X,9HDELTA (T),5X,10HNORMALIZED,6X,6HV
1(IN),11X,9HDELTA (P),5X,9HDELTA (T),5X,10HNORMALIZED,6X,6HV (IN))
 PRINT 30
 FORMAT(1H ,13X,3HATM,10X,5HDEG K,8X,8HSLOT HT.,7X,6HCM/SEC,14X,3HA
1TM,10X,5HDEG K,8X,8HSLOT HT.,7X,6HCM/SEC/1H )
 PRINT 32, (DPNS(I,M),DTNS(I,M),CSLTNS(I,M),CVINNS(I,M),DPNM(I,M),D
1TNM(I,M),CSLTNM(I,M),CVINNM(I,M),I=1,NOPINC)
 FORMAT(1H ,12X,F5.3,9X,F5.2,6X,E10.4,4X,E10.4,12X,F5.3,9X,F5.2,6X,
1F10.4,4X,F10.4)
 RETURN
 END
```

APPENDIX F

Bibliography

APPENDIX F

BIBLIOGRAPHY

1. L. Steg and G. W. Sutton, "The Prospects of MHD Power Generation", Astronautics, 5, 8, 22 (1960)

2. Z. J. J. Stekly, T. A. de Winter, and A. El Bindari, "Field Coils for Magnetohydrodynamic Generators", High Magnetic Fields (H. Kolm, B. Lax, F. Bitter, and R. Mills, ed., M. I. T. Press and John Wiley, N. Y., 1962) pp 139

3. R. A. Doragh, "Magnetohydrodynamic Propulsion Using Superconducting Magnets", presented to the annual convention of the Society of Naval Architects and Marine Engineers, N. Y., Nov. 1963

4. S. Way, "Propulsion of Submarines by Lorentz Forces in the Surrounding Sea", Westinghouse Research Laboratory Scientific Paper 63-118-265-P6, Dec. 1963

5. R. H. Levy and Z. J. J. Stekly, "Superconducting Coils", Astronautics and Aeronautics, 2, 2, 30, Feb. 1964

6. J. H. Wernick, F. J. Morin, F. S. L. Hau, D. Dorsi, J. P. Maita, and J. E. Kunzler, "Evidence for a Critical Magnetic Field in Excess of 500 Kilogauss in the Superconducting V-Ga System", High Magnetic Fields, pp 609

7. Z. J. J. Stekly, "The Feasibility of Large Superconducting Coils", Avco-Everett Research Laboratory Report 160, Sept. 1963

8. R. C. Wolgast, H. P. Hernandez, R. R. Aron, H. C. Hitchcock, and K. A. Solomon, "Superconducting Critical Currents in Wire Samples and Some Experimental Coils", Advances in Cryogenic Engineering (Plenum Press, N. Y.) 8, 601 (1963)

9. J. K. Hulm, B. S. Chandrasekhar, and H. Riemersma, "High Field Superconducting Magnets", Adv Cryo Eng, 8, 17 (1963)

10. W. F. Gauster and D. L. Coffey, "Current-Carrying Capacity and Transition State of Superconducting Solenoids", Adv Cryo Eng, 9, 316 (1964)

11. C. Laverick, "Experimental Studies on the Current-Carrying Capacity of Nb-Zr Wires under Conditions of Fixed and Swept Magnetic Field", Adv Cryo Eng, 9, 321, (1964)

12. H. Riemersma, J. K. Hulm, and B. S. Chandrasekhar, "Flux Jumping and Degradation in Superconducting Solenoids", Adv Cryo Eng, 9, 329 (1964)

13. C. B. Müller and E. J. Saur, "Influence of Mechanical Constraints on Critical Currents of Superconducting Surface Layers of Nb_3Sn on Nb and V_3Ga on V in Transverse Magnetic Fields", Adv Cryo Eng, 9, 338 (1964)

14. A. R. Kantrowitz and Z. J. J. Stekly, "A New Principle for the Construction of Stabilized Superconducting Coils", Appl Phys Letters, 6, 56 (1965)

15. J. F. Louis, J. Lothrop, and T. R. Brogan, "Fluid Dynamic Studies with a Magnetohydrodynamic Generator", Phys Fl, 7, 362 (1964)

16. J. F. Lewis, G. Gal, and P. R. Blackburn, "Detailed Theoretical and Experimental Study on a Large MHD Generator", presented to the Fifth Symposium on the Engineering Aspects of Magnetohydrodynamics, M. I. T., April 1964

17. H. L. Laquer and E. F. Hammel, "Cryogenic Electromagnets. I. Feasibility Study", Rev Sci Instr, 28, 875 (1957)

18. H. L. Laquer, "The Los Alamos High Field Magnet", Adv Cryo Eng, 2, 117 (1957)

19. J. R. Purcell, "An Aluminum Magnet Cooled with Liquid Hydrogen", High Magnetic Fields, pp 166

20. J. Hord, "Project Sherwood: Final Report on Cryogenic Aluminum Electromagnet", N. B. S. Report 8481, Nov. 1964

21. J. C. Laurence, G. V. Brown, J. Geist, and K. Zeitz, "A Large, Liquid-Neon Cooled Electromagnet", High Magnetic Fields, pp 170

22. J. M. Geist, S. Z. Kobran, G. W. Siegrist and K. Zeitz, "A He/H_2 Refrigeration System for a Large Liquid Neon Cooled Electromagnet", presented at the Cryogenic Engineering Conference, U. Penn., Aug. 1964

23. C. E. Taylor and R. F. Post, "Design of Large Cryogenic Magnet Coils", Adv Cryo Eng, 5, 31 (1960)

24. C. E. Taylor and R. L. Nelson, "Test Results for a 7-1/8" I. D. x 12" Long Sodium Cryogenic Coil", UCRL 7401 (1963)

25. R. F. Post and C. E. Taylor, "Air Core Cryogenic Magnet Coils for Fusion Research and High-Energy Nuclear Physics Applications", Adv Cryo Eng, 5, 13 (1960)

26. C. E. Taylor and R. F. Post, "Cryogenic Coils", High Magnetic Fields, pp 101

27. R. F. Post and C. E. Taylor, "Cryogenic Magnets", U. S. Patent 3,090,894, issued May 21, 1963

28. G. W. Sutton and A. W. Carlson, "End Effects in Inviscid Flow in a Magnetohydrodynamic Channel", J Fl Mech, 11, 121 (1961)

29. G. W. Sutton, H. Hurwitz, and H. Poritsky, "Electrical and Pressure Losses in a Magnetohydrodynamic Channel due to End Current Loops", AIEE Trans (Comm and Elect), 80, 687 (1962)

30. D. K. C. MacDonald, "Properties of Metals at Low Temperatures", Progress in Metal Physics (Pergammon Press, London) 3, 42 (1952)

31. A. Mathiessen, Ann Phy Chem, 110, 190 (1860), cited in (28)

32. F. Bloch, Z Phys, 53, 216 (1929), cited in (28)

33. P. Debye, Ann Phys, 39, 789 (1911), cited in (28)

34. E. Gruneisen, "Die Abhangigkeit des elektrischen Widerstandes reiner Metalle von der Temperatur", Ann Phys (5), 16, 530 (1933)

35. H. M. Rosenberg, "The Properties of Metals at Low Temperatures", Prog Met Phys, 7, 339 (1958)

36. M. Kohler, "Zur magnetischen Widerstandsanderung reiner Metalle", Ann Phys (5), 32, 211 (1938)

37. E. Justi, "Uber den elektrischen Widerstand von polykristallinem Gold, Blei, Niob, und Tantal in starken magnetischen Qurefeldern bei tiefen Temperaturen", Phys Zeit, 41, 486 (1940)

38. D. K. C. MacDonald, "Electrical Conductivity of Metals and Alloys at Low Temperatures", Encyclopedia of Physics (S. Flugge, ed, Springer-Verlag, Berlin, 1956), Vol. XIV, pp 180

39. H. K. Onnes and W. Tuyn, "Electrical Resistance of Elementary Substances at Temperatures below -80° C", International Critical Tables (McGraw-Hill, N. Y., 1929), pp 124

40. A. Maimoni, "Electrical Resistance of Aluminum at Low Temperatures", Cryogenics, 2, 4, 217 (1962)

41. S. B. Woods, "The Conductivity of Sodium at Low Temperatures", Canadian J Phys, 34, 223 (1956)

42. E. W. Fenton, J. S. Rogers, and S. B. Woods, "Lorenz Numbers of Pure Aluminum, Silver, and Gold at Low Temperatures", Canadian J Phys, 41, 2026 (1963)

43. D. K. C. MacDonald and K. Mendelssohn, "Resistivity of Pure Metals at Low Temperatures. I. The Alkali Metals", Proc Roy Soc (A), 202, 103 (1950)

44. A. N. Gerritsen and J. O. Linde, "The Electrical Resistivities of Alloys of a Noble Metal and a Transition Metal", Physica, 18, 877 (1952)

45. G. J. Los and A. N. Gerritsen, "Resistivity and Magnetoresistance of Dilute Alloys of Copper and Gold with Nickel at Low Temperatures", Physica, 23, 633 (1957)

46. R. Berman and D. K. C. MacDonald, "The Thermal and Electrical Conductivity of Copper at Low Temperatures", Proc Roy Soc (A), 211, 122 (1952)

47. D. K. C. MacDonald and W. B. Pearson, "Electron Transport in Copper and Dilute Alloys at Low Temperatures", Acta Met, 3, 392 (1955)

48. A. V. Gold, D. K. C. MacDonald, W. B. Pearson, and I. M. Templeton, "The Thermoelectric Power of Pure Copper", Phil Mag (8), 5, 765 (1960!

49. W. J. de Haas and J. de Boer, "The Electrical Resistance of Platinum at Low Temperatures", Physica, 1, 609 (1933)

50. G. K. White and S. B. Woods, "Thermal and Electrical Conductivity of Rhodium, Iridium, and Platinum at Low Temperatures", Canadian J Phys, 35, 248 (1957)

51. W. R. G. Kemp, P. G. Klemens, and G. K. White, "Thermal and Electrical Conductivities of Iron, Nickel, Titanium, and Zirconium at Low Temperatures", Australian J. Phys, 9, 180 (1956)

52. E. Mendoza and J. G. Thomas, "The Electrical Resistance of Gold, Silver, and Copper at Low Temperatures", Phil Mag (7), 42, 291 (1951)

53. B. Luthi, "Widerstandsanderung von Metallen in hohen Magnetfeldern", Helv Phys Acta, 33, 161 (1960)

54. G. K. White and S. B. Woods, "Indium Resistance Thermometer; 4 to 300° K", Rev Sci Inst, 28, 638 (1957)

55. D. K. C. MacDonald, G. K. White, and S. B. Woods, "Thermal and Electrical Conductivities of the Alkali Metals", Proc Roy Soc (A), 235, 358 (1956)

56. D. K. C. MacDonald, W. B. Pearson, and I. M. Templeton, "Thermo-Electricity at Low Temperatures. VIII. Thermo-Electricity of the Alkali Metals below 2° K", Proc Roy Soc (A), 256, 334 (1960)

57. G. Chaudron, "Preparation of Aluminum of Extreme Purity by the 'Zone Fusion' Process", Nature, 174, 923 (1954)

58. T. G. Pearson and H. W. L. Phillips, "The Production and Properties of Super-Purity Aluminum", Met Rev, 2, 8, 305 (1957)

59. J. H. Wernick, D. Dorsi, and J. J. Byrnes, "Techniques and Results of Zone Refining Some Metals", J Electrochem Soc, 106, 3, 245 (1959)

60. E. D. Tolmie, "Apparatus for the Zone-Refining of Copper", J Sci Inst, 37, 175 (1960)

61. J. S. Smart Jr, A. A. Smith Jr, and A. J. Phillips, "Preparation and Some Properties of High-Purity Copper", Trans Am Inst Mining Met Engrs, 143, 272 (1941)

62. R. B. Scott, Cryogenic Engineering (Van Nostrand, N. Y., 1959) pp 336

63. R. F. Post and C. E. Taylor, "Method for Reducing the Impurity

Resistivity of Sodium", U. S. Patent 3,100,730, issued Aug. 13, 1963

64. M. P. Orlova, D. N. Astrov, and L. A. Medvedeva, "Indium Resistance Thermometers for the Temperature Range 3.4° - 300° K", Cryogenics, 4, 2, 95 (1964)

65. B . Yates and C. H. Panter, "Indium Resistance Thermometers", J Sci Inst, 38, 196 (1961)

66. C. A. Swenson, "Properties of Indium and Thallium at Low Temperatures", Phys Rev (2), 100, 1607 (1955)

67. W. Tuyn, "Measurements on the Electrical Resistance of Some Metals Below the Boiling Point of Oxygen", Comm Phys Lab Univ Leiden 196b (1929)

68. R. W. Powell, M. J. Woodman and R. P. Tye, "The Thermal Conductivity and Electrical Resistivity of Indium", Phil Mag (8), 7, 1183 (1962)

69. W. J. de Haas and J. Voogd, "Measurements of the Electrical Resistivity of Pure In, Tl, and Ga at Low Temperatures", Comm Phys Lab Univ Leiden 212d (1931)

70. W. Tuyn and H. Kamerlingh Onnes, "Further Experiments with Liquid Helium. S. XII. Measurements Concerning the Electrical Resistivity of Indium in the Temperature Field of Liquid Helium", Comm Phys Lab Univ Leiden 167a (1923)

71. S. B. Woods, "The Conductivity of Sodium at Low Temperatures", Canadian J. Phys, 34, 223 (1956)

72. G. K. White, "Low Temperature Conductivities of Copper", Australian J Phys, 6, 397 (1953)

73. W. J. de Haas, J. de Boer, and G. J. van den Berg, "The Electrical Resistivity of Gold, Copper, and Lead at Low Temperatures", Physica, 1, 1115 (1934)

74. H. A. Boorse and H. Niewodniczanski, "Electrical Resistivity of Aluminum", Proc Roy Soc (A), 153, 463 (1936)

75. W. De Sorbo, "Quenched Imperfections and the Electrical Resistivity of Aluminum at Low Temperatures", Phys Rev (2), 111, 810 (1958)

76. E. Justi, "Magnetische Widerstandsvermehrung und Leitungstypen der Metalle", Phys Zeit, 41, 563 (1940)

77. G. K. White and S. B. Woods, "Electrical and Thermal Magneto-Resistance in Thin Rods of Pure Sodium", Phil Mag (8), 1, 846 (1956)

78. C. E. Taylor, private communication, Nov. 1964

79. E. Justi and M. Kohler, "Uber die elektrische Leitfahigkeit der Alkalimetalle im Magnetfeld", Ann d Phys (5), 36, 349 (1939)

80. J. Babiskin and P. G. Siebenmann, Phys Rev, 107, 5, 1249, cited in (78)

81. N. E. Alekseevskii and Yu. P. Gaidukov, J Exp and Theor Phys (U.S.S.R.), 36, 447 (1959), cited in (78)

82. R. G. Chambers, "Magneto-resistance in the Group I Metals at High Fields", Proc Roy Soc (A), 238, 344 (1956)

83. J. L. Olsen and L. Rinderer, "Magneto-Resistance of Copper to 150,000 Oersted at 4.2° K", Nature, 173, 682 (1954)

84. A. N. Gerritsen, "The Magnetoresistances of Alloys of a Noble Metal and a Transition Metal at Low Temperatures", Physica, 19, 61 (1953)

85. E. Gruneisen and H. Adenstedt, "Einfluss transversaler Magnetfelder auf Elektrizitats- und Warmeleitung reiner Metalle bei tiefer Temperatur", Ann d Phys (5), 31, 714 (1938)

86. A. Callaghan, "Magnetics Research at NASA", High Magnetic Fields, pp 420

87. P. Cotti, B. Luthi, and J. L. Olsen, "Pulsed Field Magnetoresistance Measurements in Metals", High Magnetic Fields, pp 523

88. E. Justi and H. Scheffers, "Uber die Widerstandsanderung von Aluminiumeinkristallen in starken magnetischen Feldern bei tiefen Temperaturen", Phys Zeit, 39, 105 (1938)

89. R. M. McClintock and R. L. Hauser, "Current Trends and Prospects in Mechanical Properties", Adv Cryo Eng, 8, 631 (1963)

90. C. A. Swenson, "The Compressive Strengths of Some Technical Metals Between 4.2° and 300° K", Adv Cryo Eng, 1, 251 (1956)

91. Cryogenic Materials Data Handbook (T. F. Durham, R. M. McClintock, and R. P. Reed, ed.), published by the Cryogenic Engineering Laboratory, N.B.S. (1961)

92. D. F. Windenburg, "Master Charts for the Design of Vessels under External Pressure", A.S.M.E. Trans, 69, 345 (1947)

93. H. Kropschot, J. E. Schrodt, M. M. Fulk, and B. J. Hunter, "Multiple Layer Insulation", Adv Cryo Eng, 5, 189 (1960)

94. M. P. Hnlicka, "Engineering Aspects of Heat Transfer in Multilayer Reflective Insulation and Perfection of NRC Insulation", Adv Cryo Eng, 5, 199 (1960)

95. P. M. Riede and D. I-J. Wang, "Characteristics and Applications of Some Superinsulations", Adv Cryo Eng, 5, 209 (1960)

96. L. C. Matsch, "Advances in Multilayer Insulations", Adv Cryo Eng, 7, 413 (1962)

97. J. L. McGrew , "A Comparative Study of Airborne Liquid Hydrogen Tank Insulation", Adv Cryo Eng, 8, 387 (1963)

98. H. Kropschot and R. W. Brugess, "Pearlite for Cryogenic Insulation", Adv Cryo Eng, 8, 425 (1963)

99. R. McFee, "Optimum Input Leads for Cryogenic Apparatus", Rev Sci Inst, 30, 98 (1959)

100. Z. J. J. Stekly and H. H. Woodson, "Rotating Machinery Utilizing Superconductors", I.E.E.E. Trans on Aerospace, AS-2, 2, 826 (1964)

101. "A Compendium of Properties of Materials at Low Temperatures (Phase 1). Part II: Properties of Solids", W. A. D. D. 60-56 (1959)

102. F. C. Hoare, L. C. Jackson, and N. Curti, Experimental Cryophysics (Butterworth, London, 1961)

103. R. E. Bernert and Z. J. J. Stekly, "Systems Analysis of Superconducting Magnets for Space Radiation Shielding", report prepared for George C. Marshall Space Flight Center (NASA) under contract No. NAS 8-5278, Mar. 1964

104. C. B. Hood, W. W. Vogelhuber, and C. B. Barnes, "Helium Refrigerators for Operation in the 10^{o}-30^{o} K Range", Adv Cryo Eng, 9, 496 (1964)

105. D. B. Mann, M. T. Norton, and T. R. Strobridge, "Interim Report on Cryogenic Magnet Refrigeration", NBS Report 8239, Feb. 1964 (Additional information will be available in Adv Cryo Eng, 10.)

106. R. E. Bernert, "Low-Temperature Refrigerators: Costs and Operating Power", Chemical Engineering, Dec. 7, 1964, pp 196

107. R. Stevenson, "Design of Two Region Solenoids" and "Design of a 300,000 Oersted Two Region Solenoid for Intermittent Operation", annual report to the Office of Naval Research under contract Nonr-3013(00), task NR 018-503, Aug. 1963

108. W. R. Rohsenow and H. Y. Choi, Heat, Mass, and Momentum Transfer (Prentice-Hall, N. Y., 1961) pp 192

109. G. F. Hagenbach and J. H. Schiffhauer, "Commercial Production of Liquid Neon", Adv Cryo Eng, 9, 557 (1964)

110. F. J. Graham, "Liquid Neon and Advanced Techniques Used in Design of Liquid Neon Equipment", Adv Cryo Eng, 7, 562 (1962)

111. J. D. Seader, W. S. Miller, and L. A. Kalvinskas, "Boiling Heat Transfer for Cryogenies: Final Report", Rocketdyne Report R-5598, prepared under George C. Marshall Space Flight Center (NASA) contract number NAS 8-5337, May, 1964

112. E. G. Brentari and R. V. Smith, "Nucleate and Film Pool Boiling Design Correlations for O_2, N_2, H_2, and He", presented at the Cryogenic Engineering Conference, U. Penn., Aug. 1964. To be published in Adv Cryo Eng, 10.

113. S. S. Kutateladze, Heat Transfer in Condensation and Boiling, Second Edition (State Scientific and Technical Publishers of Literature on Machinery, Moscow, 1952), cited in (112)

114. L. Bewilogua and H. G. Mahn, "Heat Transfer in Liquid Neon", Cryogenics, 3, 4, 232 (1963)

115. T. H. K. Frederking, "Metastable Superheat in Nucleate Boiling of Cryogenic Liquids", Adv Cryo Eng, 9, 71 (1964)

116. R. D. McCarty and R. B. Stewart, "Preliminary Thermodynamic Properties of Neon", Adv Cryo Eng, 9, 161 (1964)

117. R. B. Stewart and K. D. Timmerhaus, "The Correlation of Thermodynamic Properties of Cryogenic Fluids", Adv Cryo Eng, 9, 20 (1964)

118. C. R. Class, J. R. DeHaan, M. Piccone, and R. B. Cost, "Boiling Heat Transfer to Liquid Hydrogen from Flat Surfaces", Adv Cryo Eng, 5, 254 (1960)

119. C. W. Cowley, W. J. Timson, and J. A. Sawdye, "A Method for Improving Heat Transfer to a Cryogenic Fluid", Adv Cryo Eng, 7, 385 (1962)

120. G. G. Haselden and J. I. Peters, "Heat Transfer to Boiling Liquid Oxygen and Liquid Nitrogen", Trans Inst Chem Engrs (London), 27, 201 (1949)

121. J. C. Chen, "A Correlation for Boiling Heat Transfer to Saturated Fluids in Convective Flow", ASME Paper 63-HT-34, presented at the ASME-AIChE Heat Transfer Conference in Boston, Aug, 1963

122. T. H. K. Frederking, "Peak Heat Flux and Temperature Difference in Nucleate Boiling of Liquified Gases", Adv Cryo Eng, 8, 489 (1963)

123. A. H. Shapiro, The Dynamics and Thermodynamics of Compressible Fluid Flow, Vol. 1, (Ronald Press, N. Y., 1953), pp 80

124. D. B. Chelton and D. B. Mann, "Cryogenic Data Book", WADC TR 59-8, Mar. 1959

125. P. J. Murto, "A Gas-Shielded Storage and Transport Vessel for Liquid Helium", Adv Cryo Eng, 7, 291 (1962)

126. R. B. Jacobs, "Liquid Requirements for the Cool-Down of Cryogenic Equipment", Adv Cryo Eng, 8, 529 (1963)

127. D. B. Mann, "The Thermodynamic Properties of Helium from 3 to 300°K between 0.5 and 100 Atmospheres", NBS Tech Note 154, Jan. 1962

128. S. G. Sydoriak and T. R. Roberts, "Study of Boiling in Short Narrow Channels and Its Application to the Design of Magnets Cooled by Liquid Hydrogen and Nitrogen", J Appl Phys, 28, 143 (1957)

129. Tables of Thermodynamic and Transport Properties (formerly NBS Circular 564) (Pergammon Press, N. Y., 1960)

130. H. M. Roder and R. D. Goodwin, "Provisional Thermodynamic Functions for Parahydrogen", NBS Tech Note 130, Dec. 1961

131. R. D. Goodwin, D. E. Diller, W. J. Hall, H. M. Roder, L. A. Weber, and B. A. Younglove, "Survey of Current NBS Work on Properties of Parahydrogen", Adv Cryo Eng, 9, 316 (1964)

132. D. B. Chelton, "Safety in the Use of Liquid Hydrogen", NBS Report 7253, Apr. 1962

133. R. B. Stewart and V. J. Johnson (ed.), "A Compendium of the Properties of Materials at Low Temperatures (Phase II). Part IV," WADD 60-56 (1961), pp 127

134. T. R. Strobridge, "The Thermodynamic Properties of Nitrogen from 64 to 300 °K between 0.1 and 200 Atmospheres", NBS Tech Note 129, Jan. 1962

BIOGRAPHICAL NOTE

John Allen McMorris II was born in New York City on April 7, 1935, and graduated from Berkeley High School, Berkeley, California, in June 1952. He attended the Massachusetts Institute of Technology as a freshman, during Academic Year 1952-53, and was subsequently admitted to the United States Naval Academy, Annapolis, Maryland, in June 1953. He graduated from the Naval Academy third in a class of 848, receiving his Bachelor of Science degree in June, 1957, and was commissioned as a naval officer at that time. He served aboard the U. S. S. Alfred A. Cunningham (DD752) for eighteen months, and thereafter, as a member of the commissioning crew of the U. S. S. Morton (DD948). In June, 1960, he returned to the Massachusetts Institute of Technology, where he was awarded the degrees of Master of Science and Naval Engineer in June, 1963, and received the Brand Award of the American Society of Naval Engineers for standing first in Course XIII A at that time. He subsequently entered the doctoral program of the Department of Electrical Engineering, at M. I. T., and upon graduation from that program in 1965 will return to duties with the U. S. Navy

thesM2554
A comprehensive analysis of cryogenic ma
3 2768 001 01201 6
DUDLEY KNOX LIBRARY